Dissertations, Master's Theses and Master's Reports

2019

TOWARDS SUSTAINABLE PRODUCTION OF CHEMICALS AND FUELS FROM THE FAST PYROLYSIS OF WASTE POLYOLEFIN PLASTICS

Ulises Gracida Alvarez
Michigan Technological University, urgracid@mtu.edu

TOWARDS SUSTAINABLE PRODUCTION OF CHEMICALS AND FUELS FROM

THE FAST PYROLYSIS OF WASTE POLYOLEFIN PLASTICS

By

Ulises Raymundo Gracida Alvarez

A DISSERTATION

Submitted in partial fulfillment of the requirements for the degree of

DOCTOR OF PHILOSOPHY

In Chemical Engineering

MICHIGAN TECHNOLOGICAL UNIVERSITY

2019

This dissertation has been approved in partial fulfillment of the requirements for the Degree of DOCTOR OF PHILOSOPHY in Chemical Engineering.

Department of Chemical Engineering

Dissertation Co-Advisor: *Dr. David R. Shonnard*

Dissertation Co-Advisor: *Dr. Julio C. Sacramento Rivero*

Committee Member: *Dr. Gerard T. Caneba*

Committee Member: *Dr. Joshua M. Pearce*

Department Chair: *Dr. Pradeep K. Agrawal*

Table of Contents

List of figures

List of tables

Preface

This doctoral dissertation contains material previously reviewed and published in scientific journals along with material currently submitted to scientific journals. Full citation of these are as follows

Chapter 2

Reprinted with permission from Gracida-Alvarez, U.R.; Keenan L.M.; Sacramento-Rivero J.C.; Shonnard, D.R. Resource and Greenhouse Gas Assessments of the Thermochemical Conversion of Municipal Solid Waste in Mexico. *ACS Sustainable Chemistry and Engineering*. 4(11), 5972-5978. Copyright 2016 American Chemical Society.

DOI: 10.1021/acssuschemeng.6b01143

Author Contributions

Gracida-Alvarez	Collection, analysis, and interpretation of data, writing of the paper, responsible for submission and review of journal article.
Keenan	Collection of data and literature review.
Sacramento-Rivero	Review and editing of the paper.
Shonnard	Design of the study, analysis and interpretation of data, paper review and editing.

Chapter 3

Reprinted with permission from Gracida-Alvarez, U.R.; Mitchell, M.K.; Sacramento-Rivero J.C.; Shonnard, D.R. Effect of Temperature and Vapor Residence Time on the Micropyrolysis Products of Waste High density Polyethylene. *Industrial and Engineering Chemistry Research*. 57(6), 1912-1923. Copyright 2018 American Chemical Society.

Author Contributions

Gracida-Alvarez	Experimental planning, collection, analysis, and interpretation of data, writing of the paper, responsible for submission and review of journal article.
Mitchell	Collection and analysis of data, writing of the paper.
Sacramento-Rivero	Review and editing of the paper.
Shonnard	Design of the study, experimental planning, analysis and interpretation of data, paper writing, review and editing.

Chapter 4

Will be submitted to *ACS Sustainable Chemistry and Engineering*. Gracida-Alvarez, U.R.; Winjobi, O.; Sacramento-Rivero J.C.; Shonnard, D.R. Systems Analysis of High-value Chemicals and Fuels from a Waste High-Density Polyethylene Refinery. Part 1: Conceptual Design and Techno-economic Assessment.

Author Contributions

Gracida-Alvarez	Process modelling, collection, analysis, and interpretation of data from techno-economic assessment, writing of the paper.
Winjobi	Mentorship on process modeling and techno-economic assessment, analysis and interpretation of data.
Sacramento-Rivero	Design of the study, review and editing of the paper.
Shonnard	Design of the study, analysis and interpretation of data, paper review and editing.

Chapter 5

Will be submitted to *ACS Sustainable Chemistry and Engineering*. Gracida-Alvarez, U.R.; Winjobi, O.; Sacramento-Rivero J.C.; Shonnard, D.R. Systems Analysis of High-value Chemicals and Fuels from a Waste High-Density Polyethylene Refinery. Part 2: Carbon Footprint Analysis and Regional Electricity Effects.

Author Contributions

Gracida-Alvarez	Collection, analysis, and interpretation of data from life cycle assessment and regional energy grids evaluation, writing of the paper.
Winjobi	Mentorship on process modeling and life cycle assessment, analysis and interpretation of data.
Sacramento-Rivero	Design of the study, review and editing of the paper.
Shonnard	Design of the study, analysis and interpretation of data, paper review and editing.

Acknowledgements

List of abbreviations

AKA: Alkanes

AKD: Alkadienes

AKE: Alkenes

BC: Base case scenario

BTX: Benzene-toluene-xylenes

C: Carbon

CEPCI: Chemical Engineering plant cost index

CFA: Carbon footprint analysis

CFBR: Continuous fluidized bed reactor

CSBR: Continuous spouted bed reactor

CST: Collection, separation, and transportation

CW: Cooling water

DCFA: Discounted cash flow analysis

DCFROR: Discounted cash flow rate of return

DS: Dual stream

EAP: Estimated annual production

eGRID: Emissions and Generation Resource Integrated Database

EROI: Energy returned over invested

FBR: Fluidized bed reactor

FCI: Fixed capital investment

FOC: Fixed operation costs

GC/MS: Gas chromatography/mass spectrometry

GHG: Greenhouse gas

GWP: Global warming potential

HDPE: High-density polyethylene

HEN: Heat exchanger network

HI: Heat integration

HI-1: Heat integrated scenario 1

HI-2: Heat integrated scenario 2

IRR: Internal rate of return

LCA: Life cycle assessment

LDPE: Low-density polyethylene

LHV: Lower heating value

LP: Low pressure

MACRS: Modified accelerated cost recovery system

MAF: Moisture and ash free

MAFOW: Moisture and ash free organic waste

MAHs: monoaromatic hydrocarbons

MM USD: Million United States dollars

MRF: Materials recovery facility

MSW: Municipal solid waste

MWHCs: Molecular weight hydrocarbons

NCC: National consumption

NG: Natural gas

NPV: Net present value

PAHs: polyaromatic hydrocarbons

PE: Polyethylene

PET: Polyethylene terephthalate

PP: Polypropylene

PRW: Post-recycling waste

PS: Polystyrene

PSA: Pressure swing adsorption

PTO: Plastic-to-oil

PVC: Polyvinyl chloride

PW: Plastic waste

ROI: Return on Investment

SS: Single stream

TEA: Techno-economic assessment

TEPC: Total equipment purchase costs

TI: Total indirect costs

TIC: Total installation costs

TMLC: Total area of corresponding masses of lumped compounds

Tonne: Metric ton

TPI: Total project investment

TSMR: two-stage micropyrolysis reactor

U: Overall heat transfer coefficient

UNIQUAC: Universal quasichemical

VOC: Variable operation costs

VRT: Vapor residence time

WC: Working capital

Abstract

The increasing amount of plastic waste (PW) generation has become an important concern due to the leveled-off recycling rates. Therefore, governmental agencies around the world, including state governments in the United States, have proposed initiatives to minimize the amount of PW that is landfilled and encourage recycling or energy recovery. Circular economy is a strategy that attempts on reusing PW to produce new polymers while avoiding its disposal and the use of virgin material. Chemical recycling raises an interesting technology prospect due to the potential reduction of pollutant emissions and the establishment of a circular economy through the production of monomers and fuels.

This dissertation initially presents a resource assessment for available MSW in Mexico and concludes that when the organic and polyolefin plastic components are converted to liquid hydrocarbon transportation biofuels through a pyrolysis-based pathway, up to 7% of Mexico's transportation-fuel consumption could be met. A preliminary carbon footprint analysis (CFA) shows that liquid transportation biofuels from the organic portion of MSW (paper, packaging, wood, yard trimmings) sequesters 9.5 g CO_2 eq. per MJ biofuel, with significant pathway credits due to avoiding landfill CH_4 emissions. The greenhouse gas (GHG) emissions from the conversion of the polyolefin plastic in the MSW are positive (88 g CO_2 eq. per MJ), though still lower than current fossil transportation fuels in Mexico (95.5 g CO_2 eq. per MJ).

In this Ph.D. research, pyrolysis vapors from waste high density polyethylene (HDPE) were subjected to secondary degradation by varying the temperature and vapor residence time (VRT) in the reaction zone of a newly-designed two-stage micropyrolysis reactor (TSMR).

Temperature and VRT variations showed a strong effect on the product distribution, with low temperature (625 ºC) and short VRT (1.4 s) producing a wide range of gases and liquid products and with high temperature (675 ºC) and long VRT (5.6 s) producing mostly hydrocarbon gases (monomers) and mono- and poly-aromatics.

The last two chapters of the dissertation present a novel multiproduct/multiprocessing pyrolysis-based refinery design for the conversion of 500 tonnes/day of high-density polyethylene (HDPE) waste. The products obtained from the refinery are chemical grade ethylene and propylene, an aromatics mixture, and low- and high-molecular weight hydrocarbon mixtures (MWHCs). The energy efficiency was 72 and 77% for the base case and the heat integrated (HI) refinery, respectively. The net present values (NPVs) were 367 and 383 million U.S. dollars (MM USD), for the base case and the heat integrated process, respectively. The CFA results show that the GHG emissions of all products; ethylene, propylene, aromatics mixture, low molecular weight (MW) hydrocarbons (HCs), and high MW HCs, are equal to or less than fossil products for the HI scenario assuming US average electricity grid. Finally, the evaluation of regional electricity grids on GHG emissions for all products was conducted for all 50 states in the US. These results suggest energetic, economic, and environmental sustainability of the design and its promising application on an industrial scale.

This dissertation ends with overall conclusions and recommendations for future research.

1 Introduction

1.1 Plastic waste generation and its environmental and economic repercussions

Plastics are a group of synthetic materials that have brought many benefits to society since their introduction. Their durability, lightweight, versatility, and low-cost have brought them into many applications from food packaging to aeronautics. The impact of plastics in society is such that in 2017 their production reached 348 million tonnes, an amount that has grown annually at a rate of 4% since 2010,[1,2] also their manufacturing uses 6% of the global petroleum production.[3] Around 45% of plastics are used for packaging which is intended for a single use and immediate disposal.[4] Under this consumption pattern a plastic package has an average lifetime of one year which leads to an overall plastic waste generation of 275 million tonnes per year.[5] For over 65 years, 6,300 million tonnes of plastic waste have been generated from which only 21% has been recycled or incinerated.[4,6] The remaining 4,900 million tonnes have been discarded in landfills whose mismanagement has caused serious environmental problems, which includes leakage of plastic wastes into the oceans from major river sources across the globe. Figure 1.1 summarizes the previously mentioned fate of the plastic produced from 1950 to 2015 as analyzed by Geyer et al.[4]
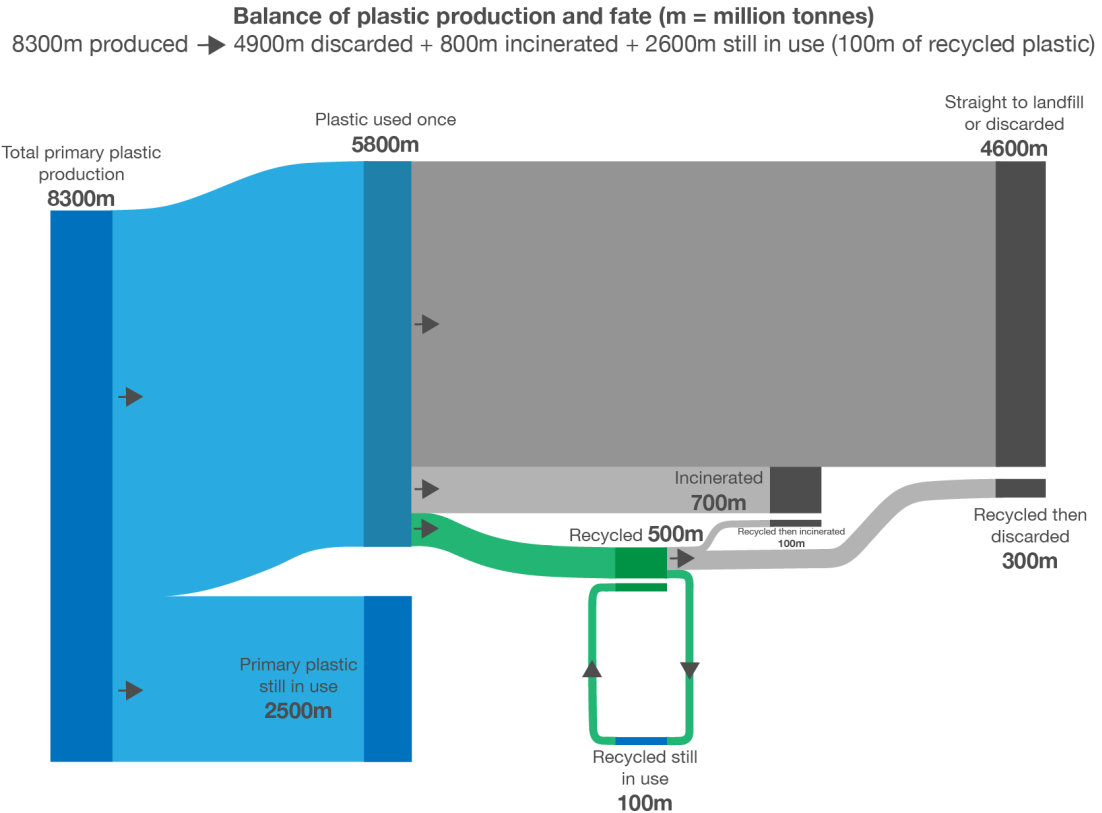
Figure 1.1. Cumulative plastic production, waste generation, and disposal scenarios from 1950 to 2015.[7]

Mismanagement of plastic waste at end of life is responsible of the leakage of 8 million tonnes of plastic waste per year into the oceans which has induced the accumulation of approximately 250,000 tonnes of plastic particles.[5,8] Subsequent degradation reduces the size of plastic particles to less than 4.5 mm which causes their ingestion by marine species. These microplastics also promote the invasion of alien species, the dissemination of harmful chemicals used in plastic production, like phthalates and bisphenols, the accumulation of other toxic compounds within the plastic particles, and the consequential toxicity of the marine food chain.[9] The threatening damage of plastic particles has also

been evidenced for terrestrial ecosystems with similar ecotoxicity and biodiversity effects to those found in marine environments.[10]

The negative effects of landfill disposal are also evident from an economic perspective. Landfill storage induces the production of new plastic to fulfill the increasing demand of the market. Recent estimations establish that between 80 and 120 billion USD are lost every year due to the extraction and manufacture of virgin materials to produce new plastics.[3] Most of the materials used in plastic production have a fossil origin which places an additional burden to the already challenging situation of the extraction of these nonrenewable resources. These statements highlight the urgent need for the substitution of landfill disposal with other alternative plastic waste management options.

1.2 Alternatives for plastic waste management

Mechanical recycling appears as a convenient option to handle plastic waste, however, the reprocessed plastics have a lower durability and inferior mechanical properties compared to those made from virgin polymers.[2] Also, the energy required for the stages of cleaning, sorting, transportation, and re-processing makes this option costly.[11] Plastic has a heating value comparable to fuels which points to their potential use for energy generation.[12] Incineration consists of the production of energy by burning waste plastics. This process apparently reduces GHG emissions by avoiding the use of fossil fuels. However, it has the inconvenience of the formation of fossil CO_2 and highly toxic pollutants such as dioxins and furans[2,13] for some of the plastics (i.e., polyvinyl chloride). In spite of reducing the amount of plastic waste to be landfilled, these alternatives still lack a solution to the

problem of requiring virgin materials to fulfill the demand of plastics in the market. To deal with this recurring issue, a new approach, known as circular economy, has been conceived by many non-governmental and governmental organizations.

1.3 Circular economy of plastics

Circular economy searches for an improved exploitation of resources through cyclic flows of material and energy that do not compromise the future availability of natural resources and reduce the reliance on virgin materials.[14] When this concept is translated to plastic manufacture, it is clear that circular economy advocates for the production of new plastic by using discarded plastic to obtain the necessary feedstocks (Figure 1.2). To advance this approach, the European Commission established in 2014, the "Strategy for Plastics in a Circular Economy". One of the major goals of this strategy is to increase the economic feasibility of recycled plastics through improved technologies and standards for recycling processes, that can promote the creation of a stable market for recycled plastics.[15] Therefore, new chemical recycling process design can offer a potential solution to achieve the goals set by the strategy of plastics in circular economy.

Closed-Loop Recycling

Collected and Processed for Recycle/Reman.

Production and Use

Energy Recovery

Virgin Feedstock

Wastes

Landfilled

Circular Dominant Economy
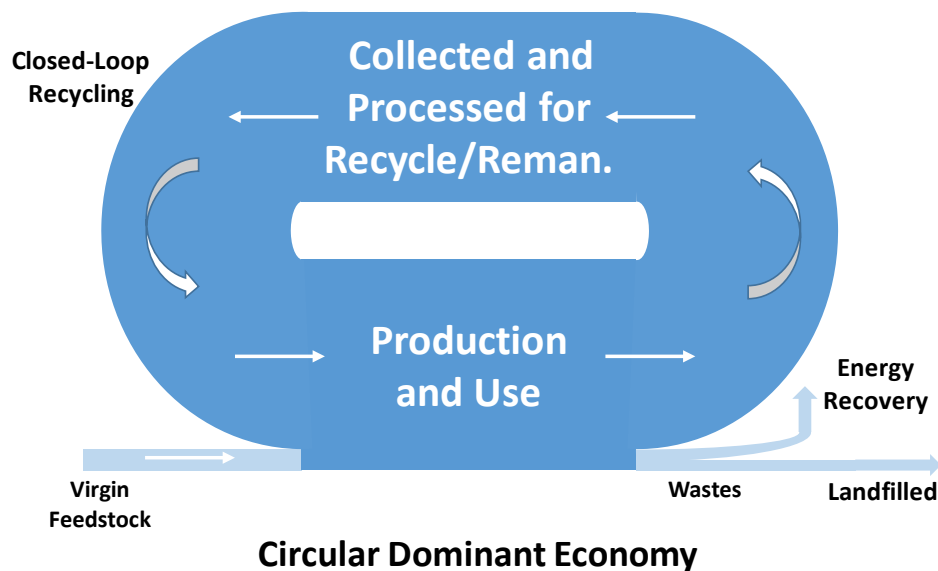
Figure 1.2. Diagram of the circular economy of plastic manufacture.[16]

Chemistry research is capable to develop new plastic additives that do not compromise the quality of products generated through continuous recycling but it also has the potential to develop feedstock materials, like monomers, from plastic waste itself.[17,18] The concept of circular chemistry, proposed by Keijer et al.,[19] broadens the impact of process design from optimizing the use resources in the production stage to the overall improvement of the performance of a system through its complete life cycle, considering the sustainable use of material and energy resources. One of the major areas of opportunity for circular chemistry is in the packaging sector, which as stated earlier has the biggest share of plastic manufacturing and the lowest product lifetime.[20]

Polyolefins are the most widely used plastic for packaging. In 2012, the U.S. generated 15.78 million tonnes of polyolefin waste which comprised 54.7% of the total plastic waste in the country.[21] In search of more sustainable options for packaging polyolefins disposal,

thermochemical conversion appears as an outstanding alternative due to its environmental benefits, compared to other disposal techniques, and the production of alternative fuels with a lower carbon footprint than fossil fuels.[22] One challenge is the design of such thermochemical process to be profitable and to achieve low emissions for the refinery products compared to comparable products produced from virgin fossil resources.

1.4 Current state of the thermochemical conversion of polyolefins

Thermochemical conversion comprises different processes from which pyrolysis is an interesting option due to the production of hydrocarbons that can be used as fuels or raw materials for the chemical industry.[23] Pyrolysis is the thermal degradation of plastic waste in the absence of oxygen, of which fast pyrolysis is the most promising approach. This process can be performed at different temperatures and reaction residence times. However, the idea of processing polyolefins by means of pyrolysis is not new. Several studies have been published describing different temperatures, reaction residence times, sample amounts, and reactor configurations to carry out this conversion.[24-39] However, few studies have been reported regarding the application of fast pyrolysis for the thermal degradation of polyolefins (See Table 1.1). In fast pyrolysis, samples are decomposed in less than two seconds due to high heating rates.[40] One of the main advantages of using these shorter reaction times is the reduction in the volume of reactors at industrial scales.

Table 1.1. Studies on fast pyrolysis of polyolefins.

Reference	Material	Temperature (°C)	Type of reactor	Sample amount
Scott et al.[40]	Waste polyethylene	515 - 790	Sand fluidized bed	30 – 60 g
Conesa et al.[41]	Commercial polyethylene	500 - 900	Fluidized bed	0.2 – 3 g
Williams and Williams[42]	Virgin plastic mixture	500 - 700	Fluidized bed	3 g
Mastral et al.[43]	Commercial HDPE	650 - 850	Fluidized bed reactor	3 – 4 g
Aguado et al.[44]	Commercial polyolefins	500 - 600	Micro-pyrolysis	1 mg
Demirbas[21]	Waste polyolefins	102 - 602	Tubular stainless steel	1 g
Elordi et al.[45]	HDPE	450 - 715	Conical spouted bed	2 g
Li et al.[46]	LDPE	650	Micro-pyrolysis	1 mg
Li et al.[47]	Commercial polyolefins	450 - 750	Micro-pyrolysis	1 mg

As shown in Table 1.1, most of the studies have been performed at temperatures over 400 ° C. The main reason is that degradation of polyolefins begins at 292 °C although an appreciable reduction in weight is observed at temperatures above 372 °C.[49] This weight loss is a consequence of a random chain scission mechanism that degrades polyolefins into shorter hydrocarbon molecules through a set of free radical-based chain reactions. [25,27,34,38,46,49-53] In this mechanism polymers are broken down through a series of steps (Figure 1.3). The first is called initiation. In this step the polymer chains are broken along the hydrocarbon backbone to form free radicals. The second step is propagation, where two general reactions occur to either stabilize the radical or break the hydrocarbon backbone again. Both intermediate radicals and products are formed. The radicals continue to cycle

through the two propagation reactions until the last step, termination, when the radicals combine to form a product.[25]

| Initiation | | | P | $\longrightarrow$ | R_p | + | R_p |
| | | | Polymer | | Primary Radical | | Primary radical |
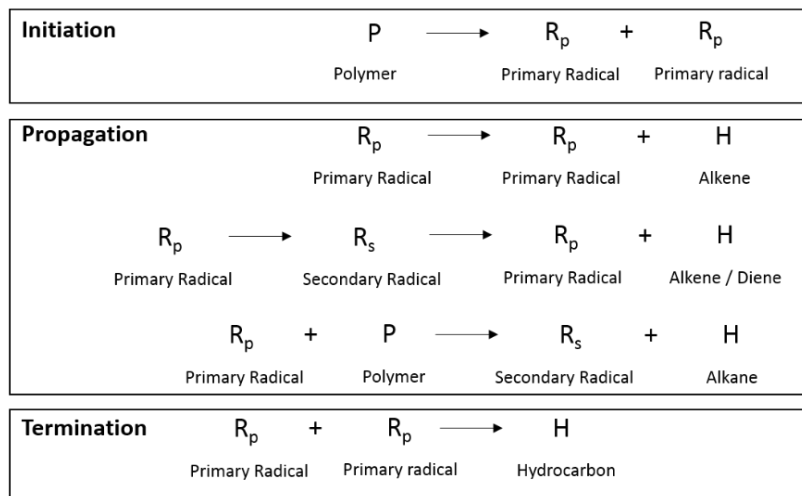
Figure 1.3. Radical mechanism of the thermal degradation of polyethylene.

This mechanism is driven by the formation of a series of primary and secondary radicals and intra and inter-molecular hydrogen transfers.[25,54] As a result the production of a variety of α,ω-dienes, 1-alkenes, and alkenes is favored over monomer formation.[25,36,39,55] This complex set of reactions has shown a strong dependence on residence time and temperature.[33] Mastral et al.[44] demonstrated that below 730 °C the main products are high carbon number waxes that are converted to liquids when temperature increases. Above this temperature only gases and liquids are formed with a stabilization of the gaseous products composition at 780 °C.

The range of products that can be obtained are strongly dependent on several operation conditions; temperature, residence time, presence of catalysts, and reactor configuration among the most important.[13,33] As an example, it is known that the increase of temperature

enhances the yield of liquid and gaseous hydrocarbons.[44,50] However, these yields have been observed at temperatures above 650 °C, with 780 °C being the temperature that produces the higher yield of gaseous products.[44] Pinto et al.[35] determined that reaction residence times should be short and reaction rates should be fast in order to achieve a good yield of fuel-range hydrocarbon.

In view of these observations, micro-pyrolysis appears as an experimental technique with many benefits to analyze and improve the performance of the fast pyrolysis of plastic waste. This technique use small quantities of samples (less than 500 μg) and has proven to be very effective to study biomass degradation.[56] Micro-pyrolysis systems can be coupled to gas chromatography-mass spectrometry (GC/MS) facilitating the identification and quantification of products. This technique offers high heating rates that help to evaluate degradation pathways at very high temperatures,[45] those that seem to be favorable for the production of fuel-range hydrocarbons. On the other hand, the short residence times of the vapors generated (15-20 ms) inhibit the formation of secondary reactions.[45,56,57] Because of this, micro-pyrolysis has limitations on probing the complete range of degradation mechanisms because secondary reactions are not prominent. On the other hand, the use of micro-pyrolysis will provide useful information about primary reactions occurring in fast pyrolysis of waste polyolefins, these being the initial reactions occurring during the rapid thermochemical breakdown of the solid sample. This fundamental knowledge of the initial degradation mechanism will help to propose operation conditions that will favor the yield of fuel-range hydrocarbons. As discussed in Chapter 3, the research program included a

novel design which added control of vapor residence time and temperature to standard micro-pyrolysis experiments.

1.5 Sustainable process design in the context of circular economy

As discussed, fast pyrolysis emerges as an interesting alternative for the recycling of plastic waste on an industrial scale while addressing the goals of a circular and sustainable economy of plastics. Sustainable development has become an important target for governments and international organizations due to overexploitation of natural resources and pollutant emissions. To be considered sustainable a technological system must properly address environmental, economic, and social concerns. This goal of sustainability can be achieved through changes in product manufacturing that optimize the production of goods, reduce the generation of residues, and provide economic profit without compromising societal benefits and protecting the environment.[58] The chemical industry has not been effective in fulfilling that objective since a single-minded development approach driven by production targets and expected profitability has been followed for several years[59] while environmental and societal concerns are relegated to secondary considerations. The incorporation of sustainability principles in the conception and design stages of chemical processes would reduce the negative effects experienced during operation, thus avoiding costly modifications.[58] On this regard, the process design should also consider other life cycle stages, aside from operation such as product use and end-of-life processes, that can lead to higher, economic, environmental, and social impacts.[59]

Life cycle assessment (LCA) and techno-economic analysis (TEA) are two essential methodologies that guide the sustainable design of chemical processes. LCA evaluates the environmental impacts of material and energy inputs of a product through its life cycle under previously established limits.[60] Important outputs of this analysis are the determination of life cycle stages with largest greenhouse gases (GHGs) emissions, to guide future improvements, and the comparison of the alternatives under study with business as usual pathways. From the few studies that carry out the LCA of plastic waste pyrolysis, the majority has focused on its comparison with other management scenarios like landfill disposal and incineration.[61-64] Another portion has evaluated the environmental impacts of fuels produced through plastic waste pyrolysis[65,66] but to date no study has focused on the analysis of a process that can produce monomers that can potentially produce feedstock to produce new plastics while maintaining a circular economy. This dissertation research will help fill this knowledge gap.

TEA estimates the economic costs and benefits of all the stages involved in the production pathway from feedstock acquisition to finished products purification. The industrial scaling of novel technologies has faced numerous barriers due the poor performance from an economic point of view, hence, TEA studies should be an important component of any process development. Compared to LCA there are fewer studies of plastic waste pyrolysis which have shown the effectiveness of the economy of scale in reducing the processing costs.[67-69] Other TEAs have found that a refinery approach is effective in improving the economic feasibility of plastic waste, due that multiple products can assure a more stable

11

market for this technology.[67,70] However, the TEA of a process that commercially exploits each product fraction from fast pyrolysis of waste polyolefins has not yet been published. This is another gap in knowledge that this dissertation will help to fill.

1.6 Research objectives

According to the information presented above, this dissertation addresses the current gaps in knowledge on the circular economy and the fast pyrolysis of waste polyolefins through the following objectives

1. Analyze if the generated amount of polyolefin and fiber municipal solid waste could produce enough transportation fuels to satisfy the annual demand in a newly industrialized country, like Mexico.

2. Carry out a carbon footprint analysis (CFA) to determine if fuels produced from pyrolysis of polyolefins waste can generate less GHG emissions than fossil-based fuels.

3. Design and operate a new two-stage laboratory scale micro-pyrolysis reactor that performs fast pyrolysis of waste HDPE with good control over primary and secondary degradation.

4. Evaluate the effect of temperature and vapor residence time on the distribution of different hydrocarbon fractions and chemical species from the two-stage micro-pyrolysis of waste high-density polyethylene.

5. Use the yields from the laboratory experiments to propose the conceptual design of a refinery that produces monomers, aromatics, and fuels from the pyrolysis of waste HDPE.

6. Carry out a TEA using a discounted cash flow analysis of the designed refinery to evaluate its net present value and compared the results with previous studies and current state of the art technologies.

7. Evaluate the CFA of the refinery to estimate the GHG emissions per tonne of waste HDPE processed and per kg of product obtained through a rigorous application of allocation methodology within the proposed refinery process units.

8. Estimate the effects of heat integration and regional electricity grids on the environmental performance of the refinery.

This dissertation is divided in four parts, Chapter 2 addresses objectives 1 and 2, Chapter 3 accomplishes objectives 4 and 5, Chapter 4 presents the progress on objectives 5 and 6, and, Chapter 5 presents the results of objectives 7 and 8. Finally, Chapter 6 presents the conclusions and future work derived from the results of the performed research.

1.7 References

(1)   Plastics Europe. Plastics - the Facts 2018. An analysis of European plastics production, demand and waste data. https://www.plasticseurope.org/application/files/6315/4510/9658/Plastics_the_facts_2018_AF_web.pdf (accessed March 14, 2019).

(2)   Burange, A. S.; Gawande, M. B.; Lam, F. L. Y.; Jayaram, R. V.; Luque, R. Heterogeneously catalyzed strategies for the deconstruction of high density polyethylene: plastic waste valorisation to fuels. *Green Chemistry* **2015,** *17* (1), 146-156.

(3)   World Economic Forum; Ellen McArthur Foundation; McKinsey & Company. The New Plastics Economy - Rethinking the future of plastics. https://www.ellenmacarthurfoundation.org/assets/downloads/EllenMacArthurFoundation_TheNewPlasticsEconomy_Pages.pdf (accessed March 14, 2019).

(4)   Geyer, R.; Jambeck, J. R.; Law, K. L. Production, use, and fate of all plastics ever made. *Sci. Adv.* **2017,** *3* (7), e1700782.

(5)   Jambeck, J. R.; Geyer, R.; Wilcox, C.; Siegler, T. R.; Perryman, M.; Andrady, A.; Narayan, R.; Law, K. L. Plastic waste inputs from land into the ocean. *Science* **2015,** *347* (6223), 768-771.

(6)   Rhodes, C. J. Plastic pollution and potential solutions. *Sci. Prog.* **2018,** *101* (3), 207-260.

(7)   Ritchie, H.; Roser, M. Plastic Pollution. https://ourworldindata.org/plastic-pollution (accessed March 23, 2019).

(8)   Eriksen, M.; Lebreton, L. C. M.; Carson, H. S.; Thiel, M.; Moore, C. J.; Borerro, J. C.; Galgani, F.; Ryan, P. G.; Reisser, J. Plastic Pollution in the World's Oceans: More than 5 Trillion Plastic Pieces Weighing over 250,000 Tons Afloat at Sea. *PLoS One* **2014,** *9* (12), 15.

(9)   Avio, C. G.; Gorbi, S.; Regoli, F. Plastics and microplastics in the oceans: From emerging pollutants to emerged threat. *Mar. Environ. Res.* **2017,** *128*, 2-11.

(10)   Machado, A. A. D.; Kloas, W.; Zarfl, C.; Hempel, S.; Rillig, M. C. Microplastics as an emerging threat to terrestrial ecosystems. *Glob. Change Biol.* **2018,** *24* (4), 1405-1416.

(11)   Lee, K.-H. In *Material Recycling, Trends and perspectives*; Achilias, D., Ed.; InTech: Rijeka, Croatia, 2012.

(12)   Arena, U.; Di Gregorio, F.; Amorese, C.; Mastellone, M. L. A techno-economic comparison of fluidized bed gasification of two mixed plastic wastes. *Waste Management* **2011,** *31* (7), 1494-1504.

(13)   Panda, A. K.; Singh, R. K.; Mishra, D. K. Thermolysis of waste plastics to liquid fuel: A suitable method for plastic waste management and manufacture of value added products—A world prospective. *Renewable and Sustainable Energy Reviews* **2010,** *14* (1), 233-248.

(14)   Korhonen, J.; Honkasalo, A.; Seppala, J. Circular Economy: The Concept and its Limitations. *Ecol. Econ.* **2018,** *143*, 37-46.

(15)   European Commision. A European Strategy for Plastics in a Circular Economy. http://ec.europa.eu/environment/circular-economy/pdf/plastics-strategy-brochure.pdf (accessed March 23, 2019).

(16)   Shonnard, D. R. In *2nd Michigan Forest Bioeconomy Conference* Midland, MI, 2019.

(17)   Clark, J. H.; Farmer, T. J.; Herrero-Davila, L.; Sherwood, J. Circular economy design considerations for research and process development in the chemical sciences. *Green Chemistry* **2016,** *18* (14), 3914-3934.

(18)   Hong, M.; Chen, E. Y. X. Chemically recyclable polymers: a circular economy approach to sustainability. *Green Chemistry* **2017,** *19* (16), 3692-3706.

(19)   Keijer, T.; Bakker, V.; Slootweg, J. C. Circular chemistry to enable a circular economy. *Nat. Chem.* **2019,** *11* (3), 190-195.

(20)   Kaur, G.; Uisan, K.; Ong, K. L.; Lin, C. S. K. Recent Trends in Green and Sustainable Chemistry & Waste Valorisation: Rethinking Plastics in a circular economy. *Curr. Opin. Green Sustain. Chem.* **2018,** *9*, 30-39.

(21)   U.S. Environmental Protection Agency *Municipal solid waste generation, recycling, and disposal in the United States: Facts and figures for 2012*; Report No. EPA-530-F-14-001; Office of Solid Waste and Emergency Response: Washington, DC, 2014.

(22)   Demirbas, A. Pyrolysis of municipal plastic wastes for recovery of gasoline-range hydrocarbons. *J Anal Appl Pyrol* **2004,** *72* (1), 97-102.

(23)   Costa, P. A.; Pinto, F. J.; Ramos, A. M.; Gulyurtlu, I. K.; Cabrita, I. A.; Bernardo, M. S. Kinetic Evaluation of the Pyrolysis of Polyethylene Waste. *Energy & Fuels* **2007,** *21* (5), 2489-2498.

(24)   Aboulkas, A.; El harfi, K.; El Bouadili, A. Thermal degradation behaviors of polyethylene and polypropylene. Part I: Pyrolysis kinetics and mechanisms. *Energy Conversion and Management* **2010,** *51* (7), 1363-1369.

(25)   Bockhorn, H.; Hornung, A.; Hornung, U. Mechanisms and kinetics of thermal decomposition of plastics from isothermal and dynamic measurements. *J Anal Appl Pyrol* **1999,** *50* (2), 77-101.

(26)   Chao-Hsiung, W.; Ching-Yuan, C.; Jwo-Luen, H.; Shin-Min, S.; Leo-Wang, C.; Feng-Wen, C. On the thermal treatment of plastic mixtures of MSW: Pyrolysis kinetics. *Waste Management* **1993,** *13* (3), 221-235.

(27)   Çit, İ.; Sınağ, A.; Yumak, T.; Uçar, S.; Mısırlıoğlu, Z.; Canel, M. Comparative pyrolysis of polyolefins (PP and LDPE) and PET. *Polym. Bull.* **2010,** *64* (8), 817-834.

(28)   Encinar, J. M.; González, J. F. Pyrolysis of synthetic polymers and plastic wastes. Kinetic study. *Fuel Processing Technology* **2008,** *89* (7), 678-686.

(29)   Kayacan, İ.; Doğan, Ö. M. Pyrolysis of Low and High Density Polyethylene. Part I: Non-isothermal Pyrolysis Kinetics. *Energy Sources, Part A: Recovery, Utilization, and Environmental Effects* **2008,** *30* (5), 385-391.

(30)   Kumar, S.; Singh, R. K. Recovery of Hydrocarbon Liquid from Waste High Density Polyethylene by Thermal Pyrolysis. *Brazilian Journal of Chemical Engineering* **2011,** *28* (4), 659-667.

(31)   López, A.; de Marco, I.; Caballero, B. M.; Laresgoiti, M. F.; Adrados, A. Influence of time and temperature on pyrolysis of plastic wastes in a semi-batch reactor. *Chemical Engineering Journal* **2011,** *173* (1), 62-71.

(32)   Miskolczi, N.; Bartha, L.; Deák, G. Thermal degradation of polyethylene and polystyrene from the packaging industry over different catalysts into fuel-like feed stocks. *Polymer Degradation and Stability* **2006,** *91* (3), 517-526.

(33)   Miskolczi, N.; Bartha, L.; Deák, G.; Jóver, B. Thermal degradation of municipal plastic waste for production of fuel-like hydrocarbons. *Polymer Degradation and Stability* **2004,** *86* (2), 357-366.

(34)   Peterson, J. D.; Vyazovkin, S.; Wight, C. A. Kinetics of the Thermal Degradation and Thermo-oxidative Degradation of Polystyrene, polyethylene and Poly(propylene). *Macromolecular Chemistry and Physics* **2001,** *202* (6), 775-784.

(35)   Pinto, F.; Costa, P.; Gulyurtlu, I.; Cabrita, I. Pyrolysis of plastic wastes. 1. Effect of plastic waste composition on product yield. *J Anal Appl Pyrol* **1999,** *51* (1–2), 39-55.

16

(36)   Soják, L.; Kubinec, R.; Jurdáková, H.; Hájeková, E.; Bajus, M. High resolution gas chromatographic–mass spectrometric analysis of polyethylene and polypropylene thermal cracking products. *J Anal Appl Pyrol* **2007,** *78* (2), 387-399.

(37)   Sørum, L.; Grønli, M. G.; Hustad, J. E. Pyrolysis characteristics and kinetics of municipal solid wastes. *Fuel* **2001,** *80* (9), 1217-1227.

(38)   Williams, E. A.; Williams, P. T. The pyrolysis of individual plastics and a plastic mixture in a fixed bed reactor. *Journal of Chemical Technology & Biotechnology* **1997,** *70* (1), 9-20.

(39)   Williams, P. T.; Williams, E. A. Interaction of Plastics in Mixed-Plastics Pyrolysis. *Energy & Fuels* **1999,** *13* (1), 188-196.

(40)   Bridgwater, A. V. Review of fast pyrolysis of biomass and product upgrading. *Biomass and Bioenergy* **2012,** *38*, 68-94.

(41)   Scott, D. S.; Czernik, S. R.; Piskorz, J.; Radlein, D. S. A. G. Fast pyrolysis of plastic wastes. *Energy & Fuels* **1990,** *4* (4), 407-411.

(42)   Conesa, J. A.; Font, R.; Marcilla, A.; Garcia, A. N. Pyrolysis of Polyethylene in a Fluidized Bed Reactor. *Energy & Fuels* **1994,** *8* (6), 1238-1246.

(43)   Williams, E. A.; Williams, P. T. Analysis of products derived from the fast pyrolysis of plastic waste. *J Anal Appl Pyrol* **1997,** *40-41*, 347-363.

(44)   Mastral, F. J.; Esperanza, E.; García, P.; Juste, M. Pyrolysis of high-density polyethylene in a fluidised bed reactor. Influence of the temperature and residence time. *J Anal Appl Pyrol* **2002,** *63* (1), 1-15.

(45)   Aguado, R.; Olazar, M.; Gaisán, B.; Prieto, R.; Bilbao, J. Kinetic Study of Polyolefin Pyrolysis in a Conical Spouted Bed Reactor. *Industrial & Engineering Chemistry Research* **2002,** *41* (18), 4559-4566.

(46)   Elordi, G.; Lopez, G.; Olazar, M.; Aguado, R.; Bilbao, J. Product distribution modelling in the thermal pyrolysis of high density polyethylene. *Journal of Hazardous Materials* **2007,** *144* (3), 708-714.

(47)   Li, X.; Zhang, H.; Li, J.; Su, L.; Zuo, J.; Komarneni, S.; Wang, Y. Improving the aromatic production in catalytic fast pyrolysis of cellulose by co-feeding low-density polyethylene. *Applied Catalysis A: General* **2013,** *455*, 114-121.

(48)   Li, X.; Li, J.; Zhou, G.; Feng, Y.; Wang, Y.; Yu, G.; Deng, S.; Huang, J.; Wang, B. Enhancing the production of renewable petrochemicals by co-feeding of biomass with

plastics in catalytic fast pyrolysis with ZSM-5 zeolites. *Applied Catalysis A: General* **2014,** *481*, 173-182.

(49)   Beyler, C. L.; Hirschler, M. M. In *SFPA Handboook of Fire Protection Engineering*; 3rd ed.; DiNenno, P. J., Ed.; National Fire Protection Association, Inc.: Quincy, MA, 2002.

(50)   Buekens, A. G.; Huang, H. Catalytic plastics cracking for recovery of gasoline-range hydrocarbons from municipal plastic wastes. *Resources, Conservation and Recycling* **1998,** *23* (3), 163-181.

(51)   Németh, A.; Blazsó, M.; Baranyai, P.; Vidóczy, T. Thermal degradation of polyethylene modeled on tetracontane. *Journal of Analytical and Applied Pyrolysis* **2008,** *81* (2), 237-242.

(52)   Singh, B.; Sharma, N. Mechanistic implications of plastic degradation. *Polymer Degradation and Stability* **2008,** *93* (3), 561-584.

(53)   Westerhout, R. W. J.; Waanders, J.; Kuipers, J. A. M.; van Swaaij, W. P. M. Kinetics of the Low-Temperature Pyrolysis of Polyethene, Polypropene, and Polystyrene Modeling, Experimental Determination, and Comparison with Literature Models and Data. *Industrial & Engineering Chemistry Research* **1997,** *36* (6), 1955-1964.

(54)   Gascoin, N.; Navarro-Rodriguez, A.; Gillard, P.; Mangeot, A. Kinetic modelling of high density polyethylene pyrolysis: Part 1. Comparison of existing models. *Polymer Degradation and Stability* **2012,** *97* (8), 1466-1474.

(55)   Ballice, L. A kinetic approach to the temperature-programmed pyrolysis of low- and high-density polyethylene in a fixed bed reactor: determination of kinetic parameters for the evolution of n-paraffins and 1-olefins. *Fuel* **2001,** *80* (13), 1923-1935.

(56)   Ronsse, F.; Dalluge, D.; Prins, W.; Brown, R. C. Optimization of platinum filament micropyrolyzer for studying primary decomposition in cellulose pyrolysis. *J Anal Appl Pyrol* **2012,** *95*, 247-256.

(57)   Patwardhan, P. R.; Dalluge, D. L.; Shanks, B. H.; Brown, R. C. Distinguishing primary and secondary reactions of cellulose pyrolysis. *Bioresource Technology* **2011,** *102* (8), 5265-5269.

(58)   Ruiz-Mercado, G. J.; Smith, R. L.; Gonzalez, M. A. Sustainability Indicators for Chemical Processes: I. Taxonomy. *Industrial & Engineering Chemistry Research* **2012,** *51* (5), 2309-2328.

(59)   Azapagic, A.; Millington, A.; Collett, A. A Methodology for Integrating Sustainability Considerations into Process Design. *Chemical Engineering Research and Design* **2006,** *84* (6), 439-452.

(60)   Shonnard, D. R.; Klemetsrud, B.; Sacramento-Rivero, J.; Navarro-Pineda, F.; Hilbert, J.; Handler, R.; Suppen, N.; Donovan, R. P. A Review of Environmental Life Cycle Assessments of Liquid Transportation Biofuels in the Pan American Region. *Environmental Management* **2015,** *56* (6), 1356-1376.

(61)   Al-Salem, S. M.; Evangelisti, S.; Lettieri, P. Life cycle assessment of alternative technologies for municipal solid waste and plastic solid waste management in the Greater London area. *Chemical Engineering Journal* **2014,** *244*, 391-402.

(62)   Alston, S. M.; Arnold, J. C. Environmental Impact of Pyrolysis of Mixed WEEE Plastics Part 2: Life Cycle Assessment. *Environ. Sci. Technol.* **2011,** *45* (21), 9386-9392.

(63)   Perugini, F.; Mastellone, M. L.; Arena, U. A life cycle assessment of mechanical and feedstock recycling options for management of plastic packaging wastes. *Environmental Progress* **2005,** *24* (2), 137-154.

(64)   Shonfield, P. LCA of Management Options for Mixed Waste Plastics. http://www.wrap.org.uk/sites/files/wrap/LCA%20of%20Management%20Options%20for%20Mixed%20Waste%20Plastics.pdf (accessed March 13, 2019).

(65)   Benavides, P. T.; Sun, P. P.; Han, J.; Dunn, J. B.; Wang, M. Life-cycle analysis of fuels from post-use non-recycled plastics. *Fuel* **2017,** *203*, 11-22.

(66)   Iribarren, D.; Dufour, J.; Serrano, D. P. Preliminary assessment of plastic waste valorization via sequential pyrolysis and catalytic reforming. *J. Mater. Cycles Waste Manag.* **2012,** *14* (4), 301-307.

(67)   Al-Salem, S. M.; Papageorgiou, L. G.; Lettieri, P. Techno-economic assessment of thermo-chemical treatment (TCT) units in the Greater London area. *Chemical Engineering Journal* **2014,** *248*, 253-263.

(68)   Fivga, A.; Dimitriou, I. Pyrolysis of plastic waste for production of heavy fuel substitute: A techno-economic assessment. *Energy* **2018,** *149*, 865-874.

(69)   Sahu, J. N.; Mahalik, K. K.; Nam, H. K.; Ling, T. Y.; Woon, T. S.; Rahman, M. S. B.; Mohanty, Y. K.; Jayakumar, N. S.; Jamuar, S. S. Feasibility Study for Catalytic Cracking of Waste Plastic to Produce Fuel Oil with Reference to Malaysia and Simulation using ASPEN Plus. *Environ. Prog. Sustain. Energy* **2014,** *33* (1), 298-307.

(70)   Vargas Santillan, A.; Farias Sanchez, J. C.; Pineda Pimentel, M. G.; Castro Montoya, A. J. Olefins and Ethanol from Polyolefins: Analysis of Potential Chemical Recycling of Poly(ethylene) Mexican Case. *Int. J. Chem. React. Eng.* **2016,** *14* (6), 1289-1300.

2 Resource and Greenhouse Gas Assessments of the Thermochemical Conversion of Municipal Solid Waste in Mexico[1]

Abstract

The use of components in municipal solid waste (MSW) as feedstock for liquid transportation biofuels and chemicals can be a sustainable solution for energy needs while minimizing impacts of landfills on the environment. This study conducts a resource assessment for available MSW in Mexico and concludes that when the organic and polyolefin plastic components are converted to liquid hydrocarbon transportation biofuels through a pyrolysis-based pathway, up to 7% of Mexico's transportation-fuel consumption needs could be met. A preliminary carbon footprint analysis (CFA) using stage-specific emission factors from the literature shows that liquid transportation biofuels from the organic portion of MSW (paper, packaging, wood, yard trimmings) sequesters 9.5 g CO_2 eq. per MJ biofuel, with significant pathway credits due to avoiding landfill CH_4 emissions. The greenhouse gas (GHG) emissions from the conversion of the polyolefin plastic in the MSW are positive (88 g CO_2 eq. per MJ), though still lower than current fossil transportation fuels in Mexico (95.5 g CO_2 eq. per MJ). Based on these resource assessments and preliminary carbon footprint results, MSW in Mexico should be

considered a promising feedstock for biofuel production through conversion research and updated carbon footprint analyses.

2.1 Introduction

The current trend of population growth in urban areas is contributing significantly to global warming and resource scarcity. According to the United Nations,[1] 66% of the world's population will be living in urban areas by the year 2050. The problems associated with greater urbanization are amplified in megacities across the world. Megacities are cities with over ten million people, and there are currently 28 megacities throughout the world, which comprise about 12% of world's population.[1] While urbanization continues to increase, income levels, living standards, and consumption will most likely also rise, especially in developing countries. Consequently, an enormous amount of waste is and will continue to be generated, leading to the problem of its management. In 2012, each inhabitant of an urban area produced 1.2 kg of waste per day, but this value is expected to increase to 1.42 kg per person per day by 2025,[2] making the rate of waste generation per capita to grow at a faster rate than urbanization. Furthermore, this increase of municipal solid waste (MSW) generation is closely linked to greenhouse gas (GHG) emissions. As a result, area available for landfills is becoming scarce and current disposal facilities are reaching their capacity.[3] Although, land availability for the landfills presents itself as an immense problem, the environmental issues associated with landfills are of greater importance. According to the U.S. Environmental Protection Agency (EPA),[4] methane emissions from waste management, including MSW disposal, are third only to those from energy and agriculture.

Degradation of solid waste in landfills is the activity with the highest impact to waste management methane emissions. In the U.S. these landfill emissions contributed up to 20% of total methane emissions in the period from 1990 to 2014, compared to 33% derived from petroleum and natural gas systems in industry and 22% generated by enteric fermentation from livestock and manure storage.[4]

Mexico, considered a newly industrialized country,[5] is experiencing the environmental and development issues described above. The country's MSW generation has increased 25% from 2003 to 2011, reaching 41 million tonnes in 2011.[6] Per capita generation has also experienced an increment of 17.6% from 1997 to 2011.[6] Mexico City, the capital and one of the ten largest megacities in the world,[1] contributes 12% of the annual national MSW generation with a per capita generation of 1.5 kg per day, the largest in the country.[6] This rising generation of MSW in the capital has caused the "Bordo Poniente" landfill to reach its capacity since 2008.[7] Mexico is also having problems of air quality. GHG emissions increased 33.4% from 1990 to 2010, with a total amount of 748 million tonnes CO_2 equiv in 2011.[6] Although the transportation sector is the main contributor to these emissions, waste-derived activities (including disposal, wastewater treatment and incineration) generated 5.9% of the national total.[6] The previously listed issues place Mexico as an interesting case study to evaluate more sustainable waste management strategies that could reduce GHG emissions in newly industrialized countries. These strategies can improve planning, in earlier stages of development, to avoid these countries experiencing current problems faced by developed countries.

The major components of MSW are food waste, yard trimmings, wood, leather and textile, rubber, plastics, metals, glass, paper, cardboard, and others.[8] According to research conducted by the Worldwatch Institute,[9] approximately 25% of the generated waste globally is recycled, composted, or digested. During 2011, Mexico recycled only 10% of their generated MSW.[6] This presents the question of what can be done with the remaining waste that is not recycled. Thermochemical conversion is a technology that uses high temperature in order to degrade complex organic molecules into simpler compounds. Among many options, the alternative of using MSW as a source of transportation fuel by means if thermochemical conversion is an intriguing one due to its low cost, existing collection infrastructure, and proximity of product fuel to consumers in urban areas. Pyrolysis, liquefaction, gasification, and supercritical fluid extraction are among the methods of thermochemical conversion. Among these processes, pyrolysis has the advantages of operating at atmospheric pressure and moderate temperatures (400-550 °C) and providing around 70% of bio-oil yield.[10,11] Pyrolysis transformation produces a volatile fraction consisting of gases and vapors, a liquid called bio-oil, and a solid residue known as biochar.[12] Plastic waste may be an ideal feedstock for pyrolysis because the resulting products present a negligible amount of oxygenated compounds which may require a minimum of further processing (i.e., catalytic upgrading).[13] However, there are very few studies in the literature reporting the environmental impact of plastic pyrolysis processes, which is an important step before operating this technology at an industrial scale.

A carbon footprint analysis (CFA) is an important first step when proposing a new process to fully comprehend the potential impacts a biofuel pathway may have once it is operating at a large scale. If the CFA is conducted once the processes are in operation rather than during the design stage, it makes it very costly and difficult to implement environmental improvements. Therefore, a preliminary CFA at the early design stage is desirable because if the pathway does not achieve favorable climate mitigation results, there is little incentive to further develop the process and to understand broader environmental and economic impacts.

The purpose of this manuscript is to conduct a resource assessment and to investigate if MSW-derived fuels produced in Mexico can make an important contribution to governmental targets for GHG emissions reduction (for example 18% reduction of transportation-related emissions by 2030 in Mexico).[14] In order to demonstrate if MSW is a significant resource for transportation fuels, estimated fuel production is also compared with Mexico's current demand. Finally, a preliminary carbon footprint analysis, using the life cycle assessment (LCA) methodology, has been performed in order to understand if thermochemical conversion of plastic and organic fractions of MSW can be a climate mitigating way to produce alternative fuels. In this preliminary carbon footprint analysis it is anticipated that avoided landfill emissions will factor in significantly to the final results.

2.2 Methods

2.2.1 Resource assessment

The Mexican Institute of Statistics and Geography (INEGI) database[15] was consulted to obtain the national MSW generation in 2010 along with that from the three most populated cities in the country: Mexico City, Guadalajara, and Monterrey. The composition of MSW of the cities was collected from various sources: composition from Mexico City and Guadalajara was obtained from Durán Moreno et al.[7] and Bernache-Pérez et al.[16], respectively; for Monterrey the MSW composition was taken as the north of Mexico waste composition reported by the Pan American Health Organization (PAHO).[17]

As shown in Tables A-1 to A-4 of Appendix A, the classification of waste materials into categories differed from city to city and nationally. The method developed to homogenize waste categories is described in the following sections. First, according to the U.S. Environmental Protection Agency (EPA)[8] and the Mexican Secretariat of Environment and Natural Resources (SEMARNAT),[6] construction industry residues and hazardous materials were not considered as part of MSW. Then, following the guidance of EPA[8] and also considering promising waste materials for thermochemical conversion, 11 waste categories were defined, as follows: food waste, yard trimmings, wood, leather and textile, rubber, plastics, metals, glass, paper, cardboard, and others. Due to the detailed information presented in the sources, data from the cities of Mexico City, Guadalajara, and Monterrey were fitted into these categories. Ferrous materials, iron packaging and aluminum were grouped together in the "metals" category, all types of polymers and synthetic fibers were

26

included in "plastics". In the same way, sanitary waste (toilet paper, diapers, and feminine pads), clayware, batteries, and fines were considered in the category "others". Then, trends found in the composition data of the cities were used for the categorization of the national composition, which originally comprised only seven categories,[15] into the 11 categories mentioned above. It was found that wood and rubber contributed on average with 0.56 and 0.30% to the national MSW generation. Also, food waste and yard trimmings presented 65.5 and 34.5% of the organics category. In the same way paper and cardboard together comprised 63.2 and 36.8% of the paper category. The computed amounts of wood and rubber were subtracted from the yard trimmings and leather and textiles categories, respectively. An example calculation is shown in section A.2 of Appendix A.

Once data were collected and categorized, the amount of MSW available per category for further processing (after recycling) was computed with equation (2.1):

$$available\ amount\ = M_R \times (1 - MC) \times (1 - PR) \qquad (2.1)$$

where M_R is the reported amount of MSW generated per category, MC is the moisture content of category, and PR is the percentage of recycling per category. Data for moisture content and percentage of recycling was gathered from Velasco Perez Alonso,[18] the Mexican Association of Tire Distributors and Renewing Plants (ANDELLAC),[19] and SEMARNAT,[6] and is shown in Table 2.1. After the available amount of MSW was computed, data for the categories of yard trimmings, wood, rubber, plastics, paper, and

cardboard was used for further analysis as potential feedstocks for thermochemical conversion.

Table 2.1. Moisture content and percentage of recycling of different waste categories.

Type of waste	Approximate moisture content [a]	Percentage of recycling
Food waste	70.0%	0.0% [a]
Yard trimmings	60.0%	0.0% [a]
Wood	20.0%	0.0% [a]
Leather and textile	10.0%	0.5% [b]
Rubber	2.0%	11.5% [c]
Plastics	0.2%	0.5% [b]
Metals	3.0%	39.0% [b]
Glass	2.0%	23.5% [b]
Paper	6.0%	14.7% [b]
Cardboard	5.0%	14.7% [b]
Other	4.0%	0.0% [a]
Sources: a: Velasco Perez Alonso[18], b: SEMARNAT[6], and c: ANDELLAC et al.[19]		

2.2.2 Estimation of fuel yields

Yields for biofuel production from yard trimmings, wood, paper, and cardboard (MSW organics) fast pyrolysis were computed from data reported by Hsu.[20] According to this study, 0.2367 kg of liquid hydrocarbon biofuel can be obtained per kilogram of water and ash-free biomass (forest residues, which serves as surrogate for MSW organics). Therefore, ash-free quantities had to be computed with equation (2.2):

$$ash\ free\ Amount\ = available\ amount \times (1 - AC) \qquad (2.2)$$

where AC is the reported ash content for each waste category. Ash content for yard trimmings, wood, paper, and cardboard in MSW is reported to be 6.4%, 9.9%, 7.9%, and 7.9%, respectively.[21] The amount of hydrocarbon products derived from plastic

(polyolefin) pyrolysis was estimated according to the BP polymer cracking process which establishes a yield of 0.86 kg of hydrocarbon products per kg of processed polyolefins.[22] The quantity of the different polymeric materials forming the plastic fraction of MSW was computed, in a similar way to the categories homogenization procedure, using an average composition from data of Mexico City and Guadalajara (details of this procedure are provided in section A.4 of Appendix A). Only polyethylene (low and high density), and polypropylene were considered as feedstock for the plastic pyrolysis products in this study.

Finally, the contribution of the pyrolysis of these MSW categories to Mexico's annual fuel consumption was obtained by using equation (2.3):

$$contribution = \frac{EAP}{NCC} \times 100 \qquad (2.3)$$

where *NCC* is the reported consumption of transportation fuels or chemicals, and *EAP* is the estimated annual production of transportation fuels by the pyrolysis pathway using MSW. Data for Mexico's annual consumption of jet fuel, diesel, and motor gasoline, in 2012, was obtained from the U.S. Energy Information Administration;[23] while annual consumption of chemicals was found in the Mexican Chemical Industry Association (ANIQ) annual report.[24]

2.2.3 Carbon footprint analysis

A preliminary CFA was conducted to obtain the GHG emissions of the production and use of renewable fuels from MSW based on literature studies of pathways using similar

feedstocks. The analysis employs the LCA approach and was conducted on a cradle-to-grave scope, which for the system under study accounts for the emissions from collection to fuel combustion stages. Because the required processes for thermochemical conversion vary with the type of waste,[20,22] both an organics and a polyolefin pathway had to be established (Figure 2.1a and 2.1b, respectively). These pathways included the same stages except for hydroprocessing and avoided landfill emissions, which are only included in the organics MSW pathway. Hydroprocessing was only included in the organics (paper, packaging, wood, yard trimmings) MSW pathway because the amount of oxygenated compounds from plastic pyrolysis is negligible compared to the amount of hydrocarbon products.[13] Likewise, emissions from landfill storage were not considered because plastic decomposition does not occur in landfills under anaerobic conditions.[25] As described, two different carbon footprint approaches were contemplated for the two pathways; a consequential analysis for the organics pathway, which evaluates the carbon footprint for biofuel product considering avoided landfill emissions, and an attributional analysis for the plastic pathway, which accounts for the GHG emissions only of the biofuel pathway. The amount of CO_2 equiv for the different types of fuels produced was estimated considering a functional unit of 1 MJ of fuel produced.

a)

```
┌────────────┐   ┌────────────┐   ┌────────────────┐   ┌────────────┐   ┌────────────┐   ┌────────────────┐   ┌────────────┐   ┌────────────┐
│ Collection │ → │ Separation │ → │   Feedstock    │ → │    Size    │ → │    Fast    │ → │ Hydroprocessing│ → │    Fuel    │ → │  Vehicle   │
│            │   │            │   │ Transportation │   │ Reduction  │   │ Pyrolysis  │   │                │   │Distribution│   │ Operation  │
└────────────┘   └────────────┘   └────────────────┘   └────────────┘   └────────────┘   └────────────────┘   └────────────┘   └────────────┘
      ↑
┌────────────┐
│  Avoided   │
│  landfill  │
│ emissions  │
└────────────┘
```

b)

```
┌────────────┐   ┌────────────┐   ┌────────────────┐   ┌────────────┐   ┌────────────┐   ┌────────────┐   ┌────────────┐
│ Collection │ → │ Separation │ → │   Feedstock    │ → │    Size    │ → │    Fast    │ → │    Fuel    │ → │  Vehicle   │
│            │   │            │   │ Transportation │   │ Reduction  │   │ Pyrolysis  │   │Distribution│   │ Operation  │
└────────────┘   └────────────┘   └────────────────┘   └────────────┘   └────────────┘   └────────────┘   └────────────┘
```
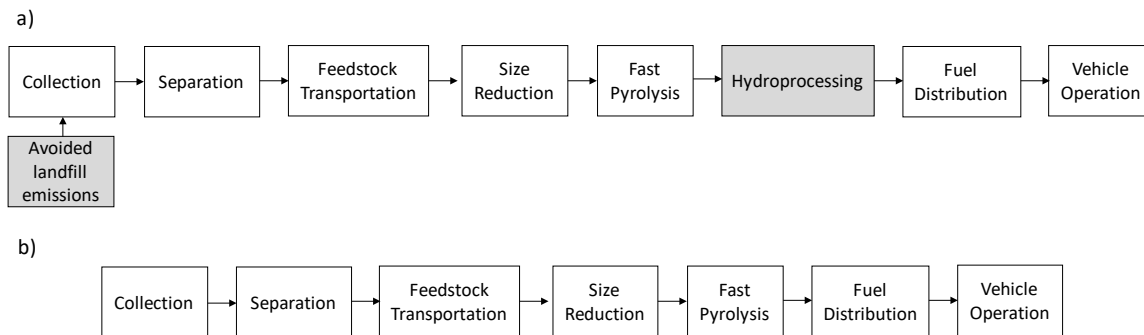
Figure 2.1. Process flow for the environmental assessment. (a) Organics (paper, cardboard, wood) MSW pathway. (b) Plastic waste pathway.

Emission factors are found in Table 2.2 for each stage in the biofuel pathways with assumptions, basis for the factors, and literature sources. The emission factors listed are in equivalent emissions of CO_2 wherein the global warming potentials of all greenhouse gases emitted at each stage were applied. The detailed calculation of these emission factors is shown in section A.6 of Appendix A, which includes not only the emissions from each stage but also upstream emissions going back to extraction from the production of material and energy inputs to the stage. To allow for the comparison of the results of this study with other LCAs or CFAs previously reported, GHG emissions are calculated in grams of CO_2 equiv per MJ of fuel. In order to calculate the biofuel carbon footprints, emissions factors from Table 2.2 were multiplied by the processed amount of MSW on an annual basis. Then, the carbon footprint value obtained was divided by the annual fuel produced according to the pathway (organics or polyolefin), converted to energy content in megajoules. This was accomplished by dividing the annual fuel amounts by the lower heating values (LHVs) of the obtained fuels which are 44 and 43.19 MJ per kg for the organics[26] and plastic (see section A.7.2 of Appendix A) pathway, respectively. These MSW fuel pathway emissions

were then compared to those from the production of fossil fuels, as reported by the National Energy Technology Laboratory.[27] Finally, a theoretical mixture composition of MSW comprising both organics and plastic was proposed to obtain 60% savings in emissions compared to the fossil fuel pathway, a level that would qualify the fuels in the United States to count toward the mandated volumes set out in the Renewable Fuel Standard (RFS2).

In this analysis we modeled the change to the environment that will occur when organic MSW is diverted from a landfill and is instead converted through pyrolysis-based processing into hydrocarbon transportation fuels. The avoided landfill emissions are the most important to model for the biogenic carbon in the MSW. Because we take a credit for the avoided landfill emissions of CH_4 and CO_2, we must "follow the carbon" for the organic MSW through the pyrolysis-based pathway and include all biogenic carbon emitted from the pyrolysis and upgrading process steps as well as the tailpipe emissions of biogenic C as CO_2. We did not take into account the biogenic CO_2 credit for photosynthesis during biomass growth that occurred, which would occur for both the landfill case as well as for the pyrolysis case, and therefore this does not change.

Table 2.2. Emission factors for the different stages of the pathways (kg CO_2 eq. per basis).

Stage	Pathway	Emission Factor	Basis	Assumptions
Collection	Organics and Plastic	41.30	Tonne of waste[a]	Emissions from a single stream collection fleet plus 9.0% more for upstream emissions for diesel. Effect of moisture was included in the emission factor.[30,31]
Separation	Organics and Plastic	12.26	Tonne of waste	Emissions from separation in a material recovery facility plus upstream emissions from Diesel (+9.0%), Electricity (+10.0%), and Natural Gas (+17.0%).[30,31]
Transportation	Organics and Plastic	12.13	Tonne of PRW[b]	Emissions from freight truck transportation from "Santa Catarina" separation facility in Mexico City to "Miguel Hidalgo" Refinery in Hidalgo, Mexico (Distance: 108 km).[30]
Size reduction	Organics and Plastic	119.13	Tonne of PRW	Emissions from the use of 0.183 kWh of electricity per kg of waste grinded. Mexican electricity mix applied (section A.6.4 of Appendix A).[30,32]
Fast Pyrolysis	Organics	382.18	Tonne of MAFOW[c]	Upstream and combustion emissions.[20]
	Plastic	394.56	Tonne of PW[d]	Upstream and combustion emissions.[22]
Hydroprocessing	Organics	471.39	Tonne of MAFOW	Upstream and combustion emissions.[20]
Fuel Distribution	Organics	1.44	Tonne of MAFOW	Emissions from pipeline distribution from refinery to Mexico City (distance: 108 km).[30]
	Plastic	7.33	Tonne of PW	Emissions from pipeline and freight truck distribution from refinery to Mexico City (distance: 108 km).[30]
Vehicle Operation	Organics	753.01	Tonne of MAFOW	Combustion emissions.[20]
	Plastic	2682.68	Tonne of PW	Combustion emissions (as presented in section A.6.8.2 of Appendix A).
Landfill	Organics	-2033.9	Tonne of MAFOW	Landfill gas production (CH_4:CO_2 - 50:50). Active organic MSW carbon in landfill: 63.3 %.[29]

[a] Tonne: metric ton, dry basis, [b] PRW: Post-recycling waste, [c] MAFOW: Moisture and ash free organic waste, [d] PW: Polyolefin waste.

For the preliminary CFA presented in this study, the carbon accounting approach is such that all the biogenic carbon was included. In the organics pathway, noncondensable gas and char produced during pyrolysis are combusted to provide heat for drying and heating of the pyrolysis reactor.[28] Some fraction of the gas is also recycled as fluidizing gas, such that bio-oil is the only product from pyrolysis. The combustion emissions from coproduct combustion have been already considered in the analysis of Hsu[20] and therefore, only combustion emissions from the pyrolysis liquid fuels (gasoline and diesel) were accounted for in the vehicle operation stage. For the pyrolysis stage in the polyolefin pathway, only a fraction of the gas is reused as fluidizing gas in the pyrolysis reactor.[22] Hence, combustion emissions from the three product fractions had to be considered, including vehicle operation. Regarding the landfill stage, only emissions from active carbon degradation were estimated as stated by the California Air Resources Board (ARB).[29] Details are presented in section A.6.9 of Appendix A on landfill emissions of CH_4 and CO_2.

2.3 Results and discussion

2.3.1 MSW resource assessment in Mexico

Mexico's MSW generation in 2010 is reported to be 41.06 million tonnes/yr,[15] which on a dry-weight basis equals to 26.16 million tonnes/yr. Food waste, plastics, and paper are the higher contributors to the national data, as shown in Figure 2.2a. These waste categories comprise 46.1% of Mexico's MSW generation. When the percentage of recycling of each waste category was considered, it was found that only 7.3% of the total waste generated is

recycled. This data is close to the 10% reported by SEMARNAT.[6] Only those materials that have a high recycling percentage (rubber, glass, metals, paper, and cardboard) experienced a decrease on their contribution compared to the pre-recycling data (Figure 2.2b). The available amounts, on a dry weight and post-recycling basis, for the six categories that were considered for further thermochemical conversion are presented in Figure A-1. They account in total for 12.18 million dry tonnes/yr comprising 46.6 % of the total waste generated on a dry-weight basis.
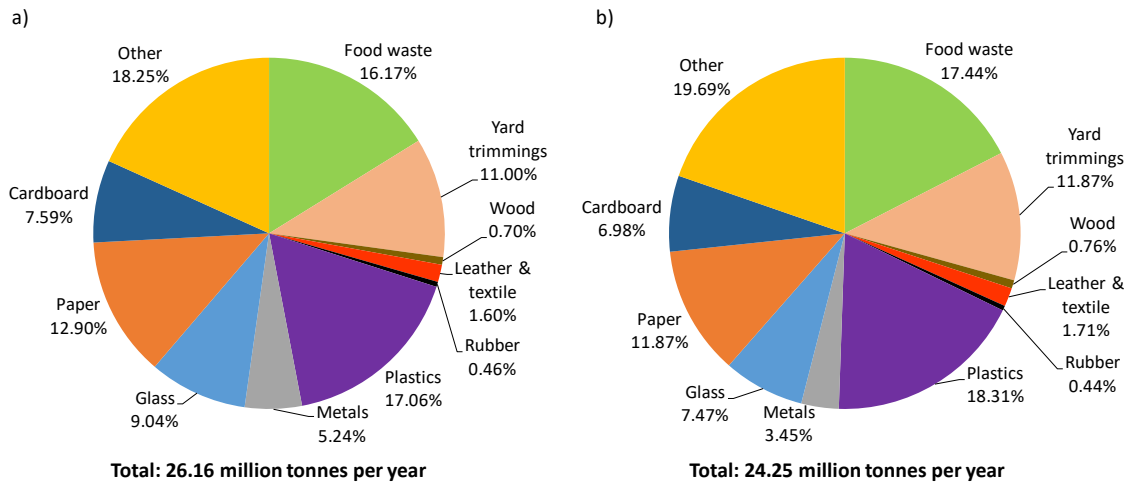
Figure 2.2. Composition of MSW in Mexico (Dry weight basis). (a) Generation. (b) Available after recycling.

Due to the fact that only polyolefins were considered for plastic pyrolysis, the national average composition of plastic waste needed to be estimated. As shown in Figure A-2, polyethylene is the most commonly generated plastic waste with more than 60% of contribution, followed by polyethylene terephthalate and polyurethane. In total, polyolefins accounted for 2.93 million dry tonnes per year, of which 30.2, 63.8, and 6.0 % are high

density polyethylene, low density polyethylene, and polypropylene, respectively. Further details and calculations are presented in section A.4 of Appendix A.

2.3.2 Pyrolysis yields for the selected feedstock

The total amount of organics waste (paper, packaging) that can be used as feedstock for thermochemical conversion is estimated to be 7.07 million tonnes/yr on a moisture and ash free (MAF) basis. In accordance with yields obtained from Hsu[20] 1.67 million tonnes of hydrocarbon fuels per year (see section 2.2.2) can be produced from these sources. Polyolefin waste accounts for 2.93 million tonnes per year which can generate 2.52 million tonnes of hydrocarbon fuels (see section 2.2.2), based on the process reported by Perugini et al.[22] Data from the U.S. Energy Information Administration (EIA)[23] states that Mexico's consumption of jet-fuel, motor gasoline, and distillate fuel oil (diesel) is 21.31, 286.81, and 166.35 million barrels per year, respectively. These quantities comprise a total 58.84 million tonnes of hydrocarbon fuels consumed per year assuming 159 L per barrel (oil) and a hydrocarbon fuel density of 0.808, 0.745, and 0.837 kg/L for jet-fuel, motor gasoline, and diesel, respectively.[26] Figure 2.3 shows a comparison between Mexico's total annual fuel consumption and the estimated amount that could be displaced by using hydrocarbon fuels produced by thermochemical conversion of available MSW organics and polyolefins. As seen in Figure 2.3, 7.1% of the national consumption could be substituted with this MSW-derived fuel, with a larger fraction derived from polyolefin plastics.
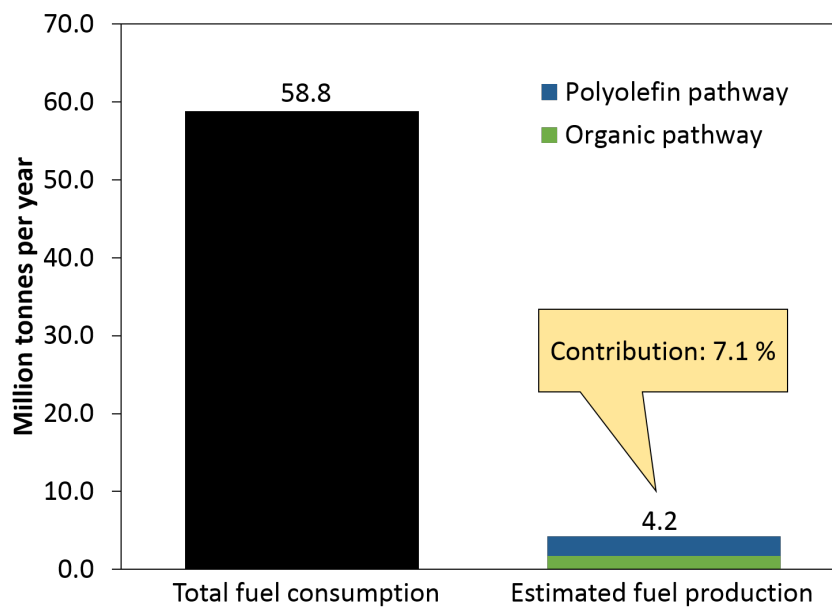
Figure 2.3. Contribution of hydrocarbon fuels produced through thermochemical conversion of MSW (organics and polyolefins) to Mexico's annual fuel consumption.

On the other hand, if chemicals were chosen as desired products instead of hydrocarbon fuels, yields of 187 and 89 kg/tonne of plastic waste for ethylene and propylene (section A.5 of Appendix A), respectively, could be achieved under favorable processing conditions.[33-38] Also several products with high potential as chemical intermediates like benzene, toluene, and xylenes can be generated with yields of 42, 70, and 44 kg/tonne of plastic waste converted by pyrolysis, respectively (section A.5 of Appendix A). When comparing literature yields for pyrolysis of Mexico's polyolefin waste with the country's annual chemicals consumption statistics in 2014,[24] it was calculated that the amount of hexane, heptane, benzene, toluene, xylenes, and hydrogen that could be obtained surpasses the annual national consumption. A detailed set of methods and calculations for the production of chemicals from plastic waste is provided in section A.5 of Appendix A.

37

2.3.3 Environmental assessment

The carbon footprint from each of the proposed pathways is shown in Figure 2.4, in which

the proposed organics pathway achieves significant savings in GHG emissions (-9.5 g CO_2

eq per MJ) in the production and use of fuels due to the avoided emissions from landfill

storage. The 88.0 g CO_2 eq emitted per MJ of fuel produced by the polyolefin pathway are

7.8% lower (See Figure 2.5) compared to the 95.5 g CO_2 eq per MJ from conventional

fossil fuel.[27] Since both pathways presented desirable outcomes in regards to the

environmental impact, further research on laboratory and pilot scale is strongly

recommended to determine optimum operation conditions for the production of fuels from

MSW.
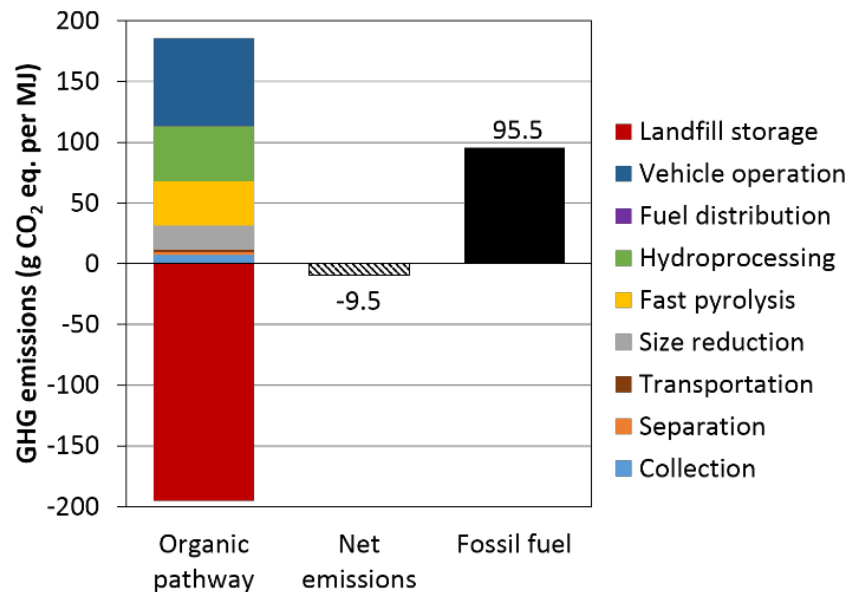
Figure 2.4. GHG emissions for the organics pathway compared to the fossil fuels production emissions.
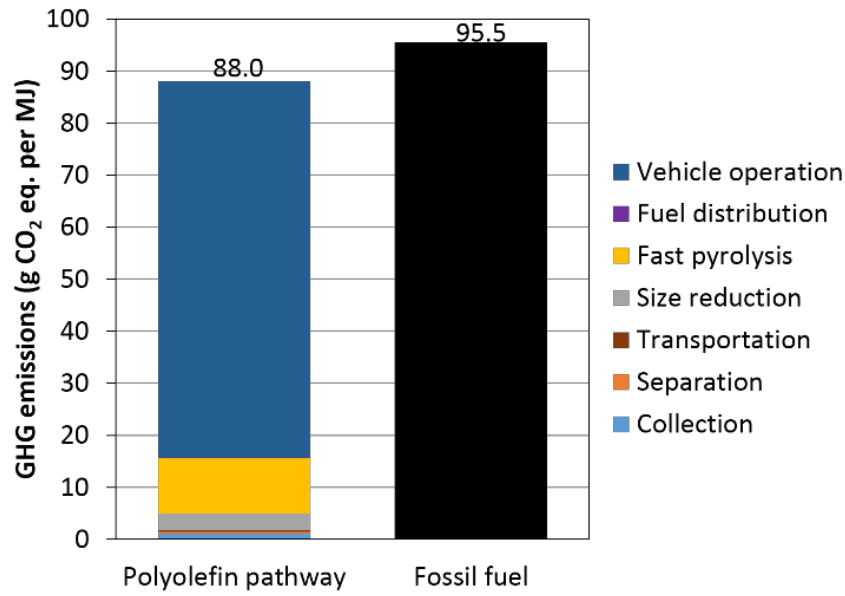
Figure 2.5. GHG emissions for the polyolefin pathway compared to the fossil fuel production emissions.

Vehicle use is the stage with the highest GHG emissions, with a contribution of 38.9 and 82% of total emissions in the organics and polyolefin pathways, respectively. However, avoiding landfill emissions for the MSW organic pathway is greater than all of the positive emission sources combined, which emphasized the importance of landfill emissions that may be avoided when MSW is converted to fuels. In contrast, the stages of separation, feedstock transportation, and fuel distribution are the ones with the lowest impact regarding emissions to the atmosphere. These stages accounted for 2.33 and 0.97% of the total emissions in the organics and polyolefin pathway, respectively. Therefore, improvements in the stages of vehicle use, pyrolysis, and size reduction could enhance the environmental performance of MSW-to-biofuel pathway.

In order to obtain an advanced biofuel with 60% savings compared to the fossil fuel pathway (38.2 g CO_2 equiv/MJ), which is necessary to qualify in the United States as a sustainable advanced biofuel, approximately 51% and 49% of the energy content (MJ) of advanced biofuels should be processed through the organics and polyolefin pathway, respectively. Then, considering the feedstock-to-biofuel yields, all the organic waste (7.07 million tonnes on MAF basis) can be processed along with 1.9 million tonnes of polyolefin waste, resulting in a mixture of 78.8% (wt) of organics waste and 21.2% (wt) of polyolefin waste. The remaining 1.03 million tonnes of polyolefin waste in Mexico could be processed for chemicals production or mechanical recycling.

These findings guide research through a sustainable pyrolysis-based biofuel pathway that blends both organics and polyolefin waste. However, mixture compositions and operation conditions still need to be tested at a laboratory and pilot scales in order to validate these findings, because the ratio of organics to plastic waste has been shown to have a strong effect on product distribution.[36] For the time being, until new pathways combining organics and polyolefin waste are developed, the pathway shown in Figure 2.6 is a proposed route to process both types of MSW in a single facility with common equipment.
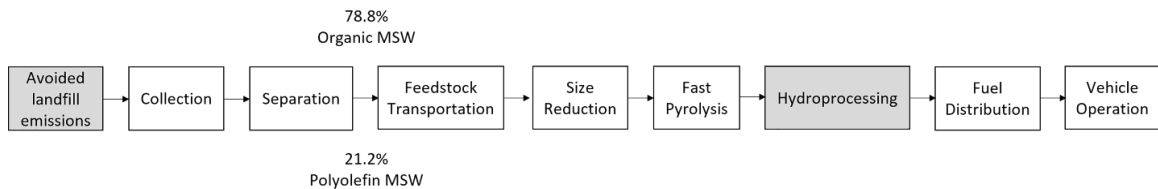
Figure 2.6. Proposed pathway for organics and polyolefin MSW for a blended fuel product.

Regarding the confidence of the carbon footprint results, it is important to mention that ideally a sensitivity analysis should be performed. However, a sensitivity analysis is important when a comprehensive CFA is conducted after process level data is available for specific feedstocks. Because the current study objective is to obtain results to justify future research, a preliminary carbon footprint approach was used, fully aware of its limitations. These limitations include uncertainty in yields of biofuel, inputs to each life cycle stage, and avoided emissions at landfills.

2.4 Conclusion

The results of the current study support MSW as a promising feedstock for the production of renewable fuels and chemicals in Mexico, which has the potential to displace up to 7% of current annual fossil transportation fuel consumption. According to the preliminary environmental assessment, this technology can provide lower emissions when compared to the fossil fuel production pathway. For the proposed organics pathway, a credit of 9.5 g CO_2 eq per MJ was estimated mostly due to the avoided emissions from the current practice of landfilling MSW organics (-195.2 g CO_2 eq per MJ). On the other hand, the polyolefin pathway presented 7.8% less GHG emissions than the well-to-wheel fossil fuels life cycle. In addition, fuels produced through utilizing MSW could avoid the use of land for the already problematic situation of landfill availability and possible competition with food for bioenergy feedstock production. Moreover, according to Mexico's MSW composition a mixture of 78.8% organics and 21.2% polyolefins, on a mass basis, would provide alternative fuels with more than 60% savings of emissions compared to the fossil fuel

pathway. Hence, the preliminary CFA has shown the environmental feasibility with regard to GHG emissions of pyrolysis-based biofuel conversion as a promising approach with a high potential to favor the sustainable management of MSW in Mexico and simultaneously contribute to transportation fuel supply.

2.5 Acknowledgements

2.6 References

(1)   United Nations. *World Urbanization Prospects: The 2014 Revision, Highlights*; Report No. ST/ESA/SER.A/352; Department of Economic and Social Affairs. Population Division: Washington, DC, 2014.

(2)   Hoornweg, D.; Bhada-Tata, P. *What a Waste. A Global Review of Solid Waste Management*; The World Bank: Washington, DC, 2012.

(3)   Azapagic, A. Energy from Municipal Solid Waste: Large-Scale Incineration or Small-Scale Pyrolysis? *Environ. Eng. Manag. J.* **2007,** *6* (5), 337-346.

(4)   U.S. Environmental Protection Agency (EPA). Overview of Greenhouse Gases. https://www3.epa.gov/climatechange/ghgemissions/gases/ch4.html (accessed March 14, 2016).

(5)   Sharif Hossain, M. Panel estimation for CO_2 emissions, energy consumption, economic growth, trade openness and urbanization of newly industrialized countries. *Energ. Policy.* **2011,** *39* (11), 6991-6999.

(6)   Mexican Secretariat of Environment and Natural Resources (SEMARNAT). *Informe de la situación del medio ambiente en México. Compendio de estadísticas ambientales. Indicadores clave y de desempeño ambiental. Edición 2012*; Mexico, 2013.

(7)   Durán Moreno, A.; Garcés Rodríguez, M.; Velasco, A. R.; Marín Enriquez, J. C.; Gutiérrez Lara, R.; Moreno Gutiérrez, A.; Delgadillo Hernández, N. A. Mexico city's municipal solid waste characteristics and composition analysis. *Rev. Int. Contam. Ambie.* **2013,** *29* (1), 39-46.

(8)   U.S. Environmental Protection Agency (EPA). *Municipal solid waste generation, recycling, and disposal in the United States: Facts and figures for 2012*; Report No. EPA-530-F-14-001; Office of Solid Waste and Emergency Response: Washington, DC, 2014.

(9)   Worldwatch Institute. Global Municipal Solid Waste Continues to Grow. http://www.worldwatch.org/global-municipal-solid-waste-continues-grow (accessed February 14, 2016).

(10)   Zhang, Q.; Chang, J.; Wang, T.; Xu, Y. Review of biomass pyrolysis oil properties and upgrading research. *Energ. Convers. Manage.* **2007,** *48* (1), 87-92.

(11)   Brown, R. C.; Holmgren, J. Fast pyrolysis and bio-oil upgrading. http://www.ars.usda.gov/sp2UserFiles/Program/307/biomasstoDiesel/RobertBrown&JenniferHolmgrenpresentationslides.pdf (accessed December 16, 2015).

(12)   Yaman, S. Pyrolysis of biomass to produce fuels and chemical feedstocks. *Energ. Convers. Manage.* **2004,** *45* (5), 651-671.

(13)   Achilias, D. S.; Roupakias, C.; Megalokonomos, P.; Lappas, A. A.; Antonakou, E. V. Chemical recycling of plastic wastes made from polyethylene (LDPE and HDPE) and polypropylene (PP). *J. Hazard. Mater.* **2007,** *149* (3), 536-542.

(14)   Mexican Secretariat of Environment and Natural Resources (SEMARNAT). México: País emergente y comprometido. Hacia un Acuerdo Global sobre Cambio Climático. http://www.semarnat.gob.mx/sites/default/files/documentos/documentos/presentaciones/mexico-secretario-guerra-climate-diplomacy-day.pdf (accessed February 17, 2016).

(15)   Mexican Institute of Statistics and Geography (INEGI). Generación estimada de residuos sólidos por entidad federativa. www.inegi.org.mx/est/contenidos/Proyectos/modulosamb/doc/rsu.zip (accessed February 6, 2015).

(16)   Bernache-Pérez, G.; Sánchez-Colón, S.; Garmendia, A. M.; Dávila-Villarreal, A.; Sánchez-Salazar, M. E. Solid waste characterisation study in the Guadalajara Metropolitan Zone, Mexico. *Waste Manage. Res.* **2001,** *19* (5), 413-424.

(17)   Pan American Health Organization (PAHO). *Evaluación general de los servicios de manejo de residuos sólidos municipales. Informe analítico de México. Evaluación 2002*; World Health Organization: Mexico, 2003.

(18)   Velasco Perez Alonso, M. G. Generation and disposition of MSW in Mexico and potential for improving waste management in Toluca municipality. MS dissertation, Columbia University, 2011.

(19)   ANDELLAC; ANILLAC; CNIH. *Plan de Manejo de Neumáticos Usados de Desecho*; Mexico, 2013.

(20)   Hsu, D. D. *Life Cycle Assessment of Gasoline and Diesel Produced via Fast Pyrolysis and Hydroprocessing*; Report No. NREL/TP-6A20-49341; National Renewable Energy Laboratory: Golden, CO, 2011.

(21)   Valkenburg, C.; Gerber, M. A.; Walton, C. W.; Jones, S. B.; Thompson, B. L.; Stevens, D. J. *Municipal Solid Waste (MSW) to Liquid Fuels Synthesis, Volume 1: Availability of Feedstock and Technology*; Report No. PNNL-18144; Richland, WA, 2008.

(22)   Perugini, F.; Mastellone, M. L.; Arena, U. A life cycle assessment of mechanical and feedstock recycling options for management of plastic packaging wastes. *Environ. Progr.* **2005,** *24* (2), 137-154.

(23)   U.S. Energy Information Administration (EIA). International Energy Statistics. http://www.eia.gov/cfapps/ipdbproject/iedindex3.cfm?tid=5&pid=54&aid=2   (accessed April 16, 2015).

(24)   Mexican Chemical Industry Association (ANIQ). Anuario Estadístico de la Industria Química Mexicana 2015. http://www.aniq.org.mx/anuario/2015/index.html (accessed May 17, 2016).

(25)   Mølgaard, C. Environmental impacts by disposal of plastic from municipal solid waste. *Resour. Conserv. Recy.* **1995,** *15* (1), 51-63.

(26)   Boundy, B.; Diegel, S. W.; Wright, L.; Davis, S. C. *Biomass Energy Data Book: Edition 4*; Oak Ridge National Laboratory: Oak Ridge, TN, 2011.

(27)   National Energy Technology Laboratory (NETL). *An Evaluation of the extraction, Transport and Refining of Imported Crude Oils and the Impact on Life Cycle Greenhouse Gas Emissions*; Report No. DOE/NETL-2009/1362; 2009.

(28)   Jones, S. B.; Holladay, J. E.; Valkenburg, C.; Stevens, D. J.; Walton, C. W.; Kinchin, C.; Elliott, D. C.; Czernik, S. *Production of Gasoline and Diesel from Biomass via Fast Pyrolysis, Hydrotreating and Hydrocracking: A Design Case.*; Report No. PNNL-18284; Pacific Northwest National Laboratory: Richland, WA, 2009.

(29)   California Air Resources Board (ARB). *Proposed Low Carbon Fuel Standard (LCFS) Pathway for the Production of Biomethane from High Solids Anaerobic Digestion (HSAD) of Organic (Food and Green) Wastes*; California Environmental Protection Agency: Sacramento, CA, 2012.

(30)   *SimaPro LCA Software*, version 8.0; PRé-Consultants: The Netherlands, 2014.

(31)   Fitzgerald, G. C.; Krones, J. S.; Themelis, N. J. Greenhouse gas impact of dual stream and single stream collection and separation of recyclables. *Resour. Conserv. Recy.* **2012,** *69*, 50-56.

(32)   Alston, S. M.; Arnold, J. C. Environmental Impact of Pyrolysis of Mixed WEEE Plastics Part 2: Life Cycle Assessment. *Environ. Sci. Technol.* **2011,** *45* (21), 9386-9392.

(33)   Buekens, A. G.; Huang, H. Catalytic plastics cracking for recovery of gasoline-range hydrocarbons from municipal plastic wastes. *Resour. Conserv. Recy.* **1998,** *23* (3), 163-181.

(34)   Çit, İ.; Sınağ, A.; Yumak, T.; Uçar, S.; Mısırlıoğlu, Z.; Canel, M. Comparative pyrolysis of polyolefins (PP and LDPE) and PET. *Polym. Bull.* **2010,** *64* (8), 817-834.

(35)   Demirbas, A. Pyrolysis of municipal plastic wastes for recovery of gasoline-range hydrocarbons. *J. Anal. Appl. Pyrol.* **2004,** *72* (1), 97-102.

(36)   Li, X.; Li, J.; Zhou, G.; Feng, Y.; Wang, Y.; Yu, G.; Deng, S.; Huang, J.; Wang, B. Enhancing the production of renewable petrochemicals by co-feeding of biomass with plastics in catalytic fast pyrolysis with ZSM-5 zeolites. *Appl. Catal. A.* **2014,** *481*, 173-182.

(37)   Scott, D. S.; Czernik, S. R.; Piskorz, J.; Radlein, D. S. A. G. Fast pyrolysis of plastic wastes. *Energ. Fuel.* **1990,** *4* (4), 407-411.

(38)   Williams, P. T.; Williams, E. A. Interaction of Plastics in Mixed-Plastics Pyrolysis. *Energ. Fuel.* **1999,** *13* (1), 188-196.

3 Effect of Temperature and Vapor Residence Time on the Micropyrolysis Products of Waste High Density Polyethylene[2]

Abstract

Thermal degradation of plastics is a promising technology for addressing the waste management issues of landfill disposal, while obtaining useful products. Primary thermal degradation of polymers usually yields a large quantity of high molecular weight compounds with a limited applicability, making necessary a secondary degradation to improve the product quality. In this study, pyrolysis vapors from waste high density polyethylene (HDPE) were subjected to secondary degradation by varying the temperature and vapor residence time (VRT) in the reaction zone of a new two-stage micropyrolysis reactor (TSMR) attached to a commercial micropyrolysis unit. Temperature and VRT variations showed a strong effect on the product distribution, with low temperature (625 ºC) and short VRT (1.4 s) producing a wide range of gases and liquid products and with high temperature (675 ºC) and long VRT (5.6 s) producing mostly hydrocarbon gases and mono- and poly-aromatics. The results showed a good agreement with previously reported product distributions for larger-scale pyrolysis reactors and were well explained by known degradation mechanisms.

3.1 Introduction

Polymers are important materials with useful and unique properties that find application in many manufactured goods including vehicular components, food packaging, and products in medical applications. To illustrate the impact of these materials, approximately 4% of the global petroleum production is embodied in polymer materials and another 4% is used to satisfy energy requirements in polymer processing.[1] The vast majority of polymers (90%) are commodity thermoplastics (consisting of mainly polyethylene (34.4%), polypropylene (24.2%), polyvinyl chloride (16.5%)), with smaller contributions from polystyrene, polyethylene terephthalate, expanded polystyrene, engineered plastics, and high-performance polymers. Depending on the region, between 22 and 43% of polymers are landfilled, thus wasting a valuable nonrenewable resource.[2] The larger portion of the nonlandfilled fraction is incinerated for energy; however, this generates hazardous solid waste and mandates expensive air pollution controls to minimize adverse health impacts.

One option to address the global challenge of plastic waste management is creating a circular material flow system where plastics are recycled at the end-of-life. Recycling of polymers involves a series of steps including waste plastic collection, washing, separation into common materials, and other recycling processes. The latter can be categorized as primary recycling, mechanical (secondary) recycling, chemical (tertiary) recycling, and energy recovery (quaternary).[3] Primary recycling occurs in an extrusion line by combining clean scraps with virgin polymers to make first generation products. Secondary recycling typically uses end-of-life thermoplastic polymers recovered from municipal solid waste or

other sources and produces items often with lower performance properties compared to the first line products due to polymer degradation. Secondary recycling of virgin polymers can be done no more than 2 to 3 times because after every recycling step the strength of the material is compromised from thermal degradation.[4] Waste polyethylene terephthalate (PET, PETE from drinking bottles) can be thermally processed into polyester fibers for clothing or other uses, or can be processed into food-contact or nonfood-contact packaging. Polyethylene (PE) is normally down-cycled into plastic lumber and other durable nonfood-contact applications. Other useful products may be obtained from waste polymers through processes of chemical recycling, which often involves subjecting waste thermoset and thermoplastic polymer wastes to high temperatures in absence of oxygen, in which the reactions may also occur in the presence of catalysts. Under these reaction conditions, the waste polymer is degraded into smaller fragments, forming a vapor phase that is condensed to a liquid product with coproduction of gaseous and, in some cases, solid char. Depending on the waste plastic type, these thermo-chemical products may be pure hydrocarbons or may be organic compounds containing oxygen, nitrogen, chlorine, or other trace elements in addition to carbon (C) and hydrogen (H).[5, 6]

Tertiary (chemical) recycling may employ processes such as pyrolysis, gasification, liquid-gas hydrogenation, steam or catalytic cracking, and others such as the direct use of plastic waste as reducing agents in blast furnaces in iron and steel making.[3] In addition, prior studies on pyrolysis of waste plastics have been conducted in various reactors, such as thermogravimetric analysis, batch and continuous well-mixed vessels, fluid beds, conical

spouted-beds, microwave or induction assisted, and auger reactors.[7] Thermochemical treatments such as pyrolysis and catalytic or steam cracking have been utilized to produce lower molecular weight monomers or mixtures of products like petrochemicals and hydrocarbon fuels. Certain polymers (PET, nylon-66) are ideal for thermochemical degradation because they yield predominantly monomers of the type that allow synthesis of the same polymers again. PE, however, degrades in a more random fashion to yield lower C number oligomer alkenes, alkanes, and alkadienes, as well as aromatics (particularly at high temperature), and gaseous alkenes and alkanes.[8] Catalysts used in thermochemical treatments, including zeolites, silica-alumina, ZSM-5, and mesoporous materials, require lower reaction temperature compared to purely thermal treatments (~400-600 ºC vs ~600-900 ºC, respectively) and produce comparatively lower molecular weight liquid products. Chemical recycling is more versatile compared to secondary recycling because both thermoplastics and thermoset polymers can be degraded to produce useful chemicals, whereas only thermoplastics can be mechanically recycled. One key advantage of chemical recycling of plastic waste is the ability to treat mixtures containing different polymer types in waste, and may be economically favorable when such mixtures are expensive to separate.

In an attempt to understand the societal impacts of chemical recycling of waste plastics, the American Chemistry Council[9] estimates that as many as 600 waste plastics-to-oil (PTO) facilities could be established in the U.S. while generating $8.9 billion in annual economic output related to PTO facilities and supporting 39,000 jobs. The oil produced

could substitute for diesel or other fossil fuels in various applications. Additional research and development activities supporting polymer remanufacturing or recycling are needed to improve economic, energy, and environmental efficiencies of these processes as well as to understand the sustainability implications at various scales, from the unit operation level, process level, facility level, and up to regional, national, and global levels.

Pyrolysis of waste plastic in an inert gas without catalysts is appealing because it avoids the cost and complexity of catalyst use,[10, 11] including catalyst deactivation during processing, and has been shown to produce gaseous and liquid products within desired molecular weight ranges by controlling reaction temperature, heating rate, and residence time (RT) of solid and vapors in the reactor. For example, pyrolysis of PE without catalysts in a fluid bed reactor was studied at temperatures between 650 and 850 ℃ and vapor residence time (VRT) between 0.64 and 2.6 s,[12] with VRT controlled by the flow rate of inert gas through the fluid bed and freeboard sections of the reactor. Yields of pyrolysis gases (H_2, C1-C5 hydrocarbons) increase from about 10% wt. to nearly 90% as temperature increased over this range, and a variation of gas yield with RT was noticeable, but not as significant as the effect of temperature. The yield of C2-C5 gaseous products peaked at intermediate temperatures and decreased between 750 and 850 ℃ because of cyclation reactions that formed aromatic compounds. The yields of wax and liquid hydrocarbons decreased sharply from 650 ℃ with increasing temperature, with a corresponding increase of gaseous products. Notable also was the modest and ambiguous effect of VRT on the yield of liquid and wax products, sometimes increasing, sometimes decreasing; this may

51

be from imprecise control of the VRT in the fluid bed reactor system. Char production was negligible in all cases studied. Another study by this research group[13] using the fluidized bed reactor showed a decrease on wax yield and an increase in the gas yield at 650 °C when increasing the VRT from 0.8 to 1.5 s. Elordi et al.[14] studied the effects of pyrolysis temperature (500-700°C) on the degradation of high density polyethylene (HDPE) in a conical spouted bed reactor, observing trends in production of C1-4 gas, C5-11 liquid, C12-20 liquid, and wax products versus temperature. Low yield of single ring aromatics was observed, suggesting that secondary reactions were kept to a minimum by the low VRT in the reactor. A study on the effects of pyrolysis temperature and VRT on yields of pyrolysis products by Artetxe et al.[11] was conducted in a two-step reactor: a conical spouted-bed reactor (510 °C) followed by a tubular cracking reactor (800-950 °C, 0.016-0.032s VRT). The conical spouted bed reactor yielded 93% wt. of C21+ waxes and C12-21 hydrocarbons while products from the tubular reactor were predominantly ethylene, propylene and butanes, and low aromatics at short VRT. The effect of VRT on product yields was insignificant over the small range studied. Butler et al.[15] reviewed pyrolysis of waste polyolefins to liquid processes, including commercial state-of-the-art and laboratory results, concluding that catalysts are generally required to yield a quality transportation-grade fuel using pyrolysis. Other advantages of using catalysis include lower pyrolysis temperature and high yields of gaseous products compared to noncatalytic pyrolysis, but disadvantages include potential for contamination and catalyst deactivation by coking.

The importance of PE pyrolysis temperature and VRT on product yield and distribution of products between gas, liquid, and wax is well-known. However, it is apparent from prior studies that a systematic investigation of these pyrolysis parameters across a wide range of expected values is lacking, especially in micropyrolysis. Thermogravimetric analysis studies cannot characterize VRT effects, only temperature. Fluid beds are imprecise with regard to VRT for both polymer particles and pyrolysis vapors due to nonideal mixing within the reactor, and prior two-step reactor arrangements, as mentioned above, probed very limited VRT ranges.

The primary research objective in this study is to present results from a new tubular reactor section that was added to a standard micropyrolysis laboratory apparatus in order to supplement its current capabilities of temperature and heating rate control with a VRT control. Our goal in this work is to show qualitative trends in the pyrolysis products data as a function of pyrolysis temperature and VRT using Gas Chromatography/Mass Spectrometry (GC/MS) peak area. Primary pyrolysis reactions occur in the standard probe of the micropyrolysis apparatus while secondary pyrolysis reactions take place in the constant temperature tubular reactor section. The new two-step micropyrolysis reactor (TSMR) apparatus design will be described along with reactor data on isothermal operation, flow characterization, and control of VRT. Micropyrolysis of small samples (< 1 mg) of waste HDPE were studied in this new apparatus over a temperature range of 625-675 °C and VRT from 1.4 to 5.6 s. Trends of pyrolysis products over these temperatures and VRT ranges are reported for gaseous, liquid, wax, and aromatic products and are

related to known mechanisms of random free-radical scission and small molecule condensation.

3.2 Experimental section

3.2.1 Sample preparation

The samples for this experiment were composed of waste undyed HDPE, obtained from clean home-disposed milk jugs. Impurities in the sample were analyzed using a Costech 4010 elemental analyzer and a PerkinElmer Optima 7000DV Inductively Coupled Plasma-Optical Emission Spectrometer. For these analyses, the sample was sliced in small stripes of 30×2 mm, that were frozen with liquid nitrogen and grinded in a commercial coffee grinder several times until obtaining small particles. The results of the elemental composition and concentration of impurities are shown in section B.2 of Appendix B. These samples were finely sliced into pieces of approximately 0.5 mm width $\times$ 3 mm length, and weighed in a microbalance with an accuracy of ± 10 μg. The weight range of the HDPE samples was determined to be 400-600 μg with the appropriate number of samples being used for each run to stay within this range. The samples were centered in a quartz tube, covered with glass wool from both sides, and inserted into the probe of a CDS 5200 HP pyroprobe (CDS Analytical).

3.2.2 Micropyrolysis Reactor and Conditions

Primary degradation was achieved in the probe of a CDS 5200 HP pyroprobe unit operating at a heating rate of 1000 °C/s for a period of 20 s. The CDS probe was inserted into a new

54

tubular reactor section which was connected to the CDS pyroprobe unit to carry out primary and secondary degradation, respectively. The probe and the tubular reactor section comprise the TSMR (Figure 3.1). The tubular reactor section was made from 22.25 in (0.57 m) long, 1/4 in ID stainless steel tubing with appropriate fittings. A heating tape, covering from 3.875 to 20.25 in (0.10 to 0.51 m) of the reactor surface, provided the heat required to increase the inner temperature up to pyrolysis conditions. The temperature in this section was manually controlled with a rheostat. To avoid condensation of the pyrolysis vapors, a second heated zone was set up for the remaining 2 in (0.05 m) of the TSMR and its union with the pyroprobe interface. A heating tape with an automatic controller was used to maintain the temperature in this section equal to that at the interface (300 °C). The purpose of the interface is to cool down the pyrolysis vapors to 300 °C to avoid further degradation before entering a system of valves within the CDS 5200 unit. Once the vapors have passed this system of valves, they are transported to the GC through a heated transfer line also operated at 300 °C. To ensure a stable temperature profile at the reactor zone (see Figure B-2 of Appendix B), the TSMR was insulated with a braided fiberglass sleeve. Details of the insulation setup are presented in Figure B-3 of Appendix B. Two type-K thermocouples connected to a temperature recorder were positioned at 10 and 16 in (0.25 and 0.41 m) from the reactor inlet edge to monitor the tube outside temperature at the reaction zone during the experiments. The above combination of temperature sensors and controllers provided an adequate control of temperature during the secondary degradation process. A detailed description regarding the criteria to define insulation positioning, reaction zone

location, temperature measurement and control, and temperature profile within the TSMR can be found in the section B.1 of Appendix B.
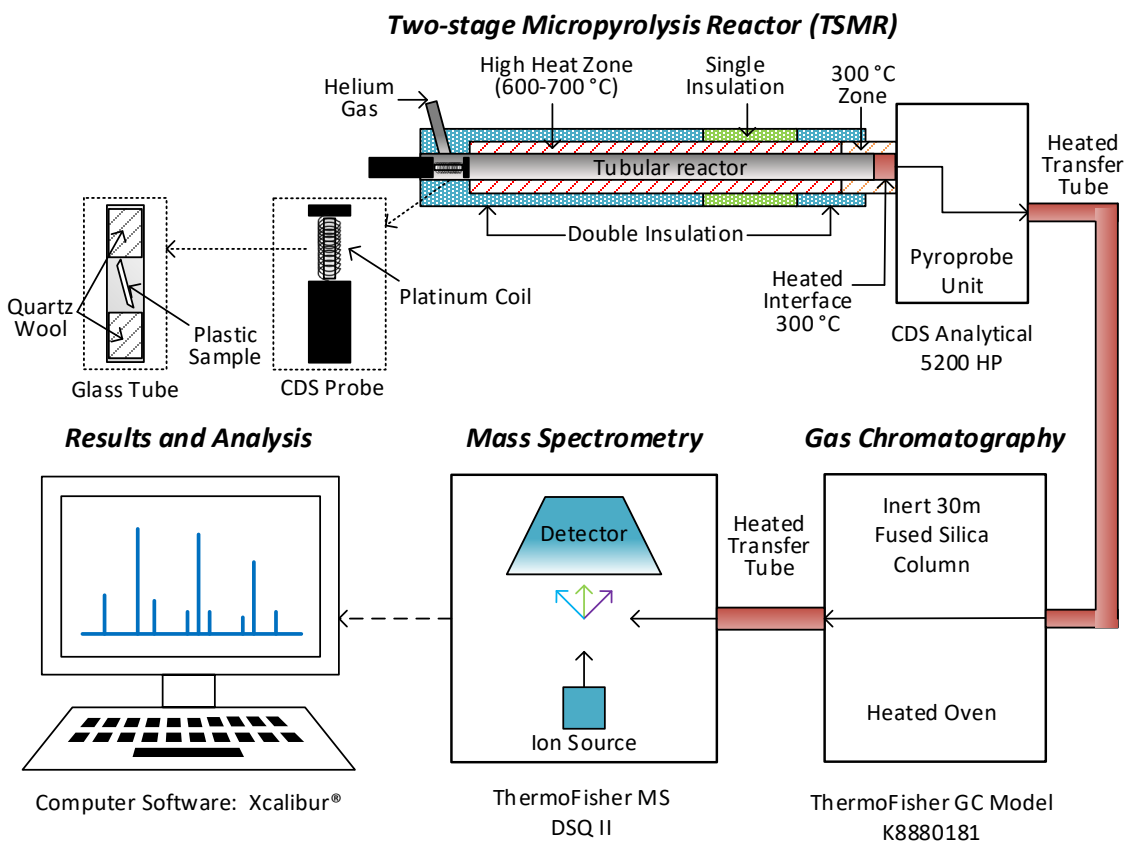
Figure 3.1. Experimental apparatus and method for the pyrolysis and data collection of HDPE samples with extended residence time.

Pyrolysis experiments were run in duplicate at temperatures of 625, 650, and 675 °C, and VRTs of 1.4, 2.8, and 5.6 s, ensuring in all cases complete degradation of the HDPE sample, with no solid residue ever detected. Both the probe and the tubular reactor section were operated at the same temperatures in every experiment. VRT was controlled by modifying the carrier gas (ultra high purity helium) flow rate coming through the reactor during pyrolysis. The calculation to convert helium flow rate to VRT is explained in the

section B.3 of Appendix B. Helium flows of 100, 50, and 25 mL/min were employed to provide VRTs of 1.4, 2.8, and 5.6 s at the reaction zone, respectively, which should be considered as average VRT values because the flow regimes transition from laminar to turbulent over this range of helium flow rates. The combination of the different temperatures and VRTs resulted in nine different operation conditions. The pyrolysis vapors from the TSMR entered the interface (at 300 °C) of the CDS Pyroprobe and then were sent, through a heated transfer line (300 °C), to the GC/MS equipment for separation and identification, as shown in Figure 3.1.

3.2.3 Analytical Methods

The pyrolysis products were separated in a GC (model K8880181 by ThermoFisher) with a Restek RXI-5MS fused silica column (low polarity phase, crossbond 5% diphenyl/95% dimethyl polysiloxane, 30m × 0.25 mm, 0.25 μm film thickness). The injector temperature was set at 275 °C and the split ratio was varied, depending of the helium flow rate in the TSMR, to ensure a constant flow of 1 mL/min through the column. To achieve the separation, the GC oven was maintained at 35 °C for 20 min, then the temperature increased at a rate of 5°C/min to 275 °C, and finally was held at this temperature for 10 min. Compounds were sent to the MS (model DSQII by Thermo Scientific) through a transfer line maintained at 275 °C. The ion source operated at 275 °C and captured ion fragments in a range of 15-600 m/z. The system was checked daily to ensure the absence of air leaks and to monitor the detector performance. Each experiment was preceded by two or three successive heatings (600°C for probe at a rate of 1000°C/s for 20 s and >600°C for tubular

reactor with GC column heating program of 35-275 °C over 2 min and hold at 275 °C for 7 min) and coolings of the pyroprobe and GC oven to remove any condensed residues. In all cases negligible traces of compounds were detected, indicating that all pyrolysis products were detected from the preceding experiments.

Pyrolysis products were identified with aid of the Xcalibur software from Thermo Fisher. For purposes of identification and peak area percent calculations, only peaks with a contribution above 0.1% of total peak area were considered. This cut off limit allowed the analysis of approximately 95 % of the total peak area of the chromatograms. The algorithm available with the Xcalibur software was used for the integration, although some few peak areas had to be manually reintegrated due to a raised baseline estimated by the algorithm. Area integration of coeluted compounds was determined using the criteria described in the section B.4 of Appendix B. It is important to clarify that the analysis performed in this study was strictly qualitative. Compound identification was performed by mass spectra comparison with the database available in the Xcalibur software. For compounds not identified by the software, usually high C number aliphatics and aromatics, the homologous ion series for organic compounds reported by Lebedev[16] and the National Institute of Standards and Technology webbook [17] were used as references. After identification, pyrolysis products were classified and grouped by C number and chemical class.

3.3 Results and discussion

3.3.1 Temperature Performance of the TSMR

As described in the section B.1 of Appendix B, several arrangements of insulation and heating tape were tested to obtain a stable temperature profile within the TSMR. The temperature profiles are shown in Figure 3.2 when this arrangement was tested at different helium flow rates and set to 700 °C. The temperature in the reaction zone (shaded region) oscillated from 670 to 725 ° C, with average values of 701, 704, and 700 °C for 100, 50, and 25 mL/min of helium flow rate, respectively. Thus, helium flow rate had little effect on reactor temperature within the two stages of the micropyrolysis reactor. The temperature in the area where the micropyrolysis probe is inserted, before 3.875 in (0.1 m), is maintained at a temperature below 380 °C which can produce melting of the sample but cannot induce its degradation. Also, the insulation arrangement provides a temperature drop after the reaction zone which allows the pyrolysis products to leave the TSMR and to enter to CDS pyroprobe close to 300 °C. This reactor exit temperature does not cause further degradation of these compounds but will keep them in a vapor state that can facilitate their delivery to the GC for analysis. The data shown in Figure 3.2 was tested without the use of the second heated zone (which was held at 300 °C in the HDPE experiments), therefore, the temperature at 22 in drops below 300 °C. However, it was later confirmed that with the second heated section in place that a stabilized temperature close to 300 °C at the reactor exit was achieved in the pyrolysis trials.
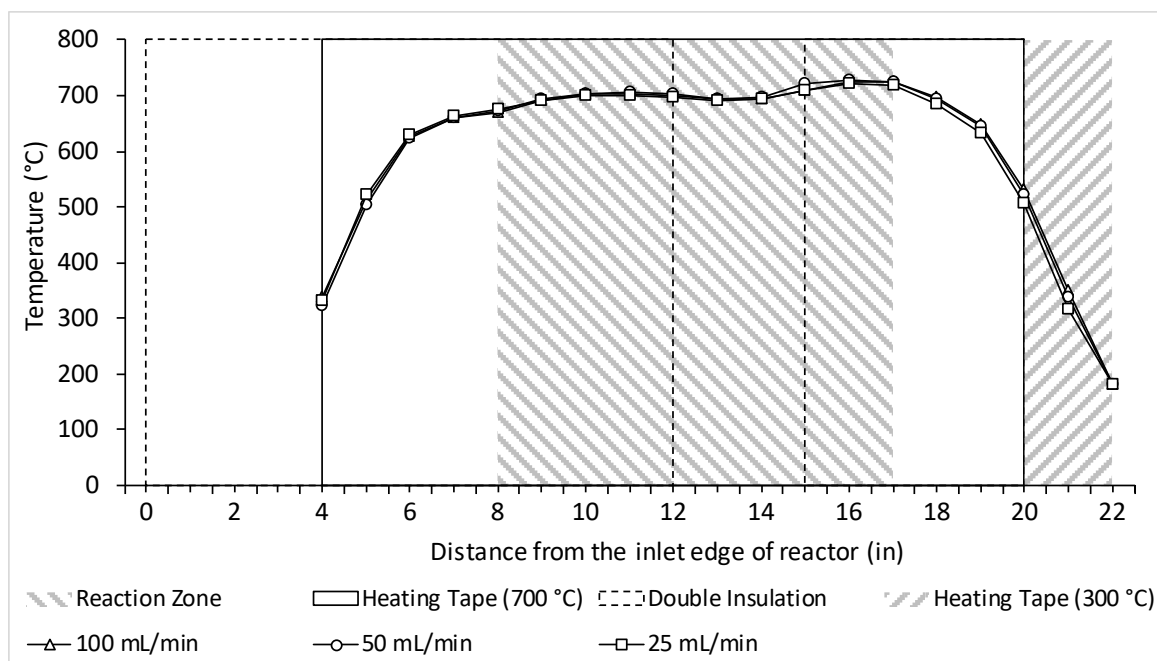
Figure 3.2. Temperature profile of the TSMR at various He flow rates.

3.3.2 GC/MS Chromatogram of the TSMR

Figure 3.3 compares the chromatograms at 625 °C and 1.4 s of VRT (least severe condition) and 675 °C and 5.6 s (most severe condition). As shown, a broad range of hydrocarbons products (C1-C31) was generated at different pyrolysis conditions. The chromatogram at 625 °C and 1.4 s shows a broad spectrum of molecular weight hydrocarbon products, from normal paraffin gases to high molecular-weight waxes and with only few small aromatic peaks. Each normal paraffin peak is a triplet with the alkadiene, alkene, and alkane of the same C number. The peak areas of the smaller alkadiene and alkane peaks are nearly equal at low C number, but at high C number the alkane peak becomes more prominent. At 625 °C and 1.4 s VRT, the pyrolysis products show peak area percentages with an almost even distribution. The chromatogram at 675 °C and 5.6 s shows a different pattern, with a great abundance of paraffin gases, lesser amounts of mono- and poly-aromatic hydrocarbons

60

(MAHs and PAHs, respectively), but with nearly negligible high C number paraffin hydrocarbons. The product distribution at severe conditions is shifted predominantly to compounds with less than six carbons. The displayed results agree with previous studies reporting that at lower temperatures and VRTs there is a wide range of aliphatic hydrocarbons formed, mostly in the medium and high C number range.[12, 18, 19] Also, the aromatic compounds observed at 675 °C and 5.6 s, have been reported as indicators of extreme conditions during the pyrolysis process.[20] The observed triplet of alkadiene, alkene, and alkane, in that ordered sequence, for each C number has also been reported before[13, 18, 21] from studies conducted at larger scale than micropyrolysis. A complete list of compounds obtained during the different combinations of temperature and VRT, along with its classification by C number and chemical class, is presented in section B.5 of Appendix B.

In the next section, results from the integration of the peaks appearing in the chromatograms are presented with respect to C number classes, reaction temperature and VRT. The data on integrated peaks do not represent a formal mass balance, rather they represent qualitative trends in the shifts of compound classes based on peak area percent.
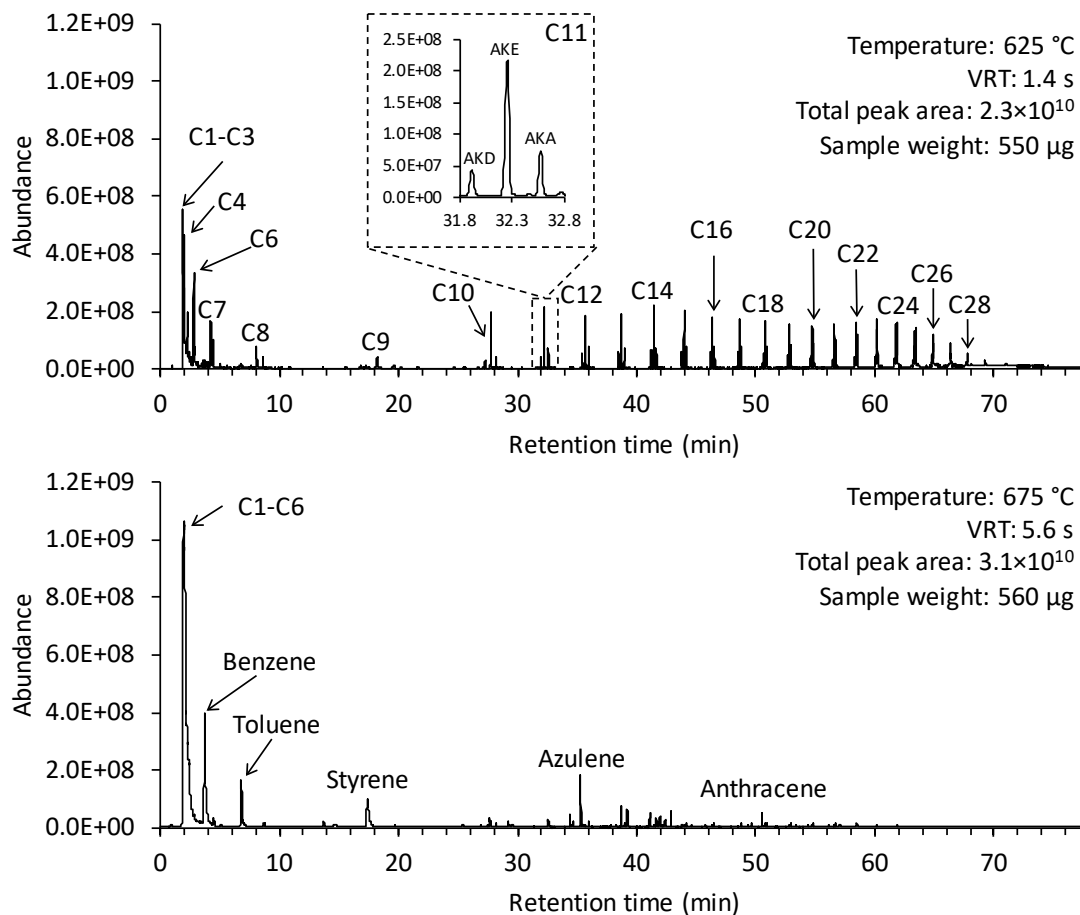
Figure 3.3. Chromatograms of the pyrolysis products from two different combinations of temperature and VRT in the Two-stage micropyrolysis reactor (AKD: Alkadiene, AKE: Alkene, AKA: Alkane).

3.3.3 Effect of temperature and VRT in the distribution of different carbon number fractions

The generation of linear and branched aliphatic and aromatic products from micropyrolysis

of waste HDPE as a function of VRT and different temperatures is shown in Figure 3.4.

The specific C number ranges are provided only for aliphatics (including alkanes, alkenes,

and alkadienes) while the category "aromatics" includes a wider C number range (C6-C27).

The data points appearing in Figure 3.4 are duplicate averages and the error bars are based

on a calculation of standard deviation, with most not visible because they are within the size of the symbols. Each VRT is a separate experiment in which the helium gas flow rate through the reactor was changed, as stated in Section 2.

At 625 °C and a VRT of 1.4 s, the generation of aliphatics with a broad range of C numbers (C1-C31) is observed. The C1-C25 aliphatics have a peak area percent ranging from 16 to 24% (see Table 3.1 for data on C number and chemical classes), whereas the production of high C number aliphatics (C26-C31) and aromatics is low (5 and 2%, respectively). As VRT increases at 625 °C, there is a decrease in the peak area percent of C11-C31 compounds with an increase in C1-C10 and aromatics. This trend is also present for temperatures of 650 and 675 °C, except that at 675 °C there is no increase in the C1-C10 range compounds and a slight decrease in the C1-C4 compounds for the highest VRT of 5.6 s. Also, the production of aromatic compounds appears to be strongly dependent on temperature. From the observed trends in Figure 4, it is clear that VRT plays an important role in the degradation of the different C number fractions and in the shift from high to low MW hydrocarbons. Finally, depending on reaction temperature and VRT, a different set of hydrocarbon products can be obtained. At the least severe conditions (625 °C, 1.4 s VRT), a high percentage of gasoline and diesel range liquids is obtained as well as hydrocarbon gases. At the most severe conditions (675 °C, 5.6 s VRT), mostly hydrocarbon gases and liquids in the gasoline range and aromatics are produced. This trend toward lower MW hydrocarbons is explained by the chain-end scission mechanism occurring during secondary degradation in the vapor phase.[22]

The pyrolysis product data at 650°C showed a similar trend as the 625°C data except that gas products had a higher percent of total product peak area (50% at VRT of 5.6 s), whereas diesel range (C11-C20) and waxes (C21-C31) aliphatics showed a lower value (see Table 3.1). At 675 °C, these trends were further evident with lower abundance of medium and high C number aliphatics and higher peak area percent reached by gases. However, at VRT of 5.6 s, gases experienced a decrease in their percentage that matched with a steep increment upward of the abundance of aromatics, which at the most severe conditions (675 °C and 5.6 s) comprised 26% of the total products (see Figure B-6 of Appendix B). The relationship between these two chemical groups suggests a chemical pathway that turns gases into aromatics. The mechanism behind this change has not been clarified yet but two pathways have been proposed already: a Diels-Alder reaction followed by dehydrogenation and unimolecular cyclation reactions followed by dehydrogenation.[23] These mechanisms highlight that increased temperature favored the production of aromatics and light aliphatics and promoted the degradation of diesel range aliphatics and waxes. The polymer thermal degradation data in Figure 4 are a result of a full range of free-radical mechanisms including initiation of degradation through random scission of C-C bonds, β-scission yielding low C number gas products, intermolecular and intramolecular H-transfer, 1,5 hydrogen transfer, and six-member ring formation.[22, 24] As temperature and VRT increase, these reactions act together to reduce the molecular weight of degradation products producing low molecular weight aliphatics, MAHs and PAHs. These interpretation on mechanisms are supported when the effect of temperature is shown at fixed VRT (see section B.6 of Appendix B for more details).
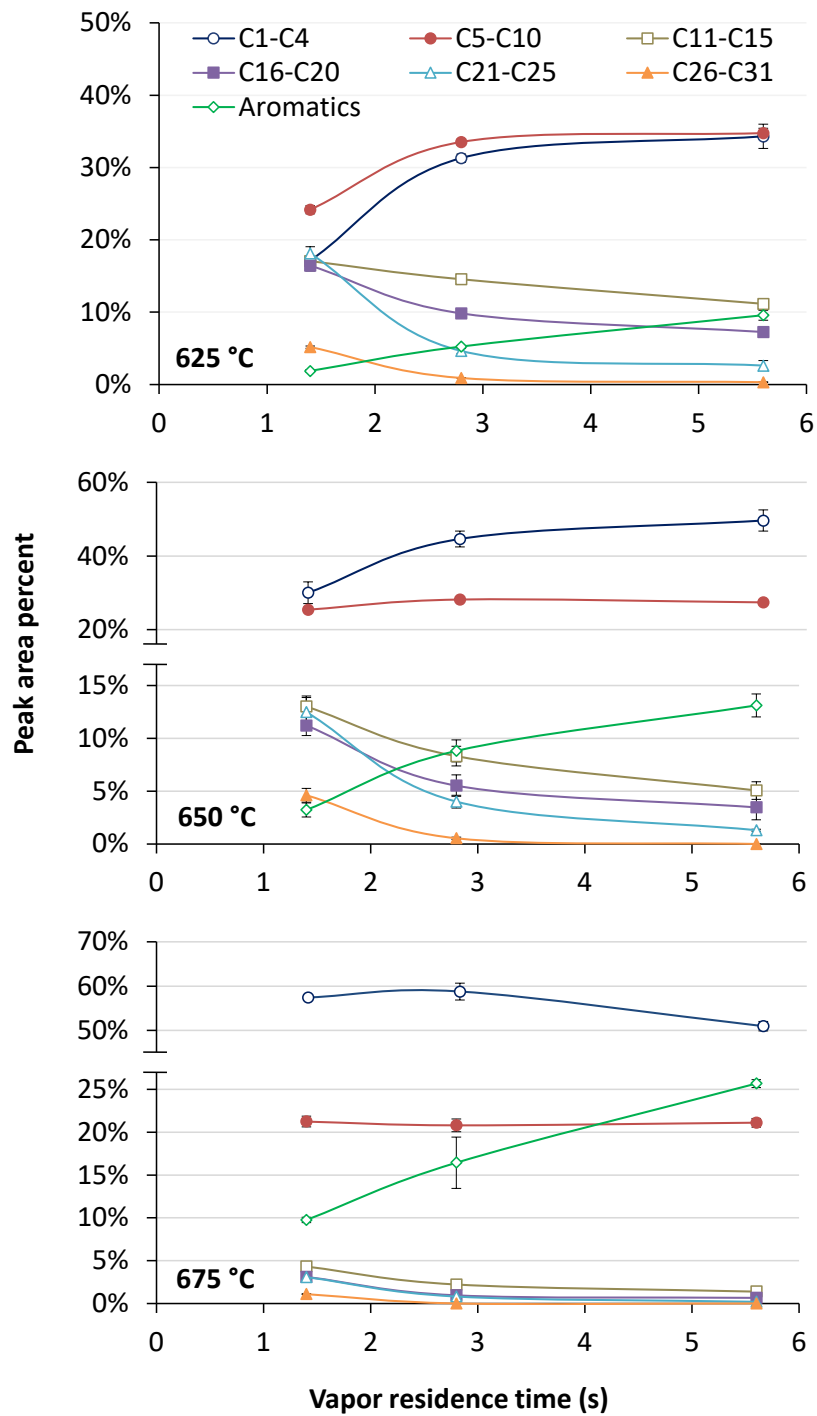
Figure 3.4. Effect of VRT at different temperatures on C number range hydrocarbon products from pyrolysis of HDPE

Table 3.1. Chemical class composition (%) of HDPE pyrolysis products at different temperatures and VRTs.

Carbon number	T = 625 °C														
	VRT = 1.4 s					VRT = 2.8 s					VRT = 5.6 s				
	AKA	AKE	AKD	MAH	PAH	AKA	AKE	AKD	MAH	PAH	AKA	AKE	AKD	MAH	PAH
C1-C4	2.45	14.70	0.00	0.00	0.00	3.83	27.47	0.00	0.00	0.00	5.88	28.44	0.00	0.00	0.00
C5-C10	4.60	14.26	5.32	1.08	0.00	7.43	16.85	9.26	3.53	0.47	7.91	17.58	9.27	7.24	0.67
C11-C15	3.35	10.76	2.95	0.00	0.00	4.24	8.73	1.58	0.08	0.58	3.99	6.23	0.93	0.25	0.90
C16-C20	4.12	9.14	3.17	0.00	0.00	4.57	4.57	0.69	0.47	0.00	3.91	3.03	0.31	0.42	0.00
C21-C25	6.77	9.00	2.35	0.37	0.11	3.19	1.36	0.09	0.11	0.00	2.03	0.59	0.00	0.09	0.00
C26-C31	2.93	1.97	0.28	0.19	0.12	0.82	0.08	0.00	0.00	0.00	0.32	0.00	0.00	0.00	0.00
Total	24.22	59.82	14.08	1.65	0.23	24.08	59.06	11.61	4.20	1.04	24.04	55.86	10.52	8.01	1.57
	T = 650 °C														
	VRT = 1.4 s					VRT = 2.8 s					VRT = 5.6 s				
	AKA	AKE	AKD	MAH	PAH	AKA	AKE	AKD	MAH	PAH	AKA	AKE	AKD	MAH	PAH
C1-C4	2.49	27.54	0.00	0.00	0.00	3.75	40.87	0.00	0.00	0.00	4.60	45.04	0.00	0.00	0.00
C5-C10	4.44	14.08	6.90	2.90	0.24	5.47	12.29	10.41	7.38	0.66	5.30	11.68	10.42	10.72	0.99
C11-C15	2.80	8.05	2.17	0.00	0.08	2.96	4.73	0.63	0.00	0.77	2.45	2.45	0.17	0.00	1.41
C16-C20	3.02	6.27	1.92	0.00	0.00	2.89	2.63	0.00	0.00	0.00	2.20	1.27	0.00	0.00	0.00
C21-C25	4.81	6.19	1.48	0.00	0.00	3.01	1.01	0.00	0.00	0.00	1.14	0.16	0.00	0.00	0.00
C26-C31	2.71	1.77	0.13	0.00	0.00	0.54	0.00	0.00	0.00	0.00	0.00	0.00	0.00	0.00	0.00
Total	20.28	63.90	12.60	2.90	0.32	18.62	61.52	11.05	7.38	1.43	15.69	60.60	10.59	10.72	2.40

Carbon number	T = 675 °C														
	VRT = 1.4 s					VRT = 2.8 s					VRT = 5.6 s				
	AKA	AKE	AKD	MAH	PAH	AKA	AKE	AKD	MAH	PAH	AKA	AKE	AKD	MAH	PAH
C1-C4	4.25	53.20	0.00	0.00	0.00	4.34	54.46	0.00	0.00	0.00	3.79	47.19	0.00	0.00	0.00
C5-C10	4.23	8.39	8.62	8.48	0.64	3.44	6.59	10.77	13.79	1.24	4.08	8.66	8.38	20.52	2.08
C11-C15	1.90	2.29	0.12	0.00	0.63	1.22	0.99	0.00	0.00	1.40	0.78	0.60	0.00	0.00	2.87
C16-C20	1.80	1.30	0.00	0.00	0.00	0.95	0.00	0.00	0.00	0.00	0.55	0.10	0.00	0.00	0.22
C21-C25	2.43	0.64	0.00	0.00	0.00	0.81	0.00	0.00	0.00	0.00	0.19	0.00	0.00	0.00	0.00
C26-C31	1.09	0.00	0.00	0.00	0.00	0.00	0.00	0.00	0.00	0.00	0.00	0.00	0.00	0.00	0.00
Total	15.69	65.83	8.74	8.48	1.26	10.76	62.04	10.77	13.79	2.65	9.40	56.54	8.38	20.52	5.16
AKA: Alkanes, AKE: Alkenes, AKD: Alkadienes, MAH: Monoaromatic hydrocarbons, PAH: Polyaromatic hydrocarbons.															

3.3.4 Relative change in yield of different C number fractions

The relative change of pyrolysis products with VRT can be determined from data in Figure 3.4. For example, as the VRT increases at 625 °C from 1.4 to 2.8 s, a drop in the abundance of medium and high C number (C11-C31) aliphatic hydrocarbons is seen. However, this drop relative to initial value at 1.4 s is not the same for each C number range. Waxes (C21-C31) are the products with the largest relative decrease in peak area percent, followed by diesel range (C11-C20) aliphatics. This relative change (decrease in peak area) is calculated using eq (3.1),

$$Relative\ change = \frac{\%A_{i,L} - \%A_{i,S}}{\%A_{i,S}} \qquad (3.1)$$

where $\%A_{i,S}$ is the peak area percent of the group of compounds i at shorter VRT (i.e., 1.4 s) and $\%A_{i,L}$ is the peak area percent of the group of compounds i at longer VRT (i.e., 2.8 s). Results are presented in Table 3.2.

It is seen that the relative change is greater in magnitude with increasing C number. Low C number aliphatics, showed the opposite behavior with a positive change in abundance. This trend is explained by considering that the vapor pyrolysis reactions only decrease molecular abundance as VRT increases at the very highest C number range, while at the lower C number ranges mechanisms are present that both add and subtract molecules from each C number class. For example, C21-C25 molecules can be added from the next higher C number range and are subtracted by degradation to lower C number ranges. The low C

68

number aliphatics show a positive change, because mechanisms for adding molecules from higher C number ranges overwhelm those for subtraction. Aromatics were the pyrolysis products with highest relative increase with VRT, with a peak area almost three times higher at 2.8 s compared to that at 1.4 s. Table 3.2 also exhibits the effect of temperature in the relative changes. Medium and high C number aliphatics exhibit an increase in their magnitude of relative change with increasing temperature, while gases and gasoline range hydrocarbons had a decrease in their relative change. Also, leveled-off trends are indicated by a relative change close to zero and total degradation, for C26-C31 aliphatics, is indicated by a value of one. Overall, similar trends are seen for relative changes from 2.8 to 5.6 s, though changes were not as high as those from 1.4-2.8 s VRT despite having a considerable difference between these two RTs.

Data from Table 3.2 provides a good insight for the framework of a kinetic model to describe these results by giving a broad view of the interrelation of the different degradation / generation reactions among the different pyrolysis products (to be covered in a subsequent paper). These data are based only in peak area percent calculations and require to be converted to mass percentages to perform the modeling.

Table 3.2. Relative change in peak area percent of different hydrocarbon groups.

Temperature (°C)	VRT increment from 1.4 to 2.8 s						
	C1-C4	C5-C10	C11-C15	C16-C20	C21-C25	C26-C31	Aromatics
625	0.83	0.9	−0.15	−0.40	−0.74	−0.83	1.80
650	0.49	0.11	−0.36	−0.51	−0.68	−0.88	1.73
675	0.02	−0.02	−0.49	−0.69	−0.74	−1.00	0.69
	VRT increment from 2.8 to 5.6 s						
	C1-C4	C5-C10	C11-C15	C16-C20	C21-C25	C26-C31	Aromatics
625	0.10	0.04	−0.23	−0.26	−0.44	−0.65	0.83
650	0.11	−0.03	−0.39	−0.37	−0.67	−1.00	0.49
675	−0.13	0.01	−0.38	−0.31	−0.76	N/A	0.56
Note: Positive values indicate increase and negative indicate decrease.							

3.3.5 Effect of temperature and VRT in the distribution of different chemical classes

Figure 3.5 shows the normalized peak area percentages related to the different chemical classes found in the HDPE pyrolysis products over ranges in C numbers from low (L) to high (H). Normalization of area percentages in each C number category was determined by using the total C number values in Table 3.1 to visually display the relative importance of alkanes, alkenes, alkadienes, and mono and polyaromatic hydrocarbons. One general trend for all pyrolysis temperatures and VRT is that alkenes are predominant at the lowest C numbers (L1) with low percentages of alkanes and a lack of alkadienes. At 625 °C and all VRTs, for the L2 fraction there appears to be a relatively large percentage of alkenes with lower but nearly equal values of alkadienes and alkanes, with monoaromatics gaining as VRT increases. Moving up through the higher C number fractions (M1, M2, H1, H2), the alkane abundance increases at the expense of alkenes and alkadienes, and the trend becomes stronger for higher VRTs. Similar trends in the hydrocarbon chemical classes are seen at 650 and 675 °C with the exception that PAHs become more prevalent at these higher

temperatures. The trends in the shifting of the chemical classes are similar when considering increases in temperature at any VRT.
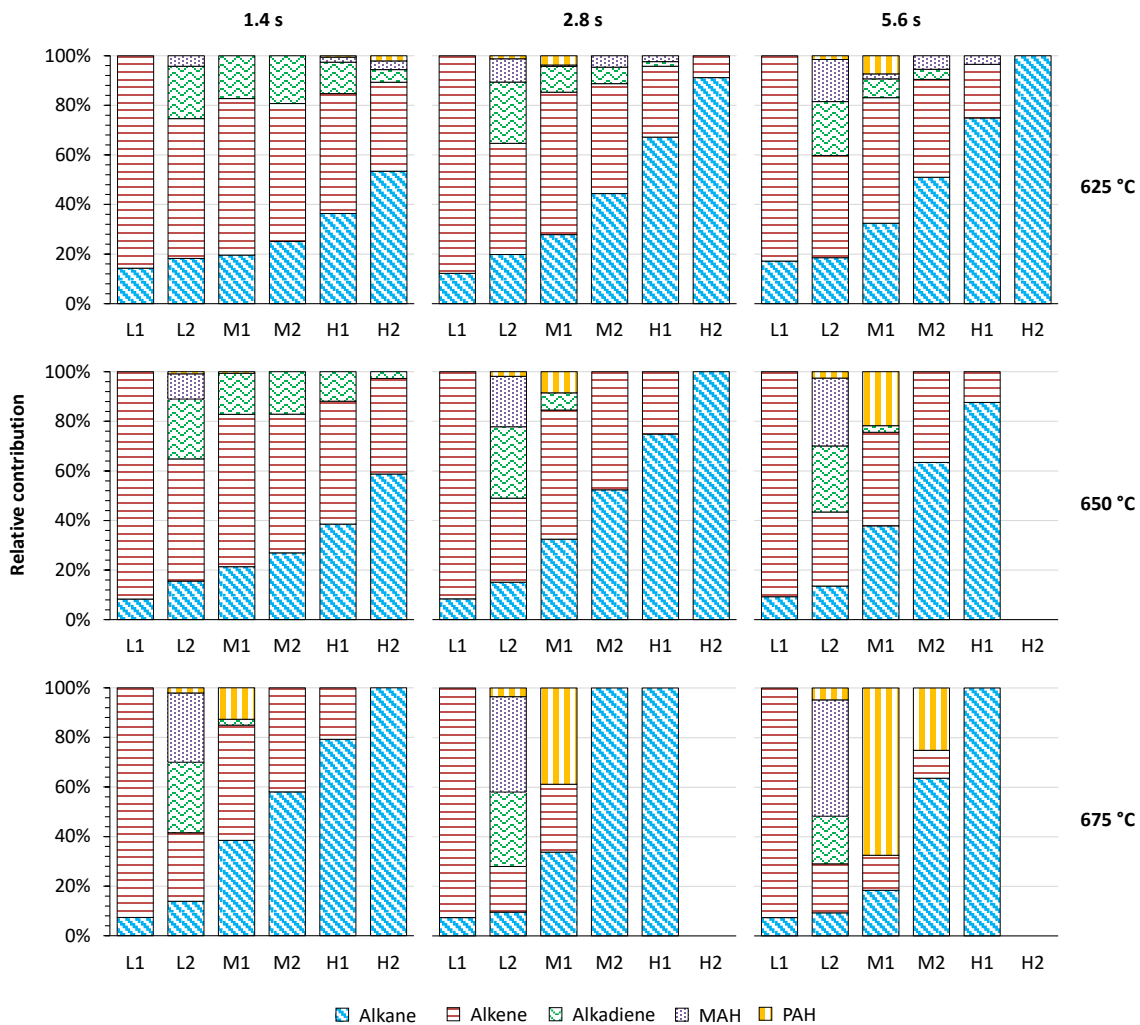
Figure 3.5. Chemical class distribution among carbon number as a function of temperature and residence time (L1: C1-C4, L2: C5-C10, M1: C11-C15, M2: C16-C20, H1: C21-C25, H2: C26-C31).

3.3.6 Pyrolysis of waste HDPE at 700 °C and zero VRT

In order to compare two-state to one-stage operation (the normal operation of the micropyrolysis apparatus), primary pyrolysis reactions were evaluated using only the probe connected to the CDS 5200 HP unit (one-stage micropyrolysis). The high heating rate and short RT (0.009 s) of the vapors in the heated coil ensure that mostly primary degradation takes place.[19, 25-27] The temperature of this experiment was increased to 700 °C compared to the lower temperatures in the TSMR experiments to avoid condensation of high C number products that occurred at lower pyrolysis temperatures. The product distribution obtained at this condition is presented in Figure 3.6 (see also Table B-17 in Appendix B). The major trend is that peak area percent increases with the increase in C number, with C21-C25 waxes as the most abundant product. However, due to the short RT and lower temperatures at the pyroprobe transfer line, condensation of higher C number waxes (above C31) may have taken place, possibly producing a lower abundance when detected in the GC/MS equipment. In contrast with the experiments carrying out secondary degradation, aromatics were just above the cut off limit with an abundance of 0.1% and benzene being the only identified compound.
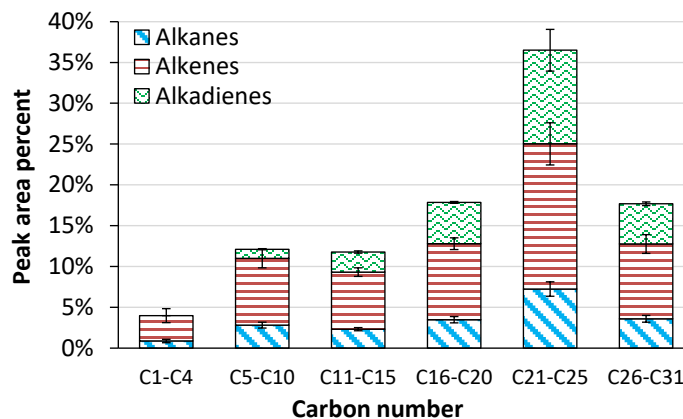
Figure 3.6. Distribution of micropyrolysis products by carbon number and chemical class for 700ºC and zero VRT.

The product distribution in Figure 3.6 is similar to that observed by other studies analyzing primary degradation in pyroprobe units[25, 28, 29] or reactor configurations with VRT close to zero seconds.[11, 30] Data from these studies showed that for C1-C8 compounds a small peak area percent is obtained. However, starting at C10 the percentage increased in those studies to a maximum at C16-C18, and then lowering again, obtaining smaller percentages at C25. Near zero VRT results reported here differ greatly from simulations of primary reactions of random scission reported previously,[24, 31] which usually show an even abundance for all C number compounds. Therefore, primary degradation of PE may be driven by not only random scission but also through a chain-end scission mechanism promoted by high temperature. This chain-end scission mechanism is based on, among others, intramolecular radical transfers, also known as back biting reactions.[32, 33] Figure 3.6 results imply that a random scission mechanism will induce first C-C dissociation followed by a backbiting mechanism; however, due to the high heating rates achieved in the pyroprobe, these two mechanisms can be considered to occur simultaneously, although backbiting seems to be

dominant. β-Scission is another mechanism favored at high temperatures, where the radical formed by backbiting forms an olefin and another primary radical.[24] This primary radical can be converted to an alkane, through intermolecular hydrogen transfer, or another olefin, by another β-scission. Hence, the amount of alkenes generated in primary degradation is greater than that of alkanes and alkadienes, as shown in Figure 3.6.

3.3.7 Comparison of the TSMR performance with different reactor configurations

Other reactor configurations from the literature that have been used to evaluate the product distribution of HDPE pyrolysis are shown in Table 3.3. Similar effects on product distribution due to temperature and VRT changes are observed between these reactors and the TSMR. For example, the literature shows that higher amounts of waxes and liquids are produced at lower temperatures and VRTs while gases rise in amount with increasing temperature and VRT. Also, a slight increment on liquid fraction is seen at the highest temperature and VRT due to aromatics formation. Table 3.3 shows that in the fluidized bed reactor (FBR),[21, 34] low temperature (600 °C) produces a small amount of gases (15%) with a similar distribution of liquids and waxes. When the temperature increases, above 660 °C, gases increase their production with liquids and waxes decreasing in amount. However, the yield of gases above 675 °C is not as high as that reported in our study (58% of peak area), although the RTs are similar (~1 s). When pyrolysis reactors operate in continuous mode (CFBR),[12, 13, 18] the effect of temperature is similar to that observed in the TSMR, at VRTs ranging from 1.5 to 2.6 s. However, at 2.6 s and 650 °C, Mastral et al.[12] found that yield of gases is lower and production of waxes is higher, than the observed values at VRT of 2.8

74

s in our study at the same temperature. These researchers also observed a reduction in the yield of gases at 650 °C while increasing VRT from 1.5 to 2.6 s, which may indicate production of aromatics in their apparatus or may be a result of nonideal mixing affecting the actual RT. A reduction in yield of gases was observed at 675 °C with a change in VRT from 2.8 to 5.6 s in our study. The small VRT (0.01 s) of the conical spouted bed reactor (CSBR),[14] provides a similar product distribution to that obtained during primary degradation (see section 3.6) which is not comparable to that observed in two-stage pyrolysis, although the trend of higher production of low C number compounds with increasing temperature is still shown.

Table 3.3. Composition of HDPE pyrolysis fractions under different reactor configurations and operation conditions.

Type of reactor	T (°C)	VRT (s)	Gases (%)	Liquids (%)	Waxes (%)	Reference
FBR[a]	600	1.5	15.2	40.9	43.9	Hernández et al.[21]
	700	1.5	32.4	37.6	30.0	
CFBR[b]	640	1.5	28.1	45.7	26.2	Mastral et al.[13]
	650	2.6	32.6	50.3	17.1	
	685	1.5	59.1	39.4	1.4	
	685	2.6	61.9	37.4	0.7	
CFBR	650	1.5	31.5	34.5	34.1	Berrueco et al.[18]
	685	1.7	67.9	30.5	1.5	
	685	2.1	59.3	40.7	0.0	
CFBR	650	1.5	31.5	68.5[e]		Mastral et al.[12]
	650	2.6	22.1	72.3[e]		
	700	1.7	64.2	32.1[e]		
	685	2.1	55.9	40.7[e]		
FBR	660	1.0	36.6	61.0	2.4	Jung et al.[34]
	680	1.0	42.8	56.7	0.5	
CSBR[c]	600	0.01	5.5	41.2	53.3	Elordi et al.[14]
	650	0.01	14.4	48.7	36.9	
	700	0.01	39.6	48.6	11.8	
TSMR[d]	625[g]	1.4	17.5	58.4	24.1	This study[f]
	625[g]	2.8	31.3	63.0	5.7	
	625[g]	5.6	34.3	62.7	3.0	
	650[g]	1.4	30.3	52.6	17.1	
	650[g]	2.8	44.6	50.8	4.6	
	650[g]	5.6	49.6	49.1	1.3	
	675[g]	1.4	57.5	38.3	4.2	
	675[g]	2.8	58.8	40.4	0.8	
	675[g]	5.6	51.0	48.8	0.2	

[a]FBR: Fluidized bed reactor. [b]CFBR: Continuous fluidized bed reactor. [c]CSBR: Continuous spouted bed reactor. [d]TSMR: Two-stage micropyrolysis reactor (this study). [e]: Percentage of oil and waxes together. [f]: Qualitative percentages taken form peak area. [g]: Temperature for both primary and secondary degradation.

Table 3.3 highlights that product distribution in the TSMR is similar to that of larger-scale FBRs and CFBRs at temperatures ranging from 600 to 700 °C, although some of these studies reported a difficult control at high temperatures[13, 34] or a nonisothermal profile within the equipment.[18, 21] The TSMR designed in our study has advantages compared to larger-scale equipment by providing a fast (~20 min) heat up period from room temperature to pyrolysis conditions and accurate temperature control that reduces the variability between experiments. The precise control of VRT through the micropyrolysis system provided a good repeatability of the experiments as exhibited by the small error bars in Figure 3.4. In addition to flow rate of inert gas in the TSMR, VRT can also be adjusted by modifying the length of the reactor surface covered by the heating tape or adjusting the inside diameter. Pyrolysis systems with a subsequent vapor degradation have been used to study PE thermal cracking[11, 30, 35, 36] and standard compounds degradation.[20] These systems have demonstrated a promising scenario for the two-stage thermal cracking, as an alternative to catalytic degradation, with increasing gases and aromatics generation with raising temperature and VRT. The TSMR reported in our work conjugates the direct analysis of the pyrolysis products through GC/MS, the ability of direct processing of solid samples and a wide range of temperatures and VRTs for testing pyrolysis. Some disadvantages of the TSMR relative to other reactor configurations are not being able to operate in a continuous mode and a concern about whether such small solid samples can actually represent the bulk of the material. Our results show that the TSMR is able to provide representative results for waste HDPE with such small samples due to the

77

homogeneous nature of the material. For biomass samples, representativeness may become an issue and may result in larger error bars on data trends.

Table 3.4 shows a comparison of the TSMR with other studies analyzing two-stage HDPE pyrolysis. Although some of the temperature ranges for primary and secondary degradation and VRTs are different, previously discussed trends of composition of gases, liquids, and waxes with respect to pyrolysis temperature and VRT are still occurring in these two-stage systems.

Table 3.4. Comparison of the TSMR with two-stage HDPE pyrolysis studies.

Type of reactor	$T_{primary}$ (°C)	$T_{secondary}$ (°C)	$VRT_{secondary}$ (s)	Gases (%)	Liquids (%)	Waxes (%)	Reference
CSBR and multitubular reactor	500	850	0.016	77.9	22.1[a]		Artetxe et al.[11]
	500	850	0.032	80.7	19.3[a]		
	500	900	0.016	79.2	20.9[a]		
	500	900	0.032	84.7	15.3[a]		
Free-fall reactors	600	600	2.08	7.7	31.9	60.4	Mastral et al.[37]
	600	600	8.98	14.3	14.4	71.3	
	600	800	1.84	46.1	16.5	37.4	
	600	800	6.80	33.8	18.3	47.9	
	600	1000	1.58	35.9	12.4	51.7	
	600	1000	5.77	34.0	4.6	61.4	
TSMR	625	625	1.4	17.5	58.4	24.1	This study[b]
	625	625	2.8	31.3	63.0	5.7	
	625	625	5.6	34.3	62.7	3.0	
	650	650	1.4	30.3	52.6	17.1	
	650	650	2.8	44.6	50.8	4.6	
	650	650	5.6	49.6	49.1	1.3	
	675	675	1.4	57.5	38.3	4.2	
	675	675	2.8	58.8	40.4	0.8	
	675	675	5.6	51.0	48.8	0.2	

[a]: Percentage of oil and waxes together. [b]: Qualitative percentages taken form peak area.

3.3.8 General mechanism of HDPE degradation at two-stages

According to the observed results and current literature, the following sequence of reactions occurs during primary and subsequent secondary degradation of the HDPE pyrolysis products. C-C bonds have a high dissociation energy (340 kJ/mol) that requires high temperature (above 550 °C) to induce initial breaking of the bonds.[5, 22] When HDPE is exposed to high temperatures (625-675 °C) in the pyroprobe, a random scission mechanism is activated in the melted HDPE (liquid phase). Random scission is rapidly followed by a chain end scission mechanism in the gas-liquid polymer interface, promoted by the breaking of C-H bonds and intramolecular transfer (back biting) of these hydrogen atoms to the primary radicals formed.[32] Both mechanisms occur simultaneously, therefore a wide variation of C number compounds is obtained. However, backbiting is the favored pathway as highlighted by the higher amount of medium and high C number alkenes and low production of gases (see Figure 3.6). When these vapors enter the second stage of the TSMR, a different series of degradation reactions and radical stabilization processes take place. At lower temperature, hydrogen abstraction (intramolecular) is the preferred mechanism because this requires less energy to stabilize the primary radicals from primary degradation.[22] As a result, high C number alkanes (Figure 3.5) and secondary radicals are formed. With temperature increase, intermolecular hydrogen transfer and radical transfer from the chain end to the fifth, ninth, 13th, and 17th carbons; as described by Ueno et al.[24], are favored increasing the production of gasoline range liquids and secondary radicals that lead to alkenes and alkadienes formation. Higher temperatures favor the stabilization of secondary radicals by hydrogen abstraction from one of the adjacent carbons, forming

alkanes or alkadienes and a primary radical in a mechanism known as β-scission.[38] Temperature increase also reduces the frequency of radical transfer leading to β-scission occurring at the chain end, which produces gaseous alkenes. High temperatures also form MAHs by Diels-Alder reaction[23, 34, 39] or cyclization[22, 23] followed by dehydrogenation, and PAHs through aryl-aryl coupling.[20]

Data in Table 3.1 shows that at 625 °C the favored mechanisms are chain end scission and intramolecular hydrogen transfer. However, when temperature increased to 650 °C radical transfer and intermolecular hydrogen transfer develop faster, and at 675 °C β-scission followed by Diels-Alder, cyclization, and aryl-aryl coupling reactions are predominant. VRT does not appear to have an effect on the mechanism of degradation; however, it has a significant impact in the extent of these mechanisms.

3.4 Conclusions

Changes in temperature and VRT had a strong influence on waste HDPE pyrolysis product distribution with respect to C number range and chemical class that is better understood from these experiments. Pyrolysis products from gases, liquids in the C-ranges of gasoline, diesel, or jet fuel, and waxes can be obtained in any relative proportion through manipulation of these variables. Low temperature and VRT produced diesel hydrocarbons combined with gasoline and gases, moderate temperature and short VRT produced gases and gasoline fuels, high temperature and short VRT produce gases that can be used as monomers for plastic production, and high temperature and long VRT generate gases and aromatics (see Table 3.3).

The TSMR has proved to be a useful tool for the study of secondary degradation of waste HDPE. Data obtained from this apparatus showed a close correlation with larger-scale equipment, but with the advantage of a precise control over heating rate and temperature not found in other reactor configurations. It also showed a significant improvement over conventional micropyrolysis, due to the opportunity to control VRT that can span a wide range of practical interest in pyrolysis. Product distribution also confirmed the known free-radical degradation mechanisms, which supports the adequate performance of the system. The results provide a strong background to formulate a kinetic mechanism that predict chemical class and C number distribution as a function of temperature and VRT.

3.5 Acknowledgements

3.6 References

(1)   United Nations Environment Programme (UNEP) *Valuing Plastic. The Business Case for Measuring, Managing and Disclosing Plastic Use in the Consumer Goods Industry*; Report No. DEP/1819/NA; UNEP: Nairobi, Kenya, 2014.

(2)   Plastics Europe. The Plastic Industry. https://committee.iso.org/files/live/sites/tc61/files/The%20Plastic%20Industry%20Berlin%20Aug%202016%20-%20Copy.pdf (accessed July 17, 2017).

(3)   Al-Salem, S. M.; Lettieri, P.; Baeyens, J. Recycling and recovery routes of plastic solid waste (PSW): A review. *Waste Manage.* **2009,** 29, 2625-2643.

(4)   Singh, N.; Hui, D.; Singh, R.; Ahuja, I. P. S.; Feo, L.; Fraternali, F. Recycling of plastic solid waste: A state of art review and future applications. *Composites Part B* **2017,** 115, 409-422.

(5)   Williams, E. A.; Williams, P. T. The pyrolysis of individual plastics and a plastic mixture in a fixed bed reactor. *J. Chem. Technol. Biotechnol.* **1997,** 70, 9-20.

(6)   Williams, P. T.; Williams, E. A. Interaction of Plastics in Mixed-Plastics Pyrolysis. *Energy Fuels* **1999,** 13, 188-196.

(7)   Anuar Sharuddin, S. D.; Abnisa, F.; Wan Daud, W. M. A.; Aroua, M. K. A review on pyrolysis of plastic wastes. *Energy Convers. Manage.* **2016,** 115, 308-326.

(8)   Lopez, G.; Artetxe, M.; Amutio, M.; Bilbao, J.; Olazar, M. Thermochemical routes for the valorization of waste polyolefinic plastics to produce fuels and chemicals. A review. *Renewable Sustainable Energy Rev.* **2017,** 73, 346-368.

(9)   American Chemistry Council. Economic Impact of Plastics-to-Oil Facilities in the U.S. https://plastics.americanchemistry.com/Stand-Alone-Content/Economic-Impact-of-Plastics-to-Oil-Facilities.pdf (accessed July 19, 2017).

(10)   Patni, N.; Shah, P.; Agarwal, S.; Singhal, P. Alternate strategies for conversion of waste plastic to fuels. *ISRN Renewable Energy* **2013,** 2013, Article ID 902053.

(11)   Artetxe, M.; Lopez, G.; Elordi, G.; Amutio, M.; Bilbao, J.; Olazar, M. Production of Light Olefins from Polyethylene in a Two-Step Process: Pyrolysis in a Conical Spouted Bed and Downstream High-Temperature Thermal Cracking. *Ind. Eng. Chem. Res.* **2012,** 51, 13915-13923.

(12)   Mastral, F. J.; Esperanza, E.; García, P.; Juste, M. Pyrolysis of high-density polyethylene in a fluidised bed reactor. Influence of the temperature and residence time. *J. Anal. Appl. Pyrolysis* **2002,** 63, 1-15.

(13)   Mastral, J. F.; Berrueco, C.; Ceamanos, J. Modelling of the pyrolysis of high density polyethylene. *J. Anal. Appl. Pyrolysis* **2007,** 79, 313-322.

(14)   Elordi, G.; Olazar, M.; Lopez, G.; Artetxe, M.; Bilbao, J. Product Yields and Compositions in the Continuous Pyrolysis of High-Density Polyethylene in a Conical Spouted Bed Reactor. *Ind. Eng. Chem. Res.* **2011,** 50, 6650-6659.

(15)   Butler, E.; Devlin, G.; McDonnell, K. Waste Polyolefins to Liquid Fuels via Pyrolysis: Review of Commercial State-of-the-Art and Recent Laboratory Research. *Waste Biomass Valorization* **2011,** 2, 227-255.

(16)   Lebedev, A. T., Introduction to Mass Spectra Interpretation: Organic Chemistry. In *Mass Spectrometry: Instrumentation, Interpretations, and Applications*, Elkman, R.; Silberring, J.; Westman-Brinkmalm, A.; Kraj, A., Eds. John Wiley & Sons, Inc.: Hoboken, NJ, 2009; pp 119-178.

(17)   Stein, S. E., Mass Spectra. In *NIST Chemistry WebBook, NIST Standard Reference Database Number 69*, Linstrom, P. J.; Mallard, W. G., Eds. National Institute of Standards and Technology: Gaithersburg, MD, 2017.

(18)   Berrueco, C.; Mastral, F. J.; Esperanza, E.; Ceamanos, J. Production of Waxes and Tars from the Continuous Pyrolysis of High Density Polyethylene. Influence of Operation Variables. *Energy Fuels* **2002,** 16, 1148-1153.

(19)   Hernández, M. d. R.; García, Á. N.; Gómez, A.; Agulló, J.; Marcilla, A. Effect of Residence Time on Volatile Products Obtained in the HDPE Pyrolysis in the Presence and Absence of HZSM-5. *Ind. Eng. Chem. Res.* **2006,** 45, 8770-8778.

(20)   Ross, A. B.; Lea-Langton, A.; Fitzpatrick, E. M.; Jones, J. M.; Williams, A.; Andrews, G. E.; Li, H.; Bartle, K. D. Investigation of Pyrolysis of Hydrocarbons and Biomass Model Compounds Using a Micropyrolysis Flow Cell. *Energy Fuels* **2011,** 25, 2945-2955.

(21)   Hernández, M. d. R.; García, Á. N.; Marcilla, A. Catalytic flash pyrolysis of HDPE in a fluidized bed reactor for recovery of fuel-like hydrocarbons. *J. Anal. Appl. Pyrolysis* **2007,** 78, 272-281.

(22)   Kumar, S.; Panda, A. K.; Singh, R. A review on tertiary recycling of high-density polyethylene to fuel. *Resour. Conserv. Recycl.* **2011,** 55, 893-910.

(23)   López, A.; de Marco, I.; Caballero, B. M.; Laresgoiti, M. F.; Adrados, A. Influence of time and temperature on pyrolysis of plastic wastes in a semi-batch reactor. *Chem. Eng. J.* **2011,** 173, 62-71.

(24)   Ueno, T.; Nakashima, E.; Takeda, K. Quantitative analysis of random scission and chain-end scission in the thermal degradation of polyethylene. *Polym. Degrad. Stab.* **2010,** 95, 1862-1869.

(25)   Hernández, M. d. R.; Gómez, A.; García, Á. N.; Agulló, J.; Marcilla, A. Effect of the temperature in the nature and extension of the primary and secondary reactions in the thermal and HZSM-5 catalytic pyrolysis of HDPE. *Appl. Catal., A* **2007,** 317, 183-194.

(26)   Klemetsrud, B.; Eatherton, D.; Shonnard, D. Effects of Lignin Content and Temperature on the Properties of Hybrid Poplar Bio-Oil, Char, and Gas Obtained by Fast Pyrolysis. *Energy Fuels* **2017,** 31, 2879-2886.

(27)   Klemetsrud, B.; Klinger, J.; Ziv, E. B.; Shonnard, D. A Kinetic Study of the Fast Micro-Pyrolysis of Hybrid Poplar. *J. Anal. Appl. Pyrolysis* **2017,** 128, 353-362.

(28)   Chen, W.; Shi, S.; Chen, M.; Zhou, X. Fast co-pyrolysis of waste newspaper with high-density polyethylene for high yields of alcohols and hydrocarbons. *Waste Manage.* **2017,** 67, 155-162.

(29)   Blazsó, M. In situ modification of pyrolysis products of macromolecules in an analytical pyrolyser. *J. Anal. Appl. Pyrolysis* **2005,** 74, 344-352.

(30)   Della Zassa, M.; Favero, M.; Canu, P. Two-steps selective thermal depolymerization of polyethylene. 1: Feasibility and effect of devolatilization heating policy. *J. Anal. Appl. Pyrolysis* **2010,** 87, 248-255.

(31)   Németh, A.; Blazsó, M.; Baranyai, P.; Vidóczy, T. Thermal degradation of polyethylene modeled on tetracontane. *J. Anal. Appl. Pyrolysis* **2008,** 81, 237-242.

(32)   Murata, K.; Hirano, Y.; Sakata, Y.; Uddin, M. A. Basic study on a continuous flow reactor for thermal degradation of polymers. *J. Anal. Appl. Pyrolysis* **2002,** 65, 71-90.

(33)   Levine, S. E.; Broadbelt, L. J. Detailed mechanistic modeling of high-density polyethylene pyrolysis: Low molecular weight product evolution. *Polym. Degrad. Stab.* **2009,** 94, 810-822.

(34)   Jung, S.-H.; Cho, M.-H.; Kang, B.-S.; Kim, J.-S. Pyrolysis of a fraction of waste polypropylene and polyethylene for the recovery of BTX aromatics using a fluidized bed reactor. *Fuel Process. Technol.* **2010,** 91, 277-284.

(35)   Artetxe, M.; Lopez, G.; Amutio, M.; Elordi, G.; Bilbao, J.; Olazar, M. Light olefins from HDPE cracking in a two-step thermal and catalytic process. *Chem. Eng. J.* **2012,** 207, 27-34.

(36)   Aguado, J.; Serrano, D.; San Miguel, G.; Castro, M.; Madrid, S. Feedstock recycling of polyethylene in a two-step thermo-catalytic reaction system. *J. Anal. Appl. Pyrolysis* **2007,** 79, 415-423.

(37)   Mastral, J. F.; Berrueco, C.; Ceamanos, J. Pyrolysis of High-Density Polyethylene in Free-Fall Reactors in Series. *Energy Fuels* **2006,** 20, 1365-1371.

(38)   Bockhorn, H.; Hornung, A.; Hornung, U. Mechanisms and kinetics of thermal decomposition of plastics from isothermal and dynamic measurements. *J. Anal. Appl. Pyrolysis* **1999,** 50, 77-101.

(39)   Lopez, G.; Erkiaga, A.; Amutio, M.; Bilbao, J.; Olazar, M. Effect of polyethylene co-feeding in the steam gasification of biomass in a conical spouted bed reactor. *Fuel* **2015,** 153, 393-401.

4 Systems Analysis of High-value Chemicals and Fuels from a Waste High-Density Polyethylene Refinery. Part 1: Conceptual Design and Techno-economic Assessment[3]

Abstract

The increasing amount of plastic waste generation has become an important concern for government agencies due to the leveled off recycling rates presented recently. On this scenario, chemical recycling raises as an interesting technology due to the potential reduction of pollutant and particle emissions and the establishment of a circular economy through the production of monomers and fuels. However, there is scarce information of industrial scale processes of this technology and their energetic, economic, and environmental performance. Therefore, the present process modeling study presents a novel multiproduct/multiprocessing pyrolysis-based refinery for the conversion of 500 tonnes/day of high-density polyethylene (HDPE) waste. The products obtained from the refinery were chemical grade ethylene and propylene, an aromatics mixture, and low- and high-molecular weight hydrocarbon mixtures (MWHCs). Part 1 of this study focuses on the energetic and economic evaluation of the refinery and the potential effects that heat integration could induce. The energy efficiency was 72 and 77% for the base case and the heat integrated refinery, respectively. The net present values (NPVs) were 367 and 383 million U.S. dollars (MM USD), for the base case and the heat integrated process,

---

[3] This chapter will be submitted to *ACS Sustainable Chemistry and Engineering*.

respectively. These results suggest energetic and economic sustainability of the design and its promising application on an industrial scale.

4.1 Introduction

Continuous population growth and its interrelated use of resources has placed a major concern in the increasing amount of waste generated in many countries. For example, in the U.S. only, 238 million tonnes of municipal solid waste were generated in 2015, the highest value ever recorded since 1960.[1] From this amount, 31.3 million tonnes (13.1%) are plastic waste (PW), which generation has increased at an average rate of 0.62 million tonnes/yr since 2000.[2] According to the U.S. Environmental Protection Agency (EPA), 75 % of this PW is discarded in landfills, 16% combusted for energy recovery, and only 9% is recycled. PW's is a valuable resource because it has a similar heating value to other fuels.[3,4] It also is a potential source for chemicals and fuels production. Thus, its disposal in landfills is considered a misspend of its benefits to the energetic and industrial sectors.[5]

Although energy recovery exploits the embodied energy of PW, the accompanying emission of hazardous compounds and particles have reduced its overall acceptability.[6,7] Therefore, chemical recycling stands as the most favorable option from an environmental perspective and also provides a base for the development of a circular economy of plastic.[8] This has been proved by various researchers studying pyrolysis, a process of chemical recycling that degrades plastic using temperature and high heating rates within an oxygen-free environment. Pyrolysis has been widely applied to polyolefins and has shown that these molecules can break into the monomers that were originally used for their production

at certain temperatures and reactor residence times.[9-11] However, due to the long hydrocarbon (HC) structure of polyolefins and the different pyrolysis reactions taking place, monomers are not the only product formed. A wide range of products are generated through pyrolysis: aromatics, low molecular weight gases, gasoline and diesel range HCs, and waxes.[11,12] It is precisely in the fuel range HCs where most of the efforts of the industrial scale-up of polyolefins pyrolysis has been focused on the recent years, possibly as a result of their capacity to fulfill HC fuels demand but with a reduced emission of greenhouse gases (GHGs).[13]

On this regard, there is a raising concern of the economic implications of pyrolysis of polyolefins beyond the laboratory and pilot plant scales. Compared to other renewable sources of fuels, i.e. woody biomass, there are few studies reporting techno-economic analyses (TEA) of plastic to fuel technologies, like the one presented by Sahu et al.[7] Their process consisted of a fluidized bed reactor (operated at 500 °C) followed by two separation units that produced light and heavy fuel oils processing 10, 60, and 100 thousand tonnes/yr of a mixture of polyolefins and polystyrene (PS). The increased capacity showed an increment from 4.2 to 35.7% in the return on investment indicator (ROI) and a reduced payback period from 24 to 3 years for the smaller and longer capacities, respectively. More recently, Fivga and Dimitriou[14] analyzed the economic performance of a pilot process from a recycling company that transformed 700 tonnes/yr of PW into heavy fuel oil. This plant showed an efficient use of energy because all the heating requirements were met by the char and gases produced, but the net present value (NPV) for 20 years was negative.

Similarly to Sahu et al.,[7] a scale up analysis showed a raise in the NPV and the payback period of the plant.

Focusing on monomer production, one of the first studies was presented by Westerhout et al.[15] who evaluated the cost of high temperature pyrolysis (625-840 °C) of a plastics mixture using different reactor types and its downstream separation. Their most important findings were that higher pyrolysis temperatures increase the capital investment, higher plant capacity favors the ROI of the plant, and the inclusion of a separation train causes a negative ROI, even for the highest capacity tested (100,000 tonnes/yr). The main reason for this was that the low processing capacity of the separation train could not compensate its high capital cost. Vargas Santillan et al.[16] targeted the pyrolysis of 182,500 tonnes/yr of polyethylene to produce chemical grade ethylene and propylene along with ethanol. The pyrolysis process occurred at 850 °C, followed by a distillation sequence where high purity ethylene and propylene are obtained. The purified ethylene was then processed through hydration to produce ethanol. The authors calculated a product sale to production costs ratio of 2.54, which proves the feasibility of the project. Comparing the results from Westerhout et al.[15] and Vargas Santillan et al.[16], it can be inferred that a multiproduct and multiprocessing approach can favor the economic performance of the chemical recycling of polyolefins. This effect is also shown by Al-Salem et al.[4] who concluded that the inclusion of a pyrolysis process to an existing recovery and incineration facility increased the NPV of the process.

The information above highlights the absence of designs that combine fuel oil and monomer production in one facility that could eventually improve the economic feasibility of both technologies. Aromatics are another product from pyrolysis at high temperatures that promote monomer production,[9,17] so there is a potential to also commercialize them an increase the offer of products from the refinery. It is also noteworthy that there are no studies that have included the conversion of light and heavy fuel oil to gasoline and diesel by means of hydrotreatment. Therefore, the present study attempts to fill these gaps by proposing the conceptual design of a multiproduct and multiprocessing refinery that converts waste HDPE into value-added chemicals like ethylene, propylene, and aromatics, and fuels that can be used as alternatives to gasoline and diesel. This first report is focused on the principles of the conceptual design and its effects on the energetic and economic sustainability of the refinery through the application of TEA and heat integration.

4.2 Materials and methods

4.2.1 Conceptual design of the refinery

The refinery was designed to process 500 tonnes of waste HDPE per day. All unit operations and material and energy balances were modeled and estimated using the software Aspen Plus v.8.8 (Aspen Technology Inc.). Thermal properties of waste HDPE were estimated using proximate and ultimate analysis from He et al.[18] and yields from pyrolysis products were taken from the reported experiments by Gracida-Alvarez et al.[9] These results were converted from qualitative to quantitative percentages using standard mixtures and correlations presented in section C.1 of Appendix C. The Peng-Robinson

equation of state predicted the vapor-liquid equilibrium for the refinery due to its reliability in modelling processes that involve HC mixtures, except for the aromatics extraction process (see section 4.2.1.3).[19] The schematic diagram of the refinery (Figure 4.1) shows the four integrity sections of the process: pyrolysis (A-100), monomer separation (A-200), aromatics extraction (A-300), and hydrotreatment (A-400) which are described in the following sections. Detailed diagrams of each section, including equipment codes and stream properties, are presented in Figures C-3 to C-6 of Appendix C.
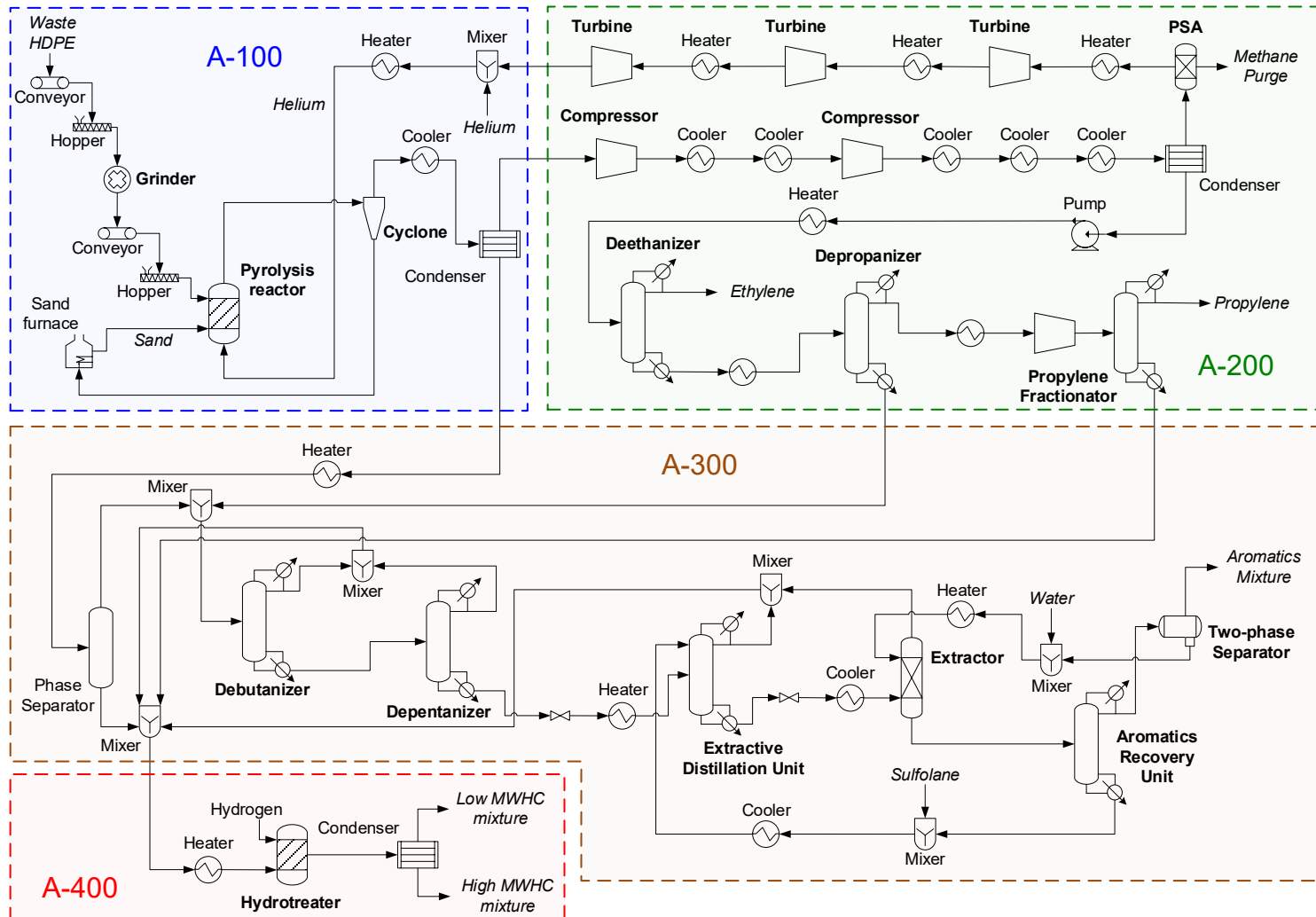
Figure 4.1. Schematic diagram of the different sections of the base case of the waste HDPE refinery. A-100: Pyrolysis, A-200: Monomer separation, A-300: Aromatics extraction, A-400: Hydrotreatment, PSA: Process swing absorption.

4.2.1.1 Pyrolysis section (A-100)

The process begins with the size reduction of the feedstock (waste HDPE) in a hammer mill (GR-101), requiring a power input of 300 kWh/tonne.[20] The granulate particles of HDPE are fed to a fluidized bed reactor (FBR) operating at 650 °C. Along with the temperature, vapor residence time is crucial to control the distribution of the pyrolysis products, therefore, the residence in the reactor (R-103) is set to 2.8 s, to ensure a wide variety of products like monomers, aromatics and fuels.[9] Helium gas is used as the fluidizing agent and supplied in a HDPE/helium mass ratio of 2.04.[21] Sand, which is modeled as silicon dioxide, is used as the heat transfer agent to keep the reactor at the required temperature. Helium from section A-200 is heated from −26 °C to 650 °C before entering the reactor (E-106). Because HDPE is fed at 25 °C to the FBR, sand is heated in a furnace (E-105) to 1200 °C to provide the necessary heat to perform the pyrolysis. The sand from the FBR outlet is recovered in a cyclone and sent back to the furnace. The pyrolysis gases and vapors are cooled down to 15 °C, using a water cooler (E-107) and a refrigeration condenser (E-108), to separate the light gases (C1-C4 HCs) from heavier fractions (C5-C29 HCs). The light gases and heavier fractions are sent to sections A-200 and A-300, respectively, for downstream processing.

4.2.1.2 Monomer separation section (A-200)

Once C1-C4 HCs and helium are separated they are pressurized up to 7 bars through a series of compressors (C-201 and C-203) and cooled down to −136 °C through a system

of refrigeration coolers (E-202 A and B and E-204 A-C) and a refrigeration condenser (E-205). The light fraction comprises helium and methane, which are separated afterwards through pressure swing adsorption (PSA). PSA under cryogenic temperatures is effective in purifying inert gases when mixed with methane.[22] Helium is depressurized, heated (units E-212 to C-217) and recycled back to the pyrolysis reactor and methane is used for heating up the sand (see section 4.3.2). Literature data from ethylene plants[23] served as the basis to set the separation sequence of the refinery. The heavy fraction from the condenser (E-205), comprising C2 to C4 HCs, is pressurized to 25 bar, heated up to 2 °C and fed to the de-ethanizer column (T-207) to obtain chemical grade (97.2% purity) ethylene in the distillate. Then, C4 HCs are removed in a depropanizer column (T-209) and the C3 fraction is separated in a propylene fractionator (T-211) where chemical grade (97.8% purity) propylene is collected in the distillate. The bottoms of the depropanizer column and the propylene fractionator are sent to sections A-300 and A-400, respectively, for further processing.

4.2.1.3 Aromatics extraction section (A-300)

The streams coming from sections A-100 and A-200 are mixed and then sent to a separation train. C4 HCs are removed in the debutanizer column (T-305), operated at 7.5 bar, and C5 HCs are taken out at the depentanizer column (T-306), that works at 4.5 bar. These fractions are sent to section A-400 to be hydrotreated. The main purpose of section A-300 is the extraction of aromatic HCs in a mixture that might be supplied to benzene-toluene-xylenes (BTX) facilities. The conceptual design of the extraction process is based on the sulfolane

process designed by UOP,[24] which has been adapted to the feed composition estimated for this refinery. Its outstanding properties like selectivity to aromatics, solubility in water, solvent capability for HCs, and high boiling point, made sulfolane the chosen solvent for extraction.[25] As suggested by various studies,[26,27] the aromatics extraction process uses the UNIQUAC equation of state for its modelling.

The bottoms of the depentanizer are sent to the extractive distillation column (T-308) where sulfolane removes around 66% of C6-C12 aliphatic HCs using a solvent-to-feed ratio of 2 (mass basis). Both the solvent and the feed are supplied at 160 °C to improve the extraction. The distillate, rich in aliphatic HCs, is sent to section A-400 while the bottoms are cooled down to 70 °C and fed to a wash column (T-310) to remove aliphatic HCs with a carbon number greater than 12. This extractor uses water at 90 °C as solvent, with a solvent-to-feed ratio of 0.06, which clears almost 95% of heavy aliphatic HCs. The raffinate is also directed to section A-400 for hydrotreatment and the extract is processed in an aromatics recovery column (T-312) working at atmospheric pressure. The distillate consists of a mixture of aromatics, traces of aliphatic HCs, and water whilst the bottoms contains sulfolane with 98.3% purity that is recycled to the extractive distillation column. A two-phase separator (V-313) reduces the water content of the distillate to yield a product with an aromatic content of 84%. Water from the bottoms of the separator is recycled to the wash column. The process requires make-up streams of sulfolane and water to maintain a constant solvent-to-feed ratio at the extractive distillation and wash columns, respectively.

4.2.1.4 Hydrotreatment section (A-400)

The aliphatic HCs from sections A-200 and A-400 are mixed and heated up to 150 °C before entering the hydrotreater (R402). Due to the negligible amount of sulfur, nitrogen, and oxygen in the feed, the hydrogenation is assumed to occur at l50 °C and atmospheric pressure over a Ni/Mo catalyst.[28] Hydrogen is supplied at the reactor temperature and stoichiometric amount according to the various hydrogenation reactions. The conversion is assumed to be 100% for alkenes and alkadienes and 50% for aromatics.[29] Subsequently, the hydrotreater outlet stream is then cooled down to 97 °C to improve the separation of the gasoline and diesel fractions that comprise the low and high MWHCs mixtures, respectively.

A summary of the design specifications of the reactors and columns used in the refinery is shown in Table 4.1.

Table 4.1. Reactors and distillation columns specifications.

Section	Unit	Specifications	Purpose
A-100	Pyrolysis reactor (R-103)	Fluidized bed reactor Temperature: 650 °C Pressure: 1.01 bar	Pyrolysis of waste HDPE.
A-200	De-ethanizer (T-207)	Stages number: 34 Feed stage: 15 Reflux ratio: 1.38 D/F ratio: 0.37 Pressure: 25 bar	Separation of ethylene.
	Depropanizer (T-209)	Stages number: 27 Feed stage: 9 Reflux ratio: 4.5 D/F ratio: 0.35 Pressure: 20.2 bar	Separation of C3 HCs.
	Propylene fractionator (T-211)	Stages number: 140 Feed stage: 70 Reflux ratio: 25 D/F ratio: 0.77 Pressure: 21.9 bar	Separation of propylene from propane.
A-300	Debutanizer (T-305)	Stages number: 13 Feed stage: 8 Reflux ratio: 1.86 D/F ratio: 0.59 Pressure: 7.6 bar	Removal of C4 HCs.
	Depentanizer (T-306)	Stages number: 14 Feed stage: 9 Reflux ratio: 2.46 D/F ratio: 0.36 Pressure: 4.5 bar	Removal of C5 HCs.
	Extractive distillation column (T-308)	Stages number: 50 Solvent stage: 4 Feed stage: 37 Reflux ratio: 2.21 D/F ratio: 0.14 Pressure: 2.53 bar	Removal of C6 to C12 aliphatic HCs.
	Wash column (T-310)	Rotary disc contactor Stages: 40 Flow: countercurrent Pressure: 1.01 bar	Removal of heavy molecular weight aliphatic HCs.
	Aromatics recovery column (T-312)	Stages number: 4 Feed stage: 2 Reflux ratio: 0.1 D/F ratio: 1 Pressure: 1.01 bar	Separation of aromatics and water from sulfolane.
A-400	Hydrotreater (R-402)	Temperature: 150 °C Pressure: 1.01 bar	Hydrogenation of alkenes, alkadienes, and aromatics.

4.2.1.5 Refrigeration cycles and heat integration

The cryogenic temperatures for the separation of the pyrolysis gases (C1 to C4) require the use of refrigeration cycles that maintain such low temperature for the process. Therefore, three single-loop refrigeration cycles and one cascade refrigeration system were designed in Aspen Plus. Each refrigeration cycle contains at least a compressor, an evaporator, a condenser, and an adiabatic valve. Their specifications (refrigerant used, temperatures, power and energy requirements) and a diagram of the cascade refrigeration system are shown in Tables C-5 and C-6 and Figure C-7 of Appendix C. For the cascade refrigeration system, heat exchange between refrigerants (see units E-01M and E-01E in Figure C-7) is necessary to achieve condensation at cryogenic temperatures and reduce electricity and cooling requirements. The electricity and cooling requirements of the compressor and condenser, respectively, were used for the calculation of variable costs and greenhouse gas (GHG) emissions of the refinery.

To analyze the effect of heat integration on the energetic, economic and environmental performance of the refinery, after the modelling the base case refinery, the heat exchanger network was designed using the software Super Target v.7.0.15 (KBC Process Technology Ltd.). Only process heaters and coolers operating above -40 °C were included in the calculation. Dowtherm fluid operating from 900 to 1000 °C (heated up with natural gas) and water going from 20 to 30 °C, served as the heating and cooling utilities, respectively. The minimum temperature difference (ΔT_{min}) for all heat exchangers (at countercurrent operation) was set at 10 K. Duties were obtained from the process flowsheet in Aspen Plus,

and overall heat transfer coefficients were obtained from literature[30] according to the corresponding cold and hot fluids. A table with the specifications of the heaters and coolers used for the heat exchanger network design are presented in Table C-7 of Appendix C. In addition to heat integration, more energy savings were achieved through the use of low-pressure steam (LP), generated from the heat released at the hydrotreatment reactor, as a heating source for the reboiler of the propylene fractionator.

4.2.2 Energetic evaluation

The energy efficiency of the refinery, was calculated to compare the performance of the proposed refinery with similar designs or with other alternative fuels technologies.[31] Total heating and electricity requirements estimations included process flowsheet data and energy savings (see section 4.3.2) that were then converted to primary energy demand in megajoules per hour (MJ/h). A factor of 2.5 was considered for the conversion of electricity to primary energy, whilst heating was itself considered primary energy, so no factor was applied for its conversion. Hence, these primary energy calculations did not consider upstream processing. The total energy embedded in input and output materials was calculated according to equation (4.1):

$$Energy\ embedded\ in\ materials = \sum_{j}^{n}\sum_{i}^{n}(LHV_{ij} \cdot Mij) \qquad (4.1)$$

where LHV_{ij} is the lower heating value (LHV) of compound i in material j in MJ/kg and M_{ij} is the mass of compound i in material j in kg. It was not possible to find the LHVs for all the compounds included in every material, therefore a combination of literature data

99

from the National Institute of Standards and Technology[32] and Aspen Plus estimations was used. Once the total energy requirements and energy embedded in material were obtained, the estimation of energy effciency was made using equation (4.2):

$$\eta_R = \frac{E_o}{E_{primary} + E_i} \tag{4.2}$$

where η_R is the energy efficiency of the refinery, E_o is the total energy embedded in material outputs (products), $E_{primary}$ are the total primary energy requirements of the refinery, and E_i is the energy embedded in the material inputs (feedstocks), including waste HDPE and hydrogen.

4.2.3 Techno-economic analysis

4.2.3.1 Cost estimations

The first step on the techno-economic assessment is the estimation of the purchase cost of plant equipment. This cost depends on the type of equipment, size, capacity, power or duty derived from the modeling in Aspen Plus. The complete information of the parameters used to obtain the cost of each unit are shown in Tables C-8 and C-9 of Appendix C. The data source of purchase costs varied according to the type of equipment. Cost of the pyrolysis and hydrotreatment reactors were based on literature data;[21,29] columns and turbines were costed using information from Peters et al.;[33] compressors, based on their power, used estimations from Peters et al.[33] or Seider et al.;[34] and costs of heat exchangers, vessels, and pumps were calculated from correlations published by Turton et al.[35] When the size or

capacity of the equipment was out of the range in the chosen methodology, the cost was adjusted with equation (4.3):

$$C_N = C_O \times \left(\frac{S_N}{S_O}\right)^n \qquad (4.3)$$

where C_N is the cost of the equipment at the new capacity in USD, C_O is the cost at the original capacity in USD, S_O is the original capacity in tonnes/h, S_N is the new capacity of the equipment in tonnes/h, and n is a scaling factor set at 0.7 as suggested by Towler and Sinnot.[36] Costs also had to be updated by means of equation (4.4):

$$C_U = C_O \times \left(\frac{CEPCI_U}{CEPCI_O}\right) \qquad (4.4)$$

where C_U is the is the updated cost in USD, established for 2017 in this study, C_O is the cost at the original year, $CEPCI_U$ is the chemical engineering plant cost index at the updated year, and $CEPCI_O$ is the chemical engineering plant cost index at the original year. The *CEPCI* is obtained from the published values of the journal Chemical Engineering.

4.2.3.2 Discounted cash flow analysis (DCFA)

A modified discounted cash flow analysis was carried out to estimate the net present value (NPV) according to Peters et al.[33] Table 4.2 summarizes principal assumptions used in the DCFA. The costs estimation for the feedstock, consumables, and products are presented in Table 4.3. The cost of waste HDPE was calculated as the difference between the average tipping fee (50 USD/tonne) that a material recovery facility (MRF) charges for its reception in the U.S.[37] and the average cost of its processing (72 USD/tonne).[4,38,39] Costs of cooling

water and low pressure (LP) steam used correlations from Ulrich and Vasudevan.[40] The selling price of the aromatic mixture was calculated from sum of the multiplication of the prices per kg of benzene, toluene, xylenes and styrene, published by Straathof and Bampouli,[41] by their corresponding mass percentage in the mixture. The low and high MWHCs are alternatives to gasoline and diesel, respectively, therefore their prices are based on those fuels. References for the costs of other consumables and products are presented in Table 4.3.

Table 4.2. Assumptions used for the DCFA.

Parameter	Value [a]
Internal rate of return (%)	10
Project economic life (years)	20
Depreciation method	7-year MACRS
Tax rate (%)	21
Working capital (WC)	15% FCI
Base year	2017
Operating days per year	350
Investment year 1	30% FCI
Investment year 2	50% FCI
Investment year 3	20% FCI + WC + FOC + 50% VOC
Investment year 4	FOC + 90% VOC
Investment year 5	FOC + VOC
MACRS: Modified accelerated cost recovery system, FCI: Fixed capital investment, FOC: Fixed operating costs, VOC: Variable operating costs. [a]: For estimations of FCI, FOC, and VOC refer to Table C-10 of Appendix C.	

Table 4.3. Feedstock, consumables and products prices from the refinery.

Product	Price
Waste HDPE (USD/tonne) [a]	22.0
Electricity (USD/kWh) [42]	0.069
Natural gas (USD/GJ) [43]	3.95
Cooling water (USD/m^3) [40]	0.053
Hydrogen (USD/kg) [29]	2.83
Helium (USD/kg) [44]	42.81
Ethylene (USD/kg) [45]	0.61
Propylene (USD/kg) [46]	0.97
Aromatics mixture (USD/kg) [b]	1.02
Low MWHC mixture (USD/kg) [47]	0.86
High MWHC mixture (USD/kg) [47]	0.84
LP steam (USD/kg) [40]	0.021
[a]: Estimated difference of processing and tipping fee at MRF, [b]: Weighed cost of major aromatics species in the mixture.	

4.2.3.3 Sensitivity analysis

When the DFCA was finished, the influence that different parameters and prices had on the NPV was tested through a sensitivity analysis. Each parameter and price were independently varied ± 15% from its reference value according to Table 4.2 and Table 4.3, and the DCFA was estimated again to check the variability of NPV from the original result. From the parameters tested only 11 showed a visible effect on NPV which are discussed in section 4.3.6.

4.2.3.4 Scenario analysis

Some parameters like waste HDPE price, internal rate of return (IRR), also known as discount rate, tax rate, and electricity cost have presented a broad variability in the different reported studies that goes beyond the 15% increase used in the sensitivity analysis. Hence, the effect of a wider range of values was analyzed using NPV as indicator. As part of the

scenario analysis, values of waste HDPE price and IRR that turn the NPV into zero were found and discussed along with the effect of state tax rates in the U.S.

4.3 Results and discussion

4.3.1 Material and energy balances

The results from the process simulation are shown in Table 4.4. The equal amounts of the total material inputs and outputs indicate that the material balance is closed. The major product (more than 53% wt.) of the refinery is a low MWHCs mixture that has similar composition to gasoline. Monomers are the second major products with contributions from ethylene and propylene of 18.5 and 13.2% wt., respectively, while aromatics and high MWHCs mixtures comprised only 8.9% of the total production of the refinery. Total process energy inputs exceed by 42.3 GJ/h the value of the total process energy outputs. This value is close the difference between the embodied energy in outputs and inputs (35.1 GJ/h), which confirms a closed energy balance for the refinery. Although the total energy between inputs and outputs differs by 7.2 GJ/h, this variation only represents an error of 0.65% in the total energy balance. This error is due to differences in the lower heating values estimated by Aspen Plus and those available in the literature (see Table C-11 of Appendix C). Table 4.4 also shows that more than 90% of the process energy inputs are in the pyrolysis and monomer separation sections, which host the most energy-intense processes in the refinery, that is, the pyrolysis of HDPE at 650 °C and the compression of the pyrolysis gases up to 7 bar. Unlike the process energy inputs, the process energy outputs are more distributed between sections, however, the monomer separation section possess

104

the highest energy loses for both the base and the heat integrated case. This is mostly due to the cooling of the pyrolysis gases to $-136\,°C$.

A close analysis of the energy balance shows that 62 GJ/h are recovered as a result of the heat integration. This value is confirmed in Table C-12 of Appendix C, which shows the interconnections and detailed savings of each heat exchanger. A significant reduction of energy inputs appears in the pyrolysis section for the heat integrated case. From Table C-1, it is seen that heat exchanger network (HEN) can provide enough energy to reduce more than a quarter the energy inputs of section A-100. However, according to Table 4.4, a more dramatic reduction takes place in the process energy outputs of the pyrolysis section. The energy losses, which relate directly to the cooling requirements, were reduced more than two thirds compared to the base case. Therefore, heat integration plays an important role when the efficient use of energy is part of the process design.

Table 4.4. Material and energy inputs and outputs of the refinery.

Stream	Parameter	Base case	Heat integrated
Material Inputs	Waste HDPE (kg/h)	20,833.33	20,833.33
	Helium (kg/h)	0.89	0.89
	Sulfolane (kg/h)	5.66	5.66
	Water for process (kg/h)	3.50	3.50
	Hydrogen (kg/h)	329.55	329.55
	Total material inputs (kg/h)	*21,172.93*	*21,172.93*
Process Energy Inputs per section	A-100 Pyrolysis (GJ/h)	135.30	99.92
	A-200 Monomer separation (GJ/h)	69.87	50.47
	A-300 Aromatics extraction (GJ/h)	12.56	10.61
	A-400 Hydrotreatment (GJ/h)	5.30	0.00
Embodied Energy for inputs	Waste HDPE (GJ/h)	891.67	891.67
	Helium (GJ/h)	0.00	0.00
	Sulfolane (GJ/h)	0.11	0.11
	Water for process (GJ/h)	0.00	0.00
	Hydrogen (GJ/h)	39.53	39.53
	Total energy inputs (GJ/h)	*1154.35*	*1092.31*
Material outputs	Ethylene (kg/h)	3,907.77	3,907.77
	Propylene (kg/h)	2,800.71	2,800.71
	Aromatics mixture (kg/h)	772.10	772.10
	Low MW HCs (kg/h)	11,255.97	11,255.97
	High MW HCs (kg/h)	1,119.92	1,119.92
	Methane purge (kg/h)	1,316.46	1,316.46
	Total material outputs (kg/h)	*21,172.93*	*21,172.93*
Process Energy outputs per section	A-100 Pyrolysis (GJ/h)	68.43	25.12
	A-200 Monomer separation (GJ/h)	76.65	60.54
	A-300 Aromatics extraction (GJ/h)	13.66	11.02
	A-400 Hydrotreatment (GJ/h)	22.04	22.04
Embodied Energy for outputs	Ethylene (GJ/h)	184.69	184.69
	Propylene (GJ/h)	128.33	128.33
	Aromatics mixture (GJ/h)	31.48	31.48
	Low MW HCs (GJ/h)	508.82	508.82
	High MW HCs (GJ/h)	48.47	48.47
	Methane purge (GJ/h)	64.64	64.64
	Total energy outputs (GJ/h)	*1147.20*	*1085.16*

4.3.2 Primary energy requirements

Besides the savings from heat integration, some of the energy outputs can be used within the refinery to reduce the energy requirements. Table C-13 of Appendix C, shows the process energy inputs and outputs per section. The information in Table C-13 suggests that the electricity produced by the turbines can fulfill a fraction of the electricity requirements of the monomer separation section (A-200). Also, the embedded energy in the purge stream of section A-100 (see Table 4.4) can provide heat for the sand fed to the pyrolysis reactor and low-pressure steam generated at the hydrotreatment reactor can supply the heating to operate the reboiler of the propylene fractionator. These energy saving strategies were included in both scenarios and reduced the total energy requirements from 223 to 151 GJ/h for the base case and from 161 to 89 GJ/h for the heat integrated case.

As visualized in Figure 4.1, an important component to obtain high purity monomers is the distillation of the pyrolysis gases at cryogenic temperatures. Hence, it is important to include the electricity requirements of the refrigeration cycles that achieve such low temperatures. These cycles are also employed when temperatures below 30 °C are required, i.e. to operate the condensers of some distillation columns. A complete list of specifications of the refrigeration cycles designed for the base and the heat integrated cases are presented in Tables C-5, C-6, C-14, and C-15 and Figure C-7 and C-8 of Appendix C.

The calculation of the primary energy requirements of the processing pathway is necessary to estimate the energy efficiency in the refinery. Energy savings and electricity for the refrigeration cycles took part of this estimation because they are an important component

of the net energy requirements of the refinery. Figure 4.2 shows the primary energy requirements per section of the refinery. According to Figure 4.2, the highest primary energy requirements occur in the monomer separation section (A-200), which tripled the values from the energy inputs. The reason behind this considerable increment is the inclusion of the electricity demand to operate the refrigeration cycles. In contrast with the results from the energy balance, the pyrolysis section does not have the highest primary energy requirements. This is an effect of the savings achieved by using the methane purge as a source of heat. On the other hand, the effects of heat integration, previously discussed, are exhibited again by the reduction of the natural gas requirements in the pyrolysis and monomer separation sections. Another important result are the null energy requirements attained in the hydrotreatment section in the heat integrated facility. Further results of the heat integration analysis like the Grand Composite Curve and the HEN grid diagram are presented in Figures C-9 and C-10 of Appendix C, respectively.
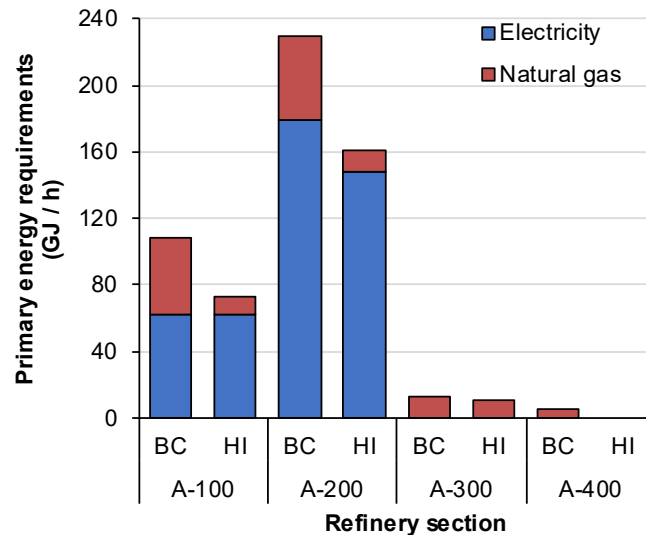
Figure 4.2. Primary energy requirements of the different refinery sections. BC: Base case. HI: Heat integrated case.

4.3.3 Product yields and energy efficiency

As mentioned in section 4.2, five products and one co-product are obtained from the refinery. The composition of each product and its recovery are shown in Table 4.5. A detailed account of every compound is available in Table C-16 of Appendix C. The purity of the produced ethylene and propylene are 97.1% and 97.8%, respectively, which qualifies both as chemical-grade products.[48,49] Among the options to increase the purity of these products are the addition of distillation columns, which would increase the capital investment and operation costs of the facility, and the modification of the pyrolysis conditions to temperatures between 675 and 700 °C, and higher residence times in the reactor.[9,50] The aromatics mixture has an aromatic composition of 93.3%, with benzene, toluene, and styrene being the mayor components that could be separated on existing BTX complex at petrochemical refineries. The generated low MWHCs mixture presents the same HC range as gasoline, hence, it is proposed as an alternative to this fuel. Nonetheless, the chemical species in this mixture are slightly different than gasoline due to the absence of branched HCs and the presence of aromatics. The total composition of C4-C12 aliphatic HCs in this mixture is 96.6%. Finally, the high MWHCs mixture comprises carbon numbers from C13 to C29 with 77.8% of its composition within the diesel range (C8-C24), therefore, it is proposed as an alternative to low-sulfur diesel. The recovery of the products is high for the monomers, but it decreases for the mixtures, mostly due to the complexity of the separations, the wide range of molecular weight in the compounds and the strong interaction between aromatic and aliphatic HCs with the same carbon number.

Table 4.5. General composition of products and recovery of products from the reactor outlet.

Product	Components: wt.%	Recovery
Ethylene	Ethylene: 97.22 Methane: 2.75 Others: 0.03	89.51
Propylene	Propylene: 97.85 Propane: 1.20 Ethylene: 0.95	99.70
Aromatics mixture	Benzene: 40.74 Toluene: 14.46 Xylenes: 5.17 Styrene: 18.87 PAHs: 5.02 C6-C10 AHCs: 12.50 Others: 3.24	57.15
Low MWHCs	Propane: 5.72 Butane: 51.43 Pentane: 22.23 C6: 9.66 C7-C12 HCs: 10.53 Others: 0.43	56.10
High MWHCs	C4-C5: 3.29 C6-C10: 15.99 C11-C15: 41.86 C16-C20: 26.52 C21-C25: 10.83 C26-C29: 1.24 Others: 0.27	76.43
PAHs: Polyaromatic hydrocarbons, AHCs: Aliphatic hydrocarbons.		

The total energy embedded of the products listed in Table 4.5 equals 905 GJ/h. On the other hand, as part of the efficient use of energy in the refinery, the exhausted heat from the hydrotreatment reactor (20 GJ/h) was used to generate low pressure steam as a co-product. In consequence, the total embedded energy from products and the co-product accounted for 925 GJ/h. The total primary energy required for the base case and heat integrated case was 372 and 262 GJ/h, respectively. As a result, the energy efficiency of

the refinery was 72 % for the base case and 77% for the heat integrated case. These efficiencies are lower than those estimated for the refining of fossil fuels like gasoline (88%) and diesel (91%).[51] The lower energy efficiency is likely due to the more complicated process design for the multi-product waste HDPE refinery.

4.3.4 Capital costs

Table 4.6 presents the investment and annual operation costs for both the base and heat integrated cases. The monomer separation section has the highest equipment cost of the both cases analyzed. According to Table C-17 of Appendix C, the highest equipment cost in this section corresponds to the compressors (8.29 MM USD), although the most expensive equipment from the entire facility is the pyrolysis reactor (8.76 MM USD). Installation, maintenance, and indirect costs (engineering, construction, etc.) are also the highest for this section A-200. Other equipment with an important contribution to the total equipment cost are the PSA unit (2.60 MMUSD), the propylene fractionator (1.35 MM USD), and the sand furnace (1.57 MM USD). Variable operation costs (VOC) are more evenly distributed between the different sections of the refinery. The monomer separation and hydrotreatment sections present the highest costs of operation for the base case and the heat integrated refinery, respectively. Therefore, the reduction of energy requirements from heat integration also produced an important reduction of the operation cost of the section A-200. Electricity is the material with the highest contribution by comprising a third of the total operation costs. Another material with important effect on the operation costs is the hydrogen used for the hydrotreatment.

The fixed capital investment (FCI) for the heat integrated case is higher compared to the base case due to an increment in the equipment purchase cost (TEPC) of the heat exchanger network. Nonetheless, the reduction of natural gas and electricity requirements decreased the variable operation costs (VOC), because of heat integration. Consequently, the HEN not only improves the energy performance of the refinery, as discussed before, but also shows positive implications from an economic perspective. Fixed operation costs (FOC) are higher for the heat integrated case because maintenance costs are directly linked to the TEPC. FCI and FOC for the heat integrated case surpass the values from the base case by 1%, whereas the VOC of the base case exceeds by 16% that of the heat integrated case. The long-term economic effects of these differences will be obtained with the analysis of the DCFA.

The FCI of the base case and the heat integrated refinery are 118.5 and 120.5 MM USD respectively. Then, the capital costs per tonne of waste HDPE processed are 677 and 688 USD for the base case and heat integrated refinery, respectively. These capital costs are higher when compared to those from previous designs focusing on fuel oil production. Fivga and Dimitriou[14] estimated 200 USD/tonne for their facility processing 70,000 tonnes/yr, while Sahu et al. estimated 488 USD/tonne for a capacity of 100,000 tonnes/yr. For multiproduct designs, Vargas Santillan et al.[16] valuated their investement in 242 USD/tonne at a capacity of 182,500 tonnes/yr, and Al-Salem et al.[4] estimated a capital cost of 709 USD/tonne for their incineration-pyrolysis plant processing 150,000 tonnes/yr. The estimated cost of the proposed refinery is closer to those estimated by Al-Salem et al.[4] due

to the higher capacity and inclusion of more processing stages on their design. It is not possible for the current design to have lower costs with processes that consist only of a reactor and a simple separation sequence. However, the operation costs of the waste HDPE refinery (41.4 and 36.7 MM USD for the base case and the heat integrated refineries, respectively) are lower compared to those from Sahu et al.[7] (52.0 MMUSD) and Vargas Santillan et al.[16] (106.6 MM USD). This can be due to the efficient use of energy in the refinery, as discussed in section 4.3.2.

Table 4.6. Total costs per section of the refinery (MM USD).

Parameter	Base case						Heat integrated					
	A-100	A-200	A-300	A-400	C&H	Total	A-100	A-200	A-300	A-400	HEN	Total
TEPC	12.09	14.01	0.58	0.19	0.62	27.49	12.00	12.67	0.58	0.19	2.51	27.95
TIC	36.52	42.31	1.76	0.58	1.86	83.03	36.24	38.28	1.76	0.58	7.57	84.42
Indirect costs	14.87	17.23	0.72	0.23	0.76	33.82	14.76	15.59	0.72	0.23	3.08	34.38
Land [a]	n/a	n/a	n/a	n/a	n/a	1.65	n/a	n/a	n/a	n/a	n/a	1.68
FCI						118.49						120.48
Working capital						17.77						18.07
TPI						136.26						138.55
Waste HDPE [b]	3.85	-	-	-	-	3.85	3.85	-	-	-	-	3.85
Electricity [b]	4.03	11.54	-	-	-	15.58	3.40	9.57	-	-	-	13.57
Natural Gas [b]	1.52	1.68	0.42	0.18	-	3.79	0.35	0.41	0.35	-	-	1.11
Cooling water [b]	0.04	0.07	0.01	-	-	0.11	0.01	0.05	0.01	-	-	0.08
Catalyst [c]	-	-	-	1.67	-	1.67	-	-	-	1.67	-	1.67
Hydrogen [b]	-	-	-	7.84	-	7.84	-	-	-	7.84	-	7.84
Sulfolane [d]	-	-	0.40	-	-	0.40	-	-	0.40	-	-	0.40
Helium [d]	0.32	-	-	-	-	0.32	0.32	-	-	-	-	0.32
Water [d]	-	-	0.03	-	-	0.03	-	-	0.03	-	-	0.03
VOC	9.76	13.29	0.86	9.69	-	33.59	8.53	10.03	0.79	9.51	-	28.86
Salaries [a]	n/a	n/a	n/a	n/a	n/a	2.21	n/a	n/a	n/a	n/a	n/a	2.21
Benefits [a]	n/a	n/a	n/a	n/a	n/a	1.99	n/a	n/a	n/a	n/a	n/a	1.99
Maintenance	1.56	1.81	0.08	0.02	0.08	3.55	1.55	1.64	0.08	0.02	0.32	3.61
FOC						7.76						7.82

C&H: Coolers and heaters. HEN: Heat exchanger network. TPEC: Total equipment purchase cost. TIC: Total installed cost. FCI: Fixed capital investment. TPI: Total project investment. VOC: variable operating costs per year. FOC: Fixed operating costs per year. [a] Estimated cost for the complete refinery and not for a single section. [b] Cost per year. [c] Regeneration cost per year. [d] Make-up feedstock cost per year.

4.3.5 Discounted cash flow analysis

The DCFA had the objective to estimate the economic feasibility of the refinery by using the net present value (NPV) as an indicator. The analysis considered revenues from five products (see Table 4.5) and one co-product (low pressure steam produced from the heat released from the hydrotreatment reactor). Revenues from the facility are estimated in 137.6 MM USD, with most of these coming from the sales of low MWHCs (59%) and chemical-grade polypropylene (16%) and ethylene (15%). The relative revenues from high MWHCs, aromatics mixture, and steam were 6, 4, and 1%, respectively. The base analysis for the DCFA is carried out considering the assumptions presented in Table 4.2 and the estimated costs from Table 4.6.

Results from the DCFA for the base case and heat integrated refineries are presented in Table 4.7 and Table 4.8, respectively. The heat integrated refinery presents a NPV of 383.1 MM USD, only 4% higher that the base case. This indicates that the economic savings achieved by the reduction from electricity and natural gas requirements are almost offset by the increased cost of equipment in the heat exchanger network. The discounted cash flow rate of return (DCFROR), which is the IRR that produces a NPV equal to zero, was also calculated. The DCFROR for the base and the heat integrated cases was 31.3 and 31.7%, respectively. As expected, the DCFROR is higher for the design with the higher NPV, however, an analysis of the effect of IRR on NPV (Figure 4.3), shows that at IRRs higher than 31% result in similar NPVs for both cases. In other words, at IRR = 31% the positive effects of reduced operation costs and increased cash flow per year (see Table 4.8)

are suppressed by the raise of FCI. Due to its benefits from an environmental (which is discussed on Chapter 5) and economic perspectives, the rest of the analysis will focus on the heat integrated case.

The DCFROR of the refinery is lower than that from Al-Salem et al.[4] (43%), although it should be considered that the refinery has a higher production capacity and a more complex process including cryogenic separation and liquid-liquid extraction. According to the methodology of Towler and Sinnot,[36] the pre-tax ROI and the payback time were calculated giving values of 52.7% and 1.8 years, respectively. Compared to the other studies the ROI is similar to the values reported by Sahu et al.[7] (35.7%) and Westerhout et al.[15] (29.5%, without cryogenic separation). The payback period is lower than the one reported by Sahu et al.[7] (3 years) and close to that from Fivga and Dimitriou[14] (1.2 years). All these comparisons were based on the closest capacity to the proposed facility in this manuscript (175,000 tonnes/yr). The discussion above highlights that the economic performance of the waste HDPE refinery is average to other facilities previously described in the literature but with advantages of the potential development of a multiproduct market from the whole exploitation of the waste HDPE.

Table 4.7. Discounted cash flow for the base case.

Year	Gross profit (MM USD)	Depreciation charge (MM USD)	Taxable income (MM USD)	Taxes paid (MM USD)	Cash flow (MM USD)	Discount factor	Present value of cash flow (MM USD)
0	-	-	-	-	−118.49	1	−118.49
1	-	-	-	-	-	0.91	-
2	-	-	-	-	-	0.83	-
3	44.75	16.70	28.05	5.89	21.08	0.75	15.84
4	86.76	28.61	58.15	12.21	74.55	0.68	50.92
5	97.26	20.44	76.83	16.13	81.13	0.62	50.37
6	97.26	14.60	82.67	17.36	79.90	0.56	45.10
7	97.26	10.43	86.83	18.23	79.03	0.51	40.55
8	97.26	10.42	86.84	18.24	79.03	0.47	36.87
9	97.26	10.43	86.83	18.23	79.03	0.42	33.52
10	97.26	5.21	92.05	19.33	77.93	0.39	30.05
11	97.26	-	97.26	20.42	76.84	0.35	26.93
12	97.26	-	97.26	20.42	76.84	0.32	24.48
13	97.26	-	97.26	20.42	76.84	0.29	22.26
14	97.26	-	97.26	20.42	76.84	0.26	20.23
15	97.26	-	97.26	20.42	76.84	0.24	18.39
16	97.26	-	97.26	20.42	76.84	0.22	16.72
17	97.26	-	97.26	20.42	76.84	0.20	15.20
18	97.26	-	97.26	20.42	76.84	0.18	13.82
19	97.26	-	97.26	20.42	76.84	0.16	12.56
20	97.26	-	97.26	20.42	76.84	0.15	11.42
Total	1,687.70						366.75

Table 4.8. Discounted cash flow for the heat integrated case.

Year	Gross profit (MM USD)	Depreciation charge (MM USD)	Taxable income (MM USD)	Taxes paid (MM USD)	Cash flow (MM USD)	Discount factor	Present value of cash flow (MM USD)
0	-	-	-	-	−120.48	1	−120.48
1	-	-	-	-	-	0.91	-
2	-	-	-	-	-	0.83	-
3	46.55	16.98	29.58	6.21	22.27	0.75	16.73
4	90.05	29.09	60.96	12.80	77.25	0.68	52.76
5	100.93	20.78	80.15	16.83	84.10	0.62	52.21
6	100.93	14.84	86.09	18.08	82.85	0.56	46.77
7	100.93	10.61	90.32	18.97	81.96	0.51	42.06
8	100.93	10.60	90.33	18.97	81.96	0.47	38.23
9	100.93	10.61	90.32	18.97	81.96	0.42	34.76
10	100.93	5.30	95.63	20.08	80.84	0.39	31.17
11	100.93	-	100.93	21.19	79.73	0.35	27.95
12	100.93	-	100.93	21.19	79.73	0.32	25.41
13	100.93	-	100.93	21.19	79.73	0.29	23.10
14	100.93	-	100.93	21.19	79.73	0.26	21.00
15	100.93	-	100.93	21.19	79.73	0.24	19.09
16	100.93	-	100.93	21.19	79.73	0.22	17.35
17	100.93	-	100.93	21.19	79.73	0.20	15.77
18	100.93	-	100.93	21.19	79.73	0.18	14.34
19	100.93	-	100.93	21.19	79.73	0.16	13.04
20	100.93	-	100.93	21.19	79.73	0.15	11.85
Total	1,751.43						383.10
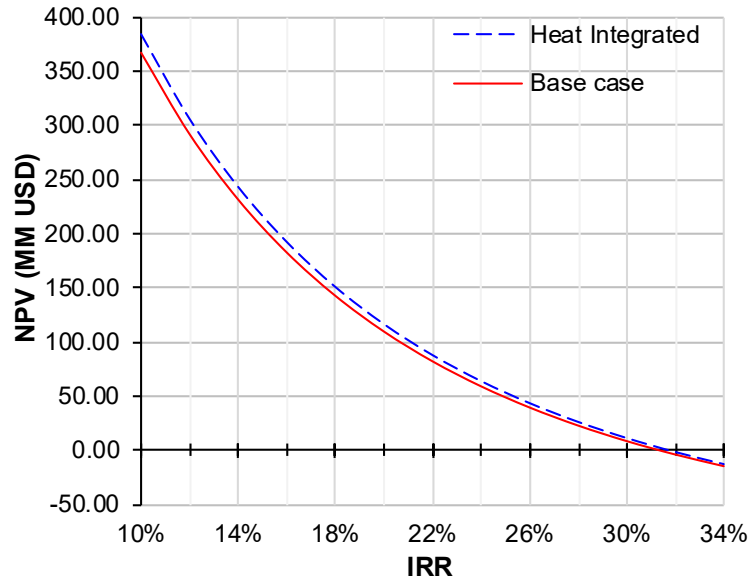
Figure 4.3. Effect of the IRR on the NPV for the base and heat integrated cases.

4.3.6 Sensitivity analysis

Similarly to the HDPE cost and the corporate tax rate, equipment and material costs as well as product prices are subjected to variability. This variability may have an important effect on the NPV of the refinery. Thus, a sensitivity analysis was carried out for 14 parameters used in the techno-economic assessment considering a variability of ± 15%. The results are shown in Figure 4.6 and demonstrate that the low MWHCs price, the IRR, and the TPI are by far the parameters with the strongest effect on the NPV of the heat integrated refinery. Being the product with the highest yield of the facility (59% wt.), a variability in the price of the low MWHCs will strongly affect the revenues and the cash flow of the project, therefore, it is important to accurately estimate the sale price of this product. The project investment is another important parameter to focus on. Accurate costs of equipment, preferably from vendor quotes, are important to obtain and reduced costs from incentives

of low carbon fuel standards can be considered to reduce investment costs. With the parameters shown in Table 4.2, the increment of one MM USD on the TPI will reduce the NPV in 0.5 MM USD. The importance of the IRR has already been discussed in section 3.5, however its effect is not as significant as that from the price of the Low MWHCs.

(Unfavorable; Base Case; Favorable)

Total Project Investment
(159.3; 138.6; 117.8 MM USD)

Internal rate of return
(11.5; 10.0; 8.5 %)

Corporate tax rate
(24.15; 21.0; 17.85 %)

HDPE cost
(25.3; 22.0; 18.7 USD/tonne)

Electricity cost
(7.94; 6.91; 5.87 cents/kWh)

Hydrogen cost
(3.26; 2.83; 2.41 USD/kg)

Ethylene price
(0.52; 0.61; 0.70 USD/kg)

Propylene price
(0.82; 0.97; 1.11 USD/kg)

Aromatics mixture price
(0.69; 0.81; 0.94 USD/kg)

Low MWHCs price
(0.73; 0.86; 0.99 USD/kg)

High MWHCs price
(0.71; 0.84; 0.96 USD/kg)

NPV (MM USD)

Figure 4.4. Sensitivity analysis of the waste HDPE refinery.

The prices of products have a stronger effect on the NPV compared to the costs of feedstocks. It is important to note the importance that product yield has on the relevance of the product's price to NPV, as exhibited by the higher impact of Low MWHCs, ethylene and propylene, the products with higher yields (see Table 4.4). The relationship between

120

feedstock costs and NPV is more complicated due to the high variability of prices and requirements. For the facility designed the costs of electricity, waste HDPE, and hydrogen are those with the highest effect on NPV and that need to be calculated consciously even considering regional effects.

4.3.7 Scenario Analysis

The costs of HDPE as feedstock for thermochemical conversion have been assumed a wide range, from studies that consider no cost[14,15] to values over 450 USD/tonne.[16] As explained in section 4.2.3.2, the current techno-economic assessment considered a cost of 22 USD/tonne, which is the difference between the operation costs per tonne at the material recovery facility (MRF) and the tipping fee paid to such facility. The waste HDPE cost can be influenced by many factors like the federal or state waste management policies and the municipal costs for collection and processing, so the effect of this price variability was evaluated and presented in Figure 4.4. Current spot prices from vendors oscillate between 10 and 100 USD/tonne,[52,53] depending on the source and quality of the waste polyethylene. The effect of these prices on the NPV is also shown in Figure 4. As seen, there is a linear relationship between the NPV and the cost of HDPE. It is also observed that HDPE costs higher than 460 USD/tonne produce a negative NPV making the project not feasible. From Figure 4.4 it is also observed that an increase in the HDPE cost of one USD/tonne reduces the NPV of the project in 0.88 MM USD.
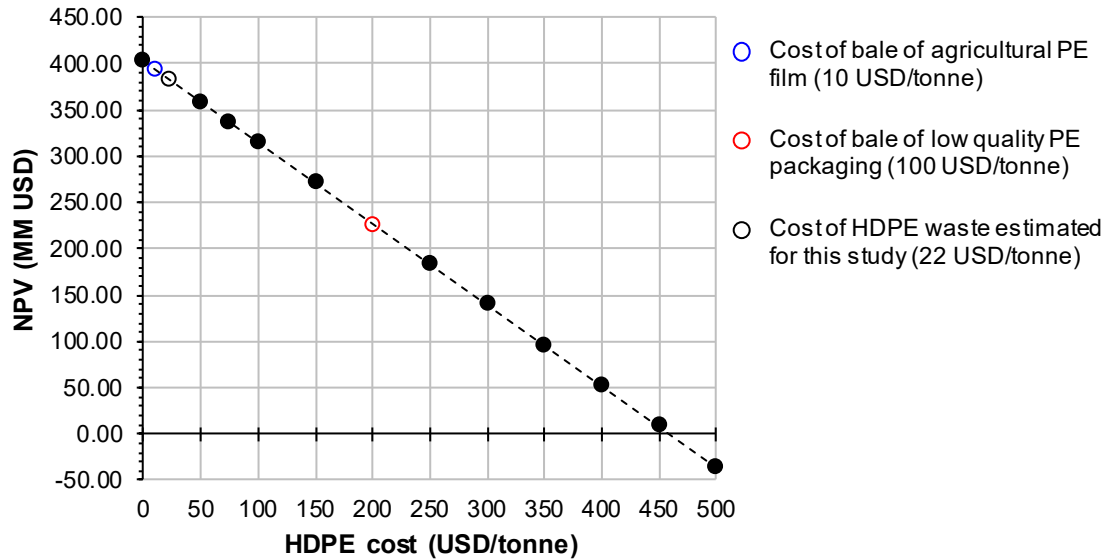
Figure 4.5. Effect of HDPE cost on the NPV for the heat integrated case.

This study used the U.S. current corporate tax rate of 21%, however previously published literature considered 35% according to the corporate tax rate applied before 2018.[52] The NPV of the heat integrated refinery with 35% corporate tax rate is of 304 MM USD, which is still a positive value that points out the proposed facility as a feasible option for the treatment of waste HDPE. Additionally, the DCFROR under this corporate tax rate was 28.7%. States corporate tax rate can also have an important effect on the NPV of the refinery because they can increase up to 12% the amount of taxes paid.[53] Figure 4.5 presents the effect of state corporate taxes on the NPV of the heat integrated refinery. This figure shows that there is a linear relationship between the two variables and that the state corporate taxes do not produce negative values of NPV. Therefore, regardless of the state were the facility is built, the project continues to be economically feasible. Furthermore, it is estimated that the increment of one percent of the corporate tax rate reduces the NPV in 5.6 MM USD.

122
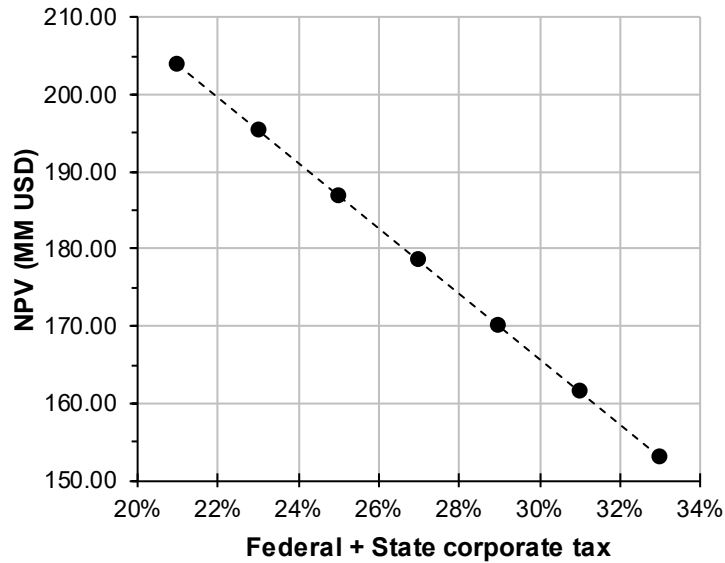
Figure 4.6. Effect of state corporate taxes on the net present value.

Another parameter that widely changes over the U.S. is the cost of electricity. According to the Energy Information Administration (EIA)[56] the price of electricity ranges from 0.047 to 0.23 USD/kWh, therefore, it is interesting to estimate the effect of this variability on the NPV of the refinery. Figure 4.7 displays the results of the analysis, which show that the maximum electricity cost (0.25 USD/kWh) do not affect the feasibility of the refinery. However, it is remarkable that the NPV diminishes to half of its value along the electricity cost interval. This points out the impact of geographical location in the economic sustainability of the refinery. Further discussion of the effects of geographical location, considering environmental sustainability, is included in Chapter 5.
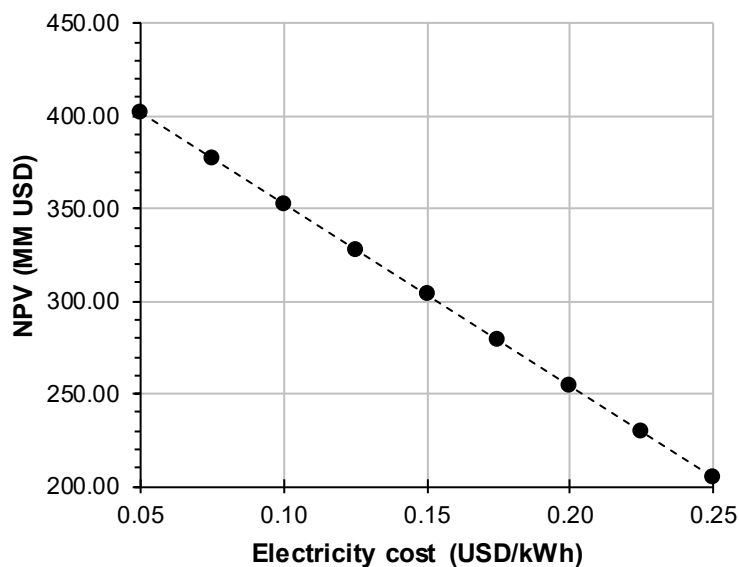
Figure 4.7. Effect of electricity cost on the net present value.

4.4 Conclusions

The analysis presented in Chapter 4 proved the energetic and economic feasibility of a multiproduct/multiprocessing refinery for the chemical recycling of waste HDPE. The energetic evaluation showed that heat integration along with the use of electricity and heating resources generated an energy efficiency of 77%. In spite of generating a higher FCI, heat integration produced lower operation costs and increased the NPV of the design. The capital cost of the heat integrated refinery was 120.5 MM USD which is higher compared to previous studies of comparable facility size, however, its operation costs 36.7 MM USD are significantly lower than the majority of the process studies previously published. The total revenues per year are 137.6 MM USD, which produced a positive NPV of 383 MM USD. The DCFROR and ROI of 31.7% and 52.7%, respectively, are acceptable and within the range of the other plastic waste pyrolysis processes. The sensitivity analysis showed that the IRR, the TPI and the price of the low MWHC mixture

124

are the factors with the highest impact on the NPV of the refinery. All these TEA results lead to the conclusion that the multiproduct/multiprocessing refinery has a favorable energetic and economic performance with the advantage of promoting new markets for the exploitation of PW while avoiding the concerns of landfill disposal and incineration. The environmental performance and the effect of energy sources will be discussed in detail in Chapter 5 of this dissertation.

4.5 Acknowledgements

4.6 References

(1)   U.S. Environmental Protection Agency (EPA). National Overview: Facts and Figures on Materials, Wastes and Recycling. https://www.epa.gov/facts-and-figures-about-materials-waste-and-recycling/national-overview-facts-and-figures-materials (accessed February 19, 2019).

(2)   U.S. Environmental Protection Agency (EPA). Facts and Figures about Materials, Waste and Recycling. Plastics: Material-Specific Data. https://www.epa.gov/facts-and-figures-about-materials-waste-and-recycling/plastics-material-specific-data (accessed February 19, 2019).

(3)   Arena, U.; Di Gregorio, F.; Amorese, C.; Mastellone, M. L. A techno-economic comparison of fluidized bed gasification of two mixed plastic wastes. *Waste Manage.* **2011,** *31* (7), 1494-1504.

(4)   Al-Salem, S. M.; Papageorgiou, L. G.; Lettieri, P. Techno-economic assessment of thermo-chemical treatment (TCT) units in the Greater London area. *Chem. Eng. J.* **2014,** *248*, 253-263.

(5)   Singh, N.; Hui, D.; Singh, R.; Ahuja, I. P. S.; Feo, L.; Fraternali, F. Recycling of plastic solid waste: A state of art review and future applications. *Compos. Pt. B-Eng.* **2017,** *115*, 409-422.

(6)   Kumar, S.; Panda, A. K.; Singh, R. K. A review on tertiary recycling of high-density polyethylene to fuel. *Resour. Conserv. Recycl.* **2011,** *55* (11), 893-910.

(7)   Sahu, J. N.; Mahalik, K. K.; Nam, H. K.; Ling, T. Y.; Woon, T. S.; Rahman, M. S. B.; Mohanty, Y. K.; Jayakumar, N. S.; Jamuar, S. S. Feasibility Study for Catalytic Cracking of Waste Plastic to Produce Fuel Oil with Reference to Malaysia and Simulation using ASPEN Plus. *Environ. Prog. Sustain. Energy* **2014,** *33* (1), 298-307.

(8)   Hong, M.; Chen, E. Y. X. Chemically recyclable polymers: a circular economy approach to sustainability. *Green Chem.* **2017,** *19* (16), 3692-3706.

(9)   Gracida-Alvarez, U. R.; Mitchell, M. K.; Sacramento-Rivero, J. C.; Shonnard, D. R. Effect of Temperature and Vapor Residence Time on the Micropyrolysis Products of Waste High Density Polyethylene. *Ind. Eng. Chem. Res.* **2018,** *57* (6), 1912-1923.

(10)   Donaj, P. J.; Kaminsky, W.; Buzeto, F.; Yang, W. Pyrolysis of polyolefins for increasing the yield of monomers' recovery. *Waste Manage.* **2012,** *32* (5), 840-846.

(11)   Lopez, G.; Artetxe, M.; Amutio, M.; Bilbao, J.; Olazar, M. Thermochemical routes for the valorization of waste polyolefinic plastics to produce fuels and chemicals. A review. *Renew. Sust. Energ. Rev.* **2017,** *73*, 346-368.

(12)   Butler, E.; Devlin, G.; McDonnell, K. Waste Polyolefins to Liquid Fuels via Pyrolysis: Review of Commercial State-of-the-Art and Recent Laboratory Research. *Waste Biomass Valorization* **2011,** *2* (3), 227-255.

(13)   Gracida-Alvarez, U. R.; Keenan, L. M.; Sacramento-Rivero, J. C.; Shonnard, D. R. Resource and Greenhouse Gas Assessments of the Thermochemical Conversion of Municipal Solid Waste in Mexico. *ACS Sustain. Chem. Eng.* **2016,** *4* (11), 5972-5978.

(14)   Fivga, A.; Dimitriou, I. Pyrolysis of plastic waste for production of heavy fuel substitute: A techno-economic assessment. *Energy* **2018,** *149*, 865-874.

(15)   Westerhout, R. W. J.; Van Koningsbruggen, M. P.; Van Der Ham, A. G. J.; Kuipers, J. A. M.; Van Swaaij, W. P. M. Techno-Economic Evaluation of High Temperature Pyrolysis Processes for Mixed Plastic Waste. *Chemical Engineering Research and Design* **1998,** *76* (3), 427-439.

(16)   Vargas Santillan, A.; Farias Sanchez, J. C.; Pineda Pimentel, M. G.; Castro Montoya, A. J. Olefins and Ethanol from Polyolefins: Analysis of Potential Chemical Recycling of Poly(ethylene) Mexican Case. *Int. J. Chem. React. Eng.* **2016,** *14* (6), 1289-1300.

(17)   Jung, S. H.; Cho, M. H.; Kang, B. S.; Kim, J. S. Pyrolysis of a fraction of waste polypropylene and polyethylene for the recovery of BTX aromatics using a fluidized bed reactor. *Fuel Process. Technol.* **2010,** *91* (3), 277-284.

(18)   He, M. Y.; Xiao, B.; Hu, Z. Q.; Liu, S. M.; Guo, X. J.; Luo, S. Y. Syngas production from catalytic gasification of waste polyethylene: Influence of temperature on gas yield and composition. *Int. J. Hydrog. Energy* **2009,** *34* (3), 1342-1348.

(19)   Wu, J.; Prausnitz, J. M. Phase Equilibria for Systems Containing Hydrocarbons, Water, and Salt: An Extended Peng−Robinson Equation of State. *Ind. Eng. Chem. Res.* **1998,** *37* (5), 1634-1643.

(20)   Alston, S. M.; Arnold, J. C. Environmental Impact of Pyrolysis of Mixed WEEE Plastics Part 2: Life Cycle Assessment. *Environ. Sci. Technol.* **2011,** *45* (21), 9386-9392.

(21)   Jones, S. B.; Meyer, P. A.; Snowden-Swan, L. J.; Padmaperuma, A. B.; Tan, E.; Dutta, A.; Jacobson, J.; Cafferty, K. *Process design and economics for the conversion of lignocellulosic biomass to hydrocarbon fuels: fast pyrolysis and hydrotreating bio-oil*

pathway; Report No. PNNL-23053; Pacific Northwest National Laboratory: Richland, WA, 2013.

(22)   Sant Anna, H. R.; Barreto, A. G.; Tavares, F. W.; do Nascimento, J. F. Methane/nitrogen separation through pressure swing adsorption process from nitrogen-rich streams. *Chem. Eng. Process.* **2016,** *103*, 70-79.

(23)   Sundaram, K. M.; Shreehan, M. M.; Olszewski, E. F. Ethylene In *Kirk-Othmer Encyclopedia of Chemical Technology*; 5th ed.; John Wiley & Sons: Hoboken, NJ, 2010.

(24)   Liu, A. UOP Sulfolane Process In *Handbook of Petroleum Refining Processes*; 4th ed.; Meyers, R. A., Ed.; McGraw Hill Professional: United States of America, 2016.

(25)   Stevens, G. W.; Lo, T. C.; Baird, M. H. I. In *Kirk-Othmer Encyclopedia of Chemical Technology*; 5th ed.; John Wiley & Sons: Hoboken, NJ, 2018.

(26)   Choi, Y. J.; Cho, K. W.; Cho, B. W.; Yeo, Y.-K. Optimization of the Sulfolane Extraction Plant Based on Modeling and Simulation. *Ind. Eng. Chem. Res.* **2002,** *41* (22), 5504-5509.

(27)   Lin, W.-C. Studies on the Extraction of Aromatics from $C9^+$ Oil. *Journal of Chemical Engineering of Japan* **2002,** *35* (12), 1257-1262.

(28)   Jeroro, E.; Zink, S. UOP Hydrotreating Technology In *Handook of Petroleum Refining Processes*; 4th ed.; Meyers, R. A., Ed.; Mc-Graw Hill Education: United States of America, 2016.

(29)   Winjobi, O.; Shonnard, D. R.; Zhou, W. Production of Hydrocarbon Fuel Using Two-Step Torrefaction and Fast Pyrolysis of Pine. Part 1: Techno-economic Analysis. *ACS Sustain. Chem. Eng.* **2017,** *5* (6), 4529-4540.

(30)   Ludwig, E. E. Heat transfer. In *Applied Process Design for Chemical & Petrochemical Plants*; 3rd ed.; Gulf Professional Publishing, 2001; Vol. 3.

(31)   Sacramento-Rivero, J. C.; Navarro-Pineda, F.; Vilchiz-Bravo, L. E. Evaluating the sustainability of biorefineries at the conceptual design stage. *Chemical Engineering Research and Design* **2016,** *107*, 167-180.

(32)   Linstrom, P. J.; Mallard, W. G.; National Institute of Standards and Technology: Gaithersburg, MD, 2018.

(33)   Peters, M. S.; Timmerhaus, K. D.; West, R. E. *Plant Design and Economics for Chemical Engineers*; 5 th. ed.; McGraw-Hill Inc.: New York, NY, 2003.

(34)   Seider, W. D.; Lewin, D. R.; Seader, J. D.; Widadgo, S. *Product and Process Design Principles*; 3rd. ed.; John Wiley & Sons, Inc.: United States of America, 2009.

(35)   Turton, R.; Bailie, R. C.; Whiting, W. B.; Shaeiwitz, J. A.; Bhattacharyya, D. *Analysis, synthesis and design of chemical processes*; 4th ed.; Pearson Education, Inc.: Ann Arbor, 2012.

(36)   Towler, G.; Sinnot, R. *Chemical Engineering Design*; 2nd. ed.; Elsevier Ltd.: United States of America, 2013.

(37)   Environmental Research and Educational Fundation. Analisis of MSW Landfill Tipping   Fees.   https://erefdn.org/wp-content/uploads/woocommerce_uploads/2017/12/MSWLF-Tipping-Fees-2018-FINAL.pdf (accessed December 03, 2018).

(38)   Cimpan, C.; Maul, A.; Wenzel, H.; Pretz, T. Techno-economic assessment of central sorting at material recovery facilities - the case of lightweight packaging waste. *J. Clean Prod.* **2016,** *112*, 4387-4397.

(39)   Kessler Consulting, I. *Material Recovery Facility Feasibility Study*; Tampa, FL, 2009.

(40)   Ulrich, G. D.; Vasudevan, P. T. How to Estimate Utility Costs. *Chemical Engineerig* **2006,** *113*, 66-70.

(41)   Straathof, A. J. J.; Bampouli, A. Potential of commodity chemicals to become bio-based according to maximum yields and petrochemical prices. *Biofuels Bioprod. Biorefining* **2017,** *11* (5), 798-810.

(42)   U.S. Energy Information Administration (EIA). Electric Power Monthly. Average Price   of   Electricity   to   Ultimate   Customers. https://www.eia.gov/electricity/monthly/epm_table_grapher.php?t=epmt_5_03 (accessed October 23, 2018).

(43)   U.S. Energy Information Administration (EIA). Selected national average natural gas   prices,   2013-2018.   https://www.eia.gov/naturalgas/monthly/pdf/table_03.pdf (accessed October 23, 2018).

(44)   U.S.   Geological   Service   (USGS).   Helium. https://minerals.usgs.gov/minerals/pubs/commodity/helium/mcs-2018-heliu.pdf (accessed October 23, 2018).

(45) Lippe, D. Uncertainty looms for US olefines industry. https://www.ogj.com/articles/print/volume-116/issue-3/special-report-us-olefins/uncertainty-looms-for-us-olefins-industry.html (accessed October 24, 2018).

(46) Independent Chemical Information Service (ICIS). US June propylene contracts settle up to 8 cents/lb on snug supply. https://www.ogj.com/articles/print/volume-116/issue-3/special-report-us-olefins/uncertainty-looms-for-us-olefins-industry.html (accessed October 24, 2018).

(47) U.S. Energy Information Administration (EIA). Petroleum and Other Liquids. Weekly Retail Gasoline and Diesel Prices. https://www.eia.gov/dnav/pet/pet_pri_gnd_dcus_nus_a.htm (accessed February 15, 2019).

(48) Whiteley, K. S. Polyethylene In *Ullmann's Encyclopedia of Industrial Chemistry*; Wiley-VCH Verlag GmbH: Weinheim, Germany, 2011.

(49) Calamur, N.; Carrera, M. Propylene In *Kirk-Othmer Encyclopedia of Chemical Technology*; 5th ed.; John Wiley & Sons: Hoboken, NJ, 2000.

(50) Elordi, G.; Arabiourrutia, M.; Bilbao, J.; Olazar, M. Energetic Viability of a Polyolefin Pyrolysis Plant. *Energy Fuels* **2018,** *32* (3), 3751-3759.

(51) Elgowainy, A.; Han, J.; Cai, H.; Wang, M.; Forman, G. S.; DiVita, V. B. Energy Efficiency and Greenhouse Gas Emission Intensity of Petroleum Products at US Refineries. *Environ. Sci. Technol.* **2014,** *48* (13), 7612-7624.

(52) Alibaba Group. Recycled Plastic Bales. https://www.alibaba.com/showroom/recycled-plastic-bales.html (accessed April 17, 2019).

(53) More Recycling Inc. Historical Scrap Plastic Pricing Interactive Chart. https://www.plasticsmarkets.org/view/commoditypricing (accessed April 17, 2019).

(54) Pormeleau, K. The United States' corporate income tax rate is now more in line with those levied by other major nations. https://taxfoundation.org/us-corporate-income-tax-more-competitive/ (accessed January 20, 2019).

(55) Scarboro, M. State corporate income tax rates and brackets for 2018. https://taxfoundation.org/state-corporate-income-tax-rates-brackets-2018/ (accessed January 20, 2018).

(56) U.S. Energy Information Administration (EIA). Electric Power Monthly. Table 5.6.A. Average Price of Electricity by End-Use Sector, by State.

https://www.eia.gov/electricity/monthly/epm_table_grapher.php?t=epmt_5_6_a (accessed April 17, 2019).

5 Systems Analysis of High-value Chemicals and Fuels from a Waste High-Density Polyethylene Refinery. Part 2: Carbon Footprint Analysis and Regional Electricity Effects[4]

Abstract

The increasing generation of plastic waste (PW) is placing severe environmental burdens in the terrestrial and marine environments due to its inappropriate management at end of life. Governmental agencies are aware of this situation and have proposed initiatives to minimize the amount of PW that is landfilled and encourage recycling or energy recovery. Circular economy is a strategy that attempts on reusing PW to produce new polymers while avoiding its disposal and the use of virgin material. Hence this study proposes a refinery design that employs fast pyrolysis and downstream separations to obtain monomers, aromatics and hydrocarbon fuels from waste high-density polyethylene (HDPE). This study focusses on a carbon footprint analysis (CFA) of the refinery and the effect of regional energy grids on greenhouse gas emissions from cradle-to-gate using a process model-based approach. The effects of heat integration (HI) on greenhouse gas (GHG) emissions were investigated in scenarios, as well as investigation of parameter sensitivity and uncertainty. The CFA results show that the GHG emissions of all products; ethylene, propylene, aromatics mixture, low molecular weight (MW) hydrocarbons (HCs), and high MW HCs, are equal to or less than fossil products for the HI scenario assuming US average

---

[4] This chapter will be submitted to *ACS Sustainable Chemistry and Engineering*.

electricity grid. Finally, the evaluation of regional electricity grids on GHG emissions for all products was conducted for all 50 states in the US.

5.1 Introduction

Since their introduction in the 1960s, plastics became widely used by society due to their outstanding properties like durability, lightweight, versatility, and low economic cost.[1] Their impact is such that the worldwide plastic production has increased 4% each year reaching 348 million tonnes produced in 2017.[2,3] However, these positive attributes have nowadays been hidden by the increasing environmental issues related to their disposal and leakage into the environment from mismanagement. Geyer et al.[4] recently reported that by 2015 around 6,300 million tonnes of plastic waste (PW) have been generated from which 79% were discarded in landfills and leaked into terrestrial and marine ecosystems. If these trends of disposal and consumption continue, by 2050 the weight of PW in the oceans will equal that of fish, the share of oil from plastic production will be of 20%, and the total PW discarded will increase to 12,000 million tonnes.[4,5] Besides, plastics are usually single-use products made from virgin fossil-based materials which impose a high burden on these non-renewable resources and promote the reliance on them.[3,6,7]

To abate these unsustainable patterns of plastic production and disposal, the European Commission established a strategy focused on reducing the consumption of single-used plastics, avoiding the fabrication of microplastics, and making all plastic packaging recyclable by 2030.[8] Under these guidelines, one of the major tasks is to promote processes that consider the reuse of PW under a circular economy perspective. From a sustainability

perspective, circular economy aims to maximize the use of virgin materials and energy by using cyclic process flows and renewable resources to provide economic, societal, and environmental benefits without compromising natural cycles.[9] The benefits of this emerging economic approach include the retention of 80 to 120 billion USD that are lost in a linear economy, reduction of 1.1 to 3.0 t of CO_2 eq. of GHG emissions from the recycling of each t of PW, and a more stable market for plastics due to a weaker dependence on fossil feedstocks.[5]

PW is an excellent feedstock for circular economy because its recycling can produce the same products that originated it. Mechanical and chemical recycling are two types of processes that convert plastics into its original products. Mechanical recycling uses decontamination, grinding of PW, melting and molding to fabricate new products however, there is a reduction of the mechanical properties and other qualities of these materials each time that mechanical recycling occurs.[10,11] This degradation causes that after some time the material is no longer suitable for mechanical recycling. Chemical recycling has the potential of forming monomers that can produce plastic with the same quality as those produced from virgin resources, and avoiding the presence of impurities that may reduce the quality of the final product.[12] Gasification, hydrocracking, and pyrolysis are the currently available alternatives for chemical recycling of olefin plastics, which pyrolysis have shown high yields of ethylene and propylene, up to 45 and 26% respectively, at temperatures above 600 °C and short reactor residence times.[13,14]

The evaluation of the environmental performance of an emerging technology like PW pyrolysis to obtain monomers, is a mandatory step to ensure that it accomplished its intended environmental goals. On this regard, life cycle assessment (LCA) arises as a useful methodology because it evaluates the environmental and health-related effects that a process or product has and guides improvements and decisions for future applications by comparison with current business as usual technologies.[15] LCA has been widely employed for the evaluation of different scenarios of PW management, which have mostly focused on the comparison of mechanical recycling, landfill disposal, and incineration.[16-18] Nonetheless, to date there are few LCAs that look into the environmental effects of the chemical recycling of plastics. Molgaard[19] was the first in reporting this type of analysis, in which he compared pyrolysis with five other PW management scenarios (two types of separation, material recycling without separation, incineration with heat recovery, and landfill) using an attributional approach and accounting for the total emissions of the process per inhabitant in the world. He found that pyrolysis has the highest environmental impact in most of the categories evaluated.

More recent studies changed the analysis from an attributional to a consequential approach by including the avoided emissions from the displacement of similar fossil-based products. Perugini et al.[20] presented the first study of this type using the British Petroleum polymer cracking process (BP process) as reference. Their functional unit was of one kg of a mixture of grinded polyethylene terephthalate (PET) and polyolefins and later mechanical recycling of PET and low temperature pyrolysis of polyolefins. The GHG emissions were of 1.7 kg

CO$_2$ eq. per kg of plastic waste processed which were lower compared to those from landfill, combustion with energy recovery, and hydrocracking coupled with mechanical recycling. Shonfield[21] also carried out a comparative LCA with system expansion for the BP process and also discovered that pyrolysis has less GHG emissions per tonne of plastic processed than landfill and incineration. These findings from a consequential approach contrasted with those from Moolgard,[19] and stated the potential benefits of this technology from an environmental perspective. More researchers have extended the evaluation of different management scenarios by considering different sources of PW or geographical locations. Alston and Arnold[22] focused on the treatment of plastics from waste electronic equipment through pyrolysis, landfilling, and incineration; Al-Salem et al.[23] compared incineration, pyrolysis and sorting in a materials recovery facility (MRF) to handle PW generated in London; and Gear et al.[24] compared incineration and landfill with an improved and scaled-up design of an existing PW pyrolysis technology in the U.K. These studies also showed less emissions for pyrolysis compared to landfill disposal and incineration and highlighted the GHG emissions savings from suppressing the use of virgin materials derived from fossil sources.

Iribarren et al.[25] used a functional unit of one kg of gasoline blendstock produced to evaluate the LCA of a pyrolysis process with subsequent catalytic reforming to obtain gasoline and diesel products employing a cradle-to-gate scope. The obtained emissions were of 2.44 kg CO$_2$ eq. per kg of gasoline blendstock, with a decline of 55% when the thermal energy demand is reduced by 80%. A carbon footprint analysis reported by

Gracida-Alvarez et al.[26] compared the GHG emissions of gasoline and diesel produced in Mexico from waste polyolefins pyrolysis with those from crude oil. These researchers found that the emissions per MJ from the pyrolysis pathway, on a cradle-to-grave scope, were 8% lower than those from crude oil production. Similarly, Benavides et al.[27] compared the emissions of ultra-low sulfur diesel obtained from PW pyrolysis and petroleum but for a U.S. scenario. Their findings demonstrated a reduction of 9% in the GHG emissions per MJ using PW pyrolysis compared to petroleum refining.

These previously published LCAs of PW pyrolysis have focused on its comparison with other management scenarios or the evaluation of the global warming potential (GWP) of the produced fuels, but none have considered advanced process designs that include monomers and aromatics production along with alternative transportation fuels. These high value products have the potential to improve the economic feasibility and product quality of the chemical recycling process, which is important in a circular economy approach. There is also a lack of studies including both environmental and economic assessments of plastic pyrolysis technologies. Hence, the present study introduces a new refinery design to produce monomers, aromatics, and hydrocarbon fuels from waste high-density polyethylene (HDPE) pyrolysis along with its economic, energy and environmental assessment. Part 1 of the study reported the conceptual design, based on previous laboratory results[28] and modelling in Aspen Plus, and the energetic and economic evaluations. This second part focusses on the evaluation of the GHG emissions of the refinery products through a carbon footprint analysis (CFA) based on the LCA

methodology, multi-product allocation, effects of heat integration, sensitivity/uncertainty analyses, and influence of the supply of different state-based regional electricity grids.

5.2 Materials and methods

5.2.1 CFA methodology

5.2.1.1 Goal and scope

The present hybrid CFA has two objectives: the calculation of the emissions of greenhouse gases (GHG) from the operation of the conceptual refinery, and the estimation of the GHG emissions per kg of product of the refinery. The information from the first objective will guide forthcoming improvements in the current design and the second objective will serve for comparing the environmental performance of the proposed pyrolysis products with the traditional fossil products. The scope of this study is cradle-to-gate because it included upstream emissions from the production of materials and energy used in the refinery although a zero burden was considered for waste HDPE before its collection. Downstream processing after the products leave the refinery was also not contemplated in the scope of the study. Therefore, the life cycle goes from the collection of waste HDPE to the final products of the refinery, as illustrated in Figure 5.1. The CFA uses a hybrid allocation approach with the main emphasis on attributional using mass allocation with taking of emission credits for exported steam from the process.
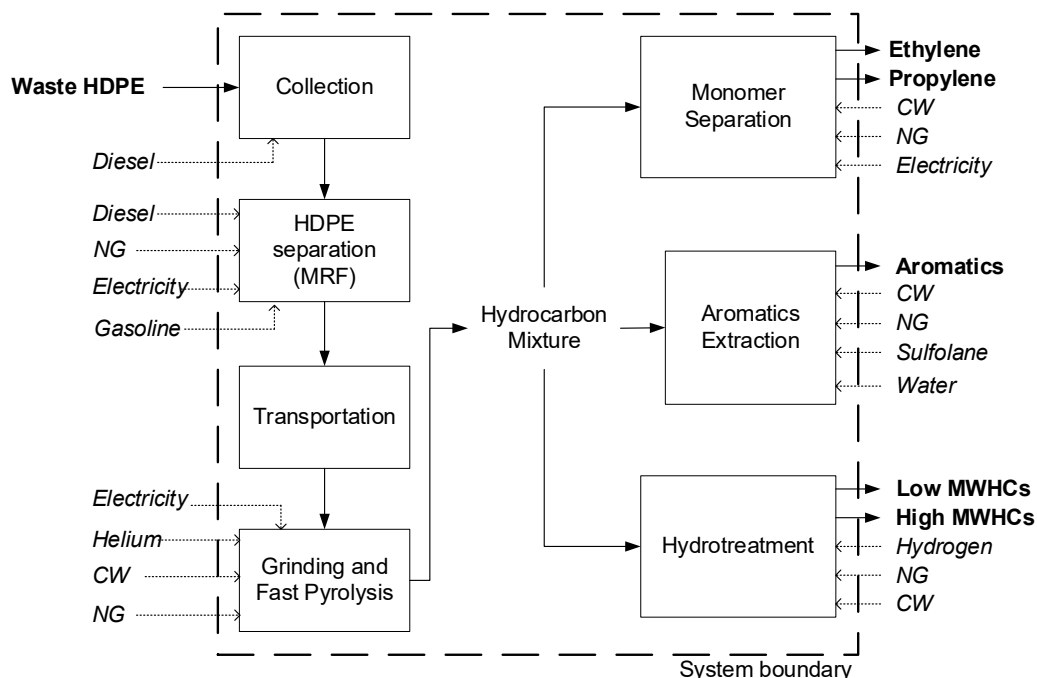
Figure 5.1. Cradle-to-gate system boundary for the proposed process. MRF: Materials recovery facility, CW: cooling water, NG: Natural gas.

5.2.1.2 System boundaries and functional units

Figure 5.1 shows the different stages included in the proposed pathway. After being discarded by households and industries the waste HDPE, mixed with all kinds of municipal solid waste, is collected by garbage trucks and sent to a materials recovery facility (MRF) where it is separated from other plastics and wastes. The waste HDPE is then transported to the designed refinery which is located at a 50 km distance from the MRF. Once in the refinery, the waste HDPE is reduced in size and fed to a fluidized bed reactor where is pyrolyzed at 650 °C for 2.8 s. Sand and helium are used as the heating and fluidizing agents, respectively. The formed pyrolysis hydrocarbon mixture is then separated into different products in the different sections of the refinery. The monomer separation section uses cryogenic temperatures and moderate pressures to separate chemical ethylene and

139

propylene through a distillation sequence. Such low temperatures are achieved by the employment of refrigeration cycles. In the aromatics extraction section, aromatics are separated from aliphatics in the C6-C12 fraction by solvent extraction with sulfolane and water. Finally, the remaining aliphatic and aromatics hydrocarbons are fed to a hydrotreater, operated at 150 °C, where they are converted to fuel-like products that are later separated into a low and a high molecular weight hydrocarbon (MWHCs) mixtures. Section 4.1 of Chapter 4 provides the detailed information of these refining processes which require electricity to run the compressors, pumps and turbines; natural gas to provide heat to distillation columns, furnaces and heaters; and cooling water to reduce the temperatures in condensers and coolers.

As stated previously, this study has two main objectives, therefore, two functional units are used in the CFA. In the calculation of the emissions of refinery operation, a functional unit of one hour of operation is employed, which accounted for the emissions generated for the processing of 20,833.33 kg of waste HDPE. For the estimation of the emissions per product, a functional unit of one kg is used, which is the main functional unit in this study because it allows the comparison of the results to virgin fossil-derived products.

5.2.1.3 Scenarios

The CFA of the refinery focusses on the three scenarios presented in Table 5.1. The first scenario is the base case (BC) that does not include heat integration but considers energy savings from the utilization of energy sources produced within the refinery. For example, electricity savings are achieved by using the electricity generated in the turbines, that

reduce the pressure of the recycled helium, of the monomer separation section (A-200) to fulfill some of the power required by the compressors used to pressurize the low molecular weight gases from the pyrolysis reactor (see Figure 4.1). Also, the purge stream generated in the pressure swing adsorption unit supplies heating for the sand furnace. The heat integrated scenario 1 (HI-1), is similar to the base case but uses the pinch analysis for the design of the heat exchanger network. Additionally, the low pressure (LP) steam generated in the hydrotreater (section 4.2.1.5 of Chapter 4) is used to provide heat for the reboiler in the propylene fractionator (T-211) which reduces the energy requirements of the monomer separation section. The heat integrated scenario 2 (HI-2) only differs from scenario HI-1 in the use of the steam from the hydrotreater. In this scenario, instead of being used internally, the savings on emissions from the use of this steam are credited to the hydrotreatment section (A-400). The main purposes of the use of these scenarios were to estimate the impact of heat integration on the environmental performance of the refinery and to evaluate how the different uses and considerations on emission savings of a co-product, like low pressure (LP) steam, affect the GHG emissions of each product in the refinery.

Table 5.1. Scenarios considered in the CFA.

Scenario	Description
Base Case (BC)	Conceptual design of the refinery without heat integration
Heat Integrated Scenario 1 (HI-1)	Refinery design with heat integration included and using steam generated in the hydrotreater to heat the reboiler of the propylene fractionator in the monomer separation section (A-200).
Heat Integrated Scenario 2 (HI-2)	Refinery design with heat integration accounting emission credits of steam generated in the hydrotreater for the hydrotreatment section (A-400).

5.2.1.4 Mass allocation

Due to the complexity of the multiproduct/multiproces refinery presented in this study, an attributional CFA is carried out. Therefore, the total emissions from the use of materials and energy in the refinery are distributed among the different products.[29] Mass allocation was the chosen approach which required the rigorous tracking of the amount of each product entering and leaving each unit of the refinery. It is important to point out, that the tracking was done to the products and not to chemical species. For example, due that both aromatics as well as low and high MWHCs products contained certain amount of aromatic hydrocarbon species (imperfect separations), these aromatic species were not considered to be exclusively part of the "aromatics" product. Certain fractions, according to the mass balances, of these aromatic species were accounted for the low and high MWHCs products.

Most LCAs use a "black box" approach that allocate the complete impacts of the refinery among each of the generated products. This approach does not consider that some products do not flow through certain units in the refinery which results in an imprecise allocation of impacts. To carry out a more accurate mass allocation, this CFA divided the refinery in nine blocks, according to Figure D-1 of Appendix D, instead of using the traditional "black box" approach. These blocks are section-specific and include inlets of materials, outlets of products, or streams that connect different sections of the plant. A brief description of the main characteristics of each block is presented in Table 5.2. The accounting for compounds in each product mass flows through the various blocks was carried out in a reverse order through the process, from products to feedstock, starting with the low and high MWHCs

142

in the hydrotreatment block. For separators, the fraction of each compound in an inlet stream going to each product or outlet streams was calculated using equation (5.1):

$$xi_{jk} = \frac{Fo_{jk}}{Fi_j} \qquad (5.1)$$

where xi_{jk} is the fraction of compound j in the inlet stream i that goes into product k, Fo_{jk} is the mass flow of compound j in product k in the outlet or product stream o in kg/h, and Fi_j is the mass flow of compound j in the inlet stream i of the separator in kg/h.

Table 5.2. Characteristics of the designated blocks for calculation of mass allocation factors.

Section	Block	Inlet materials	Outlet products	Process units
A-100	Block A	Waste HDPE Helium	None	Pyrolysis reactor, sand furnace, and cyclone.
A-200	Block B	None	Methane purge	Compressors, turbines, and pressure swing absorption unit.
	H+DE	None	Ethylene	De-ethanizer column.
	D+CP	None	None	Depropanizer column.
	H+PF	None	Propylene	Propylene fractionator column.
A-300	H+PS	None	None	Phase separator.
	DB+DP	None	None	Debutanizer and depentanizer columns.
	Block C	Sulfolane Water	Aromatics product	Extractive distillation and aromatics recovery columns, and rotary disc contactor.
A-400	HT	Hydrogen	Low MWHCs product High MWHCs product	Hydrotreater.
H+DE: Heater + De-ethanizer, H+DP: Heater + depropanizer, H+PF: Heater + Propylene fractionator, H+PS: Heater + Phase separator, DB+DB: Debutanizer + depentanizer, HT: Hydrotreatment.				

In mixers the fraction of each compound of the inlet streams going to a certain product was assumed to be equal to that of the outlet stream, as stated in equation (5.2):

$$xs_{jk} = xo_{jk} \tag{5.2}$$

Where xs_{jk} is the fraction of compound j in the inlet stream s that goes into product k and xo_{jk} is the fraction of compound j in the outlet stream that goes into product k. Thus, the mass flow of a specific compound going to a certain product in an inlet stream was estimated with equation (5.3):

$$Fs_{jk} = xs_{jk} \cdot Fs_j \tag{5.3}$$

where Fs_{jk} is the mass flow of compound j going to product k in the inlet stream s in kg/h and Fsj is the mass flow of compound j in the inlet stream s in kg/h.

In the hydrotreater only saturated hydrocarbons and aromatics are found in the outlet stream, therefore it was important to develop a method for tracking the fraction of alkenes and alkadienes, occurring in the inlet stream, that might be part of the low and high MWHCs products. The used approach consisted in neglecting one at a time the hydrotreatment reactions that consume alkenes and alkadienes, and account for their fraction distribution in low and high MWHCs products conforming to equation (5.1). A sample calculation of the reverse balances for the hydrotreatment block is shown in section D-1 of Appendix D.

Once the mass flow of each compound per product in a certain stream was estimated, the total amount of product in that stream was calculated with equation (5.4):

$$Fs_k = \sum_{j}^{n} Fs_{jk} \tag{5.4}$$

where Fs_k is the mass flow of compound k in the inlet stream s in kg/h. When the mass flows of each product in the inlet and outlet streams of each block were estimated (Figure 5.2), the mass allocation factor for each product in a block was obtained by dividing the total flow of products leaving that block by the mass flow of the specific product leaving the block as shown in equation (5.5):

$$MAF_{km} = \frac{F_{km}}{\sum_{k}^{n} F_{km}} \tag{5.5}$$

where MAF_{km} is the mass allocation factor of product k in block m, and F_{km} is the mass flow of product k leaving block m in kg/h. The complete list of mass allocation factors for each product in each block is shown in Table D-5 of Appendix D. The mass allocation factors for each block sum to one over the range of products flowing through each block.
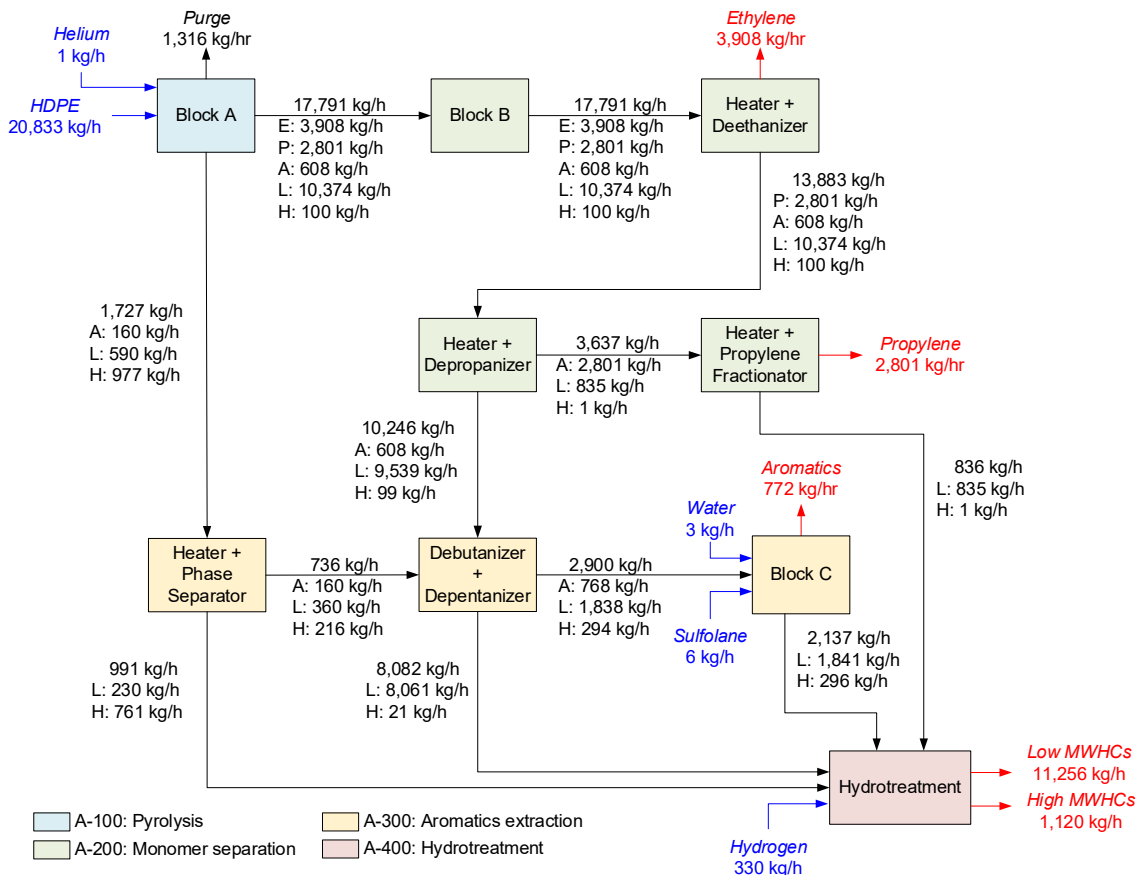
Figure 5.2. Product mass flows of the designated blocks for mass allocation. E: Ethylene, P: Propylene, A: Aromatics mixture, L: Low MWHCs mixture, H: High MWHCs mixture.

5.2.1.5 Life cycle inventory and impact assessment

Figure 5.1 shows the general material and energy inputs for the proposed pathway. According to Fitzgerald et al.,[30] the emissions for collection only account for the use of 14.25 L of diesel per tonne of solid waste processed. In the separations at the MRF, the inputs include the use of electricity (13.76 kWh/tonne processed through the MRF), natural gas (0.026 GJ/tonne), diesel (0.71 L/tonne), and gasoline (0.13 L/tonne) required for its operation. Emissions for transportation considered the shipping of the waste HDPE from

146

the MRF to the refinery through 50 km using high capacity trucks. Data from the process

modelling in Aspen Plus served to estimate the material and energy inputs for the different

refinery operations. These inputs are shown in Table 5.3 and vary among the different

scenarios. Detailed information of the inputs per block and unit operation of the refinery is

provided in Tables D-6 to D-8 of Appendix D, on an hour of operation basis.

Table 5.3. Material and energy inputs of refinery operations per tonne of waste HDPE processed.

Area	Input	BC	HI-1	HI-2
A-100	Electricity (kWh)	333.54	330.70	330.70
	Natural gas (GJ)	2.20	0.50	0.50
	Cooling water (m^3)	3.95	1.44	1.44
	Helium (kg)	0.04	0.04	0.04
A-200	Electricity (kWh)	954.55	791.57	791.57
	Natural gas (GJ)	2.42	0.59	1.49
	Cooling water (m^3)	7.37	5.75	5.75
A-300	Natural gas (GJ)	0.60	0.51	0.51
	Cooling water (m^3)	0.79	0.63	0.63
	Sulfolane (kg)	0.27	0.27	0.27
	Process water (kg)	0.17	0.17	0.17
A-400	Natural gas (GJ)	0.25	0.00	0.00
	Cooling water (m^3)	0.09	0.09	0.09
	Hydrogen (kg)	15.82	15.82	15.82

The software SimaPro v.8.5.2 (PRé Consultants B.V.) was used to obtain the CFA results of the different stages in the proposed pathway. GWP was the indicator used for the impact assessment because it expresses the environmental burdens of feedstock and processes within the life cycle in kg of CO_2 equivalent emissions per functional unit apart from having well characterized factors and concepts.[12,15] The GHG emissions for each input and process were calculated with the Intergovernmental Panel on Climate Change (IPPC) method,[31] considering a timeframe of 100 years. Ecoprofiles for the different material and energy inputs were obtained from the Ecoinvent, industrial data 2.0, and USLCI databases included in the software. The ecoprofiles and inventory data for the BC scenario are presented in Table 5.4. A more detailed inventory of the BC scenario and the inventory of scenarios HI-1 and HI-2 are shown in Tables D-6 to D-8 of Appendix D. The assumptions made for this inventory include the use of the U.S. average grid electricity mix, natural gas reforming as the production technology of the hydrogen supplied to the refinery, and replenishment rate of 5% of the water treated for cooling. Additionally, emissions from the use of materials like sand, catalyst, and refrigerants were neglected due that they are restored after a long period of time.

Table 5.4. Material and energy inputs of the BC scenario (Basis: one hour of operation, processing of 20.83 tonnes of waste HDPE).

Stage	Ecoprofile	Amount
Collection	Diesel RoW| market for | APOS, S with combustion	248.48 kg
Separation at MRF	Electricity, high voltage US| market group for | APOS, S	286.64 kWh
	Heat, district or industrial, natural gas RoW| market for heat, district or industrial, natural gas | APOS, S	541.67 MJ
	Diesel RoW| market for | APOS, S with combustion	12.38 kg
	Petrol, unleaded RoW| market for | APOS, S with combustion	2.02 kg
Transportation	Transport, freight, lorry >32 metric ton, EURO6 RoW| transport, freight, lorry >32 metric ton, EURO6 | APOS, S	1041.67 tkm[a]
Pyrolysis	Electricity, high voltage US| market group for | APOS, S	6,948.57 kWh
	Heat, district or industrial, natural gas RoW| market for heat, district or industrial, natural gas | APOS, S	45.85 GJ
	Water, completely softened, from decarbonised water, at user GLO| market for | APOS, S	81,985.47 kg
	Helium GLO| market for | APOS, S	0.89 kg
Monomer separation	Electricity, high voltage US| market group for | APOS, S	19,886.13 kWh
	Heat, district or industrial, natural gas RoW| market for heat, district or industrial, natural gas | APOS, S	50.49 GJ
	Water, completely softened, from decarbonised water, at user GLO| market for | APOS, S	153,163.8 kg
Aromatics extraction	Heat, district or industrial, natural gas RoW| market for heat, district or industrial, natural gas | APOS, S	12.57 GJ
	Water, completely softened, from decarbonised water, at user GLO| market for | APOS, S	16,310.79 kg
	Solvent, organic GLO| market for | APOS, S	5.66 kg
	Water, deionised, from tap water, at user RoW| market for water, deionised, from tap water, at user | APOS, S	3.50 kg
Hydrotreatment	Heat, district or industrial, natural gas RoW| market for heat, district or industrial, natural gas | APOS, S	5.30 GJ
	Water, completely softened, from decarbonised water, at user GLO| market for | APOS, S	1,925.56 kg
	Hydrogen (reformer) E	329.55 kg
	Steam, in chemical industry RoW| production | APOS, S	8461.24 kg[b]
[a]tkm: tonne-kilometer. [b]Emissions used as credits.		

The calculation of the GHG emissions per hour of operation of the refinery consisted in the sum of the total emissions per section of the material and energy inputs. The collection, separation at MRF, and transportation (CST) stages were not included in this analysis. The evaluation of the GHG emissions per kg of product used equation (5.6):

$$GHG_k = \frac{\sum_m^n GHG_m \cdot MAF_{km}}{F_k} \qquad (5.6)$$

where GHG_k are the greenhouse gas emissions of product k in kg of CO_2 eq. per kg; GHG_m are the greenhouse gas emissions of block m in kg of CO_2 eq. per hour of operation (processing of 20.83 tonnes of waste HDPE), MAF_{km} is the mass allocation factor for product k in block m, and F_k is the production of compound k in kg/h (see Table D-9 of Appendix D). Only the blocks that included the product being analyzed were part of the calculation. CST stages were incorporated in this evaluation of the emissions per kg of product. The GHG emissions of each product were compared to its fossil counterpart. The GHG emissions for ethylene, propylene, and aromatics were obtained from the USLCI database in SimaPro, and for the aromatics product was calculated by multiplying the GHG emissions per kg of benzene, toluene, xylenes, and styrene by their corresponding mass compositions in the aromatic product. The emissions of the low and high MWHCs were compared with the values reported by Cooney et al.[32] for gasoline and diesel, respectively.

5.2.1.6 Sensitivity analysis

To determine which parameters of the CFA have a major effect on the GHG emissions per product; the yield, the electricity, natural gas, and hydrogen requirements and the

generation of steam (for low and high MWHCs) were varied in ± 15%. The emissions per product were calculated again considering the variation of one parameter at a time and were compared with the values originally obtained.

5.2.1.7 Uncertainty analysis

The variability of the inventory data has an effect on the accuracy of the CFA results, therefore, an uncertainty analysis of the results of the current study was performed considering the uncertainty of the data from the Ecoinvent database. The uncertainty from the Ecoinvent database follows a lognormal distribution based on expert judgment.[33] The GHG emissions per kg for each product were calculated with the Monte Carlo simulatons in SimaPro. This methodology uses random values within the variability of the data in the Ecoinvent database to estimate the mean, the median, and the 95% confidence interval of the impact under study. A total of 10,000 simulations were performed for each product in the different scenarios.

5.2.2 Analysis of regional electricity grids and geographical location

Energy sources have an effect on the environmental performance of the proposed pathway because of the high electricity requirements presented. Therefore, alternative scenarios substituting the U.S. average electricity mix by other energy sources like coal, hydropower, natural gas, nuclear, solar, and wind were analyzed. This evaluation required the modification of all the ecoprofiles of electricity from U.S. average mix to that of the

analyzed source. Table D-10 of Appendix D presents the ecoprofiles in SimaPro used for each energy source.

This analysis included the effect of different electricity grid mix in different states of the U.S. The Emissions and Generation Resource Integrated Database (eGRID) from the U.S. Environmental Protection Agency (EPA)[34] provided the information of the electricity mix at each state (see Table D-11of Appendix D). The GHG emissions per kWh at each state were calculated by multiplying the percentage contribution of each source by its corresponding emissions according to the ecoprofiles from SimaPro. Same as the analysis of energy sources, these emissions substituted those from the U.S. average mixture in the calculation of the GHG emissions per kg of product from the refinery. The results from this analysis along with the comparison with their fossil-based emissions served to develop a map of potential state locations for the refinery using different criteria. This geographical location analysis was only applied to scenarios HI-1 and HI-2.

5.3 Results and discussion

5.3.1 GHG emissions of the refinery

According to the inventory presented in Table 5.3, the GHG emissions from the different sections of the refinery were calculated on the basis of one hour of operation, which are shown in Figure 5.3. For all the scenarios, the greatest rate of GHG emissions are due to the monomer separation section (A-200). This is because of the high requirements of electricity to operate the compressors to reach the pressures (7 bar) and to operate the

refrigeration cycles. This area generates between 59 to 68% of the refinery emissions depending on the scenario being evaluated. The second largest area contributing to GHG emissions is the pyrolysis section (A-100), with most of its electricity requirements coming from the shredding and grinding processes. From Figure 5.3, it can also be observed that from all the inputs to the refinery, electricity consumption causes the highest amount of emissions in the facility, contributing with at least 70% of the total emissions. Therefore, improvements in the environmental performance of this process should consider operation conditions that reduce the electricity requirements (i.e. moderate pressures and non-cryogenic temperatures) or consider greener sources of electricity than assumed in this analysis (U.S. average grid electricity).
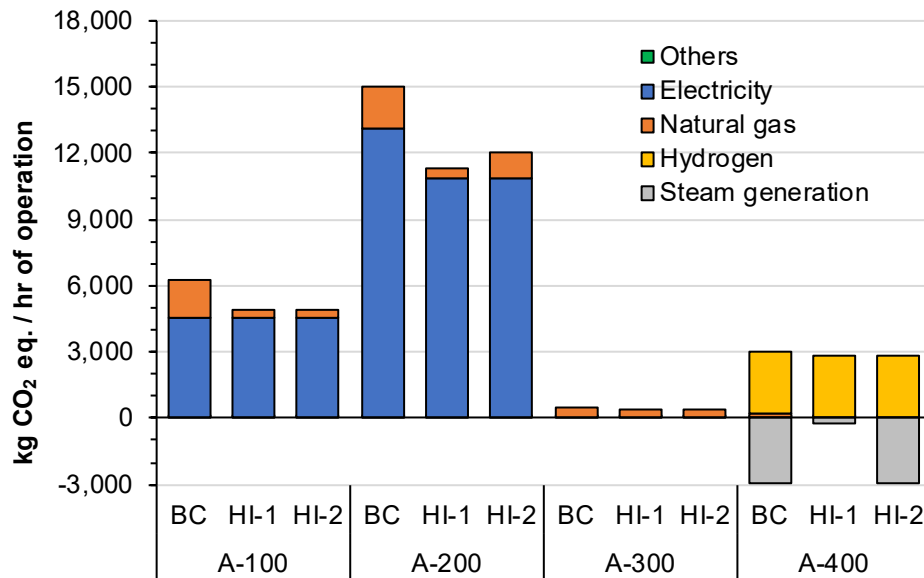
Figure 5.3. Emissions at each plant section per hour of operation. A-100: Pyrolysis, A-200: Monomer separation, A-300: Aromatics extraction, A-400: Hydrotreatment.

153

When the different scenarios are compared in Figure 5.3 (BC, HI-1, HI-2), there is a clear reduction of the emissions with the heat integrated (HI) scenarios. The reduced requirements of refrigeration in the HI cases lead to a reduction in GHG emissions from electricity of 13%, and the heat exchanger network reduced the emissions from heating by 70%, for scenario HI-1, and 54% for scenario HI-2. The different choices for use of steam generation in scenarios HI-1 and HI-2, changed the emissions in the hydrotreatment section (A-400). In scenario HI-1, the hydrotreatment (A-400) emissions accounted for 2,580 kg CO_2 eq. per hour of operation while in scenario HI-2, the emissions in this section were negative with a value of -112 kg CO_2 eq. per hour of operation. This difference has an important effect on the emissions per kg of product which will be discussed in the next section. The total emissions for one hour of plant operation for the different cases were 21,828, 19,235, and 17,242 kg CO_2 eq. for scenarios BC, HI-1, and HI-2, respectively.

If the total emissions are divided by the 20.83 t of waste HDPE fed each hour to the refinery, the GHG emissions are then 1.05, 0.92, and 0.83 kg CO_2 eq per kg of waste HDPE processed for the BC, HI-1, and HI-2 scenarios, respectively. These values are one order of magnitude higher compared with studies following system expansion,[12,21,23,27] that range between −0.35 to 0.1 kg CO_2 eq. per t of PW, which highlights the importance of the allocation method in the outcome results of the LCA. However, these emissions were lower than those reported (1.7 kg CO_2 eq. per kg of plastic) by Perugini et al.[20] for the BP process even though they considered avoided burdens of the pyrolysis products. This can be due to differences in the inventory data like sources of electricity and heat generation or other

process inputs and specifications that are not mentioned in their study. It is also interesting that current facilities in the U.S. triple the emissions (3.6 kg CO_2 eq. per kg of PW) of the proposed refinery when an attributional approach is employed and vehicular emissions are counted.[27]

Considering the inventory presented by Fitzgerald et al.,[30] the emissions from collection, transportation, and separation in a MRF (CST) were calculated. The obtained values were 933, 92, and 264 kg CO_2 eq. for the processing of 20.83 tonnes of waste HDPE per hour. These emissions are included in the analysis of the GHG emissions of the different products produced in the refinery, presented next.

5.3.2 GHG emissions of the waste HDPE refinery products

The cradle-to-gate emissions per product were obtained using the product allocation factors presented in the section 5.2.1.4 and the product yields obtained from the modelling of the refinery (see Table D-9 of Appendix D). Figure 5.4 displays the results for monomers and aromatics and the contributions of each stage of the life cycle. As revealed in the analysis of the emissions per plant section (Figure 5.3), the monomer separation section (A-200) is the biggest source of GHG emissions on each product followed by the pyrolysis section (A-100). When the GHG emissions of the HDPE pyrolysis products is compared to that from the fossil resources, it is seen that the emissions for all the scenarios are lower. For ethylene and aromatics, the emissions for the heat integrated scenarios were reduced almost by half (44%) compared to the fossil pathway. Focusing on propylene, the scenarios had an important effect on the emissions per kg. The use of steam from A-400 to provide heat

for the propylene fractionator (scenario HI-1) decreased emissions by 38%, while HI-2, which used the steam in the hydrotreatment section (A-400), produced a reduction of 25% in GHG emissions. These results are promising and represent an important improvement from an environmental perspective for chemical recycling of HDPE.
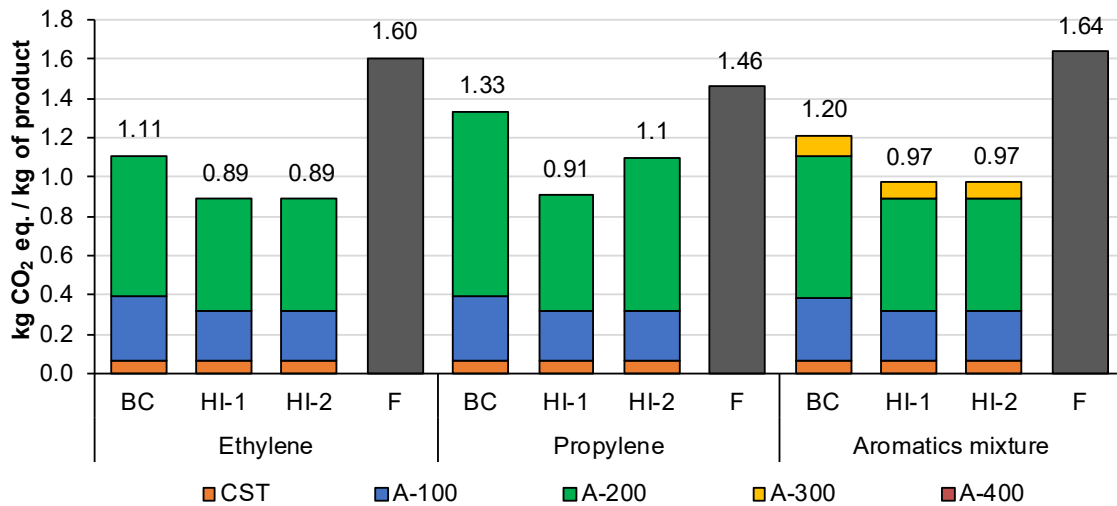
Figure 5.4. Comparison of GHG emissions per kg of product for monomers and aromatics assuming U.S. average grid electricity. BC: Base case refinery, HI-1: Heat integrated refinery Sc1, HI-2: Heat integrated refinery Sc2, F: Fossil pathway.

Figure 5.5 exhibits the cradle-to-gate GHG emissions per kg of low and high MWHCs fuels produced in the refinery. Again, the monomer separation section is the largest contributor to GHG emissions. It is noteworthy that depending on the analyzed scenario the emissions can be more distributed between process sections. Therefore, the decision on where to use the excess steam generated in A-400 made in each scenario had an important impact on the GHG emissions of each fuel. The Low MWHCs mixture showed in the BC scenario increased emissions compared to the fossil pathway for gasoline, but these are not higher than 16%. The most important change occurred for the scenario HI-2, which showed

8% reduced emissions per kg of Low MWHCs mixture compared to the GWP of fossil gasoline. The analysis of the High MWHCs mixture showed a similar pattern to that from the Low MWHCs with the difference that the emissions from the scenario HI-2 were 5% higher to those from the fossil pathway of diesel. A comparison between the performance of the BC and HI-1 scenarios demonstrated that GHG generation for both low and high MWHCs in both cases is very similar. Hence, an actual improvement in the emissions per kg of the Low and High MWHCs can only be obtained using the steam generation credits in the hydrotreatment section.
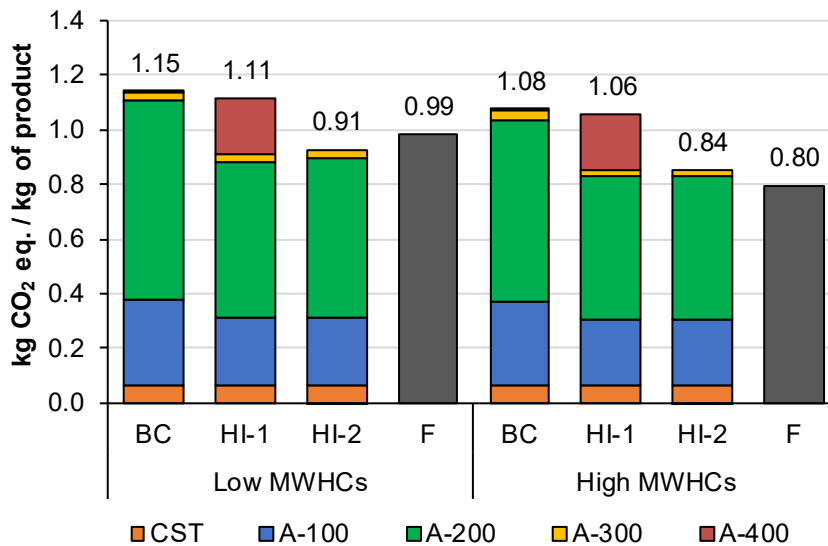
Figure 5.5. Comparison of GHG emissions per kg of product for fuels assuming U.S. average grid electricity. BC: Base case refinery, HI-1: Heat integrated refinery Sc1, HI-2: Heat integrated refinery Sc2, F: Fossil pathway.

The division of these GHG emissions by the LHV of the low and high MWHCs products gives the GHG emissions on a per MJ basis. The values for scenario HI-2 are 21 and 19.7 gCO_2 eq. per MJ of the low and high MWHCs, respectively. A comparison with the results from Iribarren et al.[25] (20.5 gCO_2 eq. per MJ) and Gracida-Alvarez et al.[26] (16 gCO_2 eq.

per MJ) shows a similar performance. This indicates the improvements that the current design has by using internal energy sources and heat integration. Future designs could include less energy intensive separation units and more alternatives of internal use of energy resources to decrease GHG emissions. However, this also depends on the targeted products in the design, as illustrated by Benavides et al.[27] who used the gas produced from pyrolysis to completely fulfill the heating and electricity requirements of the process reducing the cradle-to-gate GHG emissions of diesel to 7 gCO$_2$ eq. per MJ.

In general, these results present considerable improvements on the emissions per kg of monomers, aromatics, and fuels when compared to a fossil pathway in their life cycle. Despite being an energy intensive process, the current pyrolysis pathway has the advantage of avoiding emissions from the extraction and processing of virgin materials which improved its overall environmental performance.

5.3.3 Sensitivity analysis

The effect of the different inputs of the CFA in the emissions per kg of monomers and aromatics for the scenario HI-1 is presented in Figure 5.6. The results show that the product yield is the parameter with the highest impact in the GHG emissions per kg of product, with an increase of 17% of emissions for a decrease in yield of 15% and a reduction of 13% emissions for an increase in yield of 15%. The electricity requirements are another important factor in the environmental performance of monomers and aromatics modifying the GHG emissions between 14 and 13%, depending on the product. This shows that the use of alternatives to reduce the electricity consumption or use cleaner generation of

electricity should be encouraged. The natural gas requirements did not show an important

effect on the GHG emissions of these products.
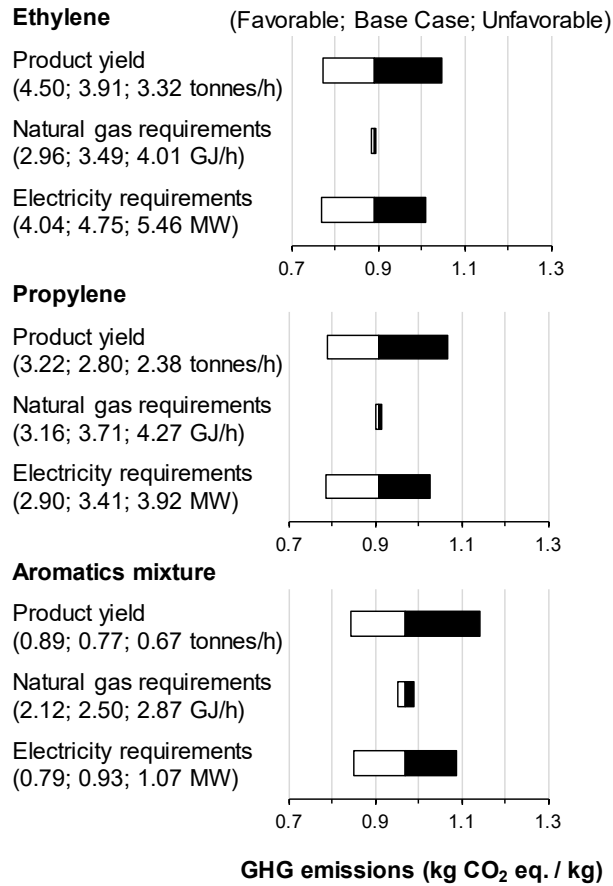
Figure 5.6. Sensitivity analysis for monomers and aromatics (scenario HI-1).

The results of the sensitivity analysis of fuels are shown in Figure 5.7, which in comparison

with those presented in Figure 5.6 include the effects of the hydrogen requirements and

steam generation. Figure 5.7 indicates that product yield also has the highest influence on

the GHG emissions for fuels, with the same increment and reduction as monomers and

aromatics, followed by the electricity requirements that showed an effect of $\pm$ 11%.

Hydrogen requirements exhibited a low effect with only a 3% of change in the emissions

of fuels due to its relatively small input requirement, whilst sensitivity to natural gas requirements and steam generation did not have a significant impact on the emissions. The results of the sensitivity analysis of Scenario HI-2 are presented and discussed in section D.4 of Appendix D.
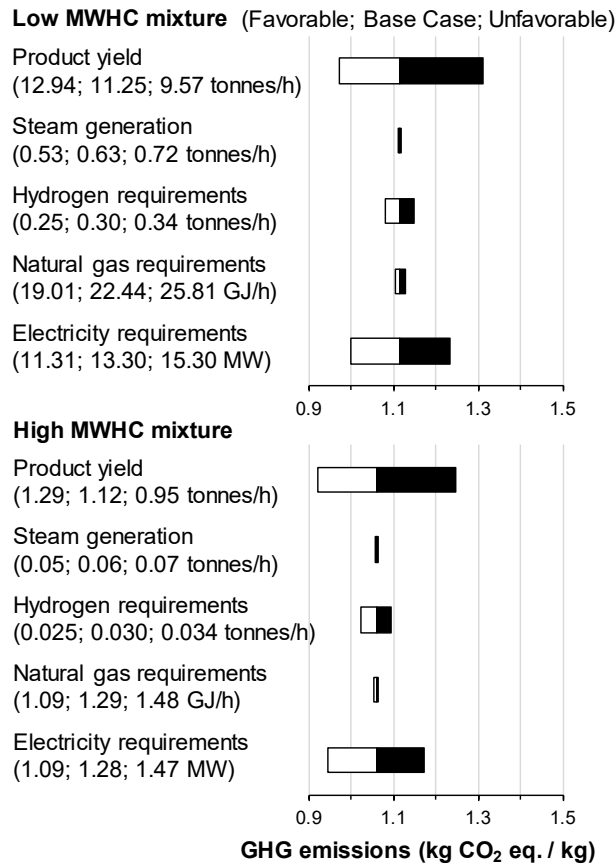
Figure 5.7. Sensitivity analysis for fuels (scenario HI-1).

5.3.4 Uncertainty analysis

The results of the Monte Carlo simulations for the estimation of the GHG emissions of ethylene are shown in Figure 5.8 for scenario HI-1. The average value is 0.89 kg CO_2 eq. per kg of product which is the same to that obtained in Figure 5.4. The range of 95% confidence goes from 0.85 to 0.94 kg CO_2 eq. per kg, which is far from the 1.60 kg CO_2

eq. per kg obtained from fossil feedstock. Therefore, there is a high confidence that the emissions from the pyrolysis-based pathway are lower than those from fossil sources for ethylene. Similar results are observed for propylene and aromatics (see Figures D-4 and D-5 of Appendix D), whose ranges go from 0.86 to 0.96 kg CO_2 eq. per kg for propylene and from 0.93 to 1.02 kg CO_2 eq. per kg for aromatics. The Monte Carlo analysis results for fuels are presented in Figures D-6 and D-7 of Appendix D, the 95% confidence intervals go from 1.07 to 1.17 and from 1.03 to 1.13 kg CO_2 eq. per kg for the low and high MWHCs products, respectively. However, in this case there is a good confidence that the GHG emissions from scenario HI-1 is higher than those from the fossil pathway for both fuels. The results from this uncertainty analysis point out the low uncertainty and high confidence in the GHG emissions estimated for the refinery products.

Method: IPCC 2013 GWP 100a V1.03, confidence interval: 95 %

Uncertainty analysis of 1 p 'Ethylene HI U (per kg of product)',
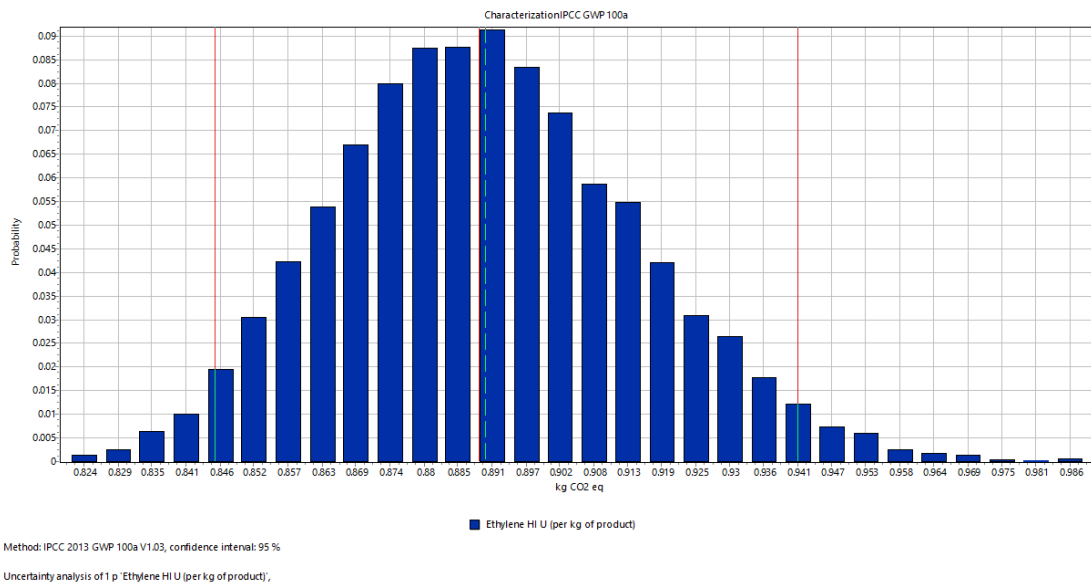
Figure 5.8. Results of the Monte Carlo simulations for the GWP of ethylene in scenario HI-1.

5.3.5 Regional electricity grids and geographical location analysis

As discussed in section 5.3.1 electricity is the input with the major contribution to GHG emissions, therefore, options to reduce its requirements or cleaner energy sources for its generation should be considered to improve the environmental sustainability of the facility. In an attempt to estimate the advantages of using cleaner energy sources, the GHG emissions of the different products of the refinery were estimated using different energy sources in the generation of electricity, as illustrated in Table 5.5. Hydropower is the source that provides the lowest GHG emissions for all the products with a reduction, depending on the product, from 70 to 94%. Other sources that also presented low emissions were nuclear and wind. On the other hand, using coal and natural gas to produce the electricity supplied to the refinery increased the emissions compared to U.S. average mix for all the products.

Table 5.5. Emissions of the refinery products in the scenario HI-1 with different electricity sources (kg CO_2 eq./ kg product).

Electricity source	Ethylene	Propylene	Aromatics mixture	Low MWHCs mixture	High MWHCs mixture
U.S. average mix	0.89	0.91	0.97	1.11	1.06
Coal	1.55	1.57	1.62	1.76	1.68
Hydropower	0.09	0.12	0.18	0.34	0.31
Natural gas	1.01	1.04	1.09	1.24	1.17
Nuclear	0.10	0.13	0.14	0.35	0.32
Solar	0.15	0.18	0.24	0.40	0.37
Wind	0.10	0.13	0.19	0.35	0.32

The results from Table 5.5, highlight the importance of primary energy sources for electricity in the reduction of emissions from the refinery products. The environmental performance of the different products generated at refineries in each state are summarized in Figure 5.9. As observed, the use of the different heat integrated scenarios has an important impact on the emissions of the different products in each state. For scenario HI-1 only in Vermont can fuels with 50% lower emissions be produced, while for scenario HI-2 this reduction in emissions can be achieved also in Washington, Oregon, Idaho, Maine, and New Hampshire. The percentage savings from fossil fuel pathways in the six states is presented in Table 5.6. These savings are due to a high contribution of clean electricity sources like hydropower (Vermont, Washington, Idaho, and Oregon) and nuclear (New Hampshire). These facts also achieved that in scenario HI-2 both Low and High MWHCs can be produced with lower emissions than fossil production in nearly half of the states.

As discussed in Chapter 4, the cost of electricity varies among the different states in the U.S. Therefore, the regional electricity analysis incorporated the effects of the electricity costs to suggest potential locations that provide both environmental and economic benefits for the refinery. The electricity prices of the six states with more than 50% reduction in emissions from the fossil-pathway are presented in Table 5.6, from which is observed that the states with lower electricity prices are Washington, Idaho, and Oregon. The analysis in Chapter 4 showed that there is a direct relation between the electricity costs and the net present value, hence, it is expected that locating the refinery in any of these states would improve its economic sustainability.
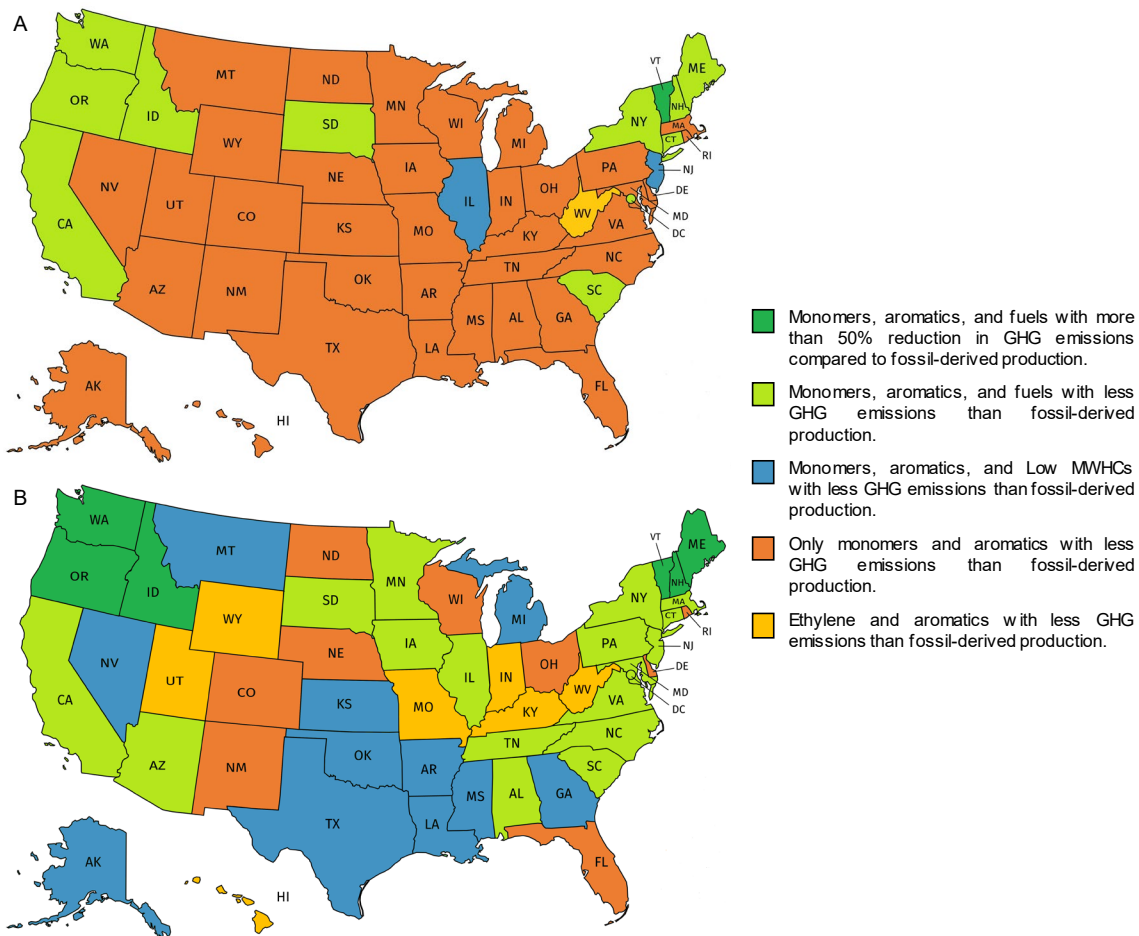
Figure 5.9. Effect of state mixture composition on the GHG emissions of the refinery products. A) Scenario HI-1, B) Scenario HI-2.

Table 5.6. Percentage savings of low and high MWHCs compared to the fossil gasoline and diesel pathways and electricity cost per state.

State	low MWHCs	high MWHCs	Electricity Cost (USD/kWh)[35]
Vermont	88.1	91.1	0.101
Washington	75.2	75.6	0.047
Idaho	70.1	69.5	0.064
New Hampshire	63.3	61.3	0.123
Oregon	62.2	60.1	0.062

Although this CFA included only greenhouse gas emissions over the cradle-to-gate life cycle, when considering the TEA results from the last chapter we might envision that other environmental impacts could be reduced. One of the potential benefits of the production of chemical and fuels from the pyrolysis of waste HDPE might be the reduction of its leakage to the oceans. The results from this study present a promising scenario for this technology which could increase the economic value of PW and therefore reduce its accumulation in landfills and leakage to the oceans with negative impacts on the marine ecosystems. This reduction may have the effect to decrease the amount of PW sent from U.S. and Europe to developing countries that have shown serious problems of mismanagement and ocean leakage.[36] However, these effects on pollution reduction and added value of PW can only be estimated with the use of economic models that predict consumption habits of the population.

5.4 Conclusions

The results of this study highlight the importance of the CFA methodology on a multiproduct/multiprocessing refinery. The use of a rigorous mass allocation, compared to the traditionally "black box" approach, appropriately assigns the GHG emissions from the different sections of the refinery to the different products. Therefore, for scenario HI-2 it was possible to lower or level the GHG emissions of all the products to their fossil production pathway, even with the inclusion of energy-intense processes usually not found in fuels production facilities (i.e., monomer separation train). The analysis of different scenarios demonstrates the impact of decision making on targeting the reduced emissions

to specific products, as observed in the shifting of GHG emissions between propylene and fuels because of the different uses of the LP steam generated in the hydrotreatment section.

Monomer separation is the process with the largest GHG emissions (between 59 to 68% of the total), due to the high electricity requirements to achieve cryogenic temperatures and high pressures. Hence, the use of alternative technologies that reduce the energy requirements of monomer separation will be of important consideration in the forthcoming improvements of the current design. Electricity requirements and product yields are the parameters with greatest influence on CFA, which encouraged the evaluation of regional U.S. electricity grids. The outcomes of this analysis show that in some states it is possible to reduce the GHG emissions per product more than 50% compared to fossil-based production. Finally, the proposed refinery can produce chemical grade ethylene, propylene, and aromatics with less GHG emissions than fossil-based production, and low and high MWHCs with a similar environmental performance of fossil gasoline and diesel, respectively. The overall results from this study encourage and sustain the development of the circular economy of plastic, which can potentially solve the current issues of plastic disposal and contamination while diminishing the use of non-renewable and virgin resources.

5.5 Acknowledgements

5.6 References

(1)   Leal Filho, W.; Saari, U.; Fedoruk, M.; Iital, A.; Moora, H.; Kloga, M.; Voronova, V. An overview of the problems posed by plastic products and the role of extended producer responsibility in Europe. *J. Clean Prod.* **2019,** *214*, 550-558.

(2)   Plastics Europe. Plastics - the Facts 2018. An analysis of European plastics production, demand and waste data. https://www.plasticseurope.org/application/files/6315/4510/9658/Plastics_the_facts_2018 _AF_web.pdf (accessed March 14, 2019).

(3)   Burange, A. S.; Gawande, M. B.; Lam, F. L. Y.; Jayaram, R. V.; Luque, R. Heterogeneously catalyzed strategies for the deconstruction of high density polyethylene: plastic waste valorisation to fuels. *Green Chem.* **2015,** *17* (1), 146-156.

(4)   Geyer, R.; Jambeck, J. R.; Law, K. L. Production, use, and fate of all plastics ever made. *Sci. Adv.* **2017,** *3* (7), e1700782.

(5)   World Economic Forum; Ellen McArthur Foundation; McKinsey & Company. The New Plastics Economy - Rethinking the future of plastics. https://www.ellenmacarthurfoundation.org/assets/downloads/EllenMacArthurFoundation _TheNewPlasticsEconomy_Pages.pdf (accessed March 14, 2019).

(6)   Hees, T.; Zhong, F.; Sturzel, M.; Mulhaupt, R. Tailoring Hydrocarbon Polymers and All-Hydrocarbon Composites for Circular Economy. *Macromol. Rapid Commun.* **2019,** *40* (1), 1800608.

(7)   Kaur, G.; Uisan, K.; Ong, K. L.; Lin, C. S. K. Recent Trends in Green and Sustainable Chemistry & Waste Valorisation: Rethinking Plastics in a circular economy. *Curr. Opin. Green Sustain. Chem.* **2018,** *9*, 30-39.

(8)   European Commision. Plastic Waste: a European strategy to protect the planet, defend our citizens and empower our industries. http://europa.eu/rapid/press-release_IP-18-5_en.htm (accessed March 14, 2019).

(9)   Korhonen, J.; Honkasalo, A.; Seppala, J. Circular Economy: The Concept and its Limitations. *Ecol. Econ.* **2018,** *143*, 37-46.

(10)   Ragaert, K.; Delva, L.; Van Geem, K. Mechanical and chemical recycling of solid plastic waste. *Waste Manage.* **2017,** *69*, 24-58.

(11)   Singh, N.; Hui, D.; Singh, R.; Ahuja, I. P. S.; Feo, L.; Fraternali, F. Recycling of plastic solid waste: A state of art review and future applications. *Compos. Pt. B-Eng.* **2017,** *115*, 409-422.

(12)   Faraca, G.; Martinez-Sanchez, V.; Astrup, T. F. Environmental life cycle cost assessment: Recycling of hard plastic waste collected at Danish recycling centres. *Resour. Conserv. Recycl.* **2019,** *143*, 299-309.

(13)   Lopez, G.; Artetxe, M.; Amutio, M.; Alvarez, J.; Bilbao, J.; Olazar, M. Recent advances in the gasification of waste plastics. A critical overview. *Renew. Sust. Energ. Rev.* **2018,** *82*, 576-596.

(14)   Lopez, G.; Artetxe, M.; Amutio, M.; Bilbao, J.; Olazar, M. Thermochemical routes for the valorization of waste polyolefinic plastics to produce fuels and chemicals. A review. *Renew. Sust. Energ. Rev.* **2017,** *73*, 346-368.

(15)   Shonnard, D. R.; Klemetsrud, B.; Sacramento-Rivero, J.; Navarro-Pineda, F.; Hilbert, J.; Handler, R.; Suppen, N.; Donovan, R. P. A Review of Environmental Life Cycle Assessments of Liquid Transportation Biofuels in the Pan American Region. *Environmental Management* **2015,** *56* (6), 1356-1376.

(16)   Bernardo, C. A.; Simoes, C. L.; Costa Pinto, L. M. AIP Conference Proceedings, 2016; p 140001.

(17)   Lazarevic, D.; Aoustin, E.; Buclet, N.; Brandt, N. Plastic waste management in the context of a European recycling society: Comparing results and uncertainties in a life cycle perspective. *Resour. Conserv. Recycl.* **2010,** *55* (2), 246-259.

(18)   Rigamonti, L.; Grosso, M.; Moller, J.; Sanchez, V. M.; Magnani, S.; Christensen, T. H. Environmental evaluation of plastic waste management scenarios. *Resour. Conserv. Recycl.* **2014,** *85*, 42-53.

(19)   Molgaard, C. Environmental impacts by disposal of plastic from municipal solid waste. *Resour. Conserv. Recycl.* **1995,** *15* (1), 51-63.

(20)   Perugini, F.; Mastellone, M. L.; Arena, U. Life cycle assessment of mechanical and feedstock recycling options for management of plastic packaging wastes. *Environ. Prog.* **2005,** *24* (2), 137-154.

(21)   Shonfield, P. LCA of Management Options for Mixed Waste Plastics. http://www.wrap.org.uk/sites/files/wrap/LCA%20of%20Management%20Options%20for%20Mixed%20Waste%20Plastics.pdf (accessed March 13, 2019).

(22)   Alston, S. M.; Arnold, J. C. Environmental Impact of Pyrolysis of Mixed WEEE Plastics Part 2: Life Cycle Assessment. *Environmental Science & Technology* **2011,** *45* (21), 9386-9392.

(23)   Al-Salem, S. M.; Evangelisti, S.; Lettieri, P. Life cycle assessment of alternative technologies for municipal solid waste and plastic solid waste management in the Greater London area. *Chem. Eng. J.* **2014,** *244*, 391-402.

(24)   Gear, M.; Sadhukhan, J.; Thorpe, R.; Clift, R.; Seville, J.; Keast, M. A life cycle assessment data analysis toolkit for the design of novel processes - A case study for a thermal cracking process for mixed plastic waste. *J. Clean Prod.* **2018,** *180*, 735-747.

(25)   Iribarren, D.; Dufour, J.; Serrano, D. P. Preliminary assessment of plastic waste valorization via sequential pyrolysis and catalytic reforming. *J. Mater. Cycles Waste Manag.* **2012,** *14* (4), 301-307.

(26)   Gracida-Alvarez, U. R.; Keenan, L. M.; Sacramento-Rivero, J. C.; Shonnard, D. R. Resource and Greenhouse Gas Assessments of the Thermochemical Conversion of Municipal Solid Waste in Mexico. *Acs Sustainable Chemistry & Engineering* **2016,** *4* (11), 5972-5978.

(27)   Benavides, P. T.; Sun, P. P.; Han, J.; Dunn, J. B.; Wang, M. Life-cycle analysis of fuels from post-use non-recycled plastics. *Fuel* **2017,** *203*, 11-22.

(28)   Gracida-Alvarez, U. R.; Mitchell, M. K.; Sacramento-Rivero, J. C.; Shonnard, D. R. Effect of Temperature and Vapor Residence Time on the Micropyrolysis Products of Waste High Density Polyethylene. *Ind. Eng. Chem. Res.* **2018,** *57* (6), 1912-1923.

(29)   Winjobi, O.; Zhou, W.; Kulas, D.; Nowicki, J.; Shonnard, D. R. Production of Hydrocarbon Fuel Using Two-Step Torrefaction and Fast Pyrolysis of Pine. Part 2: Life-Cycle Carbon Footprint. *ACS Sustainable Chemistry & Engineering* **2017,** *5* (6), 4541-4551.

(30)   Fitzgerald, G. C.; Krones, J. S.; Themelis, N. J. Greenhouse gas impact of dual stream and single stream collection and separation of recyclables. *Resour. Conserv. Recycl.* **2012,** *69*, 50-56.

(31)   Intergovernmental Panel of Climate Change (IPCC). *Climate Change 2013: The Physical Science Basis. Contribution of Working Group I to the Fifth Assessment Repost*

169

on the Intergovernmental Panel on Climate Change; Cambridge University Press: Cambridge, UK and New York, NY, USA, 2013.

(32)   Cooney, G.; Jamieson, M.; Marriott, J.; Bergerson, J.; Brandt, A.; Skone, T. J. Updating the U.S. Life Cycle GHG Petroleum Baseline to 2014 with Projections to 2040 Using Open-Source Engineering-Based Models. *Environmental Science & Technology* **2017,** *51* (2), 977-987.

(33)   Kulas, D.; Winjobi, O.; Zhou, W.; Shonnard, D. Effects of Coproduct Uses on Environmental and Economic Sustainability of Hydrocarbon Biofuel from One- and Two-Step Pyrolysis of Poplar. *Acs Sustainable Chemistry & Engineering* **2018,** *6* (5), 5969-5980.

(34)   U.S. Environmental Protection Agency (EPA). Emissions & Generation Resource Integrated Database (eGRID). https://www.epa.gov/energy/emissions-generation-resource-integrated-database-egrid (accessed December 19, 2018).

(35)   U.S. Energy Information Administration (EIA). Electric Power Monthly. Table 5.6.A. Average Price of Electricity by End-Use Sector, by State. https://www.eia.gov/electricity/monthly/epm_table_grapher.php?t=epmt_5_6_a (accessed April 17, 2019).

(36)   Jambeck, J. R.; Geyer, R.; Wilcox, C.; Siegler, T. R.; Perryman, M.; Andrady, A.; Narayan, R.; Law, K. L. Plastic waste inputs from land into the ocean. *Science* **2015,** *347* (6223), 768-771.

6 Summary, Conclusions and Recommendations for Future Work

This dissertation investigated the potential contribution of the fast pyrolysis of municipal solid waste to transportation fuel demand in Mexico and also analyzed the environmental and economic feasibility and the comparison of the greenhouse gas (GHG) emissions of their generated products with those from a fossil-derived pathway. In addition, it also evaluated the effect temperature and vapor residence time (VRT) on the product distribution of the primary and secondary pyrolysis reactions of waste high-density polyethylene (HDPE).

In Chapter 2, the resource assessment and carbon footprint analysis (CFA) of fuels produced from municipal solid waste (MSW) showed that approximately 7% of Mexico's annual transportation fuel demand can be fulfilled if the entire amount of paper, cardboard, yard trimmings, wood, and polyolefins that are discarded is pyrolyzed and catalytically upgraded to produce hydrocarbon fuels. Therefore, pyrolysis of wastes can provide an important contribution to reduce the consumption of fuels from fossil sources. The GHG emissions for the fuels derived from polyolefin pyrolysis are less (-7.8%) than those from fossil sources considering a well-to-wheels scope, as shown by the results of the CFA. Also, if avoided landfill emissions are considered in the CFA of pyrolysis of organic MSW, the resulting biofuels will have savings in GHG emissions which can help to obtain qualification as advanced biofuels in the USA when combined with polyolefin-derived

biofuels. A mixture containing at least 78.8% of organic MSW will produce a fuel with less than 60% emissions of a fossil derived fuel.

The pyrolysis experiments in the two-stage micropyrolysis reactor presented in Chapter 3 showed that increased pyrolysis temperature and VRT promote the formation of aromatics and low molecular weight hydrocarbons and monomers. The different combinations of temperature and VRT that were evaluated show that it is possible to target the production of specific compounds through the appropriate processing conditions. Therefore, pyrolysis of waste HDPE is a versatile process that can be adapted to specific needs of the industry and market. The analysis of chemical species exhibit that low carbon number species are predominantly alkenes while those with a high carbon number are comprised mostly of alkanes. Also raising temperatures and VRTs enhance the production of mono and polyaromatic hydrocarbons. Comparisons with other studies supported the occurrence of the free-radical degradation mechanism and confirmed similar product distribution in the two-stage micro-pyrolysis with that from larger scale fluidized bed reactors.

Chapter 4 used the results from Chapter 3 to guide the design of a multiproduct /multiprocessing refinery that produced monomers (ethylene, propylene), aromatics and low and high molecular weight hydrocarbon (MWHC) mixtures. The designed refinery was feasible from economic and environmental perspectives, with and energy returned over energy invested similar to other advanced alternative processes. Due to the inclusion of different processes for the separation of monomers and aromatics, the capital costs of the refinery are higher than those from previous studies, but the efficient use of energy and

heat integration reduces the annual operation costs and improve profitability. The two evaluated scenarios resulted in positive net present value with the highest value for the heat integrated design. The values that have a stronger influence on the techno-economic assessment (TEA) results are the internal rate of return, the total project investment, and the price of the low MWHCs.

The results from Chapter 5 confirm that the monomers and aromatics from the refinery have less GHG emissions from those produced with fossil-based materials. For the low and high MWHCs the result depends on the scenario that is applied, but overall the emissions are slightly lower to those from a fossil pathway, in agreement with prior life cycle assessments (LCAs). Monomer separation is the section with highest GHG emissions and capital and operating costs of the refinery which points out its importance as an area of potential improvement. For the CFA, electricity requirements and product yields are the parameters with the most significant influence on the results. From a cradle-to-gate scope, this refinery can produce low and high MWHCs with 50% less GHG emissions than fossil gasoline and diesel depending on its location. This CFA confirms the importance of using appropriate allocation and design considerations to accurately target the reduction on the emissions on the desired products.

One of the improvements to the research of this dissertation is the calibration of the detector in the mass spectrometer used in the micro-pyrolysis experiments with a higher number of standards, mainly low molecular weight hydrocarbons, to accurately estimate the mass percentages of the pyrolysis products. As a result, kinetic models based on the radical

scission mechanisms can be proposed to predict the product distribution at a wider range of temperatures and vapor residence times. Also, the micro-pyrolysis experiments can be extended to other polymers like low-density polyethylene, polypropylene, polystyrene and their mixtures with HDPE.

The refinery can be redesigned with processes that are more economic and less energy-intensive for monomer separation, of which membrane separations as one of the potential alternatives. Also, according to the results from Chapter 3, different redesigns can be carried out based on different product distribution from using combinations of temperature and VRT. Modular design and process intensification are other approaches that can be used to reduce the capital costs and energy requirements of the refinery. Modular processing allows the scalability of the refinery based on market trends, hence, some modules of the refinery can be scaled up accordingly while reducing the economic risk due to market uncertainty. Although the costs of the first modules would likely be higher, due to the economy of scale, the costs of the upcoming modules can be lowered by improved designs from the experiences gained in operating the earlier generation modules. The TEA and CFA presented in this dissertation can be applied to guide such improvements.

The designs can also be adapted to different socioeconomical regions going from small developing communities to big complexes operating in urban areas, with a special focus on countries that have shown increasing rates of plastic waste leakage into the oceans, like Thailand, Vietnam and Indonesia. The net present value (NPV) can be recalculated

according the different prices of electricity in the different states of the U.S. to highlight potential locations for the refinery from an economic perspective.

For the environmental assessment, more impact categories like water consumption, fossil energy consumption, human toxicity, aquatic ecotoxicity, terrestrial ecotoxicity, and other categories of impact can also be included. The scope of the LCA could be extended to cradle-to-grave by including distribution and combustion of the alternative transportation fuels produced, and a consequential LCA approach could capture more secondary effects of the waste plastic chemical recycling refinery such as reduced landfilling operations and their impacts. Also, social indicators can be included which can focus on the effects of the refinery on the surrounding communities like potential employment and population dynamics. The methodology of the LCA can be modified in a way that the long-term effects of avoiding the use of virgin materials and fossil resources extraction can be accounted. The analysis of regional electricity effects could also include the Mexican scenario, to extent the analysis from Chapter 2, and the South Asian countries that manages landfill storage of plastic waste from Europe and the U.S.

 Finally, the effects of regional economics from the construction of the refinery could be also evaluated. To capture all of these effects, a systems analysis for sustainability framework could be developed and used to conduct analyses of future versions of a plastics circular economy using a model-based approach in which all technical process are modeled using process simulation with the outputs from the simulations used as inputs to the TEAs, LCA, societal impact assessments, and regional economic assessments.

A   Supporting Information for Chapter 2

Resource and Greenhouse Gas Assessments of the Thermochemical Conversion of Municipal Solid Waste in Mexico

A.1   MSW generation data for different cities in Mexico

The composition tables shown below did not consider construction, hazardous, and special wastes. Data from the reviewed sources was adjusted to sum 100 % and the results were multiplied by the reported annual MSW generation.

Table A-1. MSW composition of Mexico City.[1]

Waste category	%wt	Amount (tonnes[a]/yr)
Plastics	13.16	600,425.00
Textiles	3.79	166,987.50
Organics (Food)	51.29	2,260,262.50
Sanitary waste	11.15	491,381.25
Paper	6.10	268,731.25
Cardboard	4.17	183,868.75
Ferrous material	1.20	52,925.00
Wood	0.47	20,531.25
Fines	0.83	36,500.00
Aluminum	0.30	13,231.25
Glass	2.74	120,906.25
Other	4.34	191,168.75
[a] : metric tons		

Table A-2. MSW composition of Guadalajara.[2]

Waste category	%wt	Amount (tonnes/yr)
Cotton	0.02	117.41
Cardboard-packaging	2.34	13,560.68
Cardboard-non packaging	0.14	821.86
Leather	0.47	2,700.39
Fine waste	1.22	7,103.21
Laminated cardboard-without aluminum	0.08	469.63
Laminated cardboard-with aluminum	0.09	528.34
Laminated cardboard-others	0.20	1,174.08
Laminated cardboard-non packaging	0.02	117.41
Hard plant fiber	0.48	2,759.10
Synthetic fiber-packaging	0.15	880.56
Synthetic fiber-non packaging	0.14	821.86

Bone	0.83	4,813.75
Rubber	0.40	2,348.17
Clayware-packaging	0.31	1,819.83
Clayware-non packaging	0.21	1,232.79
Wood-packaging	0.26	1,526.31
Wood-non packaging	0.38	2,230.76
Aluminum cans	0.10	587.04
Tin cans	0.46	2,641.69
Iron material-packaging	0.57	3,287.44
Iron material-non packaging	0.23	1,350.20
Non-iron material-packaging	0.08	469.63
Non-iron material-non packaging	0.06	352.23
Paper-packaging	1.10	6,398.76
Paper-non packaging	3.12	18,080.90
Toilet paper	3.48	20,194.25
Child disposable diapers	6.34	36,807.55
Adult disposable diapers	0.17	997.97
Feminine pads	0.18	1,056.68
Pet feces	0.92	5,342.08
Plastic film-snack bags	0.10	587.04
Plastic film-low density polyethylene	4.14	24,010.03
Plastic film-laminated	0.01	58.70
Rigid plastic-PET	0.92	5,342.08
Rigid plastic-high density polyethylene	1.61	9,333.97
Rigid plastic-PVC	0.27	1,585.01
Rigid plastic-others	1.11	6,457.47
Rigid plastic-non packaging	0.40	2,348.17
Polyurethane	0.03	176.11
Polystyrene foam-packaging	0.17	997.97
Polystyrene foam-non packaging	0.11	645.75
Polypropylene	0.14	821.86
Food waste	41.17	238,926.21
Yard trimmings	12.32	71,501.75
Fabrics	1.74	10,097.13
Stained glass-packaging	0.54	3,111.32
Stained glass-non packaging	0.07	410.93
Clear glass-packaging	3.03	17,611.27
Clear glass-non packaging	0.46	2,641.69
Electric batteries	0.05	293.52
Others	7.03	40,799.44

Table A-3. MSW composition of Monterrey.[3]

Waste category	%wt	Amount (tonnes/yr)
Cardboard	4.37	14,613.22
Fine waste	2.23	7,447.19
Bone	0.64	2,155.50
Rubber	0.20	669.41
Aluminum	1.41	4,715.99
Ferrous material	1.48	4,940.25
Non-ferrous material	0.65	2,182.28
Paper	10.55	35,328.11
Disposable diapers	8.31	27,807.29
Film plastic	5.12	17,136.90
Rigid plastic	3.15	10,549.90
Food waste	21.27	71,195.10
Yard trimmings	19.76	66,144.40
Textiles	2.41	8,053.00
Colored glass	0.93	3,126.14
Transparent glass	5.25	17,585.40
Others	12.27	41,058.26

Table A-4 National average of MSW composition in Mexico.[4]

Waste category	%wt	Amount (tonnes/yr)
Food, yard and organic waste	52.42	21,524,900
Paper, cardboard and paper products	13.83	5,679,000
Glass	5.88	2,414,500
Plastic	10.89	4,471,710
Metals	3.44	1,412,500
Textiles	1.43	587,190
Others	12.11	4,972,700

A.2 Categorization procedure

Categorization of the national MSW used average values from the reported composition of the cities, as shown in Tables A-5, A-6, A-7, and A-8.

Table A-5. Wood composition (percentage).

Mexico City	Guadalajara	National average
0.47	0.64	0.56

Table A-6. Rubber composition (percentage).

Guadalajara	Monterrey	National average
0.40	0.20	0.30

Table A-7. Organics category composition (percentage).

	Guadalajara	Monterrey	National average
Food waste	77.70	53.30	65.50
Yard trimmings	22.30	46.70	34.50

Table A-8. Cardboard and paper composition (percentage).

	Mexico City	Guadalajara	Monterrey	National Average
Paper	59.38	59.49	70.74	63.20
Cardboard	40.62	40.51	29.26	36.80

The national MSW generation is estimated as 41,062,500 tonnes/yr.[4] According to the established average compositions, the amount of waste products per category is:

Wood: From Table A-5

$$41,062,500 \times 0.56 = 229,950 \text{ tonnes/yr}$$

Rubber: From Table A-6

$$41,062,500 \times 0.30 = 123,187.50 \text{ tonnes/yr}$$

Food waste: Total organics, from Table A-4, are multiplied by the average composition in Table A-7

$$21,524,900 \times 0.655 = 14,098,809.50 \text{ tonnes/yr}$$

Yard Trimmings: Total organics are multiplied by the composition from Table A-7 and the amount of wood is subtracted from the result

$$(21,524,900 \times 0.345) - 229,950 = 7,196,140.50 \text{ tonnes/yr}$$

Paper: Total paper products, from Table A-4, are multiplied by the corresponding composition in Table A-8

$$5,679,000 \times 0.632 = 3,589,128 \text{ tonnes/yr}$$

Cardboard: Total paper products, from Table A-4, are multiplied by the corresponding composition in Table A-8

$$5,679,000 \times 0.368 = 2,089,872 \text{ tonnes/yr}$$

Leather and textile: The amount of rubber is subtracted from the textiles amount in Table A-4

$$587,190 - 123,187.50 = 464,002.50 \text{ tonnes/yr.}$$

179

A.3   Resource assessment of MSW

Table A-9. MSW generation in Mexico and its three most populated cities (tonnes/yr).

Type of waste	Mexico City	Guadalajara	Monterrey	National
Food waste	1,480,471.94	249,082.04	73,350.60	14,098,809.50
Yard trimmings	779,790.56	71,501.75	64,270.05	7,196,140.50
Wood	20,531.25	3,757.07	1,874.35	229,950.00
Leather & textile	153,300.00	12,914.93	8,053.00	464,002.50
Rubber	13,687.50	2,348.17	669.41	123,187.50
Plastics	600,425.00	54,066.59	27,686.80	4,471,710.00
Metals	66,156.25	7,866.37	11,838.52	1,412,500.00
Glass	120,906.25	23,775.21	20,711.55	2,414,500.00
Paper	268,731.25	24,479.66	35,328.11	3,589,128.00
Cardboard	183,868.75	16,672.00	14,613.22	2,089,872.00
Other	719,050.00	113,886.20	76,312.74	4,972,700.00
Total	4,406,918.75	580,350.00	334,708.35	41,062,500.00

Table A-10. Amount per category of Mexico's national MSW generation on a post-recycling and dry weight (DW) basis (tonnes/yr).

Type of waste	Only Post-recycling		DW & Post-recycling	
	Amount	Percentage	Amount	Percentage
Food waste	14,098,809.50	36.09%	4,229,642.85	17.44%
Yard trimmings	7,196,140.50	18.42%	2,878,456.20	11.87%
Wood	229,950.00	0.59%	183,960.00	0.76%
Leather & textile	461,682.49	1.18%	415,514.24	1.71%
Rubber	109,020.94	0.28%	106,840.52	0.44%
Plastics	4,449,351.45	11.39%	4,440,452.75	18.31%
Metals	861,625.00	2.21%	835,776.25	3.45%
Glass	1,847,092.50	4.73%	1,810,150.65	7.47%
Paper	3,061,526.18	7.84%	2,877,834.61	11.87%
Cardboard	1,782,660.82	4.56%	1,693,527.78	6.98%
Other	4,972,700.00	12.73%	4,773,792.00	19.69%
Total	39,070,559.38		24,245,947.84	
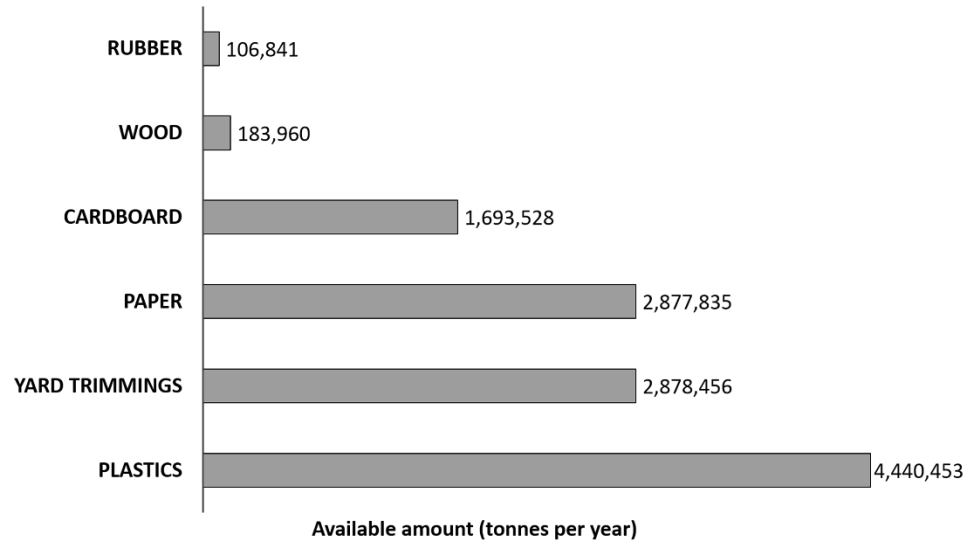
Figure A-1. Availability of MSW for thermochemical conversion (Dry weight and post-recycling basis).

A.4 Plastic waste generation

Table A-11. Composition of "plastics" category for Guadalajara.

Type of plastic	Composition
Synthetic fiber	3.15%
Low density polyethylene (LDPE)	45.49%
Polyethylene terephthalate (PET)	9.88%
High density polyethylene (HDPE)	17.26%
Polyvinyl chloride (PVC)	2.93%
Polyurethane	0.33%
Polystyrene (PS)	3.04%
Polypropylene (PP)	1.52%
Non-specified plastic	16.40%

Table A-12. Composition of "plastics" category for Mexico City.

Type of plastic	Composition
Polyethylene terephthalate (PET)	9.19%
High density polyethylene (HDPE)	9.12%
Polyvinyl chloride (PVC)	1.29%
Low density polyethylene (LDPE)	3.27%
Polypropylene (PP)	6.38%
Polystyrene (PS)	4.41%
Non-specified plastic	6.46%
Polyurethane	10.79%
plastic bag	49.09%

Total: 4.44 million tonnes per year
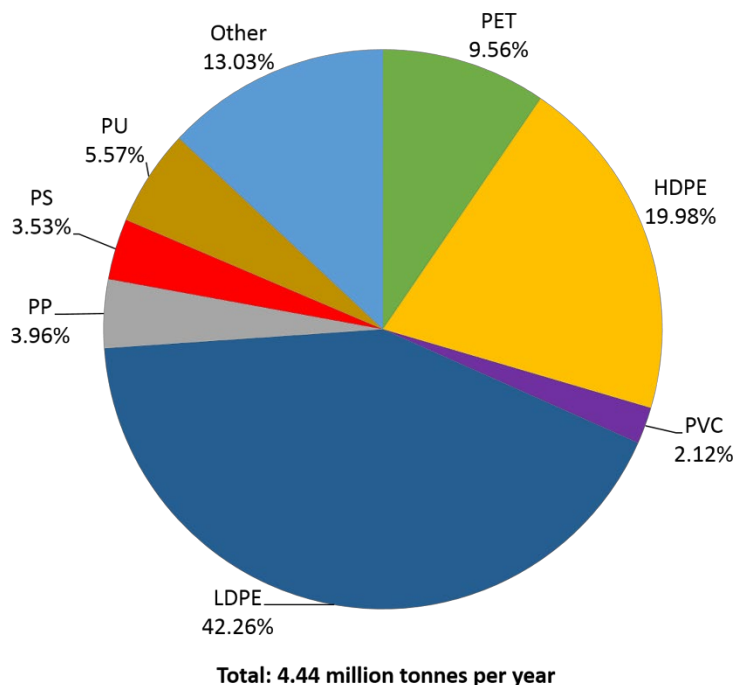
Figure A-2. Mexico's composition of plastic waste (Dry weight and post-recycling basis). LDPE: Low-density polyethylene, HDPE: High-density polyethylene, PP: polypropylene, PS: polystyrene, PVC: polyvinylchloride, PET: polyethylene terephthalate, PU: polyurethane.

A.5   Production of chemicals from MSW

Plastic pyrolysis can take place under different operation conditions that produce a wide variety of chemicals. Computation of chemicals products yields required a literature review that comprised studies using different operation parameters and equipment.[5-13] Therefore, yields were reported as a range and not as an average. In addition, yields computation considered individual pyrolysis of each polymeric material because of the effect that mixture composition has on the chemical products distribution. When total yields were missing, those were calculated using equation (A-1):

$$Total\ yield = FC_y \times CC_{comp} \qquad\qquad\qquad (A\text{-}1)$$

where FC_y is the fraction yield (gaseous, liquid, or solid) or chemical species yield (i.e. alkanes, alkenes or aromatics) and CC_{comp} is the chemical compound composition within the product or chemical species fraction. When reported grouped (i.e., C7–C12 alkanes), yields were distributed equitably within the total number of compounds. Calculation of the highest and lowest production ranges employed equations (A-2) and (A-3) and the highest and lowest yields found in literature as shown below

182

Total highest production of chemical $i = \sum G_j \cdot Hj_i$ (A-2)

Total lowest production of chemical $i = \sum G_j \cdot Lj_i$ (A-3)

where G_j is the estimated waste generation of polymeric material j, Hj_i is the highest yield of chemical i for material j and Lj_i is the lowest yield of chemical i for material j. The contribution of pyrolysis-derived chemicals to Mexico's annual chemicals consumption was calculated with equation (A-4):

$$Contribution = \frac{EAP}{NCC} \times 100$$ (A-4)

where NCC is the reported consumption of chemicals and EAP is the estimated annual production of chemicals. Mexico's annual consumption of chemicals in 2014 was obtained from the Mexican Chemical Industry Association (ANIQ)[14] annual statistics report.

Chemicals produced through plastic pyrolysis can be grouped into four categories: alkanes, alkenes, aromatics, and inorganics. According to several studies,[5-13] pyrolysis products are strongly dependent on the chemical structure of the plastic species. For example, while processing PET a high production of CO, CO_2, and complex aromatic products is expected (13.29%, 22.71%, and 34.09% of the final product, respectively). In a similar way, thermochemical conversion of PVC produces more than 52% HCl. On the other hand, PS pyrolysis presents a distinct trend in the recovery of styrene, with a composition of up to 76% in the final product. Polyolefins do not show that tendency for the production of monomers. The highest reported yield is for PP, with a composition of 31.10% in the production of propylene. In general, polyolefin pyrolysis favors production of C2–C6 alkanes and alkenes, although some aromatic compounds (i.e., toluene and naphthalene derivatives) can also be produced. Table A-13 shows a complete list of chemical products from plastic pyrolysis and their composition range.

Table A-13. Range of chemical products composition obtained by pyrolysis of different plastic materials (%).

Chemical compound	PET	HDPE	PVC	LDPE	PP	PS
Alkanes						
C1	0.71-5.5	0.01-1.90	0.77	1.14-12.80	0.69-1.75	0.21-0.53
C2	0.03-5.5	0.01-2.21	0.47	1.67-5.90	0.40-2.10	0.08-3.75
C3	0.13-3.96	0.05-1.31	0.24	0.10-6.20	0.40-7.93	0.02-3.75

C4	3.74	0.22-1.25	0.11	0.32-6.55	0.23-19.10	0.02-3.75
C5	3.96	0.37		2.41	1.00-17.10	0.60-2.68
C6	1.16	0.44		2.03	0.28-11.40	0.57-2.68
C7	1.16	0.22		2.03-3.46	0.10-6.00	0.86-2.68
C8		1.06		3.82	0.20-2.50	0.86-2.68
C9		1.19		2.74	0.10-1.68	0.71
C10		1.33		0.84-1.73	0.20-3.36	0.57
C11		1.41		0.91-3.03	0.10-2.65	0.45
C12		1.64		0.29-0.94	0.29-5.89	0.38
C13		1.33		0.87-1.00	0.13-1.16	0.35
C14		0.93		1.03	0.13-4.07	0.29
C15		1.24		1.11	0.13-3.00	0.19
C16		0.44		0.97	0.13-1.10	1.28
C17		0.31		0.99	0.64	0.86
C18		0.18		0.46	0.15-0.64	
C19		0.35		1.30	0.64	
C20		0.71		3.01	0.64-1.12	
C21				0.99	0.64	
C22				0.97	0.64	
C23					0.64	
C24				2.10	0.64	
C25				0.73		
Alkenes						
C2	1.41-5.50	0.02-6.08	0.15	2.86-31.10	0.10-4.41	0.03-3.75
C3	0.09-3.96	0.44-4.56	0.19	0.75-12.80	0.54-9.60	0.05-3.75

C4	3.74	0.36	0.15	0.40-6.55	0.14-13.10	0.06-3.75
C5	3.96			2.41	0.16-3.90	0.03-2.68
C6	1.16	0.22		2.03-3.17	0.28-7.92	0.24-2.68
C7	1.16	0.71		2.03-4.90	0.20-2.70	0.31-2.68
C8		1.72		7.86	0.24-2.20	1.18-2.68
C9		1.41		1.69-4.40	0.20-11.40	
C10		1.06		1.78-3.10	0.55-1.00	
C11		1.72		1.37-1.76	0.24-1.76	0.16
C12		3.18		1.44-1.62	0.31-1.70	0.16
C13		1.55		0.72-2.49	0.31-0.80	0.24
C14		4.51		0.29-1.84	0.20-0.31	0.24
C15		1.28		1.87		0.24
C16		2.87		2.82		
C17		0.18		1.93	0.64	
C18		0.62		2.08	0.64	
C19		0.84		8.30	0.64	
C20		0.22		2.60	0.64	
C21					0.64	
C22				2.33	0.64	
C23					0.64	
C24					0.64	
C25				1.76		
Aromatics						
Benzene and alkyl benzenes				4.02	0.20-5.38	3.60-42.35
Toluene				10.02	0.87-12.64	6.00-26.96
Xylenes		0.66		3.75-6.96	0.38-7.79	1.44-4.91
Styrene	0.20					49.60-76.20

185

	0.98	2.03		0.66-8.51	0.45-24.40	
Naphtalenes	0.98	2.03		0.66-8.51	0.45-24.40	
Other aromatics	34.09	2.40		0.61-14.85	0.11-9.63	0.10-27.11
Inorganic Compounds						
H_2	0.31	0.12	0.12	0.05-2.00	0.01-0.05	0.04-8.20
CO	13.29					
CO_2	22.71	1.26	0.26	0.56	3.31	1.16
HCl			52.93-56.00			

The amount of plastic waste converted into hydrocarbon fuels (Table A-14) was obtained considering a conversion efficiency of 86%.[15] This data and the reviewed production ranges (Table A-13) were multiplied to obtain the production ranges shown in Table A-15. According to this table, ethylene, propene, ethane, toluene, and naphthalene, compounds naturally found in crude oil, exhibit the highest production. Yields for the production of ethylene, propylene, and styrene monomers are up to 187, 87, and 33 kg per tonne of plastic waste, respectively. Several pyrolysis products have a high potential as chemical intermediates as well. For example, benzene, toluene, and xylenes presented production yields up to 42, 70, and 44 kg per tonne of plastic waste. These results point to pyrolysis as an interesting technology for the disposal of plastic waste.

Table A-14. Plastic waste converted to hydrocarbon fuels.

Type of plastic	Amount converted (tonnes/yr)
PET	364,218.82
HDPE	761,591.35
PVC	80,641.17
LDPE	1,610,488.54
PP	150,900.71
PS	134,424.70

Table A-15. Range of chemical products obtained by pyrolysis of different plastic materials (tonnes/yr).

Chemical compound	PET	HDPE	PVC	LDPE	PP	PS
Alkanes						
C1	2,586-20,032	76-14,470	621	18,360-206,143	1,041-2,641	282-712
C2	109-20,032	76-16,831	379	26,895-95,019	604-3,169	108-5,041

C3	473-14,423	381-9,977	194	1,610-99,850	604-11,966	27-5,041
C4	13,622	1,676-9,520	89	5,154-105,487	347-28,822	27-5,041
C5	14,423	2,818		38,813	1,509-25,804	807-3,603
C6	4,225	3,351		32.693	423-17,203	766-3,603
C7	4,225	1,676		32,693-55,723	151-9,054	1,156-3,603
C8		8,073		61,521	302-3,773	1,156-3,603
C9		9,063		44,127	151-2,535	954
C10		10,129		13,528-27,861	302-5,070	766
C11		10,738		14,655-48,798	151-3,999	605
C12		12,490		4,670-15,139	438-8,888	511
C13		10,129		14,011-16,105	196-1,750	470
C14		7,083		16,588	196-6,142	390
C15		9,444		17,876	196-4,527	255
C16		3,351		15,622	196-1,660	1,721
C17		2,361		15,944	966	1,156
C18		1,371		7,408	226-966	
C19		2,666		20,936	966	
C20		5,407		48,476	966-1,690	
C21				15,944	966	
C22				15,622	966	
C23					966	
C24				33,820	966	
C25				11,757		
Alkenes						
C2	5,135-20,032	152-46,305	121	46,060-500,862	151-6,655	40-5,041

C3	328-14,423	3,351-34,729	153	12,079-206,143	815-14,486	67-5,041
C4	13,622	2,742	121	6,442-105,487	211-19,768	81-5,041
C5	14,423			38,813	241-5,885	40-3,603
C6	4,225	1,676		32,693-51,052	423-11,951	323-3,603
C7	4,225	5,407		32,693-78,914	302-4,074	417-3,603
C8		13,099		126,584	362-3,320	1,586-3,603
C9		10,738		27,217-70,861	302-17,203	
C10		8,073		28,667-49,925	830-1,509	
C11		13,099		22,064-28,345	362-2,656	215
C12		21,129		23,191-26,090	468-2,565	215
C13		11,805		11,596-40,101	468-1,207	323
C14		34,348		4,670-29,633	302-468	323
C15		9,748		30,116		323
C16		21,858		45,416		
C17		1,371		31,082	966	
C18		4,722		33,498	966	
C19		6,397		133,671	966	
C20		1,676		41,873	966	
C21					966	
C22				37,524	966	
C23					966	
C24					966	
C25				28,345		
Aromatics						
Benzene and alkyl benzenes				64,742	302-8,118	4,839-56,929
Toluene				161,371	1,313-19,074	8,065-36,241
Xylenes		5,027		60,393-112,090	573-11,755	1,936-6,600

Styrene	728					66,675-102,432
Naphthalenes	3,569	15,460		10,629-137,053	679-36,820	
Other aromatics	124,162	18,278		9,824-239,158	166-14,532	134-36,443
Inorganic Compounds						
H_2	1,129	914	97	805-32,210	15-75	54-11,023
CO	48,405					
CO_2	82,714	9,596	210	9,019	4,995	1,559
HCl				42,683-45,159		

Table A-16 shows the comparison of the production ranges with Mexico's annual chemicals consumption in 2014.[14] As observed, the highest yields of hexane, heptane, benzene, toluene, xylenes, and hydrogen surpass the annual consumption. This is a good indicator of the feasibility of waste plastic pyrolysis to fulfill the Mexican consumption of certain chemical products. Likewise, estimated contributions up to 61.10, 47.56, 16.55 and 5.58 % for ethylene, propylene, styrene, and ethane also encourage the further exploitation of plastic waste. Nonetheless, more studies need to be carried out in order to find correlations between plastic feedstock and operation conditions for the production of specific chemicals.

Table A-16. Estimated range of production and contribution of different chemicals from plastic waste generated in Mexico.

Chemical product	Production range (tonnes/year)	National consumption[14] (tonnes/year)	Contribution range (%)
Alkanes			
C1	22,435-244,619		
C2	27,792-140,471	2,517,560	1.10-5.58
C3	3,095-141,451		
C4	7,203-162,580		
C5	2,316-85,460		
C6	1,189-61,074	36,867.31	3.22-165.66
C7	34,000-74,280	4,710.69	721.76-1576.84
C8	1,458-76,969		

C9	151-56,680		
C10	13,830-43,827		
C11	14,806-64,140		
C12	5,108-37,028		
C13	14,207-28,455		
C14	196-30,202		
C15	196-32,103		
C16	196-22,353		
C17	20,427		
C18	226-9,745		
C19	24,568		
C20	966-55,573		
C21	16,910		
C22	16,588		
C23	966		
C24	34,786		
C25	11,757		
Alkenes			
C2	51,539-579,015	947,684	5.44-61.10
C3	16,640-274,975	578,129	2.88-47.56
C4	6,734-146,780		
C5	282-62,724		
C6	33,438-72,507		
C7	33,411-96,223		
C8	1,948-146,606		
C9	27,519-98,803		
C10	29,497-59,507		
C11	22,426-44,315		
C12	23,659-53,089		
C13	12,063-53,436		
C14	4,972-64,771		
C15	40,187		
C16	67,273		
C17	33,419		
C18	39,186		
C19	141,034		
C20	44,514		
C21	966		
C22	38,490		
C23	966		
C24	966		

190

C25	28,435		
Aromatics			
Benzene and alkyl benzenes	5,141-129,789	114,358	4.50-113.49
Toluene	9,378-216,686	161,632	5.80-134.06
Xylenes	62,902-135,472	109,342	57.53-123.90
Styrene	66,675-103,160	623,303	10.70-16.55
Naphthalenes	11,308-192,902		
Other aromatics	10,124-432,572		
Inorganic Compounds			
H_2	874-45,448	2,759	31.68-1647.26
CO	48,405		
CO_2	108,093	228,847	47.23
HCl	42,683-45,159	111,240	38.37-40.60

A.6   Estimation of emission factors

Different sources were consulted in order to obtain the emission factors for the different stages of each MSW processing pathway. Required calculations are shown below for each of those stages.

A.6.1   Collection (organics and polyolefin pathways)

Fitzgerald et al.[16] analyzed the greenhouse gases (GHG) impact of switching from single to dual stream (SS and DS, respectively) processing for the collection and separation procedures in medium-size material recovery facilities. Due to the lower GHG emissions associated, SS processing was chosen for the established organic and polyolefin pathways.

This study reported emissions of 37.89 kg CO_2 eq. per wet tonne of MSW collected through SS processing. However, the authors did not consider upstream emissions in the analysis. According to the ecoinvent database,[17] emissions of diesel processing were assumed to be 9% of the emissions of combustion in an engine. As a result, total emissions from collection were accounted as shown below

37.89 kg CO_2 eq. per MT MSW $\times$ 1.09 = **41.30 kg CO_2 eq. per tonne MSW**.

A.6.2   Separation (organics and polyolefin pathways)

GHG emissions for the SS separation process were also taken from the study of Fitzgerald et al.,[16] which accounted 11.07 kg CO_2 eq. per wet tonne of MSW for this process. Contribution of different energy sources and the equivalences of upstream emissions[17] are presented in Table A-17.

Table A-17. Contribution and upstream emissions percentage for the separation process.

Energy source	Contribution to process (%)	Upstream emissions (%)
Electricity	67.2	10.0
Natural gas	13.0	17.0
Diesel	19.8	9.0

Then, the total emissions for the separation process were estimated as follows

Electricity: $11.07 \times 0.672 \times 1.10 = 8.18$ kg CO_2 eq. per tonne MSW

Natural gas: $11.07 \times 0.130 \times 1.17 = 1.68$ kg CO_2 eq. per tonne MSW

Diesel: $11.07 \times 0.198 \times 1.09 = 2.39$ kg CO_2 eq. per tonne MSW,

which as a result gives **12.25 kg CO_2 eq. per tonne MSW.**

A.6.3   Transportation (organics and polyolefin pathways)

The emissions of freight truck transportation were obtained from the IPCC 100a methodology used by the software SimaPro.[18] Calculations considered a distance of 108 km. This is the shortest length from the "Santa Catarina" separation facility in Mexico City to the "Miguel Hidalgo" refinery in the state of Hidalgo, (assumed location for the thermochemical conversion facility). The output from the software showed that **12.13 kg CO_2 eq.** are emitted **per wet tonne of post-recycling MSW transported.**

A.6.4   Size reduction (organics and polyolefin pathways)

For this process, estimations from Alston and Arnold[19] were taken. These authors determined an electricity input of 183 kWh to shred and grind one wet tonne of MSW. Results from SimaPro,[18] showed emissions of **119.13 kg CO_2 eq. per wet tonne of post-recycling MSW processed** if the Mexican electricity mix (Table A-18, column 3) is considered as the energy source.

Table A-18. Composition of the Mexican electricity mix.

Energy source	Contribution[20] (%)	Contribution[17] (%)
Coal	3.44	8.05
Crude Oil	63.42	3.78
Condensate	0.89	-
Natural Gas	23.56	49.95
Nuclear	1.14	3.78
Hydro	1.59	15.89
Geothermal	1.47	2.78
Solar	0.10	-
Wind	0.26	0.11
Biogas	0.02	0.03
Biomass	4.12	0.28
Import from TRE	-	0.14
Blast furnace gas	-	0.17
Coal gas	-	0.03

A.6.5 Pyrolysis

S.6.5.1 Pyrolysis for the organics pathway

The study performed by Hsu[21,22] provided the data for GHG emissions of organics waste pyrolysis. This author considered the production of diesel and gasoline from forest residues using the process reported by Jones et al.[23] In this process gasoline and diesel are obtained as the main products. Pyrolysis emissions of 0.1131 and 0.0942 kg CO_2 eq. per km traveled for gasoline and diesel, respectively, were converted to a per tonne of waste processed basis by using data from Table A-19.

Table A-19. Data for GHG emissions of the organics MSW pathway.[21]

Fuel	Fuel economy (km per kg fuel)	Fuel yield (kg fuel per tonne of moisture and ash free organic waste)
Gasoline	14.37	101.06
Diesel	17.05	135.69

Ash content of different components of organic MSW was collected from Valkenburg et al.[24] Then, the moisture and ash free organic waste (MAFOW) amount was estimated as follows

Yard trimmings: $2,878,456 \times (1 - 0.064) = 2,694,235$ tonnes/yr

Wood: $183,960 \times (1 - 0.099) = 165,748$ tonnes/yr

Paper: $2,877,835 \times (1 - 0.079) = 2,650,486$ tonnes/yr

Cardboard: $1,693,527 \times (1 - 0.079) = 1,559,739$ tonnes/yr

Total ash free organic MSW: 7,070,208 tonnes/yr

The pyrolysis emissions to produce gasoline were computed as follows

$$\frac{101.06 \text{ kg gasoline}}{\text{ton MAFOW}} \times \frac{14.37 \text{ km}}{\text{kg gasoline}} \times \frac{0.1131 \text{ kg CO}_2 \text{ eq}}{\text{km}}$$
$$= 164.25 \text{ kg CO}_2 \text{ eq per tonne MAFOW}$$

The pyrolysis emissions to produce diesel were computed as follows

$$\frac{135.69 \text{ kg diesel}}{\text{ton MAFOW}} \times \frac{17.05 \text{ km}}{\text{kg diesel}} \times \frac{0.0942 \text{ kg CO}_2 \text{ eq}}{\text{km}}$$
$$= 217.93 \text{ kg CO}_2 \text{ eq per tonne MAFOW}$$

Finally, total emissions from the pyrolysis step were **382.18 kg CO₂ eq. per tonne of MAFOW**

S.6.5.2 Pyrolysis for the polyolefin pathway

The study reported by Perugini et al.[15] provided the emission factors for the pyrolysis of polyolefins. This study took the British Petroleum polymer cracking process as a guide, which emits 0.345 kg of CO_2 per kg of polyolefin waste processed. The software SimaPro[18] was used to obtain upstream emissions for 0.131 MJ of naphtha and 0.212 MJ of electric energy (Mexican grid mix) per kg of processed polyolefins. The results for the total emissions per tonne of polyolefin waste are presented below

Process emissions: 345 kg CO_2 eq. per tonne of polyolefin waste

Naphtha (upstream emissions): 11.23 kg CO_2 eq. per tonne of polyolefin waste

Electricity (upstream emissions for Mexican mix): 38.33 kg CO_2 eq. per tonne of polyolefin waste

194

Total emissions: **394.56 kg CO₂ eq. per tonne of polyolefin MSW**.

A.6.6 Hydroprocessing (only for the organics pathway)

In a similar way to the pyrolysis step, computing of hydroprocessing emissions considered the results reported by Hsu.[21] Emission values for this process were 0.1398 and 0.116 kg CO_2 eq. per km traveled for gasoline and diesel, respectively. Again, data from Table A-19 was applied to obtain the total emissions.

Hydroprocessing emissions to produce gasoline:

$$\frac{101.06 \text{ kg gasoline}}{\text{tonne MAFOW}} \times \frac{14.37 \text{ km}}{\text{kg gasoline}} \times \frac{0.1398 \text{ kg } CO_2 \text{ eq}}{\text{km}}$$
$$= 203.02 \text{ kg } CO_2 \text{ eq per tonne of MAFOW}$$

Hydroprocessing emissions to produce diesel:

$$\frac{135.69 \text{ kg diesel}}{\text{tonne MAFOW}} \times \frac{17.05 \text{ km}}{\text{kg diesel}} \times \frac{0.116 \text{ kg } CO_2 \text{ eq}}{\text{km}}$$
$$= 268.37 \text{ kg } CO_2 \text{ eq per tonne of MAFOW}$$

Finally, total emissions from the Hydroprocessing step were **471.39 kg CO₂ eq. per tonne of MAFOW**.

A.6.7 Fuel distribution

S.6.7.1 Fuel distribution (organics pathway)

A pipeline system from the "Miguel Hidalgo" refinery to Mexico City (distance: 108 km) would transport the gasoline and diesel produced from pyrolysis and hydroprocessing. According to SimaPro 8,[18] this pipeline system emits 6 kg CO_2 per tonne of fuel produced. Then, using the overall fuel yield from biomass reported by Hsu,[21] the following calculation was performed in order to obtain the emissions per tonne of MSW (see section 2.2.2).

$$\frac{6.00 \text{ kg } CO_2 \text{ eq}}{\text{tonne fuel}} \times \frac{0.2367 \text{ tonne fuel}}{\text{tonne MAFOW}} = \mathbf{1.44 \text{ kg } CO_2 \text{ eq per tonne MAFOW}}$$

S.6.7.2 Fuel distribution (polyolefin pathway)

According to Perugini et al.,[15] polyolefins pyrolysis generates products in three different phases. Therefore, two different transportation systems were considered: a pipeline for the gas and light liquid fractions, and a freight truck for heavy waxes. Table A-20 shows the emission factors obtained from SimaPro 8,[18] which took into account the amount produced from one tonne of processed polyolefines. Total emissions accounted for **7.33 kg CO₂ eq. per dry tonne of polyolefin waste** for the fuel distribution stage.

Table A-20. Emission factors for the transportation of pyrolysis products from one tonne of processed polyolefins.

Product fraction	Amount produced (tonnes)	Emission factor[18] (kg CO_2 eq. per tonne of polyolefin waste)
Gas	0.147	0.31
Light liquid	0.265	1.59
Heavy waxes	0.448	5.43

A.6.8   Vehicle operation

S.6.8.1 Vehicle operation (organics pathway)

Emissions from combustion in engines of vehicles were estimated with data provided from Hsu.[21] This study reported emissions of 0.2152 and 0.1904 kg CO_2 eq. per km traveled for gasoline and diesel, respectively. By using the information from Table A-19 the total emissions for this stage were accounted as follows

Vehicle operation emissions to produce gasoline:

$$\frac{101.06 \text{ kg gasoline}}{\text{tonne ash free Organic residue}} \times \frac{14.37 \text{ km}}{\text{kg gasoline}} \times \frac{0.2152 \text{ kg CO}_2 \text{ eq}}{\text{km}}$$
$$= 312.52 \text{ kg CO}_2 \text{ eq per tonne ash free waste}$$

Vehicle operation emissions to produce diesel:

$$\frac{135.69 \text{ kg diesel}}{\text{tonne of MAFOW}} \times \frac{17.05 \text{ km}}{\text{kg diesel}} \times \frac{0.1904 \text{ kg CO}_2 \text{ eq}}{\text{km}}$$
$$= 440.49 \text{ kg CO}_2 \text{ eq per tonne of MAFOW}$$

Finally, total emissions from the vehicle operation stage were **753.01 kg CO₂ eq. per dry tonne of organic MSW**.

S.6.8.2 Vehicle operation (polyolefin pathway)

As seen in Table A-13, polyolefin pyrolysis products comprise diverse chemical species. In order to account for the combustion emissions, different studies[6,7,10,13] were consulted to obtain the average composition of the chemical species in each product fraction. Boiling points of the formed products aided in their classification as gases, liquids and waxes. Then, a representative compound from each chemical species in each product fraction was chosen, considering the higher compositions as reported in Table A-13. Afterwards, calculation of combustion emissions used stoichiometric calculations as shown in the example below for ethane (C_2H_6)

Ethane molecular weight: 30 mole per gram

Combustion reaction: $C_2H_6 + 3.5O_2 \rightarrow 2CO_2 + 3H_2O$
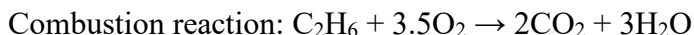
Therefore, one mole of ethane produces two moles of carbon dioxide. To obtain this relationship in terms of mass

$$\frac{2\ moles\ CO_2}{1\ mole\ C_2H_6} \times \frac{44\ g\ CO_2}{1\ mole\ CO_2} \times \frac{1\ mole\ C_2H_6}{30\ g\ C_2H_6} = 2.93\ g\ CO_2\ per\ g\ C_2H_6$$

The obtained combustion emissions for each chemical species were multiplied by the composition to obtain an average value for each product fraction. Table A-21 summarizes the results from the operations mentioned above.

Table A-21. Average chemical species composition per product fraction from polyolefin pyrolysis.

Product fraction	Chemical species	Chemical species composition	Representative compound	Combustion emissions (kg CO_2 per kg)	Fraction combustion emissions (kg CO_2 per kg of fraction)
Gas	paraffins	0.4304	C_2H_6	2.93	3.05
	olefins	0.5696	C_3H_6	3.14	
Light liquid	paraffins	0.5612	C_6H_{14}	3.07	3.11
	olefins	0.4132	C_6H_{12}	3.14	
	aromatics	0.0255	toluene	3.35	
Heavy waxes	paraffins	0.5143	$C_{20}H_{42}$	3.12	3.15
	olefins	0.4175	$C_{20}H_{40}$	3.14	
	aromatics	0.0682	naphthalene	3.44	

Fraction emissions were multiplied by the amount produced to obtain the combustion emissions per tonne of polyolefin waste processed

Gas fraction:

$$\frac{3.05 \text{ kg CO}_2 \text{ eq}}{\text{kg gas fraction}} \times \frac{0.147 \text{ kg gas fraction}}{\text{kg polyolefin waste}} \times \frac{1000 \text{ kg}}{1 \text{ tonne}}$$
$$= 448.29 \text{ kg CO}_2 \text{ eq per tonne polyolefin waste}$$

Light liquid fraction:

$$\frac{3.11 \text{ kg CO}_2 \text{ eq}}{\text{kg liquid fraction}} \times \frac{0.265 \text{ kg liquid fraction}}{\text{kg polyolefin waste}} \times \frac{1000 \text{ kg}}{1 \text{ tonne}}$$
$$= 823.11 \text{ kg CO}_2 \text{ eq per tonne polyolefin waste}$$

Heavy waxes fraction:

$$\frac{3.15 \text{ kg CO}_2 \text{ eq}}{\text{kg wax fraction}} \times \frac{0.448 \text{ kg wax fraction}}{\text{kg polyolefin waste}} \times \frac{1000 \text{ kg}}{1 \text{ tonne}}$$
$$= 1411.28 \text{ kg CO}_2 \text{ eq per tonne polyolefin waste}$$

Thus, the total emissions for the vehicle operation stage account for **2682.68 kg CO₂ eq. per tonne of polyolefin waste**.

A.6.9   Avoided Landfill (organics pathway) Emissions

Emissions from landfill storage of organics waste were accounted for according to the methodology proposed by the Air Resources Board (ARB) of the California Environmental Protection Agency.[25] According to this methodology 63.6% of the organics MSW carbon is active and the remaining fraction stays stable for a long period of time. The carbon content for the different categories of organics waste is reported to be 47, 43.5, 43.5, and 44% for yard trimmings, wood, paper, and cardboard, respectively.[26] Therefore, the total carbon stored in a landfill, on a moisture and ash free basis, is estimated as follows

Yard trimmings: $2,694,235 \times 0.47 = 1,266,290$ tonnes C

Wood: $165,748 \times 0.435 = 72,100$ tonnes C

Paper: $2,650,486 \times 0.435 = 1,151,961$ tonnes C

Cardboard: $1,559,739 \times 0.44 = 686,285$ tonnes C

Total: $3,177,637$ tonnes C/yr $= 3.18$ MMt (million tonnes)

A schematic description of the carbon degradation process presented by ARB[25] is shown in Figure A-3. This process considers a landfill with a biogas collection system in which 75% of the generated biogas is collected. Details of CO_2 calculations are provided for each conversion pathway (arrows marked with a letter).
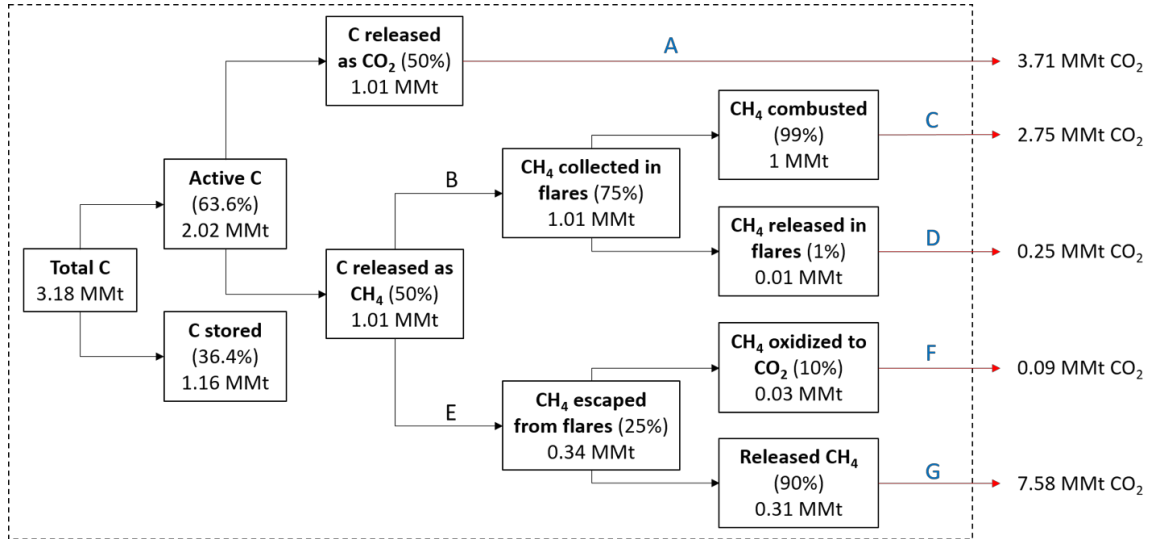
Figure A-3. Carbon degradation and emissions (CO_2 eq.) in landfill storage of organics waste.

Pathway A: From the active carbon (2.02 MMt) 50% is emitted directly as CO_2, either with or without the landfill gas collection system. The amount of CO_2 released to the atmosphere is estimated as

$$1.01 \text{ MMt C} \times \frac{44 \text{ MMt } CO_2}{12 \text{ MMt C}} = 3.71 \text{ MMt } CO_2$$

Pathway B: The other 50% (1.01 MMt) is released as CH_4, from which 75% is collected and flared

$$1.01 \text{ MMt C} \times \frac{16 \text{ MMt } CH_4}{12 \text{ MMt C}} \times 0.75 = 1.01 \text{ MMt } CH_4$$

Pathway C: From this CH_4 collected, 99% is combusted to CO_2

$$\frac{1 \text{ mole } CO_2}{1 \text{ mole } CH_4} \times \frac{44 \text{ g } CO_2}{1 \text{ mole } CO_2} \times \frac{1 \text{ mole } CH_4}{16 \text{ g } CH_4} = 2.75 \text{ g } CO_2 \text{ per g } CH_4$$

$$1.01 \text{ MMt } CH_4 \times 0.99 = 1 \text{ MMt } CH_4 \times \frac{2.75 \text{ MMt } CO_2}{\text{MMt } CH_4} = 2.75 \text{ MMt } CO_2$$

Pathway D: The remaining CH_4 collected in flares (1%) is released to the atmosphere. The emission of one kg of CH_4 is equivalent to the emission of 25 kg of CO_2 (global warming potential of 25).

$$1.01 \text{ MMt } CH_4 \times 0.01 = 0.01 \text{ MMt } CH_4 \times \frac{25 \text{ MMt } CO_2}{\text{MMt } CH_4} = 0.25 \text{ MMt } CO_2$$

Pathway E: From the active carbon released as CH_4 (1.01 MMt) 25% escapes from the collection system

$$1.01 \text{ MMt } C \times \frac{16 \text{ MMt } CH_4}{12 \text{ MMt } C} \times 0.25 = 0.34 \text{ MMt } CH_4$$

Pathway F: From the CH_4 that escaped from collection, soil bacteria metabolizes 10% of it to CO_2 by diffusion into soils that are aerobic.

$$0.34 \text{ MMt } CH_4 \times 0.1 = 0.03 \text{ MMt } CH_4 \times \frac{2.75 \text{ MMt } CO_2}{\text{MMt } CH_4} = 0.09 \text{ MMt } CO_2$$

Pathway G: The remainding CH_4 escaped from collection (90%) is released to the atmosphere

$$0.34 \text{ MMt } CH_4 \times 0.9 = 0.31 \text{ MMt } CH_4 \times \frac{25 \text{ MMt } CO_2}{\text{MMt } CH_4} = 7.58 \text{ MMt } CO_2$$

The total equivalent CO_2 emissions equal 14.38 MMt CO_2. In order to obtain the emissions per tonne of organic MSW stored in landfill, the following calculation requires to be performed.

$$\frac{14.38 \text{ MMt } CO_2}{7,070,208 \text{ tonne of MAFOW}} \times \frac{1 \times 10^9 \text{ kg } CO_2}{1 \text{ MMt } CO_2}$$
$$= 2033.9 \text{ kg } CO_2 \text{ eq per tonne of MAFOW}$$

Thus, the avoided emissions for organic MSW landfill storage account for −**2033.9 kg CO₂ eq. per tonne of organics waste**. The negative sign means the savings of these emissions when landfilling is avoided.

A.7   Emission factors in terms of MJ of fuel

With the purpose of comparing the GHG emissions of MSW-derived fuels with other sources, i.e. fossil fuels, the emission factors were converted from a per mass of waste into a per mega joule (MJ) of fuel basis. The emission factors were multiplied by the amount

of waste processed and divided by the amount of fuels produced. Then, the resulting emissions per kg of fuel produced were divided by the average lower heating value (LHV), in MJ per kg.

A.7.1 Organics pathway

As stated in Table A-9, collection and separation stages process 13.11 million tonnes of yard trimmings, wood, paper, and cardboard waste for the organics pathway. After separation, 12.27 million tonnes of organic waste are transported to the pyrolysis facility. This amount is equal to 7.07 million tonnes on an ash and moisture free basis. According to the yield of 0.2367 kg of liquid fuel per kg of MAFOW,[21,22] 1.67 million tonnes of liquid fuels are produced at the end of the hydroprocessing stage. Figure A-4, presents a summary of the information stated above.
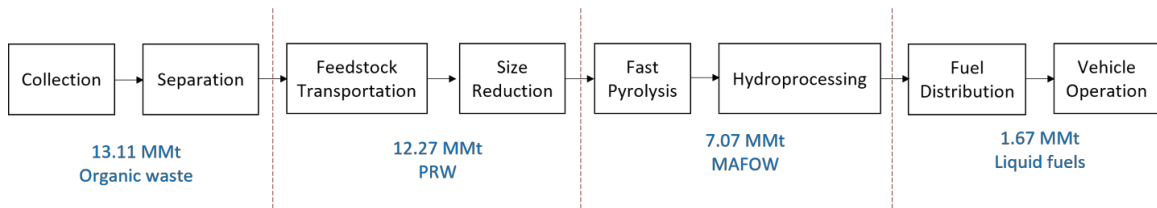
Figure A-4. Amount of waste or fuels processed on each stage of the organics pathway. Mass of organics MSW is on a wet basis for collection, separation, feedstock transportation, and size reduction.

Therefore, the emissions for each stage in g CO_2 eq. per MJ of fuel are given by

S.7.1.1 Collection

$$\frac{41.30 \text{ kg CO}_2}{\text{tonne Organics MSW}} \times \frac{13{,}109{,}091 \text{ tonne Organics MSW}}{1{,}673{,}865 \text{ tonne Liquid Fuels}} \times \frac{1 \text{ tonne fuel}}{1000 \text{ kg fuel}}$$
$$\times \frac{1000 \text{ g CO}_2}{1 \text{ kg CO}_2} = 323.45 \frac{\text{g CO}_2}{\text{kg fuel}}$$

$$\frac{323.45 \text{ g CO}_2}{\text{kg fuel}} \times \frac{\text{kg fuel}}{44 \text{ MJ}} = \mathbf{7.35 \text{ g CO}_2 \text{ eq. per MJ}}$$

S.7.1.2 Separation

$$\frac{12.26 \text{ kg CO}_2}{\text{tonne Organics MSW}} \times \frac{13{,}109{,}091 \text{ tonne Organics MSW}}{1{,}673{,}865 \text{ tonne Liquid Fuels}} \times \frac{1 \text{ tonne fuel}}{1000 \text{ kg fuel}}$$
$$\times \frac{1000 \text{ g CO}_2}{1 \text{ kg CO}_2} = 96.02 \frac{\text{g CO}_2}{\text{kg fuel}}$$

201

$$\frac{96.02 \text{ g CO}_2}{\text{kg fuel}} \times \frac{\text{kg fuel}}{44 \text{ MJ}} = \mathbf{2.18 \text{ g CO}_2 \text{ eq. per MJ}}$$

S.7.1.3 Feedstock transportation

$$\frac{12.13 \text{ kg CO}_2}{\text{tonne PRW}} \times \frac{12,270,278 \text{ tonne PRW}}{1,673,865 \text{ tonne Liquid Fuels}} \times \frac{1 \text{ tonne fuel}}{1000 \text{ kg fuel}} \times \frac{1000 \text{ g CO}_2}{1 \text{ kg CO}_2}$$
$$= 88.92 \frac{\text{g CO}_2}{\text{kg fuel}}$$

$$\frac{96.02 \text{ g CO}_2}{\text{kg fuel}} \times \frac{\text{kg fuel}}{44 \text{ MJ}} = \mathbf{2.02 \text{ g CO}_2 \text{ eq. per MJ}}$$

S.7.1.4 Size reduction

$$\frac{119.13 \text{ kg CO}_2}{\text{tonne PRW}} \times \frac{12,270,278 \text{ tonne PRW}}{1,673,865 \text{ tonne Liquid Fuels}} \times \frac{1 \text{ tonne fuel}}{1000 \text{ kg fuel}} \times \frac{1000 \text{ g CO}_2}{1 \text{ kg CO}_2}$$
$$= 873.28 \frac{\text{g CO}_2}{\text{kg fuel}}$$

$$\frac{873.28 \text{ g CO}_2}{\text{kg fuel}} \times \frac{\text{kg fuel}}{44 \text{ MJ}} = \mathbf{19.85 \text{ g CO}_2 \text{ eq. per MJ}}$$

S.7.1.5 Pyrolysis

$$\frac{382.18 \text{ kg CO}_2}{\text{tonne MAFOW}} \times \frac{7,070,208 \text{ tonne MAFOW}}{1,673,865 \text{ tonne Liquid Fuels}} \times \frac{1 \text{ tonne fuel}}{1000 \text{ kg fuel}} \times \frac{1000 \text{ g CO}_2}{1 \text{ kg CO}_2}$$
$$= 1614.28 \frac{\text{g CO}_2}{\text{kg fuel}}$$

$$\frac{1614.28 \text{ g CO}_2}{\text{kg fuel}} \times \frac{\text{kg fuel}}{44 \text{ MJ}} = \mathbf{36.69 \text{ g CO}_2 \text{ eq. per MJ}}$$

S.7.1.6 Hydroprocessing

$$\frac{471.39 \text{ kg CO}_2}{\text{tonne MAFOW}} \times \frac{7,070,208 \text{ tonne MAFOW}}{1,673,865 \text{ tonne Liquid Fuels}} \times \frac{1 \text{ tonne fuel}}{1000 \text{ kg fuel}} \times \frac{1000 \text{ g CO}_2}{1 \text{ kg CO}_2}$$
$$= 1991.1 \frac{\text{g CO}_2}{\text{kg fuel}}$$

$$\frac{1991.1 \text{ g CO}_2}{\text{kg fuel}} \times \frac{\text{kg fuel}}{44 \text{ MJ}} = \textbf{45.25 g CO}_2 \textbf{ eq. per MJ}$$

S.7.1.7 Fuel distribution

$$\frac{1.44 \text{ kg CO}_2}{\text{tonne MAFOW}} \times \frac{7,070,208 \text{ tonne MAFOW}}{1,673,865 \text{ tonne Liquid Fuels}} \times \frac{1 \text{ tonne fuel}}{1000 \text{ kg fuel}} \times \frac{1000 \text{ g CO}_2}{1 \text{ kg CO}_2}$$
$$= 6.08 \frac{\text{g CO}_2}{\text{kg fuel}}$$

$$\frac{6.08 \text{ g CO}_2}{\text{kg fuel}} \times \frac{\text{kg fuel}}{44 \text{ MJ}} = \textbf{0.14 g CO}_2 \textbf{ eq. per MJ}$$

S.7.1.8 Vehicle operation

$$\frac{753.01 \text{ kg CO}_2}{\text{tonne MAFOW}} \times \frac{7,070,208 \text{ tonne MAFOW}}{1,673,865 \text{ tonne Liquid Fuels}} \times \frac{1 \text{ tonne fuel}}{1000 \text{ kg fuel}} \times \frac{1000 \text{ g CO}_2}{1 \text{ kg CO}_2}$$
$$= 3180.62 \frac{\text{g CO}_2}{\text{kg fuel}}$$

$$\frac{3180.62 \text{ g CO}_2}{\text{kg fuel}} \times \frac{\text{kg fuel}}{44 \text{ MJ}} = \textbf{72.28 g CO}_2 \textbf{ eq. per MJ}$$

S.7.1.9 Landfill storage

$$\frac{-2033.9 \text{ kg CO}_2}{\text{tonne MAFOW}} \times \frac{7,070,208 \text{ tonne MAFOW}}{1,673,865 \text{ tonne Liquid Fuels}} \times \frac{1 \text{ tonne fuel}}{1000 \text{ kg fuel}} \times \frac{1000 \text{ g CO}_2}{1 \text{ kg CO}_2}$$
$$= -8590.9 \frac{\text{g CO}_2}{\text{kg fuel}}$$

$$\frac{-8590.9 \text{ g CO}_2}{\text{kg fuel}} \times \frac{\text{kg fuel}}{44 \text{ MJ}} = \textbf{-195.25 g CO}_2 \textbf{ eq. per MJ}$$

A.7.2   Polyolefin pathway

For the polyolefin pathway, from 4.47 million tonnes of collected and separated plastic, 4.45 million tonnes are transported to the pyrolysis facility. On a dry weight basis, this amount is equal to 4.44 million tonnes. After the pyrolysis stage, 2.52 million tonnes of hydrocarbon fuels are produced. To obtain the average LHV of these fuels, the sum of the composition of each fraction times its LHV, according to Boundy et al.[27], was computed.

The operation resulted in an average LHV of 43.19 MJ per kg of fuel. A summarized scheme of the quantities processed in the polyolefin pathway is shown in Figure A-5.

```
Collection → Separation ┆ Feedstock      → Size      → Fast     ┆ Fuel         → Vehicle
                        ┆ Transportation   Reduction   Pyrolysis ┆ Distribution   Operation

       2.95 MMt                      2.93 MMt                         2.52 MMt
     Polyolefin waste                  PRW                         Hydrocarbon fuels
```
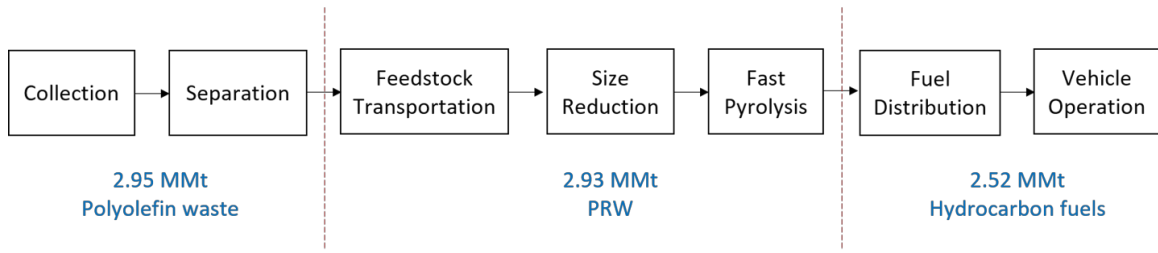
Figure A-5. Amount of waste and fuels processed for each stage in the polyolefin pathway.

The emissions for every stage on a per MJ basis were computed as follows

S.7.2.1 Collection

$$\frac{41.30 \text{ kg } CO_2}{\text{tonne Polyolefin waste}} \times \frac{2,954,349 \text{ tonne Polyolefin waste}}{2,522,981 \text{ tonne HC Fuels}} \times \frac{1 \text{ tonne HC fuel}}{1000 \text{ kg HC fuel}}$$
$$\times \frac{1000 \text{ g } CO_2}{1 \text{ kg } CO_2} = 48.36 \frac{\text{g } CO_2}{\text{kg HC fuel}}$$

$$\frac{48.36 \text{ g } CO_2}{\text{kg fuel}} \times \frac{\text{kg fuel}}{43.19 \text{ MJ}} = \mathbf{1.12 \text{ g } CO_2 \text{ eq. per MJ}}$$

S.7.2.2 Separation

$$\frac{12.26 \text{ kg } CO_2}{\text{tonne Polyolefin waste}} \times \frac{2,954,349 \text{ tonne Polyolefin waste}}{2,522,981 \text{ tonne HC Fuels}} \times \frac{1 \text{ tonne HC fuel}}{1000 \text{ kg HC fuel}}$$
$$\times \frac{1000 \text{ g } CO_2}{1 \text{ kg } CO_2} = 14.36 \frac{\text{g } CO_2}{\text{kg HC fuel}}$$

$$\frac{14.36 \text{ g } CO_2}{\text{kg HC fuel}} \times \frac{\text{kg HC fuel}}{43.19 \text{ MJ}} = \mathbf{0.33 \text{ g } CO_2 \text{ eq. per MJ}}$$

S.7.2.3 Feedstock transportation

$$\frac{12.13 \text{ kg } CO_2}{\text{tonne PRW}} \times \frac{2,939,578 \text{ tonne PRW}}{2,522,981 \text{ tonne HC Fuels}} \times \frac{1 \text{ tonne HC fuel}}{1000 \text{ kg HC fuel}} \times \frac{1000 \text{ g } CO_2}{1 \text{ kg } CO_2}$$
$$= 14.13 \frac{\text{g } CO_2}{\text{kg HC fuel}}$$

$$\frac{14.13 \text{ g } CO_2}{\text{kg HC fuel}} \times \frac{\text{kg HC fuel}}{43.19 \text{ MJ}} = \mathbf{0.33 \text{ g } CO_2 \text{ eq. per MJ}}$$

S.7.2.4 Size reduction

$$\frac{119.13 \text{ kg CO}_2}{\text{tonne PRW}} \times \frac{2{,}939{,}578 \text{ tonne PRW}}{2{,}522{,}981 \text{ tonne HC Fuels}} \times \frac{1 \text{ tonne HC fuel}}{1000 \text{ kg HC fuel}} \times \frac{1000 \text{ g CO}_2}{1 \text{ kg CO}_2}$$

$$= 138.8 \frac{\text{g CO}_2}{\text{kg HC fuel}}$$

$$\frac{138.8 \text{ g CO}_2}{\text{kg HC fuel}} \times \frac{\text{kg HC fuel}}{43.19 \text{ MJ}} = \textbf{3.21 g CO}_2 \textbf{ eq. per MJ}$$

S.7.2.5 Pyrolysis

For the pyrolysis and upcoming stages the amount of polyolefin considered needs to be expressed on a moisture free basis (Moisture content of plastic is approximately 0.5%).[26]

$$\frac{394.56 \text{ kg CO}_2}{\text{tonne PW}} \times \frac{2{,}933{,}698 \text{ tonne PW}}{2{,}522{,}981 \text{ tonne HC Fuels}} \times \frac{1 \text{ tonne HC fuel}}{1000 \text{ kg HC fuel}} \times \frac{1000 \text{ g CO}_2}{1 \text{ kg CO}_2}$$

$$= 458.79 \frac{\text{g CO}_2}{\text{kg HC fuel}}$$

$$\frac{458.79 \text{ g CO}_2}{\text{kg HC fuel}} \times \frac{\text{kg HC fuel}}{43.19 \text{ MJ}} = \textbf{10.62 g CO}_2 \textbf{ eq. per MJ}$$

S.7.2.6 Fuel distribution

$$\frac{7.33 \text{ kg CO}_2}{\text{tonne PW}} \times \frac{2{,}933{,}698 \text{ tonne PW}}{2{,}522{,}981 \text{ tonne HC Fuels}} \times \frac{1 \text{ tonne HC fuel}}{1000 \text{ kg HC fuel}} \times \frac{1000 \text{ g CO}_2}{1 \text{ kg CO}_2}$$

$$= 8.52 \frac{\text{g CO}_2}{\text{kg HC fuel}}$$

$$\frac{8.52 \text{ g CO}_2}{\text{kg HC fuel}} \times \frac{\text{kg HC fuel}}{43.19 \text{ MJ}} = \textbf{0.20 g CO}_2 \textbf{ eq. per MJ}$$

S.7.2.7 Vehicle operation

$$\frac{2682.68 \text{ kg CO}_2}{\text{tonne PW}} \times \frac{2{,}933{,}698 \text{ tonne PW}}{2{,}522{,}981 \text{ tonne HC Fuels}} \times \frac{1 \text{ tonne HC fuel}}{1000 \text{ kg HC fuel}} \times \frac{1000 \text{ g CO}_2}{1 \text{ kg CO}_2}$$

$$= 3119.39 \frac{\text{g CO}_2}{\text{kg HC fuel}}$$

$$\frac{3119.39 \text{ g CO}_2}{\text{kg HC fuel}} \times \frac{\text{kg HC fuel}}{43.19 \text{ MJ}} = \mathbf{72.22 \text{ g CO}_2 \text{ eq. per MJ}}$$

A.8   References

(1)   Durán Moreno, A.; Garcés Rodríguez, M.; Velasco, A. R.; Marín Enriquez, J. C.; Gutiérrez Lara, R.; Moreno Gutiérrez, A.; Delgadillo Hernández, N. A. Mexico city's municipal solid waste characteristics and composition analysis. *Rev. Int. Contam. Ambie.* **2013,** *29* (1), 39-46.

(2)   Bernache-Pérez, G.; Sánchez-Colón, S.; Garmendia, A. M.; Dávila-Villarreal, A.; Sánchez-Salazar, M. E. Solid waste characterisation study in the Guadalajara Metropolitan Zone, Mexico. *Waste Manage. Res.* **2001,** *19* (5), 413-424.

(3)   Pan American Health Organization (PAHO). *Evaluación general de los servicios de manejo de residuos sólidos municipales. Informe analítico de México. Evaluación 2002*; World Health Organization: Mexico, 2003.

(4)   Mexican Institute of Statistics and Geography (INEGI). Generación estimada de residuos sólidos por entidad federativa. www.inegi.org.mx/est/contenidos/Proyectos/modulosamb/doc/rsu.zip (accessed February 6, 2015).

(5)   Achilias, D. S.; Roupakias, C.; Megalokonomos, P.; Lappas, A. A.; Antonakou, E. V. Chemical recycling of plastic wastes made from polyethylene (LDPE and HDPE) and polypropylene (PP). *J. Hazard. Mater.* **2007,** *149* (3), 536-542.

(6)   Buekens, A. G.; Huang, H. Catalytic plastics cracking for recovery of gasoline-range hydrocarbons from municipal plastic wastes. *Resour. Conserv. Recy.* **1998,** *23* (3), 163-181.

(7)   Çit, İ.; Sınağ, A.; Yumak, T.; Uçar, S.; Mısırlıoğlu, Z.; Canel, M. Comparative pyrolysis of polyolefins (PP and LDPE) and PET. *Polym. Bull.* **2010,** *64* (8), 817-834.

(8)   Demirbas, A. Pyrolysis of municipal plastic wastes for recovery of gasoline-range hydrocarbons. *J. Anal. Appl. Pyrol.* **2004,** *72* (1), 97-102.

(9)   Li, X.; Li, J.; Zhou, G.; Feng, Y.; Wang, Y.; Yu, G.; Deng, S.; Huang, J.; Wang, B. Enhancing the production of renewable petrochemicals by co-feeding of biomass with plastics in catalytic fast pyrolysis with ZSM-5 zeolites. *Appl. Catal. A.* **2014,** *481*, 173-182.

(10)   Pinto, F.; Costa, P.; Gulyurtlu, I.; Cabrita, I. Pyrolysis of plastic wastes. 1. Effect of plastic waste composition on product yield. *J. Anal. Appl. Pyrol.* **1999,** *51* (1–2), 39-55.

(11)   Scott, D. S.; Czernik, S. R.; Piskorz, J.; Radlein, D. S. A. G. Fast pyrolysis of plastic wastes. *Energ. Fuel.* **1990,** *4* (4), 407-411.

(12)   Williams, E. A.; Williams, P. T. The pyrolysis of individual plastics and a plastic mixture in a fixed bed reactor. *J. Chem. Technol. Biot.* **1997,** *70* (1), 9-20.

(13)   Williams, P. T.; Williams, E. A. Interaction of Plastics in Mixed-Plastics Pyrolysis. *Energ. Fuel.* **1999,** *13* (1), 188-196.

(14)   Mexican Chemical Industry Association (ANIQ). Anuario Estadístico de la Industria Química Mexicana 2015. http://www.aniq.org.mx/anuario/2015/index.html (accessed May 17, 2016).

(15)   Perugini, F.; Mastellone, M. L.; Arena, U. A life cycle assessment of mechanical and feedstock recycling options for management of plastic packaging wastes. *Environ. Progr.* **2005,** *24* (2), 137-154.

(16)   Fitzgerald, G. C.; Krones, J. S.; Themelis, N. J. Greenhouse gas impact of dual stream and single stream collection and separation of recyclables. *Resour. Conserv. Recy.* **2012,** *69*, 50-56.

(17)   *The Ecoinvent Database*, version 3; Swiss Centre for Life Cycle Inventories: Zurich, Switzerland, 2013.

(18)   *SimaPro LCA Software*, version 8.0; PRé-Consultants: The Netherlands, 2014.

(19)   Alston, S. M.; Arnold, J. C. Environmental Impact of Pyrolysis of Mixed WEEE Plastics Part 2: Life Cycle Assessment. *Environ. Sci. Technol.* **2011,** *45* (21), 9386-9392.

(20)   Mexican Secretariat of Energy (SENER). *Balance Nacional de Energía 2014*; Mexico, 2015.

(21)   Hsu, D. D. *Life Cycle Assessment of Gasoline and Diesel Produced via Fast Pyrolysis and Hydroprocessing*; Report No. NREL/TP-6A20-49341; National Renewable Energy Laboratory: Golden, CO, 2011.

(22)   Hsu, D. D. Life cycle assessment of gasoline and diesel produced via fast pyrolysis and hydroprocessing. *Biomass Bioenerg.* **2012,** *45*, 41-47.

(23)   Jones, S. B.; Holladay, J. E.; Valkenburg, C.; Stevens, D. J.; Walton, C. W.; Kinchin, C.; Elliott, D. C.; Czernik, S. *Production of Gasoline and Diesel from Biomass via Fast Pyrolysis, Hydrotreating and Hydrocracking: A Design Case.*; Report No. PNNL-18284; Pacific Northwest National Laboratory: Richland, WA, 2009.

(24)   Valkenburg, C.; Gerber, M. A.; Walton, C. W.; Jones, S. B.; Thompson, B. L.; Stevens, D. J. *Municipal Solid Waste (MSW) to Liquid Fuels Synthesis, Volume 1: Availability of Feedstock and Technology*; Report No. PNNL-18144; Richland, WA, 2008.

(25)   California Air Resources Board (ARB). *Proposed Low Carbon Fuel Standard (LCFS) Pathway for the Production of Biomethane from High Solids Anaerobic Digestion (HSAD) of Organic (Food and Green) Wastes*; California Environmental Protection Agency: Sacramento, CA, 2012.

(26)   Velasco Perez Alonso, M. G. Generation and disposition of MSW in Mexico and potential for improving waste management in Toluca municipality. MS dissertation, Columbia University, 2011.

(27)   Boundy, B.; Diegel, S. W.; Wright, L.; Davis, S. C. *Biomass Energy Data Book*, ed. 4; Oak Ridge National Laboratory: Oak Ridge, TN, 2011.

B   Supporting Information for Chapter 3

Effect of Temperature and Vapor residence Time on the Micropyrolysis Products of Waste High Density Polyethylene

B.1   Development of a stable temperature profile of the Two-Stage Micropyrolysis Reactor

B.1.1   General description of the apparatus

In order to test longer vapor residence times (VRTs) at high temperatures, a two-stage micropyrolysis reactor (TSMR) consisting of a ¼ in ID and 22.25 in long stainless steel tube, with appropriate fittings, was connected to an existing CDS 5200 HP Pyroprobe unit (Figure B-1). With the TSMR, the probe fires and vapors are generated from the solid high density polyethylene (HDPE) particle (first stage), and then the vapors immediately enter a high temperature zone set to a stable temperature selected in the range from 625-700 °C (second stage). Ultra-high purity helium (99.999% purity) carries the vapors down the TSMR where the breakdown continues at a high temperature. After a determined length, corresponding to a particular residence time, the sample enters a 300 °C zone connected to the heated interface in the CDS pyroprobe unit. To develop a zone with an appropriate temperature profile within the TSMR, temperature measurements from several iterations of heating tape and insulation positions were completed.

High temperatures in the TSMR were achieved by wrapping a 48 in heating tape (BriskHeat BWH051040L) down 17.5 in of the reactor length, beginning at 3.875 in from the inlet edge of the reactor. This distance was set so that the probe from the Pyroprobe unit could be fully inserted to the edge of the high heat zone. The heating tape was connected to a rheostat (Staco 3PN1010 120/140V) which served as the manual temperature controller. The extent of this high temperature zone can be modified by adjusting the amount of heating tape to be wrapped along the reactor. A second heating tape (BriskHeat BWH051020L) was wrapped after the high temperature heating tape to maintain the pyrolysis products in a gaseous state but without inducing further degradation. The temperature of this second heating zone was set at 300 °C using a temperature controller (Briskheat SDC120KC-A). The entire length of the reactor was wrapped in insulation (Darco Southern Braided Fiberglass Sleeve) starting at 1.38 in from the inlet to ensure the TSMR could reach the top temperature of 750°C (initial testing temperature). Details about the insulation arrangement are provided in section B.1.2. Figure B-1 shows the TSMR with both heating tapes, insulation, and temperature control devices.
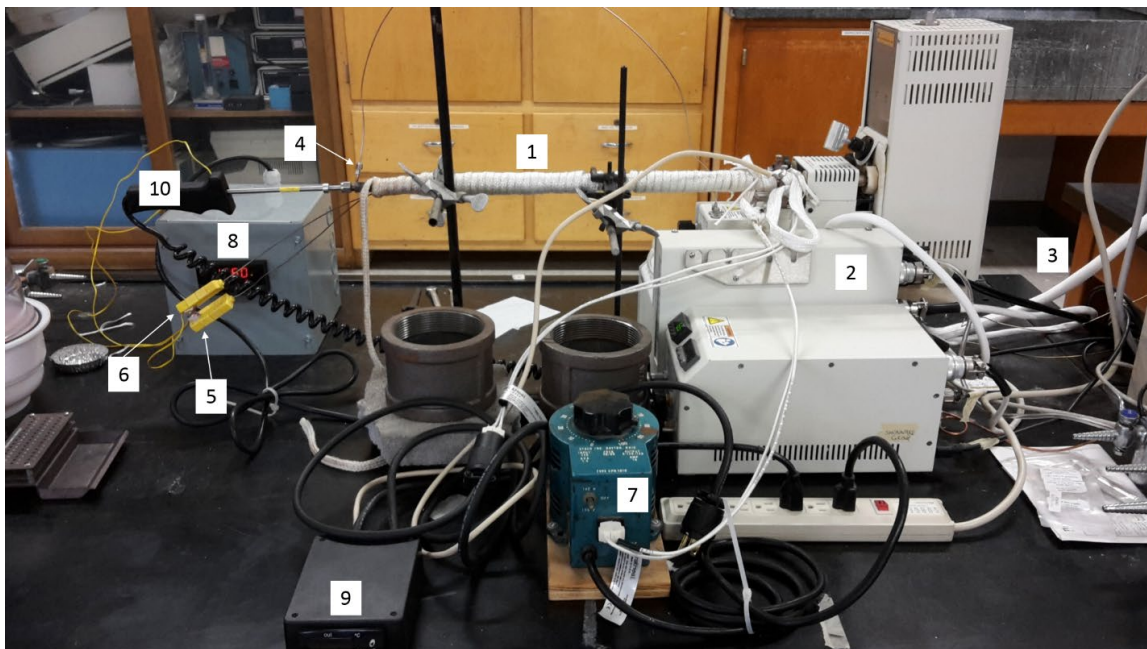
Figure B-1. Actual set up of the two-stage micropyrolysis reactor connected to the CDS 5200 HP Pyroprobe unit along with temperature measurement and control devices (1: Two-stage micropyrolysis reactor, 2: CDS 5200 HP pyroprobe unit, 3: Transfer line from pyroprobe to GC, 4: Helium flow inlet for run mode, 5: Thermocouple 1, 6: Thermocouple 2, 7: Heating tape/reactor temperature controller, 8: Thermocouple display, 9: Temperature controller/display for 300°C heated zone, 10: Probe of the CDS 5200 HP pyroprobe unit).

B.1.2   Temperature profile measurements

Temperature profile data was gathered by disconnecting the reactor extension from the Pyroprobe unit and inserting a 24 in thermocouple (Omega KQXL-116G-24) in the TSMR at an approximate distance of 15 in from the reactor inlet. Helium flow was provided and set to 100 mL/min using the CDS pyroprobe. Over the course of several iterations, the insulation wrapping was altered (Table B-1) to get the most stable temperature profile in the high temperature zone (reaction zone). With a new arrangement of insulation in place, the heating tape at the reactor zone was turned on. Once the inner measurement was stable at approximately 750°C, the thermocouple was inserted all the way to the TSMR inlet and the temperature was recorded. The thermocouple was then moved one inch farther down the reactor and another measurement was taken. This was repeated down the entire length of the reactor.

Table B-1. Insulation arrangement of each insulation test.

Insulation test number	Zones with double insulation	Zone with single insulation
1	1)1.5 to 11 in	11 to 22.25 in
2	1)1.5 to 6 in 2)16 to 22.25 in	6 to 16 in
3	1)1.5 to 9 in 2)16 to 22.25 in	9 to 16 in
4	1)1.5 to 11 in 2)16 to 22.25 in	11 to 16 in
5	1)1.5 to 12 in 2)16 to 20.25 in	12 to 16 in
6	1)1.5 to 12 in 2)15 to 20.25 in	12 to 15 in

The most stable temperature profile for the reaction zone was achieved in insulation test 6 (Figure B-2). With this set up, one layer of insulation was tightly wrapped over both heating tapes down the entire length of the reactor. A second layer of insulation was wrapped from 1.5 to 12 in from the reactor inlet, then 3 in were covered with insulation spirals separated 1 in from each other (single insulation zone), and finally, another double layer of insulation covered the TSMR from 15 to 20.25 in (see Figure B-3). The reaction zone, as shown in Figure B-2, was defined due to the stable temperature profile observed. This zone was 9 in in length with an average temperature of 759 °C. Vapor residence time (VRT) values are referred only to this reaction zone (see section B.3) and not to the entire length of the TSRM.
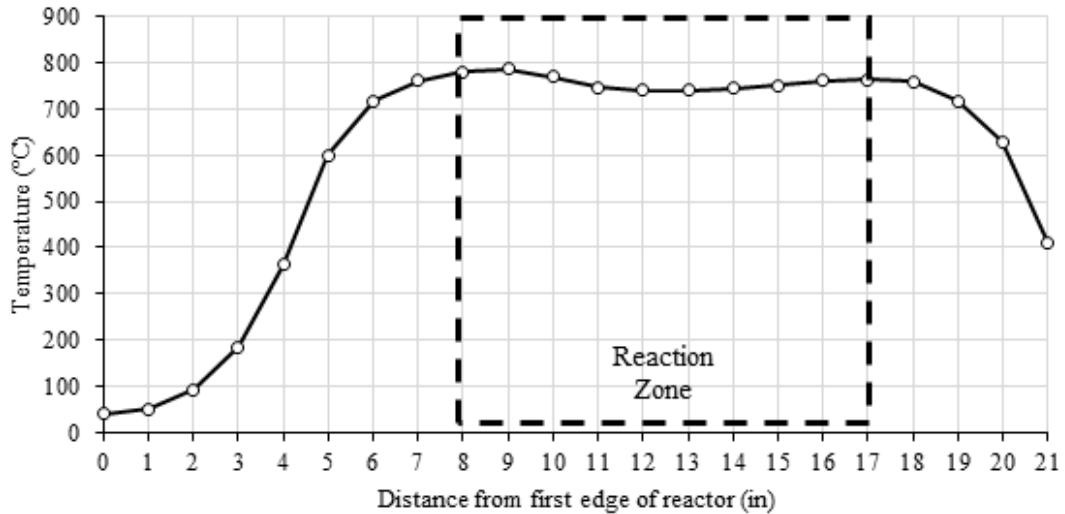
Figure B-2. Temperature profile for the most stable insulation arrangement (Insulation 6) with the reaction zone indicated.
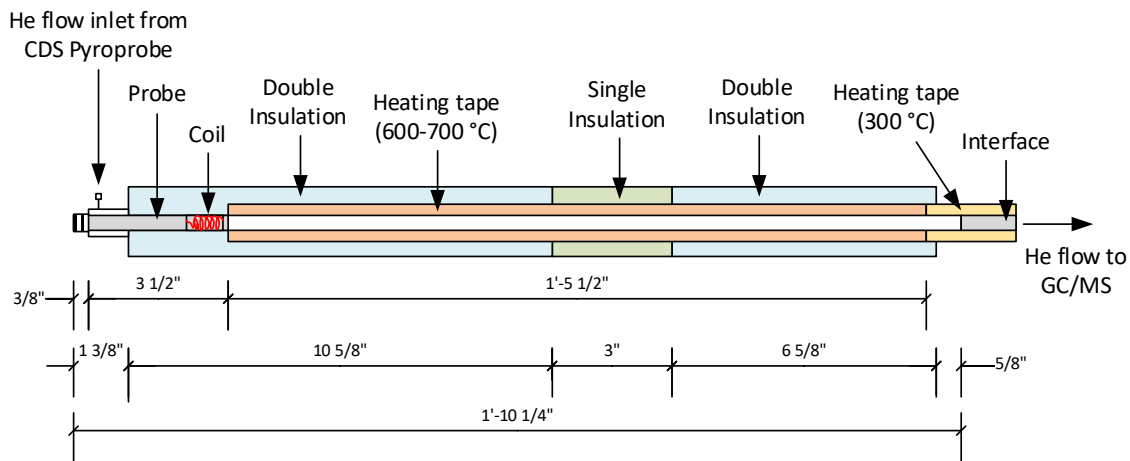
Figure B-3. Diagram of the heating zone and insulation arrangement for the TSMR.

The temperature profile measurements described above were taken with a thermocouple inside of the TSMR, however, during actual experiments; thermocouples cannot be placed inside the TSMR. The apparatus is sealed at both ends, one attached to the CDS probe and the other one to the CDS interface. To monitor the inner temperature during experiments, tests were performed with the goal to correlate outside with inside temperature measurements. Simultaneous temperature measurements were taken with one thermocouple inside the reactor and the other on the outside surface of the reactor underneath the heating tape and insulation layers. Both thermocouples were then moved up and down the reactor to take temperature readings at different points. Figure B-4 illustrates that the temperature measured inside the reactor correlated directly to the temperature measured on the outside of the reactor. Therefore, external temperature measurements were used to monitor the internal temperature during the experiments.

During actual experiments, it was not practical to get temperature information for the entire length of the reactor. Therefore, two points, based on Figure B-2, were chosen to monitor the temperature of the reaction zone. These points were located at 10 and 16 in from the reactor inlet. The average of these two temperatures was used as the "actual" temperature for every experiment.
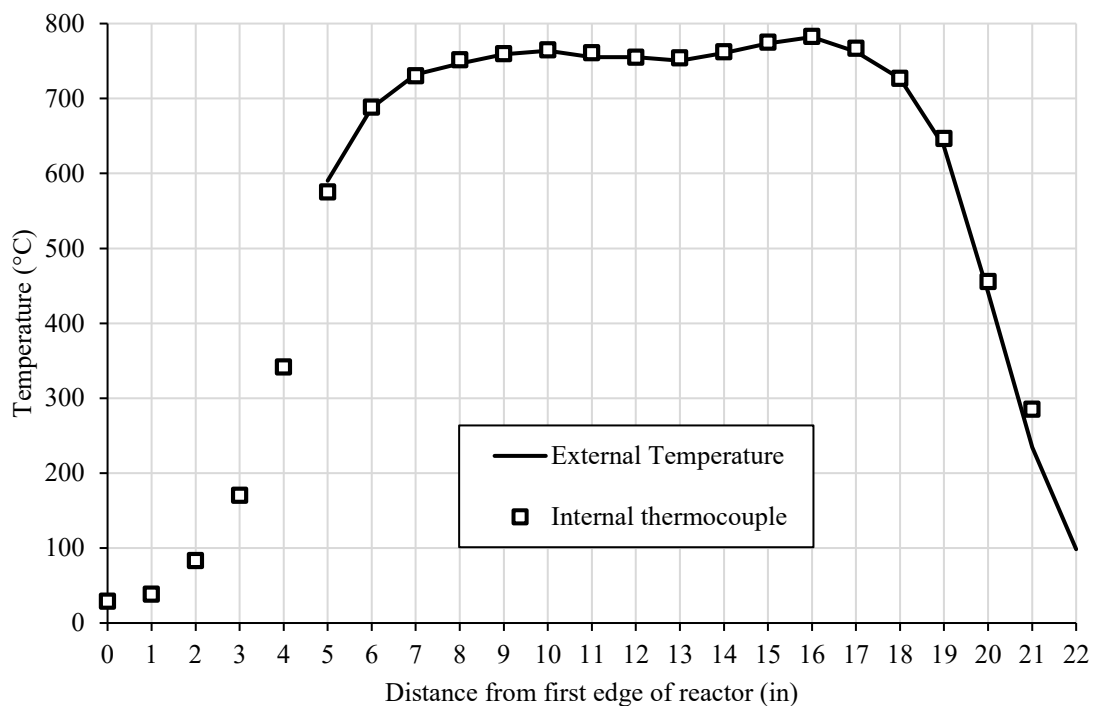
Figure B-4. Comparison of internal and external temperature in the TSMR (Helium flow rate: 100 mL/min).

B.2   Purity of the waste HDPE sample

The samples for pyrolysis were obtained from household waste milk jugs. The purity of the HDPE in these samples was analyzed using a Costech 4010 elemental analyzer that provided the elemental composition of Carbon, Hydrogen, Nitrogen, and Oxygen. Composition of other trace elements like Phosphorous, Silicon, Aluminum, Iron, Magnesium, Sodium, Titanium, and Calcium was tested with a Perkin Elmer Optima 7000DV Inductively Coupled Plasma – Optical Emission Spectrometer (ICP-OES). The results of these analysis are shown in Table B-2.

214

Table B-2. Elemental composition of the HDPE samples used in this study.

Element	Elemental Composition (%)	Trace Metals (mg/kg)
Carbon	85.40	NA
Hydrogen	15.20	NA
Nitrogen	0.07	NA
Oxygen	2.40	NA
Phosphorous	NA	15.0
Silicon	NA	298.0
Aluminum	NA	9.0
Iron	NA	20.0
Magnesium	NA	8.0
Sodium	NA	10.0
Titanium	NA	7.0
Calcium	NA	101.0
NA: Not applicable		

B.3   Calculation of VRT from helium Flow Rate

VRT in the TSMR was varied by changing the flow rate of the helium carrier gas. Three different helium flow rates (25, 50, and 100 mL/min) were tested in this experiment so that the pyrolysis products at different VRTs could be compared.

The volumetric flow rate of helium was programmed in the gas chromatographer (Thermo Fisher K8880181) and assumed to be the value at room temperature. The room temperature volumetric flow rate was converted to molar flow rate of helium through the ideal gas law in equation (B-1).

$$\dot{n} = \frac{P\dot{V}}{RT} \tag{B-1}$$

where $\dot{n}$ is molar flow rate, $\dot{V}$ is volumetric flow rate, R is the ideal gas constant, P is pressure, and T is temperature. Due to no pressurization of the TSMR, atmospheric pressure was assumed for all calculations.

Volumetric flow rate at the reaction temperature was then calculated using equation (B-2), the molar flow rate at room temperature, and the reaction temperature.

$$\dot{V} = \frac{\dot{n}TR}{P} \tag{B-2}$$

Then using the inner diameter of the cylindrical reactor, the length of the heated zone, the volumetric flow rate at high reaction temperature, and appropriate conversion factors, the residence time for the second stage reaction was determined with equation (B-3).

$$VRT = \frac{\pi L \left(\frac{D}{2}\right)^2}{\dot{V}} \tag{B-3}$$

where L is the length of the reaction zone (9 in), D is the inner diameter of the TSMR (0.25 in), and $\dot{V}$ is the volumetric flow rate.

These calculations were completed for three room temperature helium flow rates. Table B-3 shows the room temperature helium flow rate and the corresponding residence time. For comparison's sake, 25 mL/min was approximately 5.6 s, 50 mL/min was 2.8 s, and 100 mL/min was 1.4 s.

Table B-3. Estimated VRT, in seconds, at different temperatures and helium flow rates.

Temperature (°C)	Helium flow rate (mL/min)		
	25	50	100
625	5.77	2.88	1.44
650	5.61	2.81	1.40
675	5.46	2.73	1.37

Additional Reynolds number calculations were completed to characterize the flow with equation (B-4). Density and viscosity for helium were estimated using equations (B-5) and (B-6) from Petersen.[1]

$$Re = \frac{\rho v D}{\mu} \tag{B-4}$$

$$\rho = 48.14 \, \frac{P}{T}\left[1 + 0.4446 \frac{P}{T^{1.2}}\right]^{-1}, \text{ units in bar, K, and kg/m}^3 \tag{B-5}$$

$$\mu = (3.674 \times 10^{-7}) \cdot T^{0.7}, \text{ units in K, kg/(m·s)} \tag{B-6}$$

where Re is Reynolds number, ρ is density of helium, v is velocity of the fluid, D is the inner diameter of the TSMR, μ is dynamic viscosity, P is pressure, and T is temperature.

Calculated Reynolds number and corresponding flow type are listed in Table B-4. The densities and viscosities, determined throught Equations (B-5) and (B-6) that were used in the Reynolds number calculations are shown in Table B-5.

216

Table B-4. Reynolds number and flow type at different temperatures and residence times.

Temperature (°C)	Helium flow rate (mL/min)		
	25	50	100
625	1146, Laminar	2293, Transition	4586, Turbulent
650	1125, Laminar	2249, Transition	4499, Turbulent
675	1104, Laminar	2208, Transition	4415, Turbulent

Table B-5. Densities and viscosities at different temperatures and residence times.

Temperature (°C)	Helium flow rate (mL/min)					
	25		50		100	
	Density (kg/m^3)	Viscosity $(k/(m \cdot s))$	Density (kg/m^3)	Viscosity $(k/(m \cdot s))$	Density (kg/m^3)	Viscosity $(k/(m \cdot s))$
625	0.054	4.29×10^{-5}	0.054	4.29×10^{-5}	0.054	4.29×10^{-5}
650	0.053	4.37×10^{-5}	0.053	4.37×10^{-5}	0.053	4.37×10^{-5}
675	0.051	4.46×10^{-5}	0.051	4.46×10^{-5}	0.051	4.46×10^{-5}

B.4 Pyrolysis products identification at different conditions of temperature and VRT

As mentioned in the Experimental Section, pyrolysis products were analyzed through GC/MS using a 0.1 % cut off limit of contribution according the integration performed by the Xcalibur software. Adjustments in software integration had to be carried out before obtaining the final peak area percent of each compound. First, the baseline of some peaks had to be readjusted manually due to a "raising effect" observed with the software integration. Also, the areas of some peaks had to be divided into two or three compounds due to co-elution. The different compounds were identified by observing different mass fraction patterns within the same peak. A special case of identification/integration occurred with lumped C1-C5 aliphatic hydrocarbons observed at early retention times (See Figure B-5). In this case, the area of the mass with the highest relative abundance (Table B-6) for each lumped compound was considered for its identification and calculation of its corresponding area.
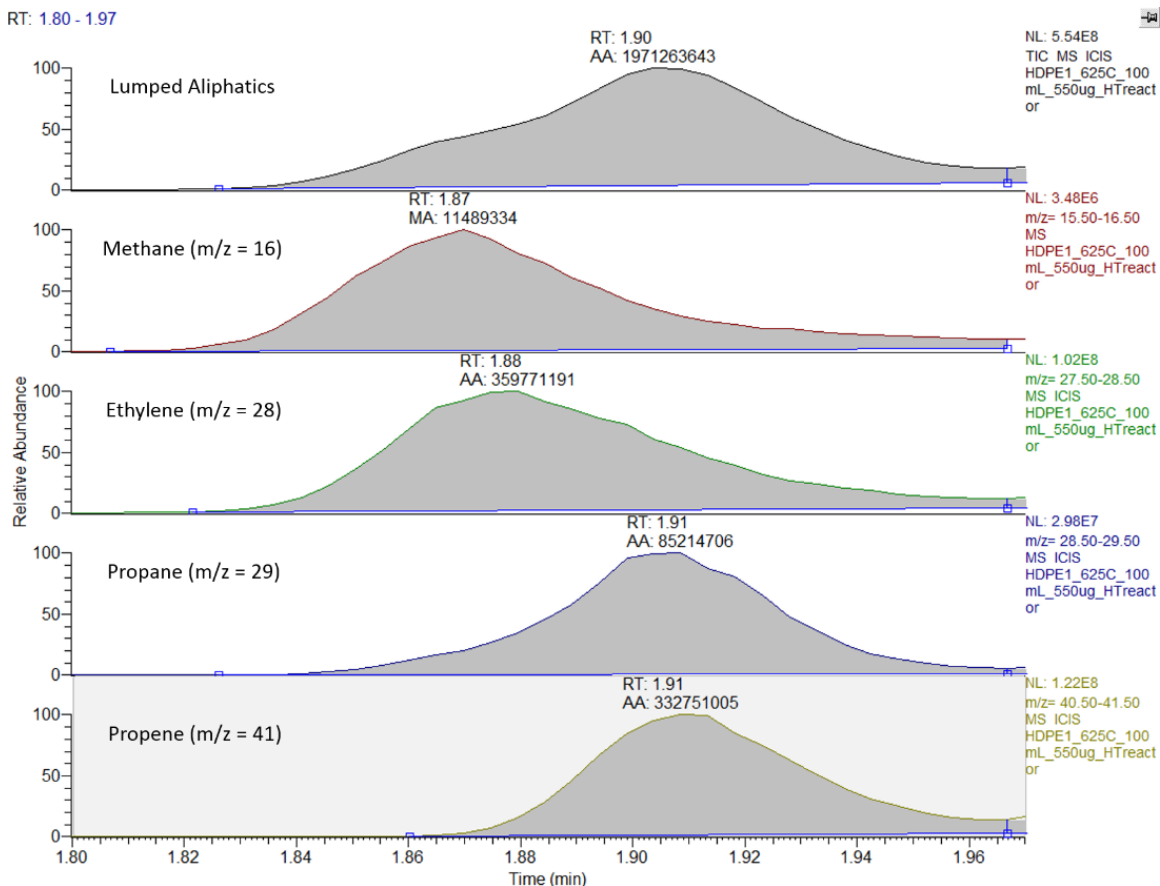
Figure B-5. Identification and integration of lumped compounds.

Table B-6. Masses used for area calculation of lumped compounds according to Kandasamy and Gökalp[2] and NIST[3]

Compound	m/z
Methane	16
Ethylene	28
Propane	29
Propene	41
Butane	43
1-butene	41
Pentane	43
1-pentene	42

The area calculation of lumped compounds was as follows: First, once the areas for the corresponding masses of each lumped compound were obtained, the total area of corresponding masses of lumped compounds (TMLC) was obtained using equation (B-7)

$$TMLC = \sum M_i \qquad \text{(B-7)}$$

where M_i is the area of each compound obtained by integration of the peak formed by its corresponding mass (Figure B-5). Then the fraction of each compound from the TMLC (x_i) is calculated with equation (B-8).

$$x_i = \frac{M_i}{TMLC} \qquad \text{(B-8)}$$

Finally, to calculate the area of each compound (A_i) based on the integrated area of the lump (ILA) equation (B-9) was applied.

$$A_i = ILA \cdot x_i \qquad \text{(B-9)}$$

For the compounds in Figure S.5, the TMLC is:

$$TMLC = M_{Methane} + M_{Ethylene} + M_{Propane} + M_{Propene}$$

$$TMLC = 1.15 \times 10^7 + 3.6 \times 10^8 + 8.52 \times 10^7 + 3.33 \times 10^8 = 7.88 \times 10^8$$

The fraction of each compound from the TMLC is:

$$x_{Methane} = \frac{1.15 \times 10^7}{7.9 \times 10^8} = 0.0145$$

$$x_{Ethylene} = \frac{3.6 \times 10^8}{7.9 \times 10^8} = 0.4558$$

$$x_{Propane} = \frac{8.52 \times 10^7}{7.9 \times 10^8} = 0.1079$$

$$x_{Propene} = \frac{3.33 \times 10^8}{7.9 \times 10^8} = 0.4218$$

The integrated area of the lump is 1.97×10^9, therefore the area of each compound is:

$$A_{Methane} = (1.97 \times 10^9)(0.0145) = 2.86 \times 10^7$$

$$A_{Ethylene} = (1.97 \times 10^9)(0.4558) = 8.98 \times 10^8$$

$$A_{Propane} = (1.97 \times 10^9)(0.1079) = 2.13 \times 10^8$$

$$A_{Propene} = (1.97 \times 10^9)(0.4218) = 8.31 \times 10^8$$

Product identification was performed by spectra comparison with the database of the Xcalibur software. Those compounds not found in the Xcalibur database were identified with the NIST WebBook[3] using the molecular ion from the spectra as an estimation of their molecular weight. Chemical classes were identified through the homologous ion series reported by Lebedev[4] (Table B-7).

Table B-7. Homologous ion series for aliphatic hydrocarbons.[4]

Class of compound	m/z
Alkanes	15, 29, 43, 57, 71, 85…
Alkenes	27, 41, 55, 69, 83…
Alkadienes	25, 39, 53, 67, 81

B.5 Product distribution at different Temperatures and VRTs

The different pyrolysis products obtained at each combination of temperature and VRT are presented in Table B-8 to Table B-17. Compounds marked as unidentified were not recognized due to similarities within isomers, however their chemical class and C number were identified with the methods explained above.

Table B-8. HDPE pyrolysis products at 625 °C and 1.4 s VRT.

Retention time (min)	Compound	Chemical class	Carbon number	Average peak area percent
1.87	methane	alkane	1	0.13%
1.88	ethylene	alkene	2	4.21%
1.91	1-propene	alkene	3	3.69%
1.91	propane	alkane	3	0.96%
2.00	1-butene	alkene	4	6.80%
2.01	butane	alkane	4	1.36%
2.24	1-pentene	alkene	5	2.78%
2.27	pentane	alkane	5	0.85%
2.31	1,2-pentadiene	alkadiene	5	0.83%
2.41	cyclopentene	alkadiene	5	0.72%
2.47	1,4-pentadiene	alkadiene	5	0.58%
2.57	isoprene	alkadiene	5	0.64%
2.73	1,5-hexadiene	alkadiene	6	0.40%
2.80	1-hexene	alkene	6	3.39%
2.87	hexane	alkane	6	0.86%
3.02	unidentified	alkadiene	6	0.50%
3.19	cyclohexane	alkene	6	0.26%
3.53	1,5-hexadiene	alkadiene	6	0.30%
3.68	benzene	MAH	6	0.30%
3.83	1,3-cyclohexadiene	MAH	6	0.29%
4.02	4-methyl,1,3-pentadiene	alkadiene	6	0.28%
4.23	1-heptene	alkene	7	2.07%
4.43	heptane	alkane	7	1.10%
5.04	cyclohexane, methyl-	alkane	7	0.21%
5.61	2-methyl-1,4-hexadiene	alkadiene	7	0.13%
6.71	toluene	MAH	7	0.22%
6.87	unidentified	alkadiene	7	0.15%
7.59	1,7-octadiene	alkadiene	8	0.17%

8.08	1-octene	alkene	8	1.45%
8.62	Octane	alkane	8	0.66%
16.85	1,8-nonadiene	alkadiene	9	0.22%
17.26	Styrene	MAH	8	0.26%
18.20	1-nonene	alkene	9	1.54%
19.60	nonane	alkane	9	0.46%
27.27	1,9-decadiene	alkadiene	10	0.41%
27.76	1-decene	alkene	10	2.77%
28.21	decane	alkane	10	0.47%
31.92	1,10-undecadiene	alkadiene	11	0.49%
32.26	1-undecene	alkene	11	2.45%
32.58	undecane	alkane	11	0.70%
35.45	1,11-dodecadiene	alkadiene	12	0.50%
35.72	1-dodecene	alkene	12	1.92%
35.98	dodecane	alkane	12	0.70%
38.48	1,12-tridecadiene	alkadiene	13	0.60%
38.72	1-tridecene	alkene	13	1.91%
38.95	tridecane	alkane	13	0.61%
41.22	1,13-tetradecadiene	alkadiene	14	0.67%
41.44	1-tetradecene	alkene	14	2.29%
41.65	tetradecane	alkane	14	0.61%
43.78	1,14-pentadecadiene	alkadiene	15	0.69%
43.98	1-pentadecene	alkene	15	2.18%
44.16	pentadecane	alkane	15	0.72%
46.18	1,15-hexadecadiene	alkadiene	16	0.68%
46.36	1-hexadecene	alkene	16	1.89%
46.53	hexadecane	alkane	16	0.75%
48.45	1,16-heptadecadiene	alkadiene	17	0.65%
48.62	1-heptadecene	alkene	17	1.82%
48.77	heptadecane	alkane	17	0.74%
50.61	1,17-octadecadiene	alkadiene	18	0.62%
50.76	1-octadecene	alkene	18	1.85%
50.90	octadecane	alkane	18	0.79%
52.66	1,18-nonadecadiene	alkadiene	19	0.61%
52.80	1-nonadecene	alkene	19	1.81%
52.93	nonadecane	alkane	19	0.88%
54.62	1,19-eicosadiene	alkadiene	20	0.61%
54.75	1-eicosene	alkene	20	1.76%

54.87	eicosane	alkane	20	0.97%
56.50	1,20-henicosadiene	alkadiene	21	0.57%
56.61	1-henicosene	alkene	21	1.81%
56.72	henicosane	alkane	21	1.08%
58.29	1,21-docosadiene	alkadiene	22	0.52%
58.40	1-docosene	alkene	22	1.89%
58.50	docosane	alkane	22	1.23%
60.01	1,22-tricosadiene	alkadiene	23	0.49%
60.11	1-tricosene	alkene	23	1.96%
60.20	tricosane	alkane	23	1.46%
60.27	Benzene, hexadecyl-	MAH	22	0.08%
61.67	1,23-tetracosadiene	alkadiene	24	0.44%
61.75	1-tetracosene	alkene	24	1.88%
61.84	tetracosane	alkane	24	1.58%
61.90	n-Heptadecylbenzene	MAH	23	0.11%
63.25	1,24-pentacosadiene	alkadiene	25	0.34%
63.33	1-pentacosene	alkene	25	1.47%
63.41	pentacosane	alkane	25	1.42%
63.47	unidentified	PAH	26	0.12%
63.59	Benzene, octadecyl-	MAH	24	0.08%
64.78	1,25-hexacosadiene	alkadiene	26	0.18%
64.85	1-hexacosene	alkene	26	0.99%
64.92	hexacosane	alkane	26	1.12%
65.16	Benzene, nonadecyl-	MAH	25	0.11%
65.25	unidentified	PAH	25	0.11%
66.25	1,26-heptacosadiene	alkadiene	27	0.09%
66.31	1-heptacosene	alkene	27	0.57%
66.38	heptacosane	alkane	27	0.79%
66.67	Benzene, eicosyl-	MAH	26	0.10%
67.73	1-octasene	alkene	28	0.29%
67.78	octacosane	alkane	28	0.52%
68.12	Benzene, heneicosyl-	MAH	27	0.09%
69.21	1-nonacosene	alkene	29	0.11%
69.26	nonacosane	alkane	29	0.34%
71.02	triacontane	alkane	30	0.16%

Table B-9. HDPE pyrolysis products at 625 °C and 2.8 s VRT.

Retention time (min)	Compound	Chemical class	Carbon number	Average peak area percent
1.84	methane	alkane	1	0.27%
1.84	ethylene	alkene	2	7.40%
1.87	1-propene	alkene	3	6.17%
1.88	propane	alkane	3	1.40%
1.96	1-butene	alkene	4	13.91%
1.97	butane	alkane	4	2.17%
2.18	1-pentene	alkene	5	4.46%
2.19	pentane	alkane	5	1.43%
2.25	unidentified	alkadiene	5	1.58%
2.33	unidentified	alkadiene	5	1.39%
2.41	unidentified	alkadiene	5	1.15%
2.51	1,4-pentadiene	alkadiene	5	1.35%
2.66	1,5-hexadiene	alkadiene	6	0.31%
2.74	1-hexene	alkene	6	3.88%
2.82	hexane	alkane	6	1.65%
2.98	unidentified	alkadiene	6	0.69%
3.14	methylcyclopentane	alkane	6	0.37%
3.33	benzene	MAH	6	0.14%
3.50	1,5-hexadiene	alkadiene	6	0.39%
3.65	benzene	MAH	6	1.06%
3.79	2,4-hexadiene	alkadiene	6	0.78%
4.00	1,6-heptadiene	alkadiene	7	0.40%
4.21	1-heptene	alkene	7	2.27%
4.41	heptane	alkane	7	1.41%
5.04	cyclohexane, methyl-	alkane	7	0.38%
5.61	unidentified	alkadiene	7	0.21%
6.31	unidentified	alkadiene	7	0.10%
6.71	toluene	MAH	7	0.69%
6.87	unidentified	alkadiene	7	0.19%
7.12	unidentified	alkadiene	7	0.10%
7.60	1,7-octadiene	alkadiene	8	0.14%
8.09	1-octene	alkene	8	1.82%
8.63	Octane	alkane	8	0.90%
13.66	Ethylbenzene	MAH	8	0.14%

14.64	p-xylene	MAH	8	0.11%
16.85	1,9-nonadiene	alkadiene	9	0.18%
17.28	Styrene	MAH	8	0.80%
17.49	xylene	MAH	8	0.17%
18.23	1-nonene	alkene	9	1.72%
19.63	nonane	alkane	9	0.64%
26.68	1,3,5-Trimethylbenzene	MAH	9	0.12%
27.28	1,9-decadiene	alkadiene	10	0.29%
27.59	Indane	MAH	9	0.11%
27.67	Indane	MAH	9	0.11%
27.77	1-decene	alkene	10	2.70%
28.22	decane	alkane	10	0.66%
31.92	1,10-undecadiene	alkadiene	11	0.35%
32.26	1-undecene	alkene	11	2.27%
32.59	undecane	alkane	11	0.92%
34.38	naphthalene	PAH	10	0.11%
34.64	1,4-divinylbenzene	MAH	10	0.10%
35.29	naphthalene	PAH	10	0.35%
35.45	1,11-dodecadiene	alkadiene	12	0.34%
35.72	1-dodecene	alkene	12	1.70%
35.98	dodecane	alkane	12	0.89%
38.48	1,12-tridecadiene	alkadiene	13	0.31%
38.72	1-tridecene	alkene	13	1.62%
38.95	tridecane	alkane	13	0.77%
41.10	biphenyl	PAH	12	0.17%
41.22	1,13-tetradecadiene	alkadiene	14	0.29%
41.44	1-tetradecene	alkene	14	1.69%
41.65	tetradecane	alkane	14	0.78%
41.95	acenaphtene	PAH	12	0.11%
42.90	acenaphtylene	PAH	12	0.10%
43.78	1,14-pentadecadiene	alkadiene	15	0.28%
43.98	1-pentadecene	alkene	15	1.46%
44.16	pentadecane	alkane	15	0.88%
45.87	Nonylbenzene	MAH	15	0.08%
46.18	1,15-hexadecadiene	alkadiene	16	0.22%
46.36	1-hexadecene	alkene	16	1.15%
46.53	hexadecane	alkane	16	0.89%
48.23	Decylbenzene	MAH	16	0.10%

48.45	1,16-heptadecadiene	alkadiene	17	0.17%
48.62	1-heptadecene	alkene	17	1.03%
48.77	heptadecane	alkane	17	0.91%
49.63	9,10-dihydro phenanthrene	PAH	14	0.11%
50.49	Undecylbenzene	MAH	17	0.12%
50.53	anthracene	PAH	14	0.09%
50.61	1,17-octadecadiene	alkadiene	18	0.18%
50.75	1-octadecene	alkene	18	0.95%
50.9	octadecane	alkane	18	0.91%
52.62	1-Phenyldodecane	MAH	18	0.13%
52.64	1,18-nonadecadiene	alkadiene	19	0.12%
52.8	1-nonadecene	alkene	19	0.83%
52.93	nonadecane	alkane	19	0.92%
53.03	unidentified	alkane	19	0.10%
54.67	1-Phenyltridecane	MAH	19	0.14%
54.74	1-eicosene	alkene	20	0.61%
54.87	eicosane	alkane	20	0.84%
56.61	1-henicosene	alkene	21	0.57%
56.72	henicosane	alkane	21	0.82%
58.39	1-docosene	alkene	22	0.31%
58.49	docosane	alkane	22	0.81%
60.1	1-tricosene	alkene	23	0.23%
60.2	tricosane	alkane	23	0.65%
60.23	1,23-tetracosadiene	alkadiene	24	0.09%
61.74	1-tetracosene	alkene	24	0.16%
61.83	tetracosane	alkane	24	0.52%
61.95	n-heptadecylbenzene	MAH	23	0.11%
63.32	1-pentacosene	alkene	25	0.10%
63.4	pentacosane	alkane	25	0.39%
64.84	1-hexacosene	alkene	26	0.08%
64.92	hexacosane	alkane	26	0.31%
66.37	heptacosane	alkane	27	0.23%
67.78	octacosane	alkane	28	0.17%
69.26	nonacosane	alkane	29	0.11%

Table B-10. HDPE pyrolysis products at 625 °C and 5.6 s VRT.

Retention time (min)	Compound	Chemical class	Carbon number	Average peak area percent
1.93	methane	alkane	1	0.30%
1.94	ethylene	alkene	2	8.32%
1.98	1-propene	alkene	3	5.18%
2.01	propane	alkane	3	1.55%
2.03	1-butene	alkene	4	14.93%
2.04	butane	alkane	4	4.03%
2.27	1-pentene	alkene	5	7.62%
2.28	pentane	alkane	5	1.86%
2.37	1,4-pentadiene	alkadiene	5	5.00%
2.58	1,5-hexadiene	alkadiene	6	2.37%
2.83	1-hexene	alkene	6	2.86%
2.87	hexane	alkane	6	2.19%
3.08	unidentified	alkadiene	6	0.88%
3.23	unidentified	alkene	6	0.35%
3.40	benzene	MAH	6	0.09%
3.58	1,5-hexadiene	alkadiene	6	0.22%
3.75	benzene	MAH	6	1.88%
3.88	benzene	MAH	6	0.84%
4.11	unidentified	alkadiene	6	0.34%
4.31	1-heptene	alkene	7	1.59%
4.50	heptane	alkane	7	1.39%
5.13	methyl, cyclohexane	alkane	7	0.31%
5.75	unidentified	alkadiene	7	0.21%
6.40	3-Ethylcyclopentene	alkene	7	0.08%
6.81	toluene	MAH	7	1.44%
8.20	1-octene	alkene	8	1.57%
8.73	octane	alkane	8	0.85%
13.75	o-xylene	MAH	8	0.22%
14.68	p-xylene	MAH	8	0.17%
16.98	1,8-nonadiene	alkadiene	9	0.08%
17.39	styrene	MAH	8	1.45%
17.61	xylene	MAH	8	0.38%
18.35	1-nonene	alkene	9	1.42%
19.76	nonane	alkane	9	0.66%

25.62	cumene	MAH	9	0.10%
26.72	1,3,5-Trimethylbenzene	MAH	9	0.13%
27.29	1,9-decadiene	alkadiene	10	0.18%
27.61	indane	MAH	9	0.17%
27.68	indane	MAH	9	0.17%
27.79	1-decene	alkene	10	2.07%
28.24	decane	alkane	10	0.65%
31.09	sec-butylbenzene	MAH	10	0.09%
31.93	1,10-undecadiene	alkadiene	11	0.22%
32.28	1-undecene	alkene	11	1.68%
32.59	undecane	alkane	11	0.89%
34.38	naphthalene	PAH	10	0.17%
34.51	Pentylbenzene	MAH	11	0.08%
34.64	1,4-divinylbenzene	MAH	10	0.11%
35.29	azulene	PAH	10	0.49%
35.45	1,11-dodecadiene	alkadiene	12	0.21%
35.73	1-dodecene	alkene	12	1.25%
36.00	dodecane	alkane	12	0.84%
38.48	1,12-tridecadiene	alkadiene	13	0.18%
38.72	1-tridecene	alkene	13	1.21%
38.96	tridecane	alkane	13	0.72%
39.20	methyl, naphthalene	PAH	11	0.13%
41.10	biphenyl	PAH	12	0.19%
41.23	1,13-tetradecadiene	alkadiene	14	0.16%
41.45	1-tetradecene	alkene	14	1.14%
41.65	tetradecane	alkane	14	0.75%
41.95	acenaphtene	PAH	12	0.16%
42.90	acenaphthylene	PAH	12	0.17%
43.35	octylbenzene	MAH	14	0.08%
43.78	1,14-pentadecadiene	alkadiene	15	0.15%
43.98	1-pentadecene	alkene	15	0.95%
44.17	pentadecane	alkane	15	0.79%
45.86	nonylbenzene	MAH	15	0.09%
46.18	1,15-hexadecadiene	alkadiene	16	0.12%
46.36	1-hexadecene	alkene	16	0.74%
46.54	hexadecane	alkane	16	0.81%
48.24	decylbenzene	MAH	16	0.09%
48.45	1,16-heptadecadiene	alkadiene	17	0.08%

48.62	1-heptadecene	alkene	17	0.67%
48.77	heptadecane	alkane	17	0.79%
49.63	9,10-dihydro phenanthrene	PAH	14	0.12%
50.49	undecylbenzene	MAH	17	0.10%
50.53	anthracene	PAH	14	0.13%
50.61	1,17-octadecadiene	alkadiene	18	0.11%
50.76	1-octadecene	alkene	18	0.65%
50.91	octadecane	alkane	18	0.79%
52.64	1-phenyldodecane	MAH	18	0.11%
52.80	1-nonadecene	alkene	19	0.55%
52.94	nonadecane	alkane	19	0.76%
53.02	unidentified	alkane	19	0.09%
54.66	1-phenyltridecane	MAH	19	0.12%
54.75	1-eicosene	alkene	20	0.41%
54.88	eicosane	alkane	20	0.68%
56.61	1-henicosene	alkene	21	0.35%
56.73	henicosane	alkane	21	0.62%
58.39	1-docosene	alkene	22	0.15%
58.50	docosane	alkane	22	0.55%
60.10	1-tricosene	alkene	23	0.09%
60.20	tricosane	alkane	23	0.38%
60.23	hexadecyl, benzene	MAH	22	0.09%
61.83	tetracosane	alkane	24	0.29%
63.40	pentacosane	alkane	25	0.19%
64.92	hexacosane	alkane	26	0.13%
66.37	heptacosane	alkane	27	0.10%
67.78	octacosane	alkane	28	0.09%

Table B-11. HDPE pyrolysis products at 650 °C and 1.4 s VRT.

Retention time (min)	Compound	Chemical class	Carbon number	Average peak area percent
1.86	methane	alkane	1	0.25%
1.87	ethylene	alkene	2	7.47%
1.90	1-propene	alkene	3	6.68%
1.90	propane	alkane	2	1.06%
2.00	1-butene	alkene	4	13.39%
2.01	butane	alkane	4	1.19%
2.24	1-pentene	alkene	5	4.12%
2.28	pentane	alkane	5	0.86%
2.32	1,4-pentadiene	alkadiene	5	1.26%
2.41	unidentified	alkadiene	5	1.11%
2.48	unidentified	alkadiene	5	0.89%
2.57	unidentified	alkadiene	5	0.84%
2.73	1,5-hexadiene	alkadiene	6	0.50%
2.81	1-hexene	alkene	6	2.98%
2.88	hexane	alkane	6	0.88%
3.02	unidentified	alkadiene	6	0.60%
3.20	unidentified	alkene	6	0.21%
3.36	unidentified	MAH	6	0.12%
3.53	unidentified	alkadiene	6	0.32%
3.68	benzene	MAH	6	0.79%
3.83	benzene	MAH	6	0.55%
4.02	unidentified	alkadiene	6	0.31%
4.24	1-heptene	alkene	7	1.82%
4.44	heptane	alkane	7	1.11%
5.05	methyl, cyclohexane	alkane	7	0.16%
5.62	2-methyl-1,4-hexadiene	alkadiene	7	0.12%
6.71	toluene	MAH	7	0.44%
6.89	unidentified	alkadiene	7	0.15%
7.13	unidentified	alkadiene	7	0.11%
7.60	1,7-octaediene	alkadiene	8	0.15%
8.09	1-octene	alkene	8	1.17%
8.64	Octane	alkane	8	0.59%
13.66	xylene	MAH	8	0.09%
16.90	1,8-nonadiene	alkadiene	9	0.19%

17.31	styrene	MAH	8	0.67%
17.52	xylene	MAH	8	0.14%
18.24	1-nonene	alkene	9	1.42%
19.66	nonane	alkane	9	0.39%
27.29	1,9-decadiene	alkadiene	10	0.36%
27.60	indane	MAH	9	0.10%
27.76	1-decene	alkene	10	2.37%
28.23	decane	alkane	10	0.44%
31.93	1,10-undecadiene	alkadiene	11	0.41%
32.26	1-undecene	alkene	11	1.93%
32.58	undecane	alkane	11	0.60%
34.39	naphthalene	PAH	10	0.09%
35.29	azulene	PAH	10	0.15%
35.45	1,11-dodecadiene	alkadiene	12	0.42%
35.72	1-dodecene	alkene	12	1.51%
35.99	dodecane	alkane	12	0.59%
38.48	1,12-tridecadiene	alkadiene	13	0.44%
38.72	1-tridecene	alkene	13	1.48%
38.95	tridecane	alkane	13	0.51%
41.23	1,13-tetradecadiene	alkadiene	14	0.45%
41.44	1-tetradecene	alkene	14	1.62%
41.65	tetradecane	alkane	14	0.50%
42.90	acenaphthylene	PAH	12	0.08%
43.79	1,14-pentadecadiene	alkadiene	15	0.45%
43.98	1-pentadecene	alkene	15	1.52%
44.16	pentadecane	alkane	15	0.60%
46.18	1,15-hexadecadiene	alkadiene	16	0.42%
46.36	1-hexadecene	alkene	16	1.34%
46.53	hexadecane	alkane	16	0.59%
48.45	1,16-heptadecadiene	alkadiene	17	0.39%
48.61	1-heptadecene	alkene	17	1.26%
48.77	heptadecane	alkane	17	0.56%
50.61	1,17-octadecadiene	alkadiene	18	0.38%
50.76	1-octadecene	alkene	18	1.26%
50.90	octadecane	alkane	18	0.56%
52.67	1,18-nonadecadiene	alkadiene	19	0.37%
52.80	1-nonadecene	alkene	19	1.22%
52.93	nonadecane	alkane	19	0.63%

54.62	1,19-eicosadiene	alkadiene	20	0.36%
54.75	1-eicosene	alkene	20	1.19%
54.87	eicosane	alkane	20	0.68%
56.50	1,20-henicosadiene	alkadiene	21	0.35%
56.61	1-henicosene	alkene	21	1.23%
56.72	henicosane	alkane	21	0.76%
58.29	1,21-docosadiene	alkadiene	22	0.33%
58.40	1-docosene	alkene	22	1.30%
58.50	docosane	alkane	22	0.89%
60.01	1,22-tricosadiene	alkadiene	23	0.33%
60.11	1-tricosene	alkene	23	1.38%
60.20	tricosane	alkane	23	1.06%
61.66	1,23-tetracosadiene	alkadiene	24	0.26%
61.75	1-tetracosene	alkene	24	1.26%
61.83	tetracosane	alkane	24	1.09%
63.25	1,24-pentacosadiene	alkadiene	25	0.21%
63.33	1-pentacosene	alkene	25	1.02%
63.41	pentacosane	alkane	25	1.01%
64.78	1,25-hexacosadiene	alkadiene	26	0.13%
64.85	1-hexacosene	alkene	26	0.77%
64.92	hexacosane	alkane	26	0.85%
66.31	1-heptacosene	alkene	27	0.54%
66.38	heptacosane	alkane	27	0.69%
67.73	1-octasene	alkene	28	0.31%
67.79	octacosane	alkane	28	0.51%
69.21	1-nonacosene	alkene	29	0.15%
69.26	nonacosane	alkane	29	0.32%
71.03	triacontane	alkane	30	0.23%
73.14	untriacontane	alkane	31	0.11%

Table B-12. HDPE pyrolysis products at 650 °C and 2.8 s VRT.

Retention time (min)	Compound	Chemical class	Carbon number	Average peak area percent
1.82	methane	alkane	1	0.41%
1.82	ethylene	alkene	2	10.06%
1.85	1-propene	alkene	3	9.34%
1.86	propane	alkane	3	1.31%
1.93	1-butene	alkene	4	21.47%
1.94	butane	alkane	4	2.03%
2.16	1-pentene	alkene	5	5.35%
2.19	pentane	alkane	5	1.06%
2.25	unidentified	alkadiene	5	2.89%
2.33	unidentified	alkadiene	5	2.05%
2.39	unidentified	alkadiene	5	1.57%
2.50	unidentified	alkadiene	5	1.65%
2.65	1,5-hexadiene	alkadiene	6	0.47%
2.73	1-hexene	alkene	6	2.14%
2.82	hexane	alkane	6	1.33%
2.99	unidentified	alkadiene	6	0.77%
3.14	unidentified	alkene	6	0.33%
3.31	unidentified	MAH	6	0.20%
3.50	unidentified	alkadiene	6	0.30%
3.65	benzene	MAH	6	2.32%
3.78	benzene	MAH	6	1.09%
3.99	unidentified	alkadiene	6	0.27%
4.21	1-heptene	alkene	7	1.19%
4.41	heptane	alkane	7	1.12%
5.03	methyl, cyclohexane	alkane	7	0.31%
5.68	2-methyl-1,4-hexadiene	alkadiene	7	0.17%
6.71	toluene	MAH	7	1.31%
6.87	unidentified	alkadiene	7	0.18%
8.09	1-octene	alkene	8	0.92%
8.64	Octane	alkane	8	0.72%
13.68	xylene	MAH	8	0.22%
14.61	xylene	MAH	8	0.15%
17.30	styrene	MAH	8	1.47%
17.58	xylene	MAH	8	0.24%

18.26	1-nonene	alkene	9	0.89%
19.68	nonane	alkane	9	0.45%
27.30	1,9-decadiene	alkadiene	10	0.10%
27.61	indane	MAH	9	0.15%
27.68	indane	MAH	9	0.12%
27.78	1-decene	alkene	10	1.48%
28.24	decane	alkane	10	0.50%
31.94	1,10-undecadiene	alkadiene	11	0.13%
32.26	1-undecene	alkene	11	1.19%
32.59	undecane	alkane	11	0.66%
34.39	naphthalene	PAH	10	0.19%
34.65	1,4-divinylbenzene	MAH	10	0.11%
35.29	azulene	PAH	10	0.47%
35.46	1,11-dodecadiene	alkadiene	12	0.13%
35.73	1-dodecene	alkene	12	0.93%
36.00	dodecane	alkane	12	0.63%
38.48	1,12-tridecadiene	alkadiene	13	0.13%
38.72	1-tridecene	alkene	13	0.99%
38.95	tridecane	alkane	13	0.53%
39.21	methyl, naphthalene	PAH	11	0.16%
41.11	biphenyl	PAH	12	0.13%
41.23	1,13-tetradecadiene	alkadiene	14	0.12%
41.45	1-tetradecene	alkene	14	0.88%
41.65	tetradecane	alkane	14	0.56%
41.96	acenaphtene	PAH	12	0.17%
42.90	acenaphthylene	PAH	12	0.20%
43.79	1,14-pentadecadiene	alkadiene	15	0.12%
43.98	1-pentadecene	alkene	15	0.75%
44.17	pentadecane	alkane	15	0.57%
46.36	1-hexadecene	alkene	16	0.62%
46.54	hexadecane	alkane	16	0.57%
48.62	1-heptadecene	alkene	17	0.57%
48.78	heptadecane	alkane	17	0.55%
50.54	anthracene	PAH	14	0.12%
50.76	1-octadecene	alkene	18	0.55%
50.91	octadecane	alkane	18	0.55%
52.80	1-nonadecene	alkene	19	0.48%
52.93	nonadecane	alkane	19	0.59%

54.75	1-eicosene	alkene	20	0.42%
54.87	eicosane	alkane	20	0.63%
56.61	1-henicosene	alkene	21	0.39%
56.73	henicosane	alkane	21	0.67%
58.40	1-docosene	alkene	22	0.28%
58.50	docosane	alkane	22	0.73%
60.11	1-tricosene	alkene	23	0.21%
60.20	tricosane	alkane	23	0.69%
61.75	1-tetracosene	alkene	24	0.13%
61.84	tetracosane	alkane	24	0.55%
63.40	pentacosane	alkane	25	0.38%
64.92	hexacosane	alkane	26	0.23%
66.38	heptacosane	alkane	27	0.13%
67.79	octacosane	alkane	28	0.11%
69.27	nonacosane	alkane	29	0.07%

Table B-13. HDPE pyrolysis products at 650 °C and 5.6 s VRT.

Retention time (min)	Compound	Chemical class	Carbon number	Average peak area percent
1.92	methane	alkane	1	0.45%
1.93	ethylene	alkene	2	10.40%
1.95	1-propene	alkene	3	9.17%
1.97	propane	alkane	3	1.24%
2.01	1-butene	alkene	4	25.47%
2.01	butane	alkane	4	2.91%
2.25	1-pentene	alkene	5	7.50%
2.26	pentane	alkane	5	1.44%
2.43	unidentified	alkadiene	5	7.04%
2.58	unidentified	alkadiene	5	2.49%
2.85	1-hexene	alkene	6	1.45%
2.88	hexane	alkane	6	1.13%
3.05	unidentified	alkadiene	6	0.51%
3.23	unidentified	alkene	6	0.25%
3.40	unidentified	MAH	6	0.11%
3.59	unidentified	alkadiene	6	0.08%
3.74	benzene	MAH	6	3.27%
3.89	benzene	MAH	6	1.02%
4.03	unidentified	alkadiene	6	0.19%
4.30	1-heptene	alkene	7	0.55%
4.50	heptane	alkane	7	0.97%
5.13	methyl, cyclohexane	alkane	7	0.23%
5.78	2-methyl-1,4-hexadiene	alkadiene	7	0.11%
6.81	toluene	MAH	7	2.25%
8.20	1-octene	alkene	8	0.54%
8.74	Octane	alkane	8	0.67%
13.77	xylene	MAH	8	0.32%
14.73	xylene	MAH	8	0.19%
17.43	styrene	MAH	8	2.27%
17.57	xylene	MAH	8	0.46%
18.37	1-nonene	alkene	9	0.42%
19.79	nonane	alkane	9	0.42%
27.62	indane	MAH	9	0.31%
27.69	indane	MAH	9	0.27%

27.79	1-decene	alkene	10	0.97%
28.25	decane	alkane	10	0.45%
29.26	indane	MAH	9	0.12%
32.27	1-undecene	alkene	11	0.63%
32.59	undecane	alkane	11	0.58%
34.39	naphthalene	PAH	10	0.25%
34.65	1,4-divinylbenzene	MAH	10	0.13%
35.29	azulene	PAH	10	0.74%
35.47	1,11-dodecadiene	alkadiene	12	0.09%
35.72	1-dodecene	alkene	12	0.46%
35.99	dodecane	alkane	12	0.52%
37.89	1-Methylnaphthalene	PAH	11	0.08%
38.72	1-tridecene	alkene	13	0.62%
38.95	tridecane	alkane	13	0.43%
39.20	methyl, naphthalene	PAH	11	0.23%
41.10	biphenyl	PAH	12	0.18%
41.44	1-tetradecene	alkene	14	0.41%
41.65	tetradecane	alkane	14	0.46%
41.96	acenaphtene	PAH	12	0.23%
42.39	Naphthalene, 2-ethenyl-	PAH	12	0.10%
42.90	acenaphthylene	PAH	12	0.28%
43.79	1,14-pentadecadiene	alkadiene	15	0.09%
43.98	1-pentadecene	alkene	15	0.32%
44.17	pentadecane	alkane	15	0.46%
46.36	1-hexadecene	alkene	16	0.27%
46.54	hexadecane	alkane	16	0.45%
48.62	1-heptadecene	alkene	17	0.26%
48.78	heptadecane	alkane	17	0.43%
49.64	9,10-dihydro phenanthrene	PAH	14	0.10%
50.54	anthracene	PAH	14	0.20%
50.76	1-octadecene	alkene	18	0.29%
50.91	octadecane	alkane	18	0.44%
52.80	1-nonadecene	alkene	19	0.25%
52.94	nonadecane	alkane	19	0.45%
54.75	1-eicosene	alkene	20	0.21%
54.87	eicosane	alkane	20	0.42%
56.61	1-henicosene	alkene	21	0.16%
56.72	henicosane	alkane	21	0.36%

58.49	docosane	alkane	22	0.31%
60.20	tricosane	alkane	23	0.23%
61.83	tetracosane	alkane	24	0.16%
63.40	pentacosane	alkane	25	0.09%

Table B-14. HDPE pyrolysis products at 675 °C and 1.4 s VRT.

Retention time (min)	Compound	Chemical class	Carbon number	Average peak area percent
1.85	methane	alkane	1	0.60%
1.86	ethylene	alkene	2	15.10%
1.89	1-propene	alkene	3	11.93%
1.90	propane	alkane	3	1.69%
1.99	1-butene	alkene	4	26.17%
2.00	butane	alkane	4	1.96%
2.23	1-pentene	alkene	5	4.67%
2.26	pentane	alkane	5	1.07%
2.31	1,4-pentadiene	alkadiene	5	2.73%
2.40	unidentified	alkadiene	5	1.74%
2.46	unidentified	alkadiene	5	1.41%
2.56	unidentified	alkadiene	5	1.22%
2.72	1,5-hexadiene	alkadiene	6	0.33%
2.80	1-hexene	alkene	6	1.17%
2.87	hexane	alkane	6	0.78%
3.04	unidentified	alkadiene	6	0.48%
3.18	unidentified	alkene	6	0.27%
3.35	unidentified	MAH	6	0.27%
3.52	unidentified	alkadiene	6	0.28%
3.67	benzene	MAH	6	3.26%
3.82	benzene	MAH	6	1.16%
4.01	unidentified	alkadiene	6	0.17%
4.23	1-heptene	alkene	7	0.69%
4.43	heptane	alkane	7	0.94%
5.04	methyl, cyclohexane	alkane	7	0.17%
5.69	2-methyl-1,4-hexadiene	alkadiene	7	0.12%
6.69	toluene	MAH	7	1.55%
6.87	unidentified	alkadiene	7	0.13%
8.08	1-octene	alkene	8	0.48%
8.62	Octane	alkane	8	0.56%
13.64	xylene	MAH	8	0.28%
14.59	xylene	MAH	8	0.17%
17.27	styrene	MAH	8	1.49%
18.22	1-nonene	alkene	9	0.40%

19.64	nonane	alkane	9	0.37%
27.59	indane	MAH	9	0.11%
27.66	indane	MAH	9	0.09%
27.76	1-decene	alkene	10	0.71%
28.22	decane	alkane	10	0.34%
32.25	1-undecene	alkene	11	0.56%
32.57	undecane	alkane	11	0.44%
34.38	naphthalene	PAH	10	0.17%
34.63	1,4-Divinylbenzene	MAH	10	0.10%
35.28	azulene	PAH	10	0.47%
35.46	1,11-dodecadiene	alkadiene	12	0.12%
35.72	1-dodecene	alkene	12	0.43%
35.98	dodecane	alkane	12	0.40%
38.71	1-tridecene	alkene	13	0.52%
38.95	tridecane	alkane	13	0.33%
39.20	1-Methylnaphthalene	PAH	11	0.14%
41.10	biphenyl	PAH	12	0.11%
41.44	1-tetradecene	alkene	14	0.42%
41.65	tetradecane	alkane	14	0.38%
41.96	acenaphtene	PAH	12	0.10%
42.90	acenaphthylene	PAH	12	0.17%
43.97	1-pentadecene	alkene	15	0.37%
44.16	pentadecane	alkane	15	0.35%
46.35	1-hexadecene	alkene	16	0.29%
46.53	hexadecane	alkane	16	0.34%
48.61	1-heptadecene	alkene	17	0.27%
48.77	heptadecane	alkane	17	0.33%
50.54	anthracene	PAH	14	0.11%
50.75	1-octadecene	alkene	18	0.27%
50.90	octadecane	alkane	18	0.34%
52.80	1-nonadecene	alkene	19	0.25%
52.93	nonadecane	alkane	19	0.38%
54.74	1-eicosene	alkene	20	0.23%
54.87	eicosane	alkane	20	0.41%
56.61	1-henicosene	alkene	21	0.23%
56.72	henicosane	alkane	21	0.46%
58.39	1-docosene	alkene	22	0.16%
58.49	docosane	alkane	22	0.49%

60.11	1-tricosene	alkene	23	0.13%
60.20	tricosane	alkane	23	0.51%
61.74	1-tetracosene	alkene	24	0.12%
61.83	tetracosane	alkane	24	0.49%
63.41	pentacosane	alkane	25	0.48%
64.92	hexacosane	alkane	26	0.43%
66.38	heptacosane	alkane	27	0.35%
67.79	octacosane	alkane	28	0.22%
69.27	nonacosane	alkane	29	0.09%

Table B-15. HDPE pyrolysis products at 675 °C and 2.8 s VRT.

Retention time (min)	Compound	Chemical class	Carbon number	Average peak area percent
1.80	methane	alkane	1	0.69%
1.81	ethylene	alkene	2	14.57%
1.83	1-propene	alkene	3	11.44%
1.86	propane	alkane	3	1.54%
1.93	1-butene	alkene	4	28.44%
1.94	butane	alkane	4	2.12%
2.15	1-pentene	alkene	5	5.05%
2.18	pentane	alkane	5	1.03%
2.22	1,4-pentadiene	alkadiene	5	3.43%
2.30	unidentified	alkadiene	5	2.49%
2.37	unidentified	alkadiene	5	1.64%
2.49	unidentified	alkadiene	5	1.76%
2.63	1,5-hexadiene	alkadiene	6	0.31%
2.71	1-hexene	alkene	6	0.57%
2.79	hexane	alkane	6	0.66%
2.97	unidentified	alkadiene	6	0.45%
3.13	unidentified	alkene	6	0.22%
3.30	unidentified	MAH	6	0.30%
3.47	unidentified	alkadiene	6	0.15%
3.63	benzene	MAH	6	5.44%
3.77	benzene	MAH	6	1.29%
3.96	unidentified	alkadiene	6	0.23%
4.19	1-heptene	alkene	7	0.20%
4.38	heptane	alkane	7	0.67%
5.01	methyl, cyclohexane	alkane	7	0.16%
5.65	2-methyl-1,4-hexadiene	alkadiene	7	0.10%
6.68	toluene	MAH	7	2.57%
6.85	unidentified	alkadiene	7	0.22%
8.06	1-octene	alkene	8	0.14%
8.60	Octane	alkane	8	0.44%
13.60	xylene	MAH	8	0.38%
14.52	xylene	MAH	8	0.24%
17.26	styrene	MAH	8	2.41%
17.47	xylene	MAH	8	0.33%

18.19	1-nonene	alkene	9	0.10%
19.61	nonane	alkane	9	0.24%
25.35	1-Ethyl-2-methylbenzene	MAH	9	0.10%
25.57	1,3,5-Trimethylbenzene	MAH	9	0.09%
27.58	indane	MAH	9	0.23%
27.65	indane	MAH	9	0.17%
27.75	1-decene	alkene	10	0.32%
28.21	decane	alkane	10	0.24%
29.23	indane	MAH	9	0.14%
32.25	1-undecene	alkene	11	0.19%
32.57	undecane	alkane	11	0.30%
34.38	naphthalene	PAH	10	0.25%
34.63	1,4-Divinylbenzene	MAH	10	0.11%
35.28	azulene	PAH	10	0.99%
35.72	1-dodecene	alkene	12	0.14%
35.98	dodecane	alkane	12	0.27%
38.71	1-tridecene	alkene	13	0.42%
38.95	tridecane	alkane	13	0.21%
39.20	1-Methylnaphthalene	PAH	11	0.30%
41.10	biphenyl	PAH	12	0.20%
41.43	1-tetradecene	alkene	14	0.15%
41.65	tetradecane	alkane	14	0.24%
41.95	acenaphtene	PAH	12	0.19%
42.39	Naphthalene, 2-ethenyl-	PAH	12	0.10%
42.90	acenaphthylene	PAH	12	0.29%
43.97	1-pentadecene	alkene	15	0.09%
44.16	pentadecane	alkane	15	0.21%
46.52	hexadecane	alkane	16	0.20%
48.77	heptadecane	alkane	17	0.18%
49.63	9,10-dihydro phenanthrene	PAH	14	0.08%
50.53	anthracene	PAH	14	0.24%
50.90	octadecane	alkane	18	0.18%
52.93	nonadecane	alkane	19	0.20%
54.87	eicosane	alkane	20	0.19%
56.72	henicosane	alkane	21	0.20%
58.49	docosane	alkane	22	0.20%
60.19	tricosane	alkane	23	0.18%
61.83	tetracosane	alkane	24	0.15%

| 63.40 | pentacosane | alkane | 25 | 0.09% |

Table B-16. HDPE pyrolysis products at 675 °C and 5.6 s VRT.

Retention time (min)	Compound	Chemical class	Carbon number	Average peak area percent
1.90	methane	alkane	1	0.78%
1.91	ethylene	alkene	2	14.27%
1.91	1-propene	alkene	3	9.61%
1.93	propane	alkane	3	1.44%
1.98	1-butene	alkene	4	23.32%
1.99	butane	alkane	4	1.57%
2.22	1-pentene	alkene	5	8.51%
2.26	pentane	alkane	5	1.82%
2.37	unidentified	alkadiene	5	4.82%
2.65	unidentified	alkadiene	5	2.87%
2.86	hexane	alkane	6	0.98%
2.98	unidentified	alkadiene	6	0.30%
3.2	unidentified	alkene	6	0.15%
3.4	unidentified	MAH	6	0.16%
3.72	benzene	MAH	6	9.33%
4.05	unidentified	alkadiene	6	0.38%
4.48	heptane	alkane	7	0.49%
5.12	methyl, cyclohexane	alkane	7	0.12%
6.78	toluene	MAH	7	4.10%
8.7	Octane	alkane	8	0.34%
13.72	xylene	MAH	8	0.54%
14.65	xylene	MAH	8	0.36%
17.41	styrene	MAH	8	3.45%
17.56	xylene	MAH	8	0.52%
19.71	nonane	alkane	9	0.17%
25.38	1-Ethyl-2-methylbenzene	MAH	9	0.12%
25.62	1,2,4-Trimethylbenzene	MAH	9	0.14%
26.73	1,3,5-Trimethylbenzene	MAH	9	0.11%
27.5	unidentified	MAH	9	0.10%
27.6	indane	MAH	9	0.40%
27.68	indane	MAH	9	0.32%
27.78	Allylbenzene	MAH	9	0.35%
28.23	decane	alkane	10	0.16%
29.24	indane	MAH	9	0.25%

29.56	indane	MAH	9	0.09%
32.58	undecane	alkane	11	0.20%
34.39	naphthalene	PAH	10	0.37%
34.63	1,4-divinylbenzene	MAH	10	0.19%
35.3	azulene	PAH	10	1.71%
35.99	dodecane	alkane	12	0.17%
37.87	1-Methylnaphthalene	PAH	11	0.11%
38.72	1-tridecene	alkene	13	0.60%
38.95	tridecane	alkane	13	0.12%
39.2	methyl, naphthalene	PAH	11	0.52%
41.1	biphenyl	PAH	12	0.41%
41.65	tetradecane	alkane	14	0.19%
41.95	acenaphtene	PAH	12	0.34%
42.39	Naphthalene, 2-ethenyl-	PAH	12	0.24%
42.9	acenaphthylene	PAH	12	0.50%
43.81	Naphthalene, 1-methylethenyl	PAH	13	0.13%
44.16	pentadecane	alkane	15	0.11%
46.53	hexadecane	alkane	16	0.11%
48.77	heptadecane	alkane	17	0.10%
49.63	9,10-dihydro phenanthrene	PAH	14	0.14%
50.54	anthracene	PAH	14	0.48%
50.75	1-octadecene	alkene	18	0.10%
50.9	octadecane	alkane	18	0.09%
52.92	nonadecane	alkane	19	0.14%
54.86	eicosane	alkane	20	0.11%
56.08	Pyrene	PAH	16	0.11%
56.71	henicosane	alkane	21	0.10%
57.04	fluoranthene	PAH	16	0.11%
58.49	docosane	alkane	22	0.10%

Table B-17. HDPE pyrolysis products at 700 °C and zero VRT.

Retention time (min)	Compound	Chemical class	Carbon number	Average peak area percent
1.76	ethylene	alkene	2	0.85%
1.78	1-propene	alkene	3	1.13%
1.79	propane	alkane	3	0.29%
1.85	1-butene	alkene	4	1.12%
1.85	butane	alkane	4	0.59%
2.00	1-pentene	alkene	5	1.07%
2.01	pentane	alkane	5	0.37%
2.11	1,4-pentadiene	alkadiene	5	0.13%
2.15	cyclopropene,1,2-dimethyl	alkene	5	0.12%
2.23	cyclopentene	alkene	5	0.11%
2.37	1-hexene	alkene	6	2.21%
2.40	hexane	alkane	6	0.44%
2.51	1,3-butadiene-2,ethyl-	alkadiene	6	0.11%
2.61	cyclohexane	alkane	6	0.14%
2.79	unidentified	alkadiene	6	0.11%
2.88	benzene	MAH	6	0.09%
3.07	1,6-heptadiene	alkadiene	7	0.12%
3.13	1-heptene	alkene	7	1.17%
3.23	heptane	alkane	7	0.62%
3.57	cyclohexane, methyl-	alkane	7	0.13%
4.57	1,4-octadiene	alkadiene	8	0.14%
4.74	1-octene	alkene	8	0.80%
4.92	octane	alkane	8	0.49%
7.02	1,8-nonadiene	alkadiene	9	0.21%
7.27	1-nonene	alkene	9	0.95%
7.52	nonane	alkane	9	0.31%
10.01	1,9-decadiene	alkadiene	10	0.29%
10.28	1-decene	alkene	10	1.76%
10.54	decane	alkane	10	0.33%
13.09	1,10-undecadiene	alkadiene	11	0.31%
13.35	1-undecene	alkene	11	1.46%
13.61	undecane	alkane	11	0.47%
16.08	1,11-dodecadiene	alkadiene	12	0.40%
16.32	1-dodecene	alkene	12	1.12%

16.56	dodecane	alkane	12	0.47%
18.91	1,12-tridecadiene	alkadiene	13	0.49%
19.14	1-tridecene	alkene	13	1.19%
19.36	tridecane	alkane	13	0.41%
21.59	1,13-tetradecadiene	alkadiene	14	0.59%
21.80	1-tetradecene	alkene	14	1.63%
22.00	tetradecane	alkane	14	0.43%
24.12	1,14-pentadecadiene	alkadiene	15	0.66%
24.31	1-pentadecene	alkene	15	1.61%
24.49	pentadecane	alkane	15	0.53%
26.50	1,15-hexadecadiene	alkadiene	16	0.73%
26.68	1-hexadecene	alkene	16	1.49%
26.84	hexadecane	alkane	16	0.54%
28.75	1,16-heptadecadiene	alkadiene	17	0.82%
28.92	1-heptadecene	alkene	17	1.53%
29.07	heptadecane	alkane	17	0.55%
30.90	1,17-octadecadiene	alkadiene	18	0.92%
31.06	1-octadecene	alkene	18	1.75%
31.19	octadecane	alkane	18	0.64%
32.96	1,18-nonadecadiene	alkadiene	19	1.11%
33.09	1-nonadecene	alkene	19	2.01%
33.22	nonadecane	alkane	19	0.77%
34.92	1,19-eicosadiene	alkadiene	20	1.49%
35.04	1-eicosene	alkene	20	2.52%
35.16	eicosane	alkane	20	0.99%
36.79	1,20-henicosadiene	alkadiene	21	1.95%
36.91	1-henicosene	alkene	21	3.05%
37.01	henicosane	alkane	21	1.24%
38.59	1,21-docosadiene	alkadiene	22	2.29%
38.70	1-docosene	alkene	22	3.53%
38.79	docosane	alkane	22	1.38%
40.31	1,22-tricosadiene	alkadiene	23	2.53%
40.41	1-tricosene	alkene	23	3.84%
40.49	tricosane	alkane	23	1.56%
41.96	1,23-tetracosadiene	alkadiene	24	2.53%
42.05	1-tetracosene	alkene	24	3.91%
42.13	tetracosane	alkane	24	1.61%
43.55	1,24-pentacosadiene	alkadiene	25	2.17%

43.63	1-pentacosene	alkene	25	3.45%
43.70	pentacosane	alkane	25	1.46%
45.08	1,25-hexacosadiene	alkadiene	26	1.62%
45.15	1-hexacosene	alkene	26	2.81%
45.21	hexacosane	alkane	26	1.13%
46.55	1,26-heptacosadiene	alkadiene	27	1.21%
46.62	1-heptacosene	alkene	27	2.01%
46.68	heptacosane	alkane	27	0.83%
47.97	1,27-octacosadiene	alkadiene	28	0.92%
48.03	1-octacosene	alkene	28	1.54%
48.08	octacosane	alkane	28	0.56%
49.50	1,28-nonacosadiene	alkadiene	29	0.57%
49.56	1-nonacosene	alkene	29	1.13%
49.61	nonacosane	alkane	29	0.43%
51.31	1,29-triacontadiene	alkadiene	30	0.30%
51.39	1-triacontene	alkene	30	0.84%
51.44	triacontane	alkane	30	0.27%
53.32	1,30-hentriacontadiene	alkadiene	31	0.20%
53.59	1-hentriacontene	alkene	31	0.56%
53.66	hentriacontane	alkane	31	0.22%
56.22	1,31-dotriacontadiene	alkadiene	32	0.11%
56.29	1-dotriacontene	alkene	32	0.30%
56.36	dotriacontane	alkane	32	0.14%

B.6 Analysis of the effect of temperature at given VRT

The effect of pyrolysis temperature on peak area percentages at different VRT is shown in Figure B-6. This data shows that for all VRTs increasing pyrolysis temperature shows an accelerating decline in peak area percent for gasoline and diesel aliphatics and waxes, while that from C1-C4 gases and aromatics presented a sharp increase. Increasing VRTs exhibit a stronger downward trend with increasing temperature for C11-C31 range aliphatics, while aromatics continue a strong upward trend. However, at the highest VRT (5.6 s) the peak area of gases leveled off at 650 °C. This straight abundance showed a correspondence with a steep increase in peak area percent for aromatics. A comparison between Figure 4, from the main article, and Figure B-6 indicate that the degradation of C11-C31 aliphatics is favored by the increase in VRT while changes in peak area percent of C5-C10 aliphatics, C1-C4 gases and aromatics are mostly influenced by temperature.
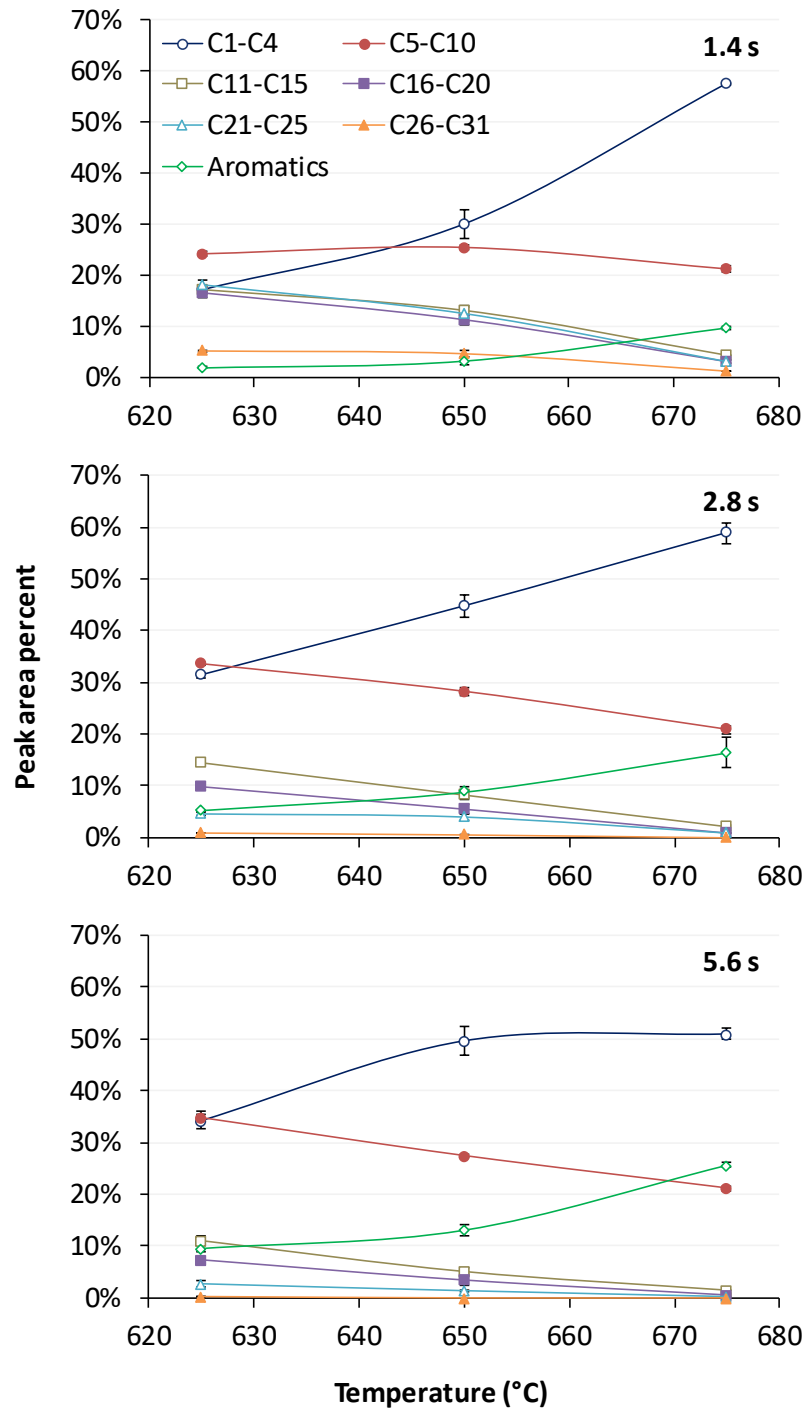
Figure B-6. Effect of temperature at different VRTs in the product distribution of waste HDPE degradation.

B.7 References

(1)   Petersen, H. The properties of helium: Density, specific heats, viscosity, and thermal conductivity at pressures from 1 to 100 bar and from room temperature to about 1800 K.; Report No. Commision, D. A. E.: Copenhagen, Denmark, 1970.

(2)   Kandasamy, J.; Gökalp, I. Pyrolysis, Combustion, and Steam Gasification of Various Types of Scrap Tires for Energy Recovery. Energy Fuels **2015,** 29, 346-354.

(3)   Stein, S. E., Mass Spectra. In NIST Chemistry WebBook, NIST Standard Reference Database Number 69, Linstrom, P. J.; Mallard, W. G., Eds. National Institute of Standards and Technology: Gaithersburg, MD, 2017.

(4)   Lebedev, A. T., Introduction to Mass Spectra Interpretation: Organic Chemistry. In Mass Spectrometry: Instrumentation, Interpretations, and Applications, Elkman, R.; Silberring, J.; Westman-Brinkmalm, A.; Kraj, A., Eds. John Wiley & Sons, Inc.: Hoboken, NJ, 2009; pp 119-178.

C   Supporting Information for Chapter 4

Systems Analysis of High-value Chemicals and Fuels from a Waste High-Density Polyethylene Refinery. Part 1: Conceptual Design and Techno-economic Assessment

C.1   Calculation of product distribution in mass percentages

In a previous publication,[1] a two-stage micropyrolysis reactor (TSMR) was developed and used to study the thermal degradation of waste high-density polyethylene. The main objective of the study was to evaluate the effect of pyrolysis temperature and vapor residence time (VRT) on the carbon numbers and chemical species (alkanes, alkenes, alkadienes, and mono- and poly-aromatic hydrocarbons) distribution of the formed products. The results were reported in a qualitative basis using area percentages to express the product distribution. To obtain the response factors that could allow an estimation of the mass percentages, the mass-spectrometry detector (ThermoFisher DSQ III) was calibrated using four different standard mixtures, shown in Table C-1, representing the different chemical species and carbon numbers observed in the pyrolysis products. The standard mixtures were injected at different volumes, using an autosampler (ThermoFisher AI 1310), to modify the concentration in the detector (see Table C-1). Due that, the VRT was controlled varying the helium flowrate through the TSMR, the split ratio had to be modified for each a different VRT tested. The operation conditions for the current study are temperature of 650 °C and a VRT of 2.8 s, which corresponds to a split ratio of 50. A more detailed information about the setting for the analysis is shown in the published manuscript.

252

Table C-1. Standards for the mass-spectrometry detector calibration.

Standard	Compounds	Concentration (μg/mL)	Observations
Alkanes	Decane	1999.2	Injection volumes: 1, 2, 3, 4, and 5 μL.
	Tetradecane	1998.4	
	Octadecane	1988.8	
Alkenes	1-pentene	1611.5	Injection volumes: 1, 2, 3, and 4 μL.
	1-decene	1900.8	
	1-tetradecene	2003.8	
	1-octadecene	2027.5	
Alkadienes	1,4-pentadiene	1960.2	Injection volumes: 1, 2, and 3 μL.
	1,9-decadiene	1928.4	
	1,13-tetradecadiene	1792.8	
Aromatics	Benzene	2001.0	Injection volumes: 3, 4, and 5 μL. Commercial standard: Michigan GRO mix Vendor: Restek
	Toluene	2007.0	
	Ethylbenzene	2000.0	
	p- & m-xylene	4013.0	
	O-xylene	2001.2	
	cumene	2006.0	
	1,3,5-trimmethyl benzene	1997.6	
	1,2,4-trimethyl benzene	1999.6	
	Naphthalene	1998.8	
	2-methylnaphthalene	1998.8	

The slope of the linear correlation between the standard concentration and the peak areas from the chromatograph served to calculate the response factors for each compound. Figure C-1 shows the results of the linear correlations, indicating a relationship between carbon number and response factor. As a result, power correlations between carbon number and response factor were obtained for each chemical species (Figure C-2). These correlations made possible to estimate the individual response factors for each carbon number, from C1 to C29, of the aliphatic hydrocarbon species. Table C-2 and Table C-3 present the calculated response factors for aliphatic and aromatic hydrocarbons, respectively. The estimated mass percentages are compared to the previously published area percentages in Table C-4. The modelling of the performance of the pyrolysis reactor took into consideration the mass percentages obtained with the methodology presented in this section.
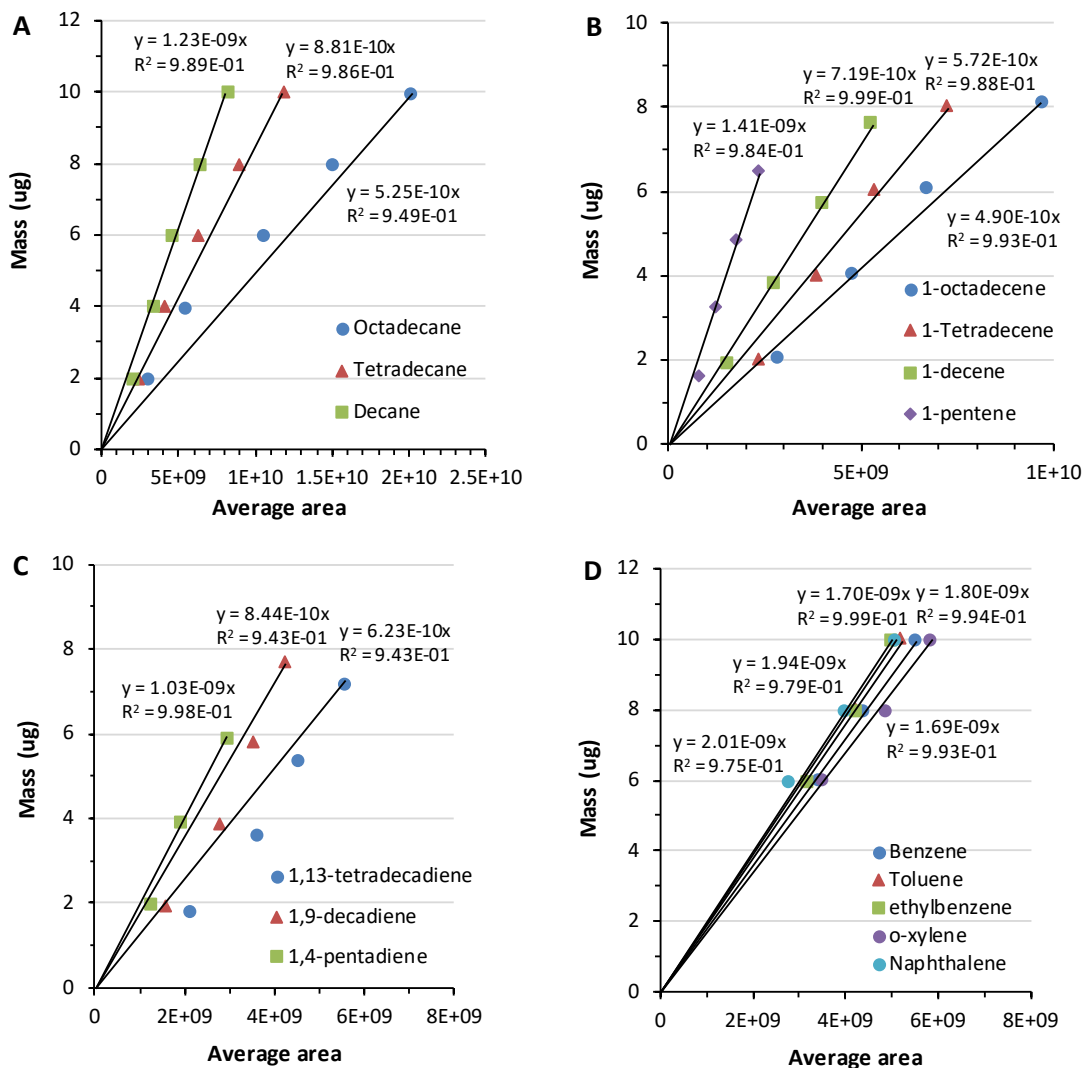
Figure C-1. Estimation of the response factors of different chemical species. A) Alkanes, B) Alkenes, C) Alkadienes, D) Aromatics.
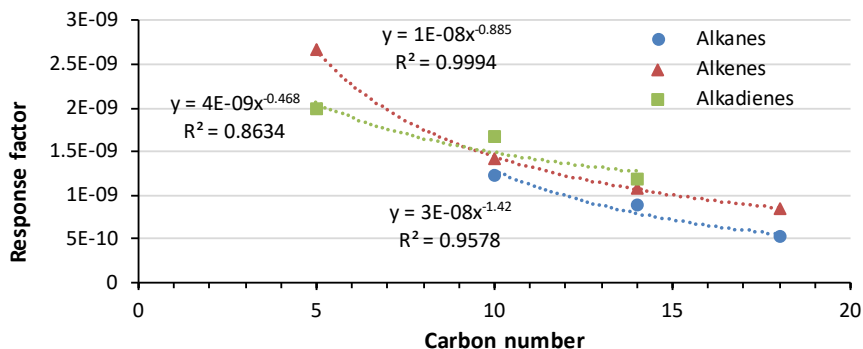
Figure C-2. Response factors and carbon number correlation of aliphatic hydrocarbons.

254

Table C-2. Response factors for aliphatic hydrocarbons.

Carbon Number	Alkanes	Alkenes	Alkadienes
1	3.45536E-08	1.10422E-08	4.37608E-09
2	1.29161E-08	5.98035E-09	3.16326E-09
3	7.26337E-09	4.17766E-09	2.61628E-09
4	4.82799E-09	3.23888E-09	2.28657E-09
5	3.51711E-09	2.66627E-09	1.98655E-09
6	2.71503E-09	2.26257E-09	1.89119E-09
7	2.18138E-09	1.97411E-09	1.7595E-09
8	1.80469E-09	1.75414E-09	1.65285E-09
9	1.5268E-09	1.58055E-09	1.56417E-09
10	1.22938E-09	1.42117E-09	1.66316E-09
11	1.14831E-09	1.32344E-09	1.42389E-09
12	1.05653E-09	1.22538E-09	1.36705E-09
13	9.05858E-10	1.1416E-09	1.31676E-09
14	8.80844E-10	1.08632E-09	1.18052E-09
15	7.39317E-10	1.00585E-09	1.23143E-09
16	6.96249E-10	9.50021E-10	1.19477E-09
17	6.18957E-10	9.00408E-10	1.16133E-09
18	5.25813E-10	8.51119E-10	1.13066E-09
19	5.28547E-10	8.16023E-10	1.1024E-09
20	4.6224E-10	7.79819E-10	1.07624E-09
21	4.5854E-10	7.46873E-10	1.05193E-09
22	4.40515E-10	7.16758E-10	1.02927E-09
23	4.02984E-10	6.89116E-10	1.00806E-09
24	4.22474E-10	6.63651E-10	9.88175E-10
25	3.57996E-10	6.4011E-10	9.69466E-10
26	4.10456E-10	6.18279E-10	9.51825E-10
27	3.20943E-10	5.97975E-10	9.35153E-10
28	3.82353E-10	5.79041E-10	9.19364E-10
29	2.89981E-10	5.6134E-10	9.04382E-10

Table C-3. Response factors for aromatic hydrocarbons

Compound	Response factor	Compound	Response factor
benzene	1.80024E-09	cumene	1.62748E-09
toluene	1.91585E-09	trimethyl benzene	1.76599E-09
ethylbenzene	1.94349E-09	naphthalene	2.00567E-09
xylenes	1.77434E-09	2-methyl naphthalene	1.51438E-09

Table C-4. Comparison of area and mass percentages of the pyrolysis products of waste HDPE at 650 °C and VRT of 2.8 s.

Compound	Chemical class	Carbon number	Average peak area percent	Average mass area percent
methane	alkane	1	0.41%	4.81%
ethylene	alkene	2	10.06%	20.37%
1-propene	alkene	3	9.34%	13.19%
propane	alkane	3	1.31%	3.23%
1-butene	alkene	4	21.47%	23.67%
butane	alkane	4	2.03%	3.35%
1-pentene	alkene	5	5.35%	4.85%
pentane	alkane	5	1.06%	1.27%
unidentified	alkadiene	5	2.89%	1.96%
unidentified	alkadiene	5	2.05%	1.39%
unidentified	alkadiene	5	1.57%	1.06%
unidentified	alkadiene	5	1.65%	1.11%
1,5-hexadiene	alkadiene	6	0.47%	0.30%
1-hexene	alkene	6	2.14%	1.64%
hexane	alkane	6	1.33%	1.23%
unidentified	alkadiene	6	0.77%	0.50%
unidentified	alkene	6	0.33%	0.25%
unidentified	aromatic	6	0.20%	0.12%
unidentified	alkadiene	6	0.30%	0.19%
benzene	aromatic	6	2.32%	1.41%
benzene	aromatic	6	1.09%	0.67%
unidentified	alkadiene	6	0.27%	0.17%
1-heptene	alkene	7	1.19%	0.80%
heptane	alkane	7	1.12%	0.83%
methyl, cyclohexane	alkane	7	0.31%	0.23%
2-methyl-1,4-hexadiene	alkadiene	7	0.17%	0.10%
toluene	aromatic	7	1.31%	0.85%
unidentified	alkadiene	7	0.18%	0.11%
1-octene	alkene	8	0.92%	0.55%
Octane	alkane	8	0.72%	0.44%
xylene	aromatic	8	0.22%	0.13%
xylene	aromatic	8	0.15%	0.09%
styrene	aromatic	8	1.47%	0.97%

xylene	aromatic	8	0.24%	0.14%
1-nonene	alkene	9	0.89%	0.48%
nonane	alkane	9	0.45%	0.23%
1,9-decadiene	alkadiene	10	0.10%	0.06%
indane	aromatic	9	0.15%	0.09%
indane	aromatic	9	0.12%	0.07%
1-decene	alkene	10	1.48%	0.72%
decane	alkane	10	0.50%	0.21%
1,10-undecadiene	alkadiene	11	0.13%	0.06%
1-undecene	alkene	11	1.19%	0.54%
undecane	alkane	11	0.66%	0.26%
naphthalene	aromatic	10	0.19%	0.13%
1,4-divinylbenzene	aromatic	10	0.11%	0.07%
azulene	aromatic	10	0.47%	0.32%
1,11-dodecadiene	alkadiene	12	0.13%	0.06%
1-dodecene	alkene	12	0.93%	0.39%
dodecane	alkane	12	0.63%	0.23%
1,12-tridecadiene	alkadiene	13	0.13%	0.06%
1-tridecene	alkene	13	0.99%	0.38%
tridecane	alkane	13	0.53%	0.17%
methyl, naphthalene	aromatic	11	0.16%	0.08%
biphenyl	aromatic	12	0.13%	0.07%
1,13-tetradecadiene	alkadiene	14	0.12%	0.05%
1-tetradecene	alkene	14	0.88%	0.33%
tetradecane	alkane	14	0.56%	0.17%
acenaphtene	aromatic	12	0.17%	0.09%
acenaphthylene	aromatic	12	0.20%	0.10%
1,14-pentadecadiene	alkadiene	15	0.12%	0.05%
1-pentadecene	alkene	15	0.75%	0.26%
pentadecane	alkane	15	0.57%	0.15%
1-hexadecene	alkene	16	0.62%	0.20%
hexadecane	alkane	16	0.57%	0.14%
1-heptadecene	alkene	17	0.57%	0.17%
heptadecane	alkane	17	0.55%	0.12%
anthracene	aromatic	14	0.12%	0.06%
1-octadecene	alkene	18	0.55%	0.16%
octadecane	alkane	18	0.55%	0.10%
1-nonadecene	alkene	19	0.48%	0.13%

nonadecane	alkane	19	0.59%	0.11%
1-eicosene	alkene	20	0.42%	0.11%
eicosane	alkane	20	0.63%	0.10%
1-henicosene	alkene	21	0.39%	0.10%
henicosane	alkane	21	0.67%	0.11%
1-docosene	alkene	22	0.28%	0.07%
docosane	alkane	22	0.73%	0.11%
1-tricosene	alkene	23	0.21%	0.05%
tricosane	alkane	23	0.69%	0.10%
1-tetracosene	alkene	24	0.13%	0.03%
tetracosane	alkane	24	0.55%	0.08%
pentacosane	alkane	25	0.38%	0.05%
hexacosane	alkane	26	0.23%	0.03%
heptacosane	alkane	27	0.13%	0.01%
octacosane	alkane	28	0.11%	0.01%
nonacosane	alkane	29	0.07%	0.01%

C.2   Detailed information of the conceptual design
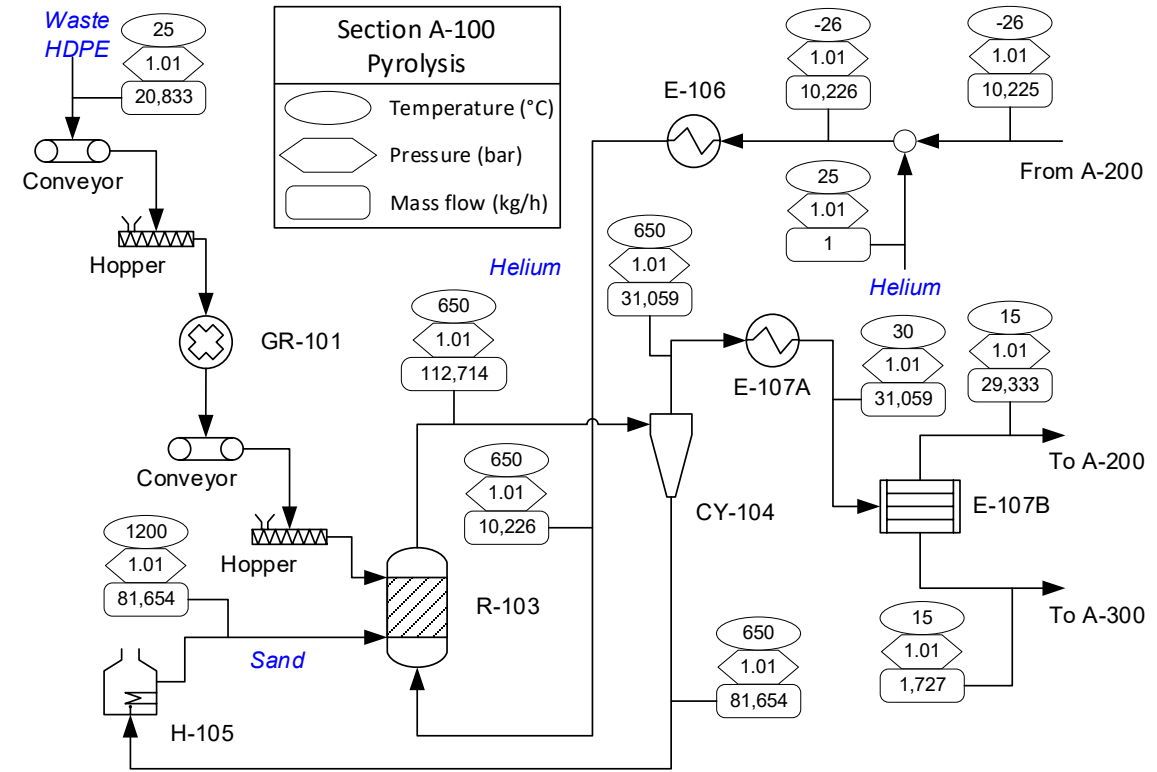
Figure C-3. Process flow diagram of section A-100.
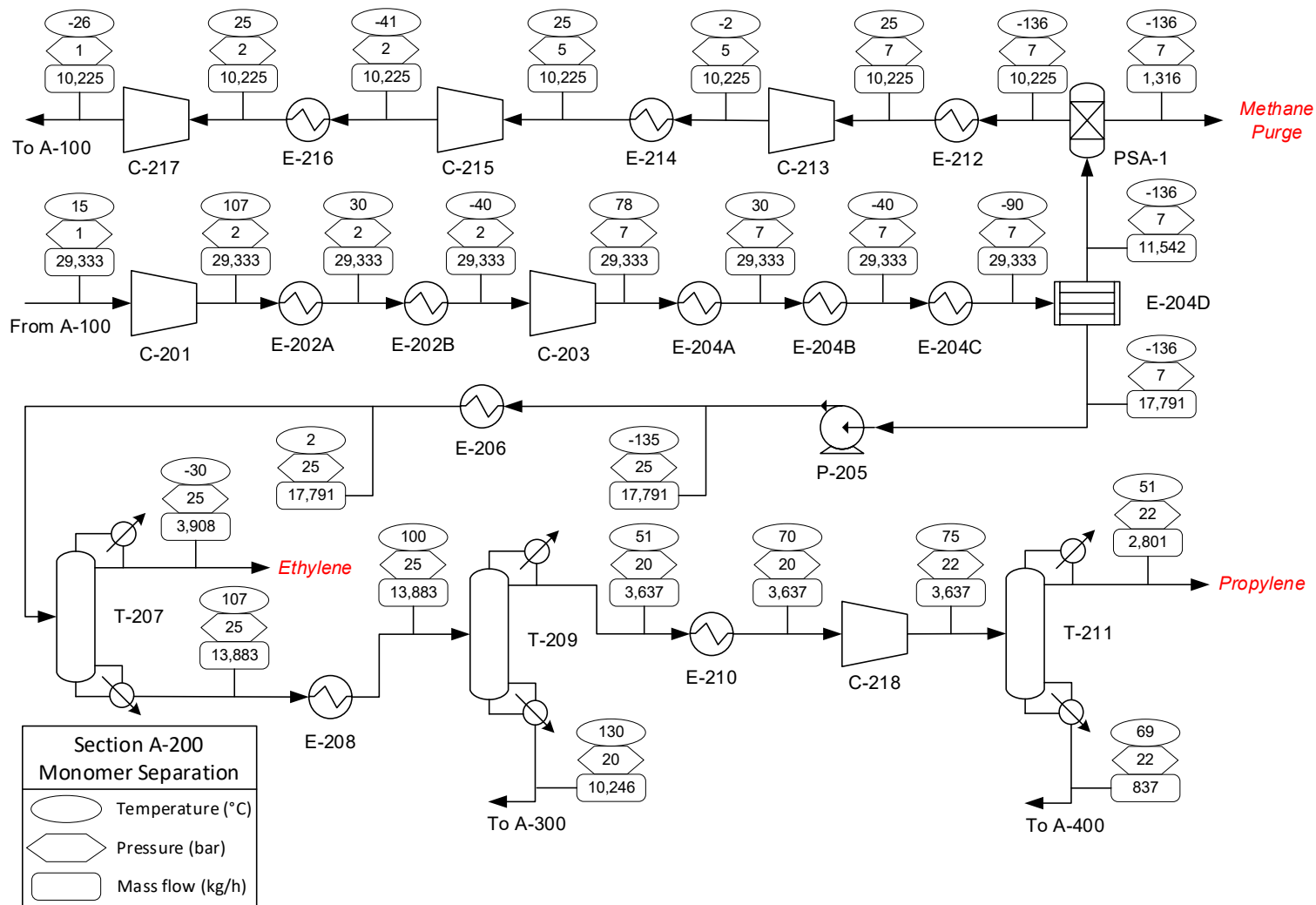
Figure C-4. Process flow diagram of section A-200
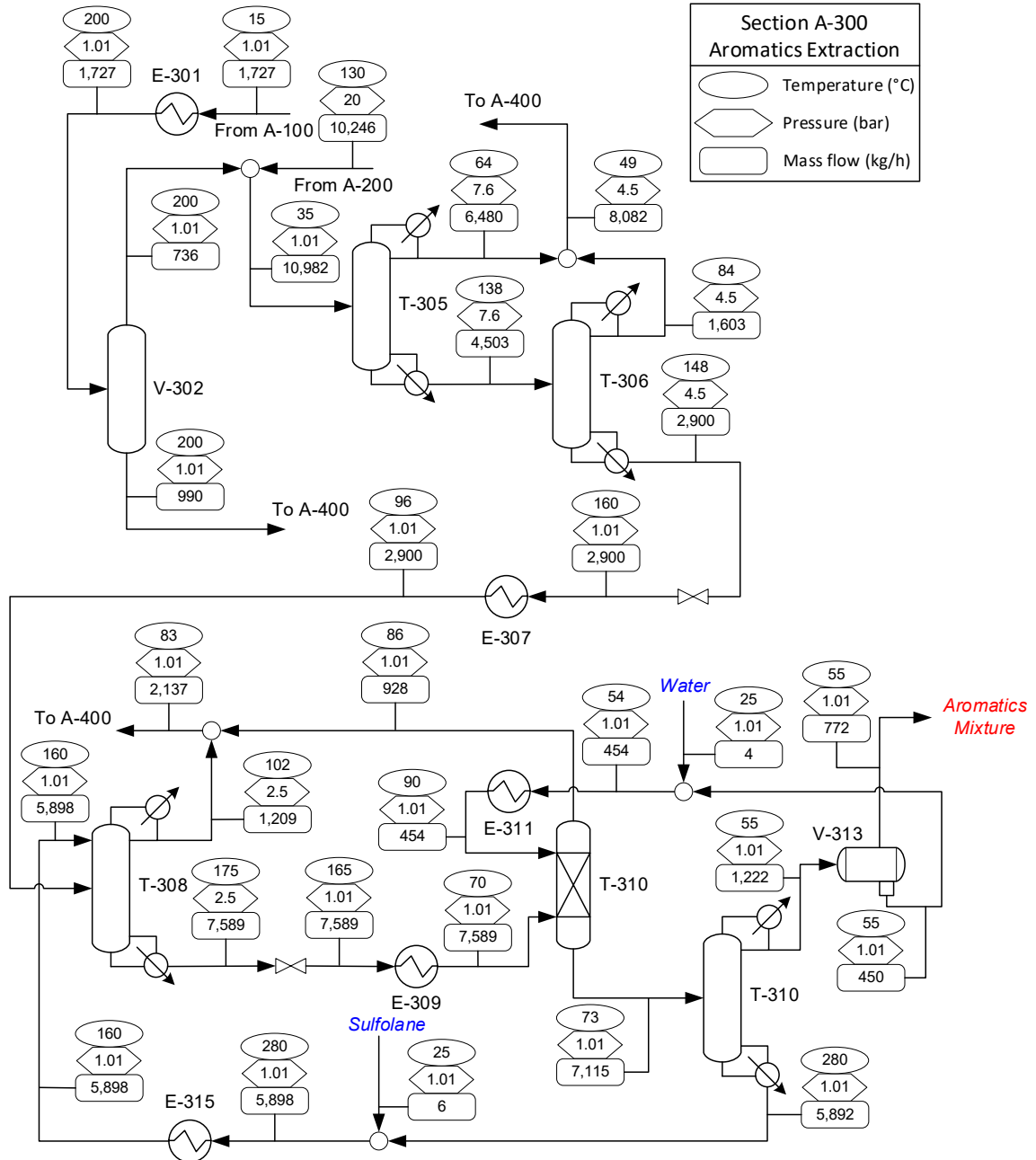
Figure C-5. Process flow diagram of section A-300
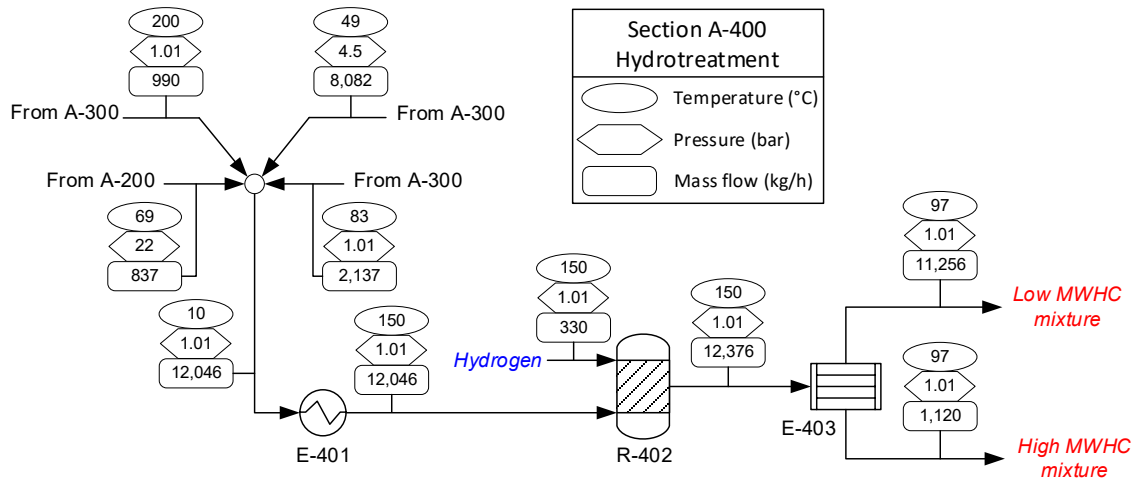
Figure C-6. Process flow diagram of section A-400.

Table C-5. Single-loop refrigeration cycles for the base case refinery.

Process stream	Refrigerant	Evaporator Duty (MJ/h)	Compressor work (kW)	Condenser Duty (MJ/h)
E-107B	1,1,1,2-Tetrafluoroethane	1428.07	59.13	1641.11
E-202B	Propene	7353.47	1516.04	12811.15
Condenser T-207	Propene	2952.49	494.93	4734.24

Table C-6. Cascade refrigeration cycle for the base case refinery.

Stream	Refrigerant	Evaporator 1 Duty (MJ/h)	Evaporator 2 Duty (MJ/h)	Condenser Duty (MJ/h)	Compressor work (kW)
E-204B	Propane	8,951.73	33,202.11	74,018.2611	8,851.23
E-204C	Ethane	6,785.50	13,382.57	33,202.1107	3,620.57
E-204D	Methane	5,651.54	-	13,382.57	2,147.50
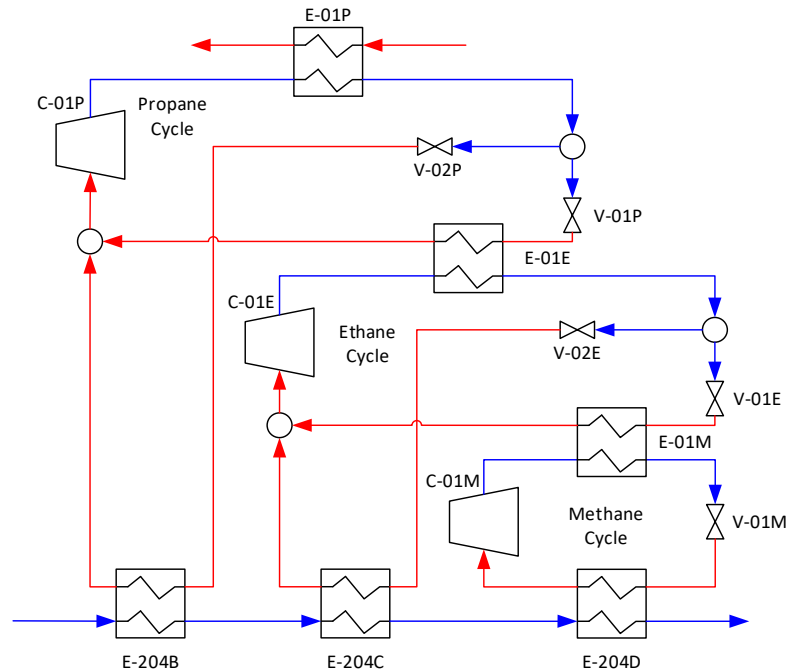
Figure C-7. Diagram of the cascade refrigeration system for the base case refinery.

Table C-7. Heaters and coolers used in the heat exchanger network design.

Code	Heat load (MJ/h)	Thot,in (°C)	Tcold,out (°C)	Thot,out (°C)	Tcold,in (°C)	U (kW/m² C)
E-106	35905.32	1000	650	900	-26	0.11
E-107A	66997.12	650	30	30	20	0.16
E-107B	1428.07	30	5	15	5	0.44
E-202A	6622.35	107	30	30	20	0.16
E-202B	7353.47	30	-50	-40	-50	0.4259
E-204A	4198.18	78	30	30	20	0.16
E-204B	8951.73	30	-50	-40	-50	0.0596
E-206	4755.78	1000	2	900	-135	0.11
E-208	286.89	131	30	100	20	0.16
E-210	1156.97	1000	75	900	50	0.11
E-212	8556.17	1000	25	900	-136	0.11
E-214	1434.58	1000	25	900	-28	0.11
E-216	3496.46	1000	25	900	-85	0.11
E-301	928.76	1000	200	900	15	0.175
E-307	960.51	1000	160	900	148	0.175
E-309	1526.42	173	30	155	20	0.5
E-311	70.50	1000	90	900	80	2.25
E-315	1402.94	248	30	160	20	0.5
E-401	5303.90	1000	150	900	11	0.1425
E-403	1612.08	150	30	97	20	0.3925

C.3 Techno-economic analysis inputs

Table C-8. Costing parameters for refinery equipment.

Section	Equipment	Description	Costing parameter	Source
A-100	GR-101	Grinder	Capacity: 500 tonnes/day	Jones et al.[2]
	SC-102	Screen	Capacity: 500 tonnes/day	Jones et al.[2]
	R-103	CFM Pyrolyzer	Capacity: 500 tonnes/day	Jones et al.[2]
		Hopper	Capacity: 500 tonnes/day	Winjobi et al.[3]
		Conveyor	Capacity: 500 tonnes/day	Winjobi et al.[3]
	CY-104	Cyclone	Capacity: 500 tonnes/day	Jones et al.[2]
	E-105	Furnace	Duty: 74,588 MJ/h	Peters et al.[4]
	V-108	Flash separator	Volume: 21.62 m^3	Turton et al.[5]
	COMP-107	Refrigeration compresor (E-107B)	Power: 59.13 kW	Seider et al.[6]
	COND-107	Refrigeration condenser (E-107B)	Area: 54.65 m^2	Turton et al.[5]
A-200	C-201	Compresor	Power: 2,218.62 kW	Peters et al.[4]
	C-203	Compresor	Power: 3,172.80 kW	Peters et al.[4]
	V-205	flash separator	Volume: 6.08 m^3	Turton et al.[5]
	PSA-1	Pressure swing absorption unit	Capacity: 25,444 lb/hr	Winjobi et al.[3]
	C-213	Turbine	Power: 399.94 kW	Peters et al.[4]
	C-215	Turbine	Power: 973.40 kW	Peters et al.[4]
	C-217	Turbine	Power: 754.63 kW	Peters et al.[4]
	P-205	Pump	Power: 22.70 kW	Turton et al.[5]
	T-207	Deethanizer	Diameter: 1.07 m Height: 31.70 m No. trays: 32	Peters et al.[4]
			Condenser area: 183.5 m^2 Reboiler area: 18.9 m^2	Turton et al.[5]

			Diameter: 1.07 m Height: 25.60 m No. trays: 25	Peters et al.[4]
	T-209	Depropanizer	Condenser area: 83.1 m^2 Reboiler area: 18.6 m^2	Turton et al.[5]
	C-218	Compresor	Power: 5.71 kW	Seider et al.[6]
	T-211	Propylene fractionator	Two columns of Diameter: 1.83 m Height: 62.18 m No. trays: 69	Peters et al.[4]
			Condenser area: 291.5 m^2 Reboiler area: 53.8 m^2	Turton et al.[5]
	E-204C	C1-C4 condenser (-40 to -90)	Area: 792.77 m^2	Turton et al.[5]
	E-204D	C1-C4 condenser (-90 to -136)	Area: 690.07 m^2	Turton et al.[5]
	COMP-202	Refrigeration compresor (E-202B)	Power: 1,516.04 kW	Peters et al.[4]
	COND-202	Refrigeration condenser (E-202B)	Area: 73.54 m^2	Turton et al.[5]
	C-01P	Refrigeration compresor (E-204B)	Power: 8,851.23 kW	Seider et al.[6]
	E-01P	Refrigeration condenser (E-204B)	Area: 1249.08 m^2	Turton et al.[5]
	C-01E	Refrigeration compresor (E-204C)	Power: 3620.57 kW	Peters et al.[4]
	E-01E	Refrigeration condenser (E-204C)	Area: 573.55 m^2	Turton et al.[5]
	C-01M	Refrigeration compresor (E-204D)	Power: 2,147.50 kW	Peters et al.[4]
	E-01M	Refrigeration condenser (E-204D)	Area: 216.04 m^2	Turton et al.[5]
	COMP-207	Refrigeration compresor (T-207)	Power: 494.93 kW	Peters et al.[4]
	COND-207	Refrigeration condenser (T-207)	Area: 73.54 m^2	Turton et al.[5]
A-300	V-302	flash tank	Volume: 2.40 m^3	Turton et al.[5]

	T-305	Debutanizer	Diameter: 0.91 m Height: 13.41 m No. trays: 11	Peters et al.[4]
			Condenser area: 58.5 m^2 Reboiler area: 14.3 m^2	Turton et al.[5]
	T-306	Depentanizer	Diameter: 0.61 m Height: 14.63 m No. trays: 12	Peters et al.[4]
			Condenser area: 11.2 m^2 Reboiler area: 5.1 m^2	Turton et al.[5]
	T-308	Extractive distillation column	Diameter: 0.61 m Height: 45.72 m No. trays: 48	Peters et al.[4]
			Condenser area: 12.3 m^2 Reboiler area: 1.2 m^2	Turton et al.[5]
	T-310	Extractor (Sizing from correlations and formulas of Frank et al.[7], Choi et al.[8], and Kłeczek et al.[9])	Diameter: 0.60 m Height: 6.69 m	Peters et al.[4]
	T-312	Aromatics recovery column	Diameter: 0.76 m Height: 5.48 m No. trays: 2	Peters et al.[4]
			Condenser area: 37.6 m^2 Reboiler area: 9.1 m^2	Turton et al.[5]
	V-313	2-phase separator	Volume: 2.40 m^3	Turton et al.[5]
A-400	V-404	flash separator (condenser)	Volume: 4.27 m^3	Turton et al.[5]
	R-402	Hydrotreater	Capacity: 19.46 liq scfh	Jones et al.[2]

Table C-9. Costing of coolers and heaters of the heat exchanger network of the base case refinery.

Code	Heat load (MJ/h)	Area (m²)	Cost (USD, 2017)	Source
E-106	35905.32	153.15	39,897.43	Turton et al.[5]
E-107A	66997.12	786.96	94,564.08	Turton et al.[5]
E-107B	1428.07	55.07	28,221.33	Turton et al.[5]
E-202A	6622.35	350.27	64,069.15	Turton et al.[5]
E-202B	7353.47	142.47	42,180.58	Turton et al.[5]
E-204A	4198.18	300.86	54,473.38	Turton et al.[5]
E-204B	8951.73	1239.39	125,526.73	Turton et al.[5]
E-206	4755.78	11.82	24,261.56	Turton et al.[5]
E-208	286.89	5.53	25,470.02	Turton et al.[5]
E-210	1156.97	3.29	4,580.34	Turton et al.[5]
E-212	8556.17	21.49	23,433.20	Turton et al.[5]
E-214	1434.58	3.81	4,530.78	Turton et al.[5]
E-216	3496.46	9.01	24,087.95	Turton et al.[5]
E-301	928.76	1.75	3,685.92	Turton et al.[5]
E-307	960.51	1.92	3,785.30	Turton et al.[5]
E-309	1526.42	6.10	4,886.94	Turton et al.[5]
E-311	70.50	0.01	150.02	Peters et al.[4]
E-315	1402.94	4.43	4,557.48	Peters et al.[4]
E-401	5303.90	11.89	22,179.76	Turton et al.[5]
E-403	1612.08	11.77	22,168.97	Turton et al.[5]

Table C-10. Inputs for capital cost estimation.[3]

Parameter	Estimation factor
Total purchased equipment cost (TPEC)	100%
Purchased equipment installation	39% of TPEC
Instrumentation and controls	26% of TPEC
Piping	31% of TPEC
Electrical Systems	10% of TPEC
Buildings (including services)	29% of TPEC
Yard Improvements	12% of TPEC
Service Facilities	55% of TPEC
Total installed cost (TIC)	302% of TPEC
Engineering	32% of TPEC
Construction	34% of TPEEC
Legal and Contractors Fees	23% of TPEC
Project Contingency	34% of TPEC
Total indirect costs (TI)	123% of TPEC
Land	6% of TPEC
Fixed Capital investment (FIC)	TIC + TI + Land
Working capital (WC)	15% of TIC + TI
Total project investment (TPI)	FIC + WC

C.4   Energy balances and primary energy calculations

Table C-11. Difference between embodied energy calculation results (GJ/h) using Lower Heating Values estimated from Aspen plus and obtained from literature.

	Aspen Plus	Literature
Waste HDPE		42.8
Ethylene	184.34	184.74
Propylene	128.17	128.28
Aromatics mixture	33.05	33.15
Low MW HCs	506.77	504.84
High MW HCs	57.10	53.87
Methane purge	63.27	64.64

Table C-12. Energy savings per heat exchanger after heat integration.

Heat exchanger code	Hot stream	Cold stream	Cooling Savings (MJ/h)
N1	E-107	E-106	1,646.5
N2	E-202	E-106	1,062.3
N3	E-107	E-106	32,665.4
N5	E-107	E-301	928.8
N6	E-107	E-307	960.5
N7	E-107	E-401	3,901.0
N9	E-107	E-216	1,430.4
N10	E-107	E-214	1,434.6
N11	E-107	E-206	337.5
N13	E-202	E-216	2,066.1
N14	E-202	E-206	4,418.3
N15	E-202	E-212	198.2
N17	E-204	E-212	8,358.0
N19	E-309	E-210	1,1557.0
N20	E-309	E-311	70.5
N22	E-315	E-401	1,402.9
Total			62,038.0

Note: Exchanger N4 is a heater and exchangers N8, N12, N16, N18, N21, and N23 are coolers.

Table C-13. Process energy inputs and outputs (GJ/h) by source and per section of the refinery.

Stream	Section	Source	Base case	Heat integrated
Inputs	A-100	Electricity	24,802.00	24,802.00
		Heating	110,493.28	75,119.06
	A-200	Electricity	19,381.83	19,381.83
		Heating	50,487.79	31,087.33
	A-300	Electricity	0.00	0.00
		Heating	12,566.68	10,606.91
	A-400	Electricity	0.00	0.00
		Heating	5,303.90	0.00
Outputs	A-100	Electricity	0.00	0.00
		Cooling	68,425.19	25,120.50
	A-200	Electricity	7,660.72	7,660.72
		Cooling	68,988.79	52,885.98
	A-300	Electricity	0.00	0.00
		Cooling	13,655.31	11,024.85
	A-400	Electricity	0.00	0.00
		Cooling	22,040.27	22,040.27

Table C-14. Single-loop refrigeration cycle for the heat integrated refinery.

Process stream	Refrigerant	Evaporator Duty (MJ/h)	Compressor work (kW)	Condenser Duty (MJ/h)
E-107B	1,1,1,2-Tetrafluoroethane	-	-	-
E-202B	Propene	-	-	-
Condenser T-207	Propene	2952.49	494.93	4734.24
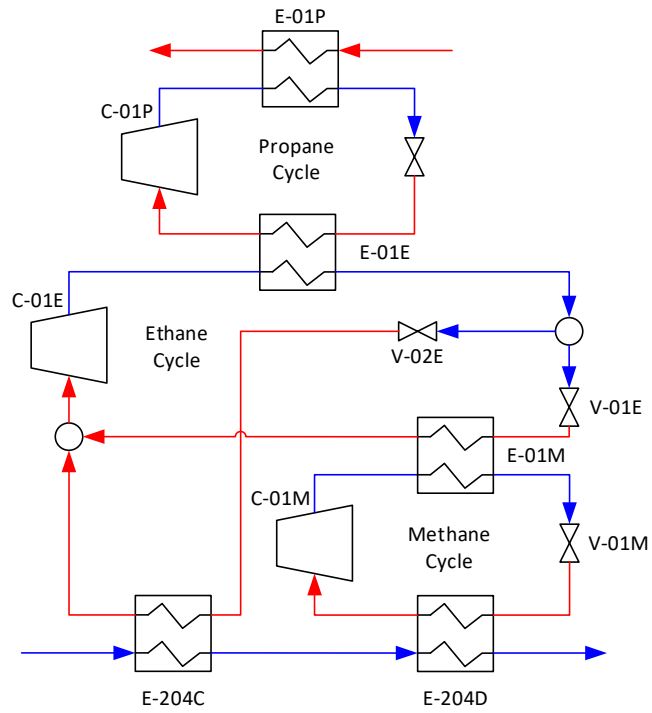
Figure C-8. Diagram of the cascade refrigeration system for the heat integrated refinery.

Table C-15. Cascade refrigeration cycle for the heat integrated refinery.

Stream	Refrigerant	Evaporator 1 Duty (MJ/h)	Evaporator 2 Duty (MJ/h)	Condenser Duty (MJ/h)	Compressor work (kW)
E-204B	Propane	-	33,202.11	58,300.57	6,971.94
E-204C	Ethane	6,785.50	13,382.57	33,202.11	3,620.57
E-204D	Methane	5,651.54	-	13,382.57	2,147.50
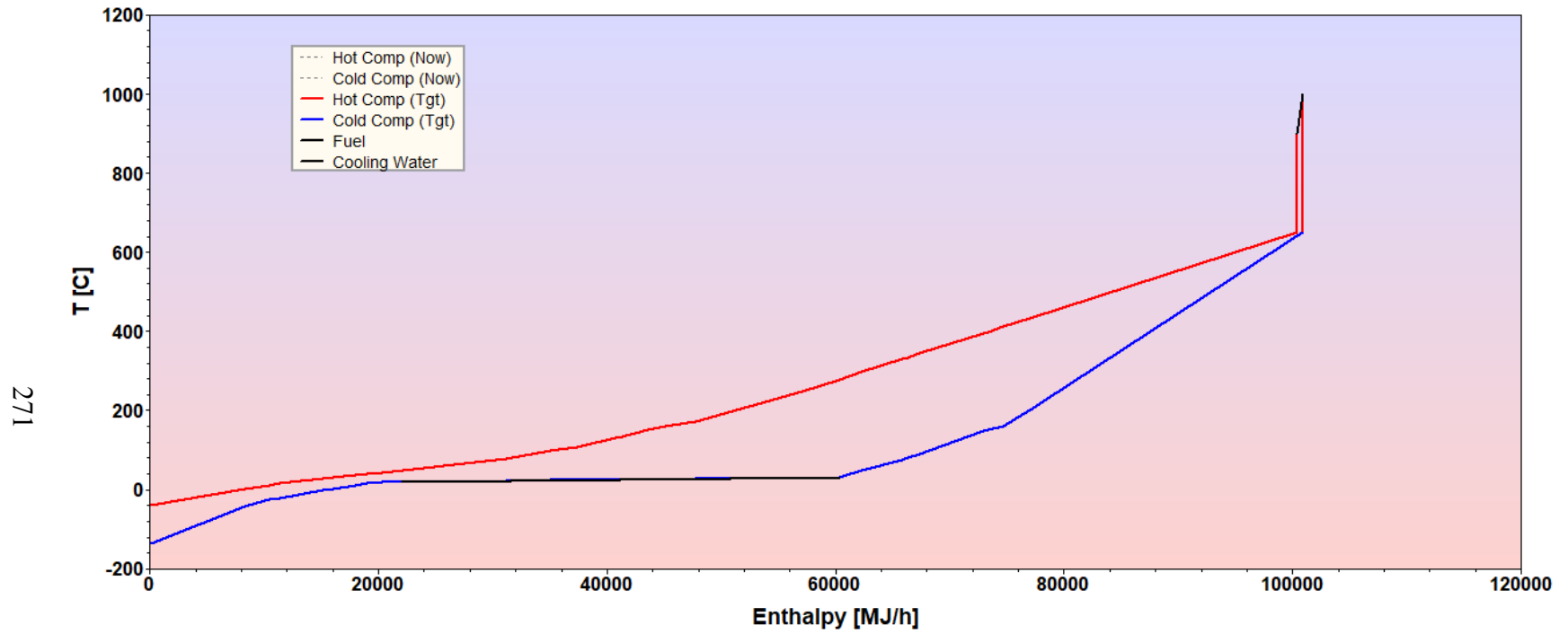
Figure C-9. Grand composite curve from the heat integration of the refinery.
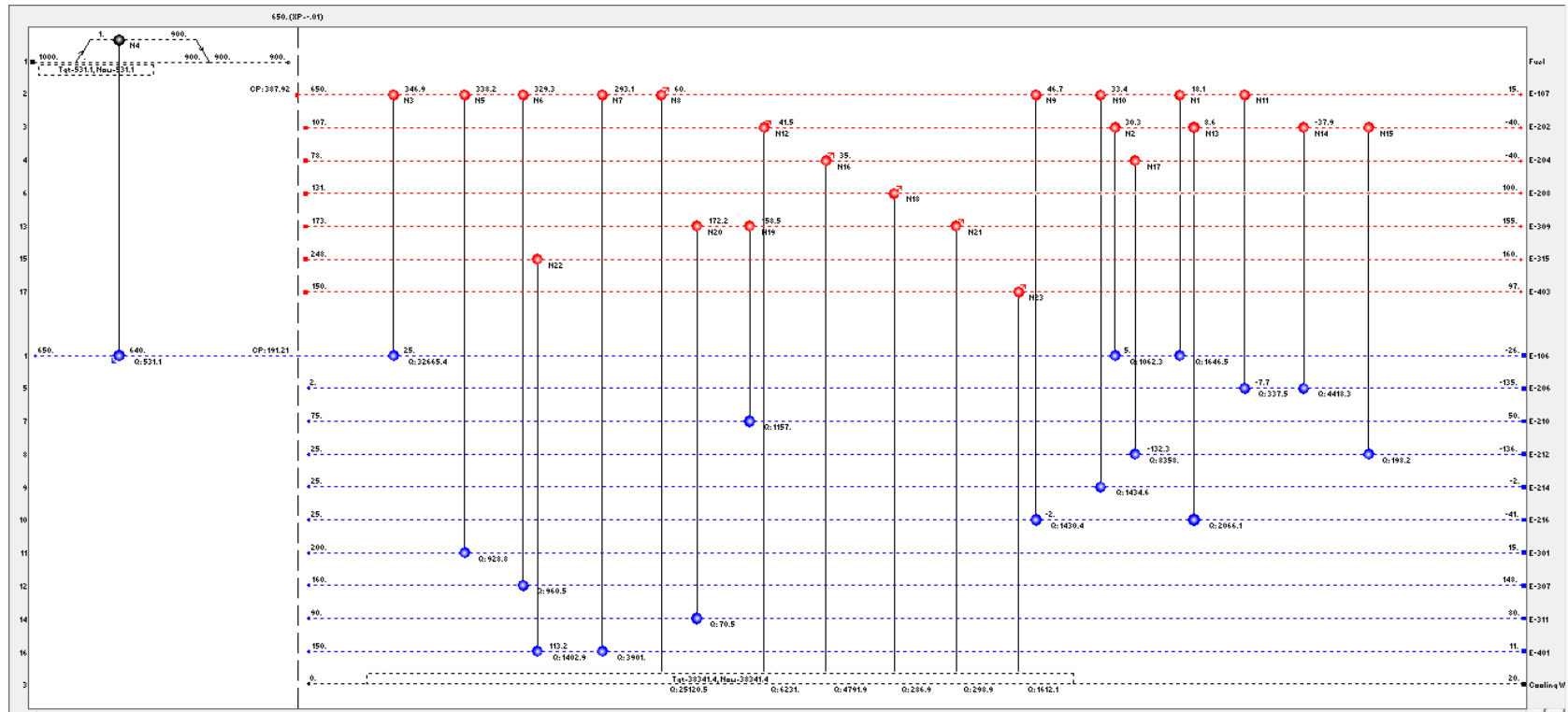
Figure C-10. Heat Exchanger Network (HEN) grid diagram from the heat integration of the refinery.

Table C-16. Detailed composition of each product from the refinery.

Compound	Ethylene	Propylene	Aromatics	Low MWHCs	High MWHCs
Methane	107.59	0.00	0.00	0.02	0.00
Ethylene	3799.30	26.61	0.00	0.00	0.00
Ethane	0.00	0.00	0.00	0.42	0.00
Propane	0.00	33.63	0.00	643.40	0.84
Propylene	0.01	2740.47	0.00	0.00	0.00
N-butane	0.00	0.00	0.00	5788.95	18.31
1-butene	0.00	0.00	0.00	0.00	0.00
N-pentane	0.00	0.00	0.00	2502.25	18.58
1-pentene	0.00	0.00	0.00	0.00	0.00
1,4-pentadiene	0.00	0.00	0.00	0.00	0.00
N-hexane	0.00	0.00	0.00	940.81	15.99
1-hexene	0.00	0.00	0.00	0.00	0.00
1,5-hexadiene	0.00	0.00	2.54	0.00	0.00
Benzene	0.00	0.00	314.58	70.79	1.27
cyclohexane	0.00	0.00	0.00	76.00	1.64
N-heptane	0.00	0.00	0.05	324.70	12.31
1-heptene	0.00	0.00	6.61	0.00	0.00
Methylcyclohexane	0.00	0.00	1.65	77.87	3.14
Toluene	0.00	0.00	111.66	31.48	1.43
N-octane	0.00	0.00	4.45	173.19	14.71
1-octene	0.00	0.00	16.59	0.00	0.00
o-xylene	0.00	0.00	17.13	5.77	0.65
1,2-Dimethylcyclohexane	0.00	0.00	0.00	6.29	0.49
m-xylene	0.00	0.00	9.07	4.28	0.44
1,3-Dimethylcyclohexane	0.00	0.00	0.00	4.67	0.31
p-xylene	0.00	0.00	13.74	6.40	0.65
1,4-Dimethylcyclohexane	0.00	0.00	0.00	6.96	0.49
Styrene	0.00	0.00	145.73	25.12	2.83
Ethylcyclohexane	0.00	0.00	0.00	27.66	2.45
N-nonane	0.00	0.00	6.97	102.97	18.94
1-nonene	0.00	0.00	20.55	0.00	0.00
Indane	0.00	0.00	12.94	8.17	2.11
Bicyclo[4,3,0]nonane	0.00	0.00	0.00	8.96	1.85
N-decane	0.00	0.00	4.10	164.47	65.06
1-decene	0.00	0.00	20.06	0.00	0.00

1,9-Decadiene	0.00	0.00	12.93	0.00	0.00
Naphthalene	0.00	0.00	20.03	21.38	15.13
Decalin	0.00	0.00	0.00	26.25	13.13
1,4-Divinylbenzene	0.00	0.00	4.47	3.18	2.18
1:4-Diethylcyclohexane	0.00	0.00	0.00	3.94	1.83
N-undecane	0.00	0.00	2.34	87.30	68.49
1-undecene	0.00	0.00	9.13	0.00	0.00
1-methylnaphthalene	0.00	0.00	0.78	2.86	5.08
1-methyldecalin	0.00	0.00	0.00	4.75	3.75
1-dodecane	0.00	0.00	3.78	0.00	0.00
N-dodecene	0.00	0.00	1.04	46.47	77.75
Diphenyl	0.00	0.00	0.26	1.66	5.01
Bicyclohexyl	0.00	0.00	0.00	2.15	5.04
Acenaphthene	0.00	0.00	0.08	2.45	15.37
Acenaphthalene	0.00	0.00	0.18	3.55	17.96
N-tridecane	0.00	0.00	0.99	23.77	88.67
1-tridecene	0.00	0.00	2.03	0.00	0.00
1-tetradecane	0.00	0.00	0.89	0.00	0.00
N-tetradecane	0.00	0.00	0.25	12.11	90.34
Anthracene	0.00	0.00	0.00	0.19	12.56
1-pentadecene	0.00	0.00	0.35	0.00	0.00
N-pentadecane	0.00	0.00	0.08	5.13	78.83
1-hexadecene	0.00	0.00	0.11	0.00	0.00
N-hexadecane	0.00	0.00	0.05	2.26	68.17
1-heptadecene	0.00	0.00	0.05	0.00	0.00
N-heptadecane	0.00	0.00	0.02	0.92	59.76
1-octadecene	0.00	0.00	0.02	0.00	0.00
N-octadecane	0.00	0.00	0.01	0.43	53.79
1-nonadecene	0.00	0.00	0.01	0.00	0.00
N-nonadecane	0.00	0.00	0.00	0.20	50.08
1-eicosene	0.00	0.00	0.00	0.00	0.00
N-eicosane	0.00	0.00	0.00	0.13	65.17
N-heneicosane	0.00	0.00	0.00	0.02	21.86
1-docosene	0.00	0.00	0.00	0.00	0.00
N-docosane	0.00	0.00	0.00	0.03	47.18
N-tricosane	0.00	0.00	0.00	0.01	19.80
1-tricosene	0.00	0.00	0.00	0.00	0.00
N-tetracosane	0.00	0.00	0.00	0.00	22.87
N-pentacosane	0.00	0.00	0.00	0.00	9.55
N-hexacosane	0.00	0.00	0.00	0.00	6.53

N-heptacosane	0.00	0.00	0.00	0.00	2.92
N-octacosane	0.00	0.00	0.00	0.00	3.04
N-nonacosane	0.00	0.00	0.00	0.00	1.41
Silicon dioxide	0.00	0.00	0.00	0.00	0.00
Helium	0.87	0.00	0.00	0.02	0.00
Sulfolane	0.00	0.00	2.83	0.66	2.17
Water	0.00	0.00	0.96	2.52	0.01
Hydrogen	0.00	0.00	0.00	0.00	0.00
Total	3907.77	2800.71	772.10	11255.97	1119.92

Table C-17. Total equipment costs per section of the refinery (USD).

Section	Equipment	Description	Base case cost (2007)	Heat integrated cost (2007)
		Total heat exchanger network	616,710.94	2,506,500.71
A-100	GR-101	Hammer mill	81,099.46	81,099.46
	SC-102	Screen	39,934.31	39,934.31
	R-103	CFB Pyrolyzer	8,766,341.78	8,766,341.78
		Hopper, live bottom, 9m drg chain conv	236,452.39	236,452.39
		Conveyor, belted 33.5m length	297,661.70	297,661.70
	CY-104	Cyclone	982,510.70	982,510.70
	E-105	Furnace	1,566,589.78	1,566,589.78
	V-108	Flash separator	27,896.71	27,896.71
	COMP-107	Refrigeration compresor (E-107B)	65,213.21	0.00
	COND-107	Refrigeration condenser (E-107B)	28,284.34	0.00
A-200	C-201	Compresor	805,571.70	805,571.70
	C-203	Compresor	1,036,508.05	1,036,508.05
	V-205	flash separator	11,833.50	11,833.50
	PURGE-1	PSA	2,598,692.19	2,598,692.19
	C-213	Turbine	162,051.66	162,051.66
	C-215	Turbine	273,616.48	273,616.48
	C-217	Turbine	235,523.98	235,523.98
	P-205	Pump	7,995.95	7,995.95
	T-207	Deethanizer	307,436.85	307,436.85
	T-209	Depropanizer	246,487.92	246,487.92
	C-218	Compresor	10,050.56	10,050.56

	T-211	Propylene fractionator	1,354,937.18	1,354,937.18
	E-204C	C1-C4 condenser (-40 to -90)	95,152.59	95,152.59
	E-204D	C1-C4 condenser (-90 to -136)	87,132.99	87,132.99
	COMP-202	Refrigeration compresor (E-202B)	630,178.91	0.00
	COND-202	Refrigeration condenser (E-202B)	44,014.60	0.00
	PCOMP3	Refrigeration compresor (E-204B)	3,585,217.78	2,962,073.09
	PCOND3	Refrigeration condenser (E-204B)	128,131.32	111,458.00
	ECOMP3	Refrigeration compresor (E-204C)	1,132,932.84	1,132,932.84
	PEVAP3E	Refrigeration condenser (E-204C)	77,993.16	57,334.77
	MCOMP	Refrigeration compresor (E-204D)	796,813.90	796,813.90
	EEVAP3M	Refrigeration condenser (E-204D)	53,340.91	53,340.91
	COMP-207	Refrigeration compresor (T-207)	296,403.99	296,403.99
	COND-207	Refrigeration condenser (T-207)	31,189.29	31,189.29
A-300	V-302	flash tank	6,946.59	6,946.59
	T-305	Debutanizer	121,473.72	121,473.72
	T-306	Depentanizer	95,756.21	95,756.21
	T-308	Extractive distillation column	244,413.90	244,413.90
	T-310	Extractor	25,732.02	25,732.02
	T-312	Aromatics recovery column	81,210.89	81,210.89
	V-313	2-phase separator	7,437.77	7,437.77
A-400	V-404	flash separator (condenser)	9,571.43	9,571.43
	R-402	Hydrotreater	181,427.66	181,427.66

Table C-18. Costing of equipment of the heat exchanger network of the heat integrated refinery.

Code	Heat load (MJ/h)	Area (m²)	Cost (USD, 2017)	Source
N1	1646.5	424.56	102,589.67	Turton et al.[5]
N2	1062.3	475.5833	95,392.68	Turton et al.[5]
N3	32665.4	489.801	632,911.03	Turton et al.[5]
N4	531.1	61.62	35,431.25	Turton et al.[5]
N5	928.8	178.93	27,468.00	Turton et al.[5]
N6	960.5	230.12	29,789.01	Turton et al.[5]
N7	3901	376.19	64,924.60	Turton et al.[5]
N8	25120.5	480.0782	201,144.95	Turton et al.[5]
N9	1430.4	476.045	71,110.82	Turton et al.[5]
N10	1434.6	471.3567	98,468.16	Turton et al.[5]
N11	337.5	484.425	31,737.67	Turton et al.[5]
N12	6231	446.12	131,072.64	Turton et al.[5]
N13	2066.1	471.8083	104,995.58	Turton et al.[5]
N14	4418.3	490.2018	174,706.39	Turton et al.[5]
N15	198.2	115	23,282.16	Turton et al.[5]
N16	4791.9	467.2911	141,925.04	Turton et al.[5]
N17	8358	498.7024	385,921.36	Turton et al.[5]
N18	286.9	79.29	22,045.34	Turton et al.[5]
N19	1157	449.62	23,518.68	Turton et al.[5]
N20	70.5	7.09	22,307.84	Turton et al.[5]
N21	298.9	21.79	26,056.57	Turton et al.[5]
N22	1402.9	328.82	37,920.77	Turton et al.[5]
N23	1612.1	192.49	21,780.50	Turton et al.[5]

C.5   References

(1)   Gracida-Alvarez, U. R.; Mitchell, M. K.; Sacramento-Rivero, J. C.; Shonnard, D. R. Effect of Temperature and Vapor Residence Time on the Micropyrolysis Products of Waste High Density Polyethylene. *Ind. Eng. Chem. Res.* **2018,** *57* (6), 1912-1923.

(2)   Jones, S. B.; Meyer, P. A.; Snowden-Swan, L. J.; Padmaperuma, A. B.; Tan, E.; Dutta, A.; Jacobson, J.; Cafferty, K. *Process design and economics for the conversion of lignocellulosic biomass to hydrocarbon fuels: fast pyrolysis and hydrotreating bio-oil pathway*; Report No. 2013.

(3)   Winjobi, O.; Shonnard, D. R.; Zhou, W. Production of Hydrocarbon Fuel Using Two-Step Torrefaction and Fast Pyrolysis of Pine. Part 1: Techno-economic Analysis. *ACS Sustain. Chem. Eng.* **2017,** *5* (6), 4529-4540.

(4)   Peters, M. S.; Timmerhaus, K. D.; West, R. E. *Plant Design and Economics for Chemical Engineers*; 5 th. ed.; McGraw-Hill Inc.: New York, NY, 2003.

(5)   Turton, R.; Bailie, R. C.; Whiting, W. B.; Shaeiwitz, J. A.; Bhattacharyya, D. *Analysis, synthesis and design of chemical processes*; 4th ed.; Pearson Education, Inc.: Ann Arbor, 2012.

(6)   Seider, W. D.; Lewin, D. R.; Seader, J. D.; Widadgo, S. *Product and Process Design Principles*; 3rd. ed.; John Wiley & Sons, Inc.: United States of America, 2009.

(7)   Frank, T. C.; Dahuron, L.; Holden, B. S.; Prince, W. D.; Seibert, A. F.; Wilson, L. C. In *Perry's Chemical Engineers' Handbook*; 8th. ed.; Green, D. W.;Perry, R. H., Eds.; McGraw-Hill Inc.: United States of America, 2008.

(8)   Choi, Y. J.; Cho, K. W.; Cho, B. W.; Yeo, Y.-K. Optimization of the Sulfolane Extraction Plant Based on Modeling and Simulation. *Ind. Eng. Chem. Res.* **2002,** *41* (22), 5504-5509.

(9)   Kłeczek, F.; Niedziałkowski, W.; Kaczmarski, K. Design algorithm for rotating disc contactors. **1992,** *15* (1), 63-68.

D   Supporting Information for Chapter 5

Systems Analysis of High-value Chemicals and Fuels from a Waste High-Density Polyethylene Refinery. Part 2: Carbon Footprint Analysis and Regional Electricity Effects

D.1   Carbon footprint analysis (CFA) methodology

The calculation of the mass allocation factors for the different products in the refinery required the division of the plant in different blocks that comprise the outlet of products and inlet of materials. The diagram of the different section in the designed refinery is shown in Figure D-1.
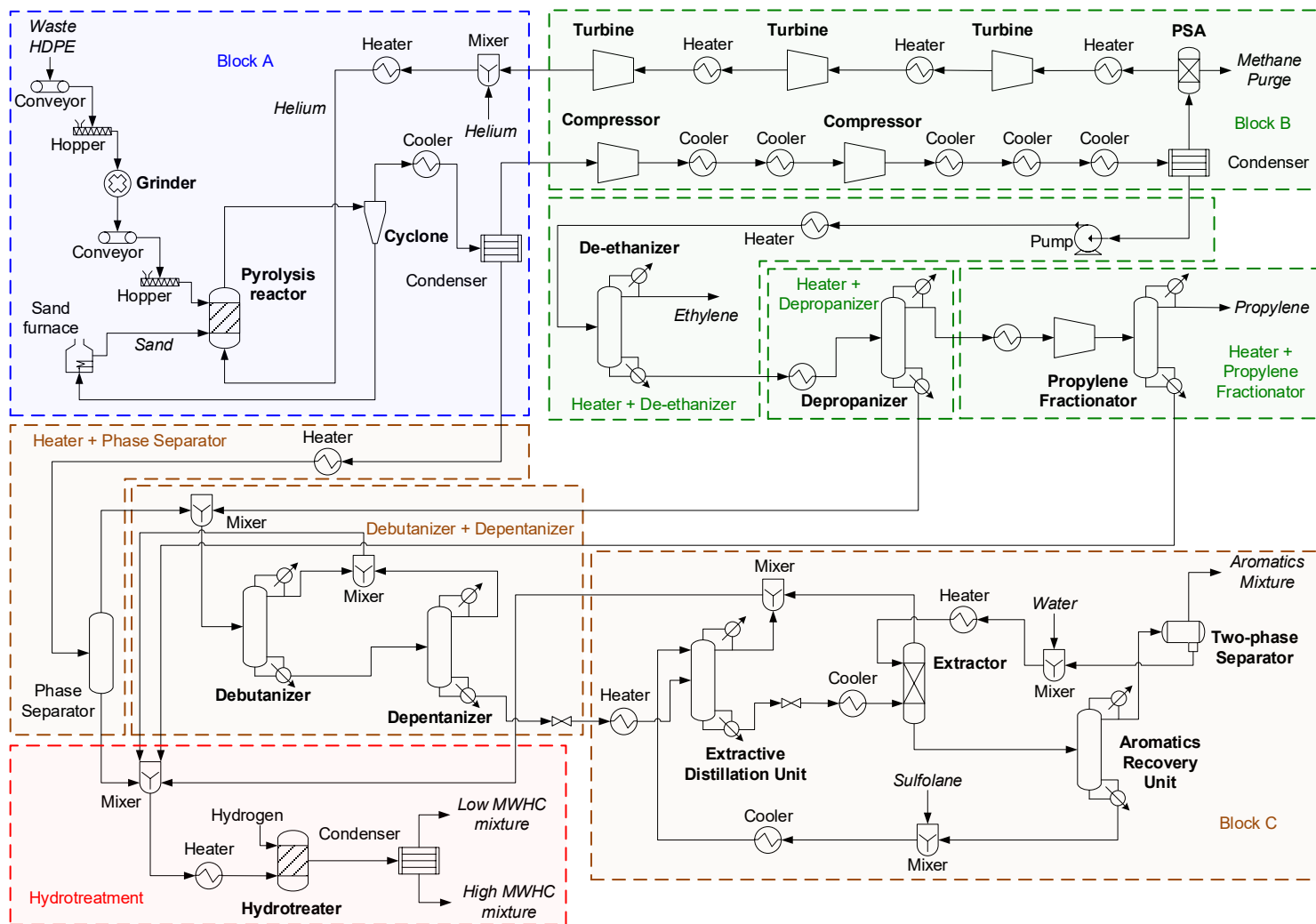
Figure D-1. Designated blocks for mass allocation factors calculation.

Section 5.2 presents the detailed explanation of the calculation of the allocation factors. This section presents a sample calculation of the methodology using the hydrotreatment block as example. Figure D-2 shows the diagram of the hydrotreatment block, which serve as a reference for the calculations.
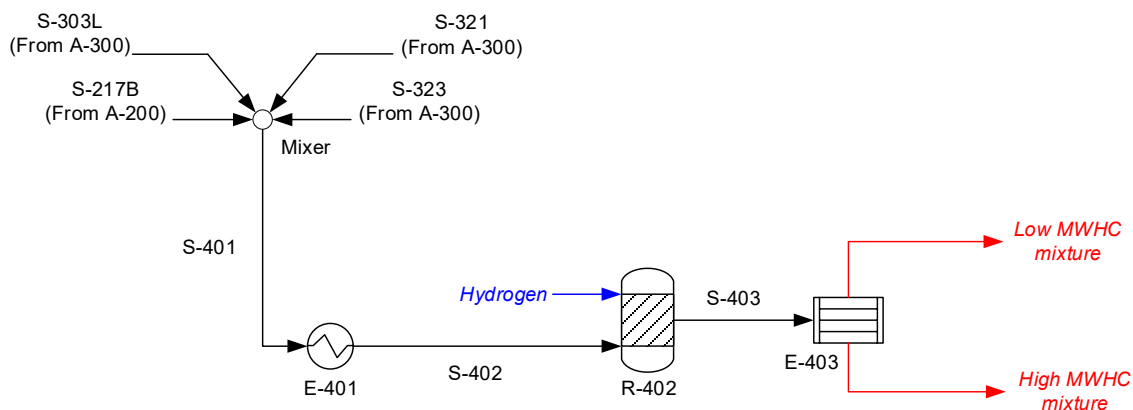
Figure D-2. Diagram of the hydrotreatment block.

As mentioned in the main manuscript, the calculations occur on a reverse mode starting from the products. In this example, the products are the low and high molecular weight hydrocarbons (MWHCs) mixture. Table D-1 shows the mass flows of the compounds in the streams of the hydrotreatment block.

Table D-1. Mass flows of each compound in the hydrotreatment block.

Compound	High MWHCs	Low MWHCs	S-403	X_{LHC}	S-402
Methane	0.00	0.02	0.02	0.9998	0.02
Ethylene	0.00	0.00	0.00	0.9996	0.39
Ethane	0.00	0.42	0.42		0.00
Propane	0.84	643.40	644.23	0.9987	638.89
Propylene	0.00	0.00	0.00	0.9988	5.10
N-butane	18.31	5788.95	5807.26	0.9984	698.06
1-butene	0.00	0.00	0.00	0.9986	4932.00
N-pentane	18.58	2502.25	2520.83	0.9951	264.31
1-pentene	0.00	0.00	0.00	0.9958	1009.75
1,4-pentadiene	0.00	0.00	0.00	0.9959	1149.70
N-hexane	15.99	940.81	956.80	0.9851	256.04
1-hexene	0.00	0.00	0.00	0.9871	394.59
1,5-hexadiene	0.00	0.00	0.00	0.9881	282.84
Benzene	1.27	70.79	72.06	0.9829	144.12
cyclohexane	1.64	76.00	77.64		0.00

N-heptane	12.31	324.70	337.01	0.9641	173.85
1-heptene	0.00	0.00	0.00	0.9685	159.88
Methylcyclohexane	3.14	77.87	81.01	0.9616	45.94
Toluene	1.43	31.48	32.91	0.9570	65.82
N-octane	14.71	173.19	187.90	0.9225	87.54
1-octene	0.00	0.00	0.00	0.9319	98.58
o-xylene	0.65	5.77	6.42	0.8989	12.84
1,2-Dimethylcyclohexane	0.49	6.29	6.78		0.00
m-xylene	0.44	4.28	4.72	0.9067	9.43
1,3-Dimethylcyclohexane	0.31	4.67	4.99		0.00
p-xylene	0.65	6.40	7.05	0.9077	14.10
1,4-Dimethylcyclohexane	0.49	6.96	7.45		0.00
Styrene	2.83	25.12	27.95	0.8994	55.90
Ethylcyclohexane	2.45	27.66	30.11		0.00
N-nonane	18.94	102.97	121.91	0.8458	41.76
1-nonene	0.00	0.00	0.00	0.8614	78.89
Indane	2.11	8.17	10.28	0.7951	20.57
Bicyclo[4,3,0]nonane	1.85	8.96	10.81		0.00
N-decane	65.06	164.47	229.53	0.7221	39.57
1-decene	0.00	0.00	0.00	0.7441	129.06
1,9-Decadiene	0.00	0.00	0.00	0.7703	57.38
Naphthalene	15.13	21.38	36.51	0.5857	73.02
Decalin	13.13	26.25	39.38		0.00
1,4-Divinylbenzene	2.18	3.18	5.36	0.5933	10.72
1,4-Diethylcyclohexane	1.83	3.94	5.78		0.00
N-undecane	68.49	87.30	155.78	0.5622	51.99
1-undecene	0.00	0.00	0.00	0.5710	102.45
1-methylnaphthalene	5.08	2.86	7.94	0.4630	15.88
1-methyldecalin	3.75	4.75	8.50		0.00
1-dodecane	0.00	0.00	0.00	0.3877	76.90
N-dodecene	77.75	46.47	124.22	0.3754	46.40
Diphenyl	5.01	1.66	6.67	0.2487	13.35
Bicyclohexyl	5.04	2.15	7.20		0.00
Acenaphthene	15.37	2.45	17.82	0.1377	17.82
Acenaphthalene	17.96	3.55	21.51	0.1652	21.51
N-tridecane	88.67	23.77	112.44	0.2124	33.48
1-tridecene	0.00	0.00	0.00	0.2284	78.09
1-tetradecane	0.00	0.00	0.00	0.1236	66.94

Compound					
N-tetradecane	90.34	12.11	102.45	0.1186	34.82
Anthracene	12.56	0.19	12.75	0.0145	12.75
1-pentadecene	0.00	0.00	0.00	0.0657	53.26
N-pentadecane	78.83	5.13	83.96	0.0613	30.19
1-hexadecene	0.00	0.00	0.00	0.0330	41.74
N-hexadecane	68.17	2.26	70.43	0.0321	28.31
1-heptadecene	0.00	0.00	0.00	0.0177	36.16
N-heptadecane	59.76	0.92	60.69	0.0152	24.22
1-octadecene	0.00	0.00	0.00	0.0088	33.09
N-octadecane	53.79	0.43	54.22	0.0079	20.86
1-nonadecene	0.00	0.00	0.00	0.0045	27.77
N-nonadecane	50.08	0.20	50.28	0.0041	22.30
1-eicosene	0.00	0.00	0.00	0.0021	44.09
N-eicosane	65.17	0.13	65.30	0.0019	20.89
N-heneicosane	21.86	0.02	21.89	0.0010	21.89
1-docosene	0.00	0.00	0.00	0.0006	24.21
N-docosane	47.18	0.03	47.20	0.0006	22.83
N-tricosane	19.80	0.01	19.81	0.0003	19.81
1-tricosene	0.00	0.00	0.00	0.0002	6.34
N-tetracosane	22.87	0.00	22.88	0.0001	16.50
N-pentacosane	9.55	0.00	9.55	0.0001	9.55
N-hexacosane	6.53	0.00	6.53	0.0000	6.53
N-heptacosane	2.92	0.00	2.92	0.0000	2.92
N-octacosane	3.04	0.00	3.04	0.0000	3.04
N-nonacosane	1.41	0.00	1.41	0.0000	1.41
Silicon dioxide	0.00	0.00	0.00		0.00
Helium	0.00	0.02	0.02	1.0000	0.02
Sulfolane	2.17	0.66	2.83	0.2326	2.83
Water	0.01	2.52	2.53	0.9964	2.53
Hydrogen	0.00	0.00	0.00	1.0000	0.00

The fraction of each compound being part of a certain product is estimated using equation (D-1):

$$xi_{jk} = \frac{Fo_{jk}}{Fi_j} \qquad \text{(D-1)}$$

where xi_{jk} is the fraction of compound j in the inlet stream i that goes into product k, Fo_{jk} is the mass flow of compound j in product k in the outlet or product stream o in kg/h, and Fi_j is the mass flow of compound j in the inlet stream i of the separator in kg/h. For a chemical species that does not participate in the hydrotreatment reactions like water, the

fraction of water being part of the low MWHCs product in stream S-402 would be given by

$$xi_{jk} = \frac{2.52\ kg/h}{2.83\ kg/h} = 0.9964$$

where i refers to stream S-402, j to water, and k to the low MWHCs product.

The calculation of fractions of chemical species that undergo hydrotreatment, like 1-pentene and 1,4-pentadiene, contained in the reactor feed considered the mass flows if the reaction would not have occurred (see Table D-2). Thus, the fractions for each product and reactant involved in the reaction would be

n-pentane:
$$xi_{jk} = \frac{263.01\ kg/h}{264.31\ kg/h} = 0.9951$$

1-pentene:
$$xi_{jk} = \frac{1005.47\ kg/h}{1009.75\ kg/h} = 0.9958$$

1,4-pentadiene:
$$xi_{jk} = \frac{1144.96\ kg/h}{1149.70\ kg/h} = 0.9959$$

where i refers to stream S-402, j to the analyzed compound (n-pentane, 1-pentene, or 1,4-pentadiene), and k to the low MWHCs product.

Table D-2. Mass flows (kg/h) of C10 aliphatics through the hydrotreatment block without reaction.

Compound	High MWHCs	Low MWHCs	S-403	X_{LHC}	S-402
n-pentane	1.30	263.01	264.31	0.9951	264.31
1-pentene	4.28	1005.47	1009.75	0.9958	1009.75
1,4-pentadiene	4.74	1144.96	1149.70	0.9959	1149.70

Table D-1 also shows the fraction of each compound in stream S-402 that is part of the low MWHCs (X_{LHC}). With this information and equations (D-2) and (D-3), it is possible to obtain the mass flow of each compound in every inlet stream of the mixer that will be part of the low MWHCs product. Equations (D-2) and (D-3) are as follows

$$xs_{jk} = xo_{jk} \tag{D-2}$$

284

where xs_{jk} is the fraction of compound j in the inlet stream s that goes into product k and xo_{jk} is the fraction of compound j in the outlet stream that goes into product k.

$$Fs_{jk} = xs_{jk} \cdot Fs_j \tag{D-3}$$

where Fs_{jk} is the mass flow of compound j going to product k in the inlet stream s in kg/h and Fs_j is the mass flow of compound j in the inlet stream s in kg/h. Then considering the compounds used in our example the fractions of water, n-pentane, 1-pentene, and 1,4-pentadiene being part of the low MWHCs product are 0.9964, 0.9951, 0.9958, and 0.9959, respectively. These fractions are the same in streams S-217B, S-303L, S-321, and S-323 (inlet streams of the mixer). Table D-3 shows the mass flows of these compounds in these inlet streams.

Table D-3. Mass flows (kg/h) of n-pentane, 1-pentene, 1,4-pentadiene, and water in the inlet streams of the mixer of the hydrotreatment block.

Compound	S-217B	S-303L	S-321	S-323
n-pentane	0.01	0.08	256.90	7.32
1-pentene	0.08	0.22	998.29	11.15
1,4-pentadiene	0.16	0.21	1135.79	13.54
water	0.00	0.00	0.00	2.53

Applying equation (D-3) on each compound results in the amount that will be part of the low MWHCs product as shown below

For stream S-217B

n-pentane: $\qquad Fs_{jk} = xs_{jk} \cdot Fs_j = 0.9951 \cdot 0.01 = 0.01\ kg/h$

1-pentene: $\qquad Fs_{jk} = xs_{jk} \cdot Fs_j = 0.9958 \cdot 0.08 = 0.08\ kg/h$

1,4-pentadiene: $\qquad Fs_{jk} = xs_{jk} \cdot Fs_j = 0.9959 \cdot 0.16 = 0.16\ kg/h$

Water: $\qquad Fs_{jk} = xs_{jk} \cdot Fs_j = 0.9964 \cdot 0.00 = 0.00\ kg/h$

For stream S-303L

n-pentane: $\qquad Fs_{jk} = xs_{jk} \cdot Fs_j = 0.9951 \cdot 0.08 = 0.08\ kg/h$

1-pentene: $\qquad Fs_{jk} = xs_{jk} \cdot Fs_j = 0.9958 \cdot 0.22 = 0.22\ kg/h$

1,4-pentadiene: $\qquad Fs_{jk} = xs_{jk} \cdot Fs_j = 0.9959 \cdot 0.21 = 0.21\ kg/h$

Water: $\qquad Fs_{jk} = xs_{jk} \cdot Fs_j = 0.9964 \cdot 0.00 = 0.00\ kg/h$

For stream S-321

n-pentane: $\qquad Fs_{jk} = xs_{jk} \cdot Fs_j = 0.9951 \cdot 256.90 = 255.64\ kg/h$

1-pentene: $\qquad Fs_{jk} = xs_{jk} \cdot Fs_j = 0.9958 \cdot 998.29 = 994.06\ kg/h$

| 1,4-pentadiene: | $Fs_{jk} = xs_{jk} \cdot Fs_j = 0.9959 \cdot 1135.79 = 1131.11\ kg/h$ |
| Water: | $Fs_{jk} = xs_{jk} \cdot Fs_j = 0.9964 \cdot 0.00 = 0.00\ kg/h$ |

For stream S-323

n-pentane:	$Fs_{jk} = xs_{jk} \cdot Fs_j = 0.9951 \cdot 7.32 = 7.29\ kg/h$
1-pentene:	$Fs_{jk} = xs_{jk} \cdot Fs_j = 0.9958 \cdot 11.15 = 11.10\ kg/h$
1,4-pentadiene:	$Fs_{jk} = xs_{jk} \cdot Fs_j = 0.9959 \cdot 13.54 = 13.49\ kg/h$
Water:	$Fs_{jk} = xs_{jk} \cdot Fs_j = 0.9964 \cdot 2.54 = 2.52\ kg/h$

When this equation is applied for each compound in the streams, the mass flow of low MWHCs product in each stream can be obtained through equation (D-4)

$$Fs_k = \sum_{j}^{n} Fs_{jk} \qquad (D\text{-}4)$$

where Fs_k is the mass flow of compound k in the inlet stream s in kg/h. The results for each inlet stream of the mixer are shown in Table S.4. The sum of the mass flows of each compound at every stream (final row of each column) represents its total flow of low MWHCs.

Table D-4. Mass flow (kg/h) per compounds being part of the low MWHCs product in the inlet streams of the mixer.

Compound	S-217B	S-303L	S-321	S-323
Methane	0.00	0.00	0.02	0.00
Ethylene	0.00	0.00	0.39	0.00
Ethane	0.00	0.00	0.00	0.00
Propane	635.07	0.00	2.98	0.00
Propylene	1.48	0.02	3.60	0.00
N-butane	9.83	0.03	687.07	0.00
1-butene	188.83	0.18	4736.03	0.00
N-pentane	0.01	0.08	255.64	7.29
1-pentene	0.08	0.22	994.06	11.10
1,4-pentadiene	0.16	0.21	1131.11	13.49
N-hexane	0.00	0.43	30.05	221.73
1-hexene	0.00	0.49	100.37	288.66
1,5-hexadiene	0.00	0.29	99.44	179.74
Benzene	0.00	0.92	19.97	120.75

cyclohexane	0.00	0.00	0.00	0.00
N-heptane	0.00	1.48	0.04	166.08
1-heptene	0.00	1.11	0.11	153.62
Methylcyclohexane	0.00	0.45	0.01	43.72
Toluene	0.00	2.21	0.01	60.77
N-octane	0.00	3.32	0.00	77.44
1-octene	0.00	3.37	0.00	88.51
o-xylene	0.00	1.75	0.00	9.79
1,2-Dimethylcyclohexane	0.00	0.00	0.00	0.00
m-xylene	0.00	0.95	0.00	7.60
1,3-Dimethylcyclohexane	0.00	0.00	0.00	0.00
p-xylene	0.00	1.40	0.00	11.40
1,4- Dimethylcyclohexane	0.00	0.00	0.00	0.00
Styrene	0.00	11.81	0.00	38.47
Ethylcyclohexane	0.00	0.00	0.00	0.00
N-nonane	0.00	4.99	0.00	30.33
1-nonene	0.00	8.96	0.00	58.99
Indane	0.00	5.05	0.00	11.30
Bicyclo[4,3,0]nonane	0.00	0.00	0.00	0.00
N-decane	0.00	8.09	0.00	20.48
1-decene	0.00	26.14	0.00	69.89
1,9-Decadiene	0.00	11.26	0.00	32.94
Naphthalene	0.00	22.21	0.00	20.56
Decalin	0.00	0.00	0.00	0.00
1,4-Divinylbenzene	0.00	3.50	0.00	2.86
1,4-Diethylcyclohexane	0.00	0.00	0.00	0.00
N-undecane	0.00	12.05	0.00	17.18
1-undecene	0.00	24.57	0.00	33.93
1-methylnaphthalene	0.00	4.56	0.00	2.79
1-methyldecalin	0.00	0.00	0.00	0.00
1-dodecane	0.00	16.42	0.00	13.39
N-dodecene	0.00	9.57	0.00	7.85
Diphenyl	0.00	2.26	0.00	1.06
Bicyclohexyl	0.00	0.00	0.00	0.00
Acenaphthene	0.00	1.92	0.00	0.54
Acenaphthalene	0.00	2.67	0.00	0.88
N-tridecane	0.00	4.86	0.00	2.25
1-tridecene	0.00	11.89	0.00	5.94
1-tetradecane	0.00	6.29	0.00	1.99
N-tetradecane	0.00	3.16	0.00	0.97
Anthracene	0.00	0.17	0.00	0.01

1-pentadecene	0.00	2.90	0.00	0.59
N-pentadecane	0.00	1.54	0.00	0.31
1-hexadecene	0.00	1.22	0.00	0.16
N-hexadecane	0.00	0.81	0.00	0.10
1-heptadecene	0.00	0.59	0.00	0.05
N-heptadecane	0.00	0.34	0.00	0.03
1-octadecene	0.00	0.28	0.00	0.02
N-octadecane	0.00	0.16	0.00	0.01
1-nonadecene	0.00	0.12	0.00	0.00
N-nonadecane	0.00	0.09	0.00	0.00
1-eicosene	0.00	0.09	0.00	0.00
N-eicosane	0.00	0.04	0.00	0.00
N-heneicosane	0.00	0.02	0.00	0.00
1-docosene	0.00	0.01	0.00	0.00
N-docosane	0.00	0.01	0.00	0.00
N-tricosane	0.00	0.01	0.00	0.00
1-tricosene	0.00	0.00	0.00	0.00
N-tetracosane	0.00	0.00	0.00	0.00
N-pentacosane	0.00	0.00	0.00	0.00
N-hexacosane	0.00	0.00	0.00	0.00
N-heptacosane	0.00	0.00	0.00	0.00
N-octacosane	0.00	0.00	0.00	0.00
N-nonacosane	0.00	0.00	0.00	0.00
Silicon dioxide	0.00	0.00	0.00	0.00
Helium	0.00	0.00	0.02	0.00
Sulfolane	0.00	0.00	0.00	0.66
Water	0.00	0.00	0.00	2.52
Hydrogen	0.00	0.00	0.00	0.00
Total	835.47	229.57	8060.92	1840.76

Table D-5. Mass allocation factors for each product in the designated blocks.

Block	Ethylene	Propylene	Aromatics	Low MWHCs	High MWHCs
CST	0.2002	0.1435	0.0394	0.5617	0.0552
Block A	0.2002	0.1435	0.0394	0.5617	0.0552
Block B	0.2002	0.1435	0.0394	0.5617	0.0552
Heater + De-ethanizer	0.2196	0.1574	0.0342	0.5831	0.0057
Heater + Depropanizer	-	0.2017	0.0438	0.7472	0.0073
Heater + Propylene fractionator	-	0.77	-	0.2297	0.0003
Heater + phase separator	-	-	0.0928	0.3415	0.5657
Debutanizer + Depentanizer	-	-	0.0700	0.9013	0.0287
Block C	-	-	0.02654	0.6327	0.1019
Hydrotreatment	-	-	-	0.9095	0.0905
CST: Collection, separation at municipal recovery facility, and transportation.					

D.2 Life cycle inventory

Tables show the Inventory data for scenarios BC, HI-1, and H-2, respectively.

Table D-6. Life cycle inventory for the base case (BC) scenario. Basis: one hour of operation.

Section	Block	Input	Ecoprofile	Amount
CST	Collection	Fuel for collection	Diesel RoW| market for | APOS, S with combustion	248.48 kg
	Separation at MRF	Electricity for facility operation	Electricity, high voltage US| market group for | APOS, S	286.67 kWh
		Heating for facility operation	Heat, district or industrial, natural gas RoW| market for heat, district or industrial, natural gas | APOS, S	541.67 MJ
		Diesel for facility operation	Diesel RoW| market for | APOS, S with combustion	12.38 kg
		Gasoline for facility operation	Petrol, low-sulfur RoW| market for | APOS, S with combustion	2.02 kg
	Transportation	Truck transportation for 50 km	Transport, freight, lorry >32 metric ton, EURO6 RoW| transport, freight, lorry >32 metric ton, EURO6 | APOS, S	1041.67 tkm
A-100	Block A	Grinder/Schredder (GR-101)	Electricity, high voltage US| market group for | APOS, S	6,889.45 kWh
		Sand Heater (E-105)	Heat, district or industrial, natural gas RoW| market for heat, district or industrial, natural gas | APOS, S	9,944.72 MJ
		Condenser cooler (E-107A)	Water, completely softened, from decarbonised water, at user GLO| market for | APOS, S	80,025.23 kg
		Electricity for refrigeration cycle (E-107B)	Electricity, high voltage US| market group for | APOS, S	59.13 kWh
		Water for refrigeration cycle (E-107B)	Water, completely softened, from decarbonised water, at user GLO| market for | APOS, S	1,960.24 kg

		Helium Heater 4 (E-106)	Heat, district or industrial, natural gas RoW| market for heat, district or industrial, natural gas | APOS, S	35,905.32 MJ
		Make-up helium	Helium GLO| market for | APOS, S	0.89 kg
A-200	Block B	Compresor electricity (C-201 & C-203)	Electricity, high voltage US| market group for | APOS, S	3,227.45 kWh
		Condenser cooler (E-202A)	Water, completely softened, from decarbonised water, at user GLO| market for | APOS, S	7,910.11 kg
		Electricity for refrigeration cycle (E-202B)	Electricity, high voltage US| market group for | APOS, S	1,516.04 kWh
		Cooling water for refrigeration cycle (E-202B)	Water, completely softened, from decarbonised water, at user GLO| market for | APOS, S	15,302.38 kg
		Condenser cooler (E-204A)	Water, completely softened, from decarbonised water, at user GLO| market for | APOS, S	5,014.55 kg
		Electricity for refrigeration cycle (E-204B to D)	Electricity, high voltage US| market group for | APOS, S	14,619.30 kWh
		Cooling water for refrigeration cycle (E-204B to D)	Water, completely softened, from decarbonised water, at user GLO| market for | APOS, S	88,411.68 kg
		Helium heater 1 (E-212)	Heat, district or industrial, natural gas RoW| market for heat, district or industrial, natural gas | APOS, S	8,556.17 MJ
		Helium heater 2 (E-214)	Heat, district or industrial, natural gas RoW| market for heat, district or industrial, natural gas | APOS, S	1,434.58 MJ
		Helium heater 3 (E-216)	Heat, district or industrial, natural gas RoW| market for heat, district or industrial, natural gas | APOS, S	3,496.46 MJ
	H + DE	Pump electricity (P-205)	Electricity, high voltage US| market group for | APOS, S	22.70 kWh

		C2-C4 heater (E-206)	Heat, district or industrial, natural gas RoW| market for heat, district or industrial, natural gas | APOS, S	4,755.78 MJ
		Electricity for refrigeration cycle (T-207)	Electricity, high voltage US| market group for | APOS, S	494.93 kWh
		Cooling water for refrigeration cycle (T-207)	Water, completely softened, from decarbonised water, at user GLO| market for | APOS, S	5,654.85 kg
		Deethanizer reboiler (T-207)	Heat, district or industrial, natural gas RoW| market for heat, district or industrial, natural gas | APOS, S	6,305.94 MJ
	H + DP	C3-C4 cooler (E-208)	Water, completely softened, from decarbonised water, at user GLO| market for | APOS, S	342.68 kg
		Depropanizer condenser (T-209)	Water, completely softened, from decarbonised water, at user GLO| market for | APOS, S	6,768.80 kg
		Depropanizer reboiler (T-209)	Heat, district or industrial, natural gas RoW| market for heat, district or industrial, natural gas | APOS, S	6,014.65 MJ
	H + PF	C3 heater (E-210)	Heat, district or industrial, natural gas RoW| market for heat, district or industrial, natural gas | APOS, S	1,156.97 MJ
		Compresor electricity (C-218)	Electricity, high voltage US| market group for | APOS, S	5.71 kWh
		Propylene Fractionator condenser (T-211)	Water, completely softened, from decarbonised water, at user GLO| market for | APOS, S	23,758.81 kg
		Propylene Fractionator reboiler (T-211)	Heat, district or industrial, natural gas RoW| market for heat, district or industrial, natural gas | APOS, S	18,767.24 MJ

A-300	H + PS	C5-C29 heater (E-301)	Heat, district or industrial, natural gas RoW| market for heat, district or industrial, natural gas | APOS, S	928.76 MJ
	DB + DP	Debutanizer condenser (T-305)	Water, completely softened, from decarbonised water, at user GLO| market for | APOS, S	7,196.45 kg
		Debutanizer reboiler (T-305)	Heat, district or industrial, natural gas RoW| market for heat, district or industrial, natural gas | APOS, S	4,578.75 MJ
		Depentanizer condenser (T-306)	Water, completely softened, from decarbonised water, at user GLO| market for | APOS, S	2,094.59 kg
		Depentanizer reboiler (T-306)	Heat, district or industrial, natural gas RoW| market for heat, district or industrial, natural gas | APOS, S	1,604.10 MJ
	Block C	C6-C12 heater (E-307)	Heat, district or industrial, natural gas RoW| market for heat, district or industrial, natural gas | APOS, S	960.51 MJ
		Extractive Distillation condenser (T-308)	Water, completely softened, from decarbonised water, at user GLO| market for | APOS, S	1,590.42 kg
		Extractive Distillation reboiler (T-308)	Heat, district or industrial, natural gas RoW| market for heat, district or industrial, natural gas | APOS, S	575.14 MJ
		Sulfolane for extraction (T-308)	Solvent, organic GLO| market for | APOS, S	5.66 kg
		C6-C12 cooler (E-309)	Water, completely softened, from decarbonised water, at user GLO| market for | APOS, S	1,823.24 kg
		Aromatics column condenser (T-312)	Water, completely softened, from decarbonised water, at user GLO| market for | APOS, S	1,887.57 kg

		Aromatics column reboiler (T-312)	Heat, district or industrial, natural gas RoW| market for heat, district or industrial, natural gas | APOS, S	3,848.92 MJ
		Water heater (E-311)	Heat, district or industrial, natural gas RoW| market for heat, district or industrial, natural gas | APOS, S	70.50 MJ
		Water for extraction (T-310)	Water, deionised, from tap water, at user RoW| market for water, deionised, from tap water, at user | APOS, S	3.50 kg
		Water for 2-phase separation (V-313)	Water, completely softened, from decarbonised water, at user GLO| market for | APOS, S	42.65 kg
		Sulfolane cooler (E-315)	Water, completely softened, from decarbonised water, at user GLO| market for | APOS, S	1,675.75 kg
A-400	Hydrotreatment	Aliphatics heater (E-401)	Heat, district or industrial, natural gas RoW| market for heat, district or industrial, natural gas | APOS, S	5,303.90 MJ
		Hydrogen (R-402)	Hydrogen (reformer) E	329.55 kg
		Condenser cooling (E-403)	Water, completely softened, from decarbonised water, at user GLO| market for | APOS, S	1,925.56 kg
		Steam generation	Steam, in chemical industry RoW| production | APOS, S	8,461.24 kg
CST: Collection, separation, and transportation, H + DE: heater + De-ethanizer, H+DP: Heatre + depropanizer, H+PF: Heater + Propylene Fractionator, H+PS: Heater + phase separator, DB+DP: Debutanizer + depentanizer.				

Table D-7. Life cycle inventory for the heat integrated scenario 1 (HI-1). Basis: one hour of operation.

Section	Block	Input	Ecoprofile	Amount
CST	Collection	Fuel for collection	Diesel RoW| market for | APOS, S with combustion	248.48 kg
	Separation at MRF	Electricity for facility operation	Electricity, high voltage US| market group for | APOS, S	286.67 kWh
		Heating for facility operation	Heat, district or industrial, natural gas RoW| market for heat, district or industrial, natural gas | APOS, S	541.67 MJ
		Diesel for facility operation	Diesel RoW| market for | APOS, S with combustion	12.38 kg
		Gasoline for facility operation	Petrol, low-sulfur RoW| market for | APOS, S with combustion	2.02 kg
	Transportation	Truck transportation for 50 km	Transport, freight, lorry >32 metric ton, EURO6 RoW| transport, freight, lorry >32 metric ton, EURO6 | APOS, S	1041.67 tkm
A-100	Block A	Grinder/Schredder (GR-101)	Electricity, high voltage US| market group for | APOS, S	6,889.45 kWh
		Sand Heater (E-105)	Heat, district or industrial, natural gas RoW| market for heat, district or industrial, natural gas | APOS, S	9,944.72 MJ
		Condenser cooler (E-107A)	Water, completely softened, from decarbonised water, at user GLO| market for | APOS, S	30,005.38 kg
		Electricity for refrigeration cycle (E-107B)	Electricity, high voltage US| market group for | APOS, S	-
		Water for refrigeration cycle (E-107B)	Water, completely softened, from decarbonised water, at user GLO| market for | APOS, S	-

		Helium Heater 4 (E-106)	Heat, district or industrial, natural gas RoW| market for heat, district or industrial, natural gas | APOS, S	531.10 MJ
		Make-up helium	Helium GLO| market for | APOS, S	0.89 kg
A-200	Block B	Compresor electricity (C-201 & C-203)	Electricity, high voltage US| market group for | APOS, S	3,227.45 kWh
		Condenser cooler (E-202A)	Water, completely softened, from decarbonised water, at user GLO| market for | APOS, S	7,442.67 kg
		Electricity for refrigeration cycle (E-202B)	Electricity, high voltage US| market group for | APOS, S	-
		Cooling water for refrigeration cycle (E-202B)	Water, completely softened, from decarbonised water, at user GLO| market for | APOS, S	-
		Condenser cooler (E-204A)	Water, completely softened, from decarbonised water, at user GLO| market for | APOS, S	5,723.72 kg
		Electricity for refrigeration cycle (E-204B to D)	Electricity, high voltage US| market group for | APOS, S	12,740.01 kWh
		Cooling water for refrigeration cycle (E-204B to D)	Water, completely softened, from decarbonised water, at user GLO| market for | APOS, S	69,637.57 kg
		Helium heater 1 (E-212)	Heat, district or industrial, natural gas RoW| market for heat, district or industrial, natural gas | APOS, S	-
		Helium heater 2 (E-214)	Heat, district or industrial, natural gas RoW| market for heat, district or industrial, natural gas | APOS, S	-
		Helium heater 3 (E-216)	Heat, district or industrial, natural gas RoW| market for heat, district or industrial, natural gas | APOS, S	-
	H + DE	Pump electricity (P-205)	Electricity, high voltage US| market group for | APOS, S	22.70 kWh

		C2-C4 heater (E-206)	Heat, district or industrial, natural gas RoW| market for heat, district or industrial, natural gas | APOS, S	-
		Electricity for refrigeration cycle (T-207)	Electricity, high voltage US| market group for | APOS, S	494.93 kWh
		Cooling water for refrigeration cycle (T-207)	Water, completely softened, from decarbonised water, at user GLO| market for | APOS, S	5,654.85 kg
		Deethanizer reboiler (T-207)	Heat, district or industrial, natural gas RoW| market for heat, district or industrial, natural gas | APOS, S	6,305.94 MJ
	H + DP	C3-C4 cooler (E-208)	Water, completely softened, from decarbonised water, at user GLO| market for | APOS, S	342.68 kg
		Depropanizer condenser (T-209)	Water, completely softened, from decarbonised water, at user GLO| market for | APOS, S	6,768.80 kg
		Depropanizer reboiler (T-209)	Heat, district or industrial, natural gas RoW| market for heat, district or industrial, natural gas | APOS, S	6,014.65 MJ
	H + PF	C3 heater (E-210)	Heat, district or industrial, natural gas RoW| market for heat, district or industrial, natural gas | APOS, S	-
		Compresor electricity (C-218)	Electricity, high voltage US| market group for | APOS, S	5.71 kWh
		Propylene Fractionator condenser (T-211)	Water, completely softened, from decarbonised water, at user GLO| market for | APOS, S	23,758.81 kg
		Propylene Fractionator reboiler (T-211)	Heat, district or industrial, natural gas RoW| market for heat, district or industrial, natural gas | APOS, S	-

A-300	H + PS	C5-C29 heater (E-301)	Heat, district or industrial, natural gas RoW| market for heat, district or industrial, natural gas | APOS, S	-
	DB + DP	Debutanizer condenser (T-305)	Water, completely softened, from decarbonised water, at user GLO| market for | APOS, S	7,196.45 kg
		Debutanizer reboiler (T-305)	Heat, district or industrial, natural gas RoW| market for heat, district or industrial, natural gas | APOS, S	4,578.75 MJ
		Depentanizer condenser (T-306)	Water, completely softened, from decarbonised water, at user GLO| market for | APOS, S	2,094.59 kg
		Depentanizer reboiler (T-306)	Heat, district or industrial, natural gas RoW| market for heat, district or industrial, natural gas | APOS, S	1,604.10 MJ
	Block C	C6-C12 heater (E-307)	Heat, district or industrial, natural gas RoW| market for heat, district or industrial, natural gas | APOS, S	-
		Extractive Distillation condenser (T-308)	Water, completely softened, from decarbonised water, at user GLO| market for | APOS, S	1,590.42 kg
		Extractive Distillation reboiler (T-308)	Heat, district or industrial, natural gas RoW| market for heat, district or industrial, natural gas | APOS, S	575.14 MJ
		Sulfolane for extraction (T-308)	Solvent, organic GLO| market for | APOS, S	5.66 kg
		C6-C12 cooler (E-309)	Water, completely softened, from decarbonised water, at user GLO| market for | APOS, S	357.02 kg
		Armatics column condenser (T-312)	Water, completely softened, from decarbonised water, at user GLO| market for | APOS, S	1,887.57 kg

		Aromatics column reboiler (T-312)	Heat, district or industrial, natural gas RoW| market for heat, district or industrial, natural gas | APOS, S	3,848.92 MJ
		Water heater (E-311)	Heat, district or industrial, natural gas RoW| market for heat, district or industrial, natural gas | APOS, S	-
		Water for extraction (T-310)	Water, deionised, from tap water, at user RoW| market for water, deionised, from tap water, at user | APOS, S	3.50 kg
		Water for 2-phase separation (V-313)	Water, completely softened, from decarbonised water, at user GLO| market for | APOS, S	42.65 kg
		Sulfolane cooler (E-315)	Water, completely softened, from decarbonised water, at user GLO| market for | APOS, S	-
A-400	Hydrotreatment	Aliphatics heater (E-401)	Heat, district or industrial, natural gas RoW| market for heat, district or industrial, natural gas | APOS, S	-
		Hydrogen (R-402)	Hydrogen (reformer) E	329.55 kg
		Condenser cooling (E-403)	Water, completely softened, from decarbonised water, at user GLO| market for | APOS, S	1,925.56 kg
		Steam generation	Steam, in chemical industry RoW| production | APOS, S	687.96 kg
CST: Collection, separation, and transportation, H + DE: heater + De-ethanizer, H+DP: Heatre + depropanizer, H+PF: Heater + Propylene Fractionator, H+PS: Heater + phase separator, DB+DP: Debutanizer + depentanizer.				

Table D-8. Life cycle inventory for the heat integrated scenario 2 (HI-2). Basis: one hour of operation.

Section	Block	Input	Ecoprofile	Amount
CST	Collection	Fuel for collection	Diesel RoW| market for | APOS, S with combustion	248.48 kg
	Separation at MRF	Electricity for facility operation	Electricity, high voltage US| market group for | APOS, S	286.67 kWh
		Heating for facility operation	Heat, district or industrial, natural gas RoW| market for heat, district or industrial, natural gas | APOS, S	541.67 MJ
		Diesel for facility operation	Diesel RoW| market for | APOS, S with combustion	12.38 kg
		Gasoline for facility operation	Petrol, low-sulfur RoW| market for | APOS, S with combustion	2.02 kg
	Transportation	Truck transportation for 50 km	Transport, freight, lorry >32 metric ton, EURO6 RoW| transport, freight, lorry >32 metric ton, EURO6 | APOS, S	1041.67 tkm
A-100	Block A	Grinder/Schredder (GR-101)	Electricity, high voltage US| market group for | APOS, S	6,889.45 kWh
		Sand Heater (E-105)	Heat, district or industrial, natural gas RoW| market for heat, district or industrial, natural gas | APOS, S	9,944.72 MJ
		Condenser cooler (E-107A)	Water, completely softened, from decarbonised water, at user GLO| market for | APOS, S	30,005.38 kg
		Electricity for refrigeration cycle (E-107B)	Electricity, high voltage US| market group for | APOS, S	-
		Water for refrigeration cycle (E-107B)	Water, completely softened, from decarbonised water, at user GLO| market for | APOS, S	-

		Helium Heater 4 (E-106)	Heat, district or industrial, natural gas RoW| market for heat, district or industrial, natural gas | APOS, S	531.10 MJ
		Make-up helium	Helium GLO| market for | APOS, S	0.89 kg
A-200	Block B	Compresor electricity (C-201 & C-203)	Electricity, high voltage US| market group for | APOS, S	3,227.45 kWh
		Condenser cooler (E-202A)	Water, completely softened, from decarbonised water, at user GLO| market for | APOS, S	7,442.67 kg
		Electricity for refrigeration cycle (E-202B)	Electricity, high voltage US| market group for | APOS, S	-
		Cooling water for refrigeration cycle (E-202B)	Water, completely softened, from decarbonised water, at user GLO| market for | APOS, S	-
		Condenser cooler (E-204A)	Water, completely softened, from decarbonised water, at user GLO| market for | APOS, S	5,723.72 kg
		Electricity for refrigeration cycle (E-204B to D)	Electricity, high voltage US| market group for | APOS, S	12,740.01 kWh
		Cooling water for refrigeration cycle (E-204B to D)	Water, completely softened, from decarbonised water, at user GLO| market for | APOS, S	69,637.57 kg
		Helium heater 1 (E-212)	Heat, district or industrial, natural gas RoW| market for heat, district or industrial, natural gas | APOS, S	-
		Helium heater 2 (E-214)	Heat, district or industrial, natural gas RoW| market for heat, district or industrial, natural gas | APOS, S	-
		Helium heater 3 (E-216)	Heat, district or industrial, natural gas RoW| market for heat, district or industrial, natural gas | APOS, S	-
	H + DE	Pump electricity (P-205)	Electricity, high voltage US| market group for | APOS, S	22.70 kWh

		C2-C4 heater (E-206)	Heat, district or industrial, natural gas RoW| market for heat, district or industrial, natural gas | APOS, S	-
		Electricity for refrigeration cycle (T-207)	Electricity, high voltage US| market group for | APOS, S	494.93 kWh
		Cooling water for refrigeration cycle (T-207)	Water, completely softened, from decarbonised water, at user GLO| market for | APOS, S	5,654.85 kg
		Deethanizer reboiler (T-207)	Heat, district or industrial, natural gas RoW| market for heat, district or industrial, natural gas | APOS, S	6,305.94 MJ
	H + DP	C3-C4 cooler (E-208)	Water, completely softened, from decarbonised water, at user GLO| market for | APOS, S	342.68 kg
		Depropanizer condenser (T-209)	Water, completely softened, from decarbonised water, at user GLO| market for | APOS, S	6,768.80 kg
		Depropanizer reboiler (T-209)	Heat, district or industrial, natural gas RoW| market for heat, district or industrial, natural gas | APOS, S	6,014.65 MJ
	H + PF	C3 heater (E-210)	Heat, district or industrial, natural gas RoW| market for heat, district or industrial, natural gas | APOS, S	-
		Compresor electricity (C-218)	Electricity, high voltage US| market group for | APOS, S	5.71 kWh
		Propylene Fractionator condenser (T-211)	Water, completely softened, from decarbonised water, at user GLO| market for | APOS, S	23,758.81 kg
		Propylene Fractionator reboiler (T-211)	Heat, district or industrial, natural gas RoW| market for heat, district or industrial, natural gas | APOS, S	18,767.24 MJ

A-300	H + PS	C5-C29 heater (E-301)	Heat, district or industrial, natural gas RoW| market for heat, district or industrial, natural gas | APOS, S	-
	DB + DP	Debutanizer condenser (T-305)	Water, completely softened, from decarbonised water, at user GLO| market for | APOS, S	7,196.45 kg
		Debutanizer reboiler (T-305)	Heat, district or industrial, natural gas RoW| market for heat, district or industrial, natural gas | APOS, S	4,578.75 MJ
		Depentanizer condenser (T-306)	Water, completely softened, from decarbonised water, at user GLO| market for | APOS, S	2,094.59 kg
		Depentanizer reboiler (T-306)	Heat, district or industrial, natural gas RoW| market for heat, district or industrial, natural gas | APOS, S	1,604.10 MJ
	Block C	C6-C12 heater (E-307)	Heat, district or industrial, natural gas RoW| market for heat, district or industrial, natural gas | APOS, S	-
		Extractive Distillation condenser (T-308)	Water, completely softened, from decarbonised water, at user GLO| market for | APOS, S	1,590.42 kg
		Extractive Distillation reboiler (T-308)	Heat, district or industrial, natural gas RoW| market for heat, district or industrial, natural gas | APOS, S	575.14 MJ
		Sulfolane for extraction (T-308)	Solvent, organic GLO| market for | APOS, S	5.66 kg
		C6-C12 cooler (E-309)	Water, completely softened, from decarbonised water, at user GLO| market for | APOS, S	357.02 kg
		Armatics column condenser (T-312)	Water, completely softened, from decarbonised water, at user GLO| market for | APOS, S	1,887.57 kg

		Aromatics column reboiler (T-312)	Heat, district or industrial, natural gas RoW| market for heat, district or industrial, natural gas | APOS, S	3,848.92 MJ
		Water heater (E-311)	Heat, district or industrial, natural gas RoW| market for heat, district or industrial, natural gas | APOS, S	-
		Water for extraction (T-310)	Water, deionised, from tap water, at user RoW| market for water, deionised, from tap water, at user | APOS, S	3.50 kg
		Water for 2-phase separation (V-313)	Water, completely softened, from decarbonised water, at user GLO| market for | APOS, S	42.65 kg
		Sulfolane cooler (E-315)	Water, completely softened, from decarbonised water, at user GLO| market for | APOS, S	-
A-400	Hydrotreatment	Aliphatics heater (E-401)	Heat, district or industrial, natural gas RoW| market for heat, district or industrial, natural gas | APOS, S	-
		Hydrogen (R-402)	Hydrogen (reformer) E	329.55 kg
		Condenser cooling (E-403)	Water, completely softened, from decarbonised water, at user GLO| market for | APOS, S	1,925.56 kg
		Steam generation	Steam, in chemical industry RoW| production | APOS, S	8,461.24 kg
CST: Collection, separation, and transportation, H + DE: heater + De-ethanizer, H+DP: Heatre + depropanizer, H+PF: Heater + Propylene Fractionator, H+PS: Heater + phase separator, DB+DP: Debutanizer + depentanizer.				

Table D-9. Product yields from waste HDPE pyrolysis at 650 °C and 2.8 s of vapor residence time.

Products	Yield (kg/h)
Ethylene	3,907.77
Propylene	2,800.71
Aromatics mixture	772.10
Low MWHCs mixture	11,255.97
High MWHCs mixture	1,119.92
Total	19,856.47

D.3 Regional electricity sources and geographical location

Table D-10. Ecoprofiles in SimaPro for the different electricity sources.

Source	Ecoprofile
Coal	Electricity, hard coal, at power plant/US US-EI U
Hydropower	Electricity, hydropower, at power plant/US* US-EI U
Natural gas	Electricity, natural gas, at power plant/US US-EI U
Nuclear	Electricity, nuclear, at power plant/US US-EI U
Solar	Electricity, production mix photovoltaic, at plant/US US-EI U
Wind	Electricity, at wind power plant/US- US-EI U

Table D-11. Contribution of different sources (fraction) to the electricity mixture in each state of the U.S.[1]

State	Coal	Oil	Natural gas	Nuclear	Hydro	Biomass	Wind	Solar	Geothermal
AK	0.0938	0.1312	0.4798	0.0000	0.2618	0.0068	0.0267	0.0000	0.0000
AL	0.2398	0.0003	0.4047	0.2793	0.0522	0.0233	0.0000	0.0002	0.0000
AR	0.3938	0.0007	0.3007	0.2221	0.0597	0.0227	0.0000	0.0004	0.0000
AZ	0.2796	0.0005	0.3144	0.2978	0.0665	0.0020	0.0050	0.0344	0.0000
CA	0.0016	0.0009	0.4964	0.0968	0.1468	0.0313	0.0688	0.0988	0.0586
CO	0.5509	0.0001	0.2332	0.0000	0.0296	0.0030	0.1733	0.0099	0.0000
CT	0.0049	0.0025	0.4919	0.4542	0.0063	0.0393	0.0003	0.0007	0.0000
DC	0.0000	0.0131	0.2969	0.0000	0.0000	0.6901	0.0000	0.0000	0.0000
DE	0.0567	0.0074	0.9212	0.0000	0.0000	0.0080	0.0006	0.0060	0.0000
FL	0.1667	0.0119	0.6699	0.1240	0.0007	0.0258	0.0000	0.0009	0.0000
GA	0.2853	0.0016	0.3981	0.2596	0.0143	0.0344	0.0000	0.0066	0.0000
HI	0.1532	0.6795	0.0000	0.0000	0.0093	0.0569	0.0654	0.0091	0.0266
IA	0.4633	0.0051	0.0544	0.0865	0.0169	0.0046	0.3692	0.0000	0.0000
ID	0.0019	0.0000	0.2130	0.0000	0.5792	0.0341	0.1653	0.0019	0.0046
IL	0.3176	0.0004	0.0936	0.5279	0.0007	0.0025	0.0571	0.0003	0.0000

IN	0.7316	0.0062	0.2017	0.0000	0.0043	0.0046	0.0494	0.0023	0.0000
KS	0.4852	0.0006	0.0426	0.1732	0.0006	0.0012	0.2964	0.0000	0.0000
KY	0.8329	0.0152	0.1026	0.0000	0.0434	0.0058	0.0000	0.0001	0.0000
LA	0.1155	0.0463	0.6350	0.1649	0.0106	0.0277	0.0000	0.0000	0.0000
MA	0.0587	0.0132	0.6618	0.1695	0.0066	0.0645	0.0068	0.0190	0.0000
MD	0.3720	0.0043	0.1459	0.3971	0.0375	0.0234	0.0142	0.0056	0.0000
ME	0.0062	0.0097	0.3106	0.0000	0.2663	0.2591	0.1480	0.0000	0.0000
MI	0.3673	0.0074	0.2655	0.2859	0.0074	0.0239	0.0426	0.0001	0.0000
MN	0.3873	0.0005	0.1490	0.2313	0.0202	0.0364	0.1751	0.0002	0.0000
MO	0.7674	0.0009	0.0768	0.1200	0.0184	0.0018	0.0143	0.0004	0.0000
MS	0.0850	0.0003	0.7967	0.0938	0.0000	0.0242	0.0000	0.0000	0.0000
MT	0.5199	0.0168	0.0173	0.0000	0.3673	0.0007	0.0780	0.0000	0.0000
NC	0.2877	0.0019	0.3017	0.3288	0.0339	0.0196	0.0000	0.0262	0.0000
ND	0.7037	0.0008	0.0284	0.0000	0.0506	0.0001	0.2164	0.0000	0.0000
NE	0.5884	0.0000	0.0145	0.2513	0.0411	0.0026	0.1021	0.0001	0.0000
NH	0.0219	0.0020	0.2460	0.5581	0.0594	0.0902	0.0224	0.0000	0.0000
NJ	0.0170	0.0019	0.5651	0.3855	0.0000	0.0196	0.0003	0.0106	0.0000
NM	0.5578	0.0016	0.3025	0.0000	0.0045	0.0005	0.1095	0.0232	0.0004
NV	0.0553	0.0003	0.7377	0.0000	0.0456	0.0014	0.0088	0.0654	0.0855
NY	0.0132	0.0048	0.4212	0.3101	0.1971	0.0232	0.0294	0.0010	0.0000
OH	0.5816	0.0100	0.2448	0.1422	0.0042	0.0061	0.0105	0.0006	0.0000
OK	0.2436	0.0002	0.4646	0.0000	0.0316	0.0047	0.2552	0.0001	0.0000
OR	0.0315	0.0001	0.2543	0.0000	0.5741	0.0173	0.1189	0.0007	0.0031
PA	0.2549	0.0017	0.3172	0.3866	0.0084	0.0147	0.0162	0.0003	0.0000
RI	0.0000	0.0040	0.9582	0.0000	0.0003	0.0312	0.0040	0.0022	0.0000
SC	0.2167	0.0012	0.1688	0.5759	0.0129	0.0245	0.0000	0.0001	0.0000
SD	0.2024	0.0003	0.0893	0.0000	0.4016	0.0000	0.3064	0.0000	0.0000
TN	0.3930	0.0015	0.1427	0.3730	0.0765	0.0118	0.0005	0.0010	0.0000
TX	0.2689	0.0004	0.5013	0.0934	0.0030	0.0037	0.1276	0.0016	0.0000
UT	0.6849	0.0008	0.2295	0.0000	0.0201	0.0023	0.0217	0.0278	0.0128
VA	0.1783	0.0058	0.4420	0.3212	0.0033	0.0492	0.0000	0.0002	0.0000
VT	0.0000	0.0021	0.0010	0.0000	0.5638	0.2498	0.1524	0.0309	0.0000
WA	0.0405	0.0002	0.0966	0.0847	0.6891	0.0182	0.0707	0.0000	0.0000
WI	0.5138	0.0023	0.2383	0.1563	0.0431	0.0228	0.0233	0.0000	0.0000
WV	0.9418	0.0016	0.0161	0.0000	0.0216	0.0000	0.0189	0.0000	0.0000

Table D-12. Global warming potential (GWP) of the electricity produced in each state (kg CO_2 eq. /kWh).

State	GWP	State	GWP	State	GWP	State	GWP
AK	0.6297	ID	0.1716	MT	0.6599	RI	0.7359
AL	0.6021	IL	0.4618	NC	0.5849	SC	0.3998
AR	0.7075	IN	1.0405	ND	0.8709	SD	0.3175
AZ	0.5826	KS	0.6223	NE	0.7232	TN	0.5891
CA	0.3930	KY	1.0966	NH	0.2288	TX	0.7086
CO	0.8426	LA	0.6789	NJ	0.4600	UT	1.0010
CT	0.3918	MA	0.5961	NM	0.9050	VA	0.5643
DC	0.2724	MD	0.5705	NV	0.6355	VT	0.0213
DE	0.7788	ME	0.2702	NY	0.3492	WA	0.1292
FL	0.7271	MI	0.6577	OH	0.8991	WI	0.8052
GA	0.6535	MN	0.5867	OK	0.6503	WV	1.1460
HI	0.9636	MO	0.9837	OR	0.2373	WY	1.0558
IA	0.6101	MS	0.7116	PA	0.5563		

D.4   Sensitivity analysis

Ethylene   (Favorable; Base Case; Unfavorable)

Product yield
(4.49; 3.91; 3.32 tonnes/h)

Natural gas requirements
(2.96; 3.49; 4.01 GJ/h)

Electricity requirements
(4.04; 4.75; 5.46 MW)

0.7   0.9   1.1   1.3

Propylene

Product yield
(2.90; 3.41; 3.92 tonnes/h)

Natural gas requirements
(15.44; 18.16; 20.89 GJ/h)

Electricity requirements
(2.64; 3.10; 3.57 MW)

0.7   0.9   1.1   1.3

Aromatics mixture

Product yield
(0.89; 0.77; 0.66 tonnes/h)

Natural gas requirements
(2.12; 2.50; 2.87 GJ/h)

Electricity requirements
(0.79; 0.93; 1.07 MW)

0.7   0.9   1.1   1.3

Low MWHC mixture

Product yield
(12.94; 11.25; 9.57 tonnes/h)

Steam generation
(6.54; 7.70; 8.85 tonnes/h)

Hydrogen requirements
(0.25; 0.30; 0.34 tonnes/h)

Natural gas requirements
(22.74; 26.75; 30.76 GJ/h)

Electricity requirements
(11.31; 13.30; 15.30 MW)

0.7   0.9   1.1   1.3

High MWHC mixture

Product yield
(1.29; 1.12; 0.95 tonnes/h)

Steam generation
(0.88; 0.77; 0.65 tonnes/h)

Hydrogen requirements
(0.025; 0.030; 0.034 tonnes/h)

Natural gas requirements
(1.10; 1.29; 1.49 GJ/h)

Electricity requirements
(1.09; 1.28; 1.47 MW)

0.7   0.9   1.1   1.3

GHG emissions (kg CO_2 eq. / kg)

Figure D-3. Sensitivity analysis for scenario HI-2.

308

The sensitivity of CFA inputs for propylene and fuels changed when scenario HI-2 was analyzed. Figure D-3 shows the results and clearly indicates the difference in kg of CO_2 equivalents for the three products. In the case of propylene, apart from the raise on the base GHG emissions, there is a considerable increase on the impact of natural gas, from 1 to 3%, due to the substitution of heat from steam generated internally. For the Low and High MWHCs the largest changes observed were the lower GHG emissions per kg of product (0.87 and 0.80 kg CO_2 eq., respectively) and the higher impact of steam generation. The raise on the steam generation impact went from 0.3 to 4% for both fuels, indicating a similar behavior to that from the hydrogen requirements. These observations imply not only a change in the overall GWP but also in the parameters that are more critical to control or estimate with different scenarios of credit emissions allocation.

D.5 Uncertainty analysis

Method: IPCC 2013 GWP 100a V1.03, confidence interval: 95 %

Uncertainty analysis of 1 p 'Propylene HI U (per kg of product)',
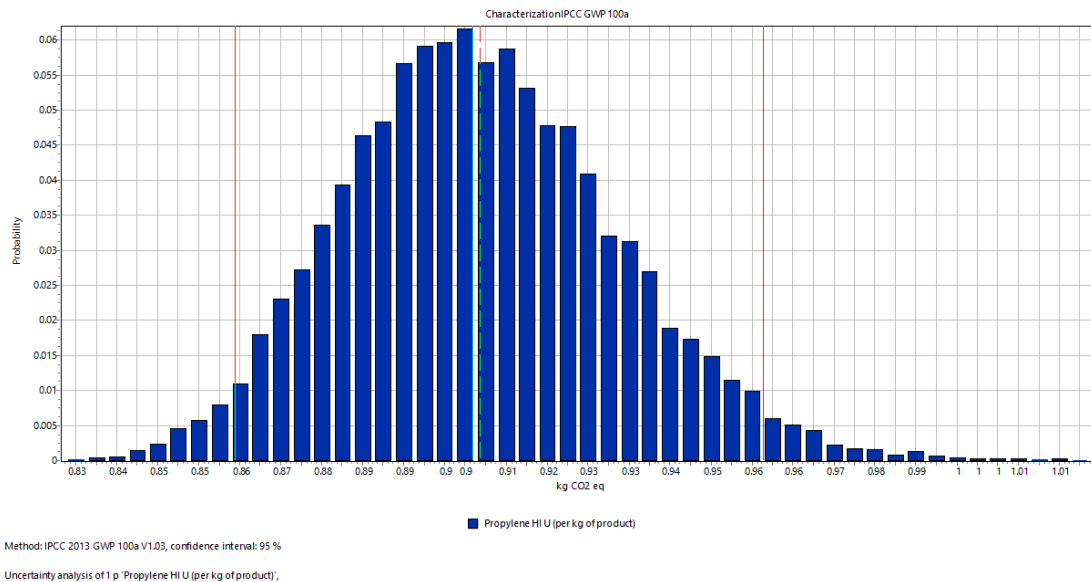
Figure D-4. Results of the Monte Carlo simulations for the GWP of propylene in scenario HI-1.
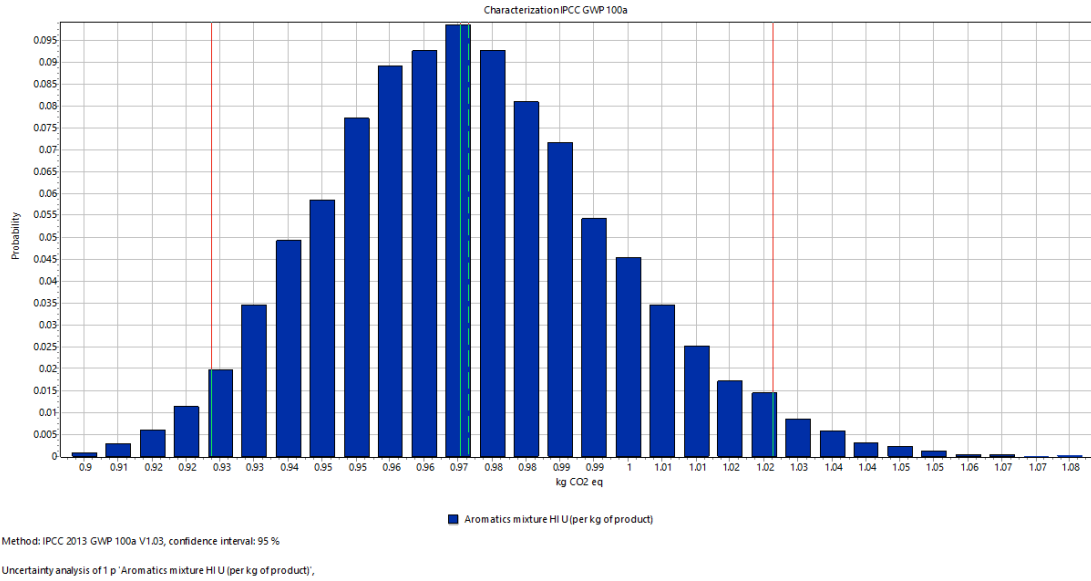
Figure D-5. Results of the Monte Carlo simulations for the GWP of the aromatics product in scenario HI-1.
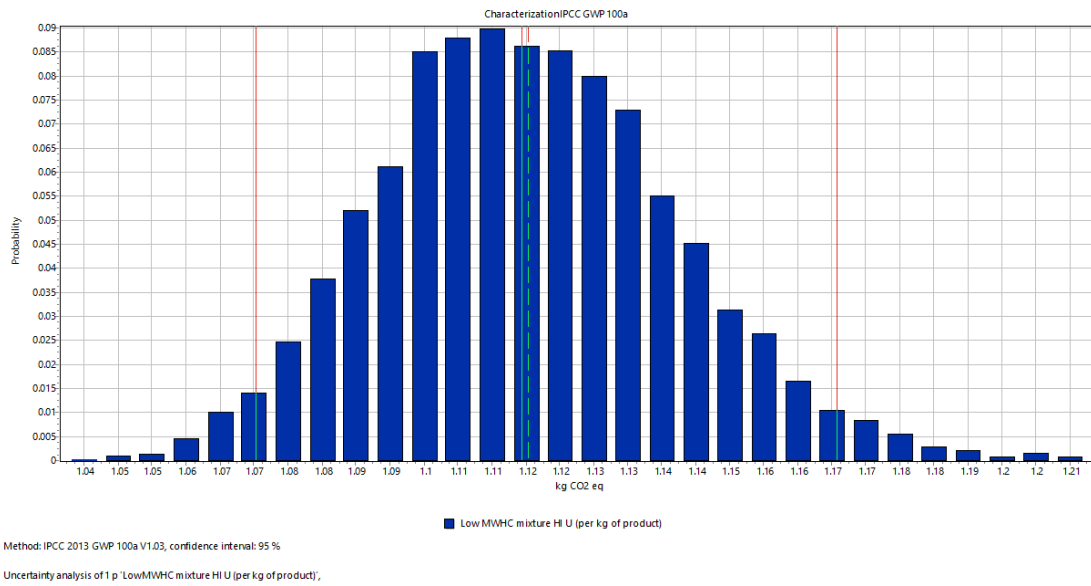
Figure D-6. Results of the Monte Carlo simulations for the GWP of the low MWHCs product in scenario HI-1.
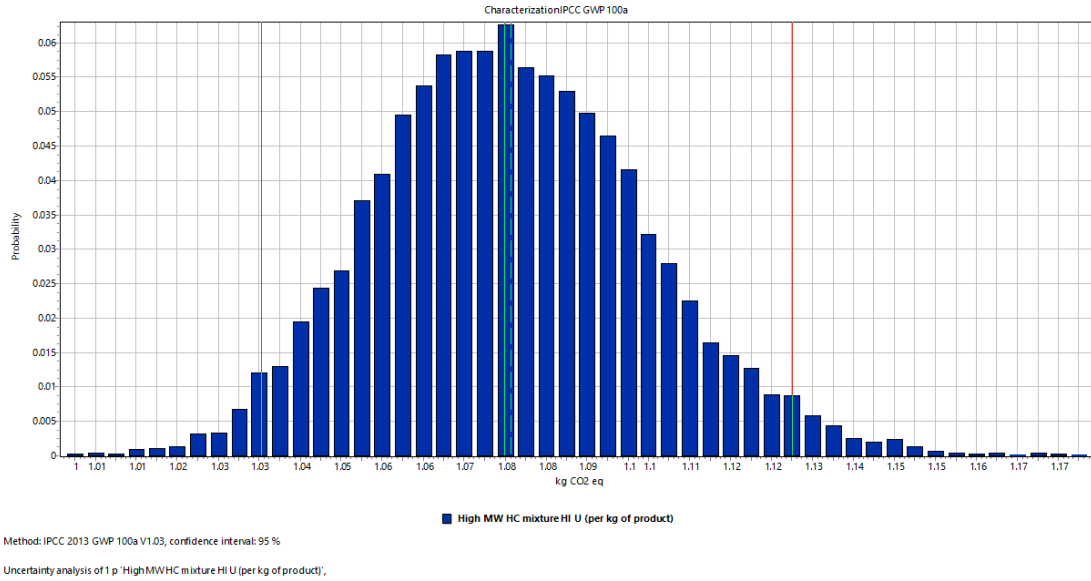
Figure D-7. Results of the Monte Carlo simulations for the GWP of the high MWHCs product in scenario HI-1.

D.6 References

(1)   U.S. Environmental Protection Agency (EPA). Emissions & Generation Resource Integrated   Database   (eGRID).   https://www.epa.gov/energy/emissions-generation-resource-integrated-database-egrid (accessed December 19, 2018).

E   Copyright documentation

Figure E-1. Copyright clearance for Chapter 2.

Figure E-2. Copyright clearance for Chapter 3.

Copyright clearance for Figure 1.1

Figure 1.1. "Cumulative plastic production, waste generation, and disposal scenarios from 1950 to 2015". Licensed under CC-BY-SA by Ritchie, H. and Roser, M. (2018) via Our World in Data.